UNIVERSITY OF COPENHAGEN
FACULTY OF SCIENCE

Measurement of the $t\bar{t}$ production cross section in the $e\mu$ channel with b-tagged events at $\sqrt{s} = 13$ TeV and its interpretation towards a high precision top quark mass measurement.

Author: Rosanna Ignazzi
Supervisor: Prof. Peter H. Hansen

A thesis presented for the degree of
Doctor of Philosophy

Niels Bohr Institute
University of Copenhagen
Denmark

Submitted: 14-09-2019

ABSTRACT

The study of the top quark is fundamental to the field of particle physics, because its high mass of approximately 173 GeV, the highest in the Standard Model, is close to the electro-weak vacuum expectation value of 246 GeV, which hints to the fact that this particle might be special and it could be the key to unveil physics beyond the Standard Model. Therefore a precise study of the properties and mass of the top quark is necessary. In particular the mass of the top quark, which is a free parameter in the Standard Model, needs to be measured precisely, because it is one of the parameters used to constrain the global fit to check for the validity of the Standard Model and its consistency with the measured data. Also, the measured inclusive $t\bar{t}$ production cross section can be compared to theoretically predicted values, allowing for a further check of the Standard Model.

The $t\bar{t}$ production total fiducial and inclusive cross section and the $t\bar{t}$ production absolute and normalised differential cross section for seven different leptonic kinematic variables are measured using the data collected in the ATLAS experiment at $\sqrt{s} = 13\,\text{TeV}$ during the full Run 2 period (2015−2018) with a total integrated luminosity of $139\,\text{fb}^{-1}$. The measurement is performed using dilepton $e\mu$ events with opposite sign and with either one or two associated b-jets. The total $t\bar{t}$ production fiducial cross section is measured with a total relative uncertainty of 2.34% and the total inclusive $t\bar{t}$ production cross section with a total relative uncertainty of 2.91%. The value of the total inclusive cross section and the contributions to its uncertainty are as such:

$$\sigma_{t\bar{t}} = 839.8 \pm 1.3 \pm 16.0 \pm 18.4\,\text{pb}$$

where the first uncertainty is the statistical one, the second is the luminosity uncertainty and the last is the total systematic uncertainty from all of the other sources other than the luminosity.

The normalised differential distributions are used to extract the top pole mass for five leptonic kinematic variables, $p_\text{T}(\ell^+\ell^-)$, $p_\text{T}(\ell^+) + p_\text{T}(\ell^-)$, $p_\text{T}(\ell)$, $E(\ell^+) + E(\ell^-)$, $m(\ell^+\ell^-)$, due to their sensitivity to the mass of the top quark. The extraction is done by comparing the measured distributions to Monte Carlo templates at different top mass values. The results show that the uncertainty on the top pole mass can be reduced compared to previous measurements, thanks to the lower uncertainty on the normalised differential cross section distributions, but the templates used in this thesis are not adequate and more proper templates, including correction to the top p_T spectrum and NNLO processes, would improve the results.

RESUMÉ

Undersøgelsen af top kvarken er grundlæggende for partikelfysik, fordi dens høje masse på ca. 173 GeV, den højeste i Standardmodellen, er tæt på den elektrosvage skala vacuum værdi på 246 GeV, som antyder, at denne partikel kan være speciel, og at den kan være nøglen til at afsløre fysik ud over Standardmodellen. Derfor er en nøjagtig undersøgelse af egenskaberne og massen af top kvarken nødvendig. Især skal massen af top kvarken, som er en fri parameter i Standardmodellen, måles nøjagtigt, da det er en af de parametre, der bruges til at begrænse den globale fit til at kontrollere gyldigheden af Standardmodellen og dens overensstemmelse med de målte data. Desuden kan det målte inklusive $t\bar{t}$ produktions tværsnit sammenlignes med teoretisk forudsagte værdier, hvilket muliggør en yderligere kontrol af Standardmodellen.

Det totale $t\bar{t}$ produktions tværsnit og $t\bar{t}$ absolutte og normaliserede produktions differentielle tværsnit for syv leptoniske kinemaiske variabler måles ved hjælp af data indsamlet i ATLAS eksperimentet ved $\sqrt{s} = 13\,\text{TeV}$ i hele Run 2 perioden ($2015 - 2018$) med en total integreret luminositet på $139\,\text{fb}^{-1}$. Målingen udføres ved hjælp af dilepton $e\mu$ begivenheder med modsat ladning og med enten en eller to tilknyttede b-jets. Den totale $t\bar{t}$ fiducial produktions tværsnit er målt med en samlet relativ usikkerhed på $2,34\%$, mens den inklusive $t\bar{t}$ produktions tværsnit er målt med en samlet relativ usikkerhed på $2,91\%$. Den inklusive $t\bar{t}$ produktions tværsnit og bidragene til dens samlede usikkerhed er som sådan:

$$\sigma_{t\bar{t}} = 839.8 \pm 1.3 \pm 16.0 \pm 18.4\,\text{pb}$$

hvor den første usikkerhed er den statistiske, den anden er luminositetsusikkerheden, og den sidste er den samlede systematiske usikkerhed fra alle de andre kilder bortset fra luminositet.

De normaliserede differentielle fordelinger for fem leptoniske kinematiske variabler, $p_\text{T}(\ell^+\ell^-)$, $p_\text{T}(\ell^+) + p_\text{T}(\ell^-)$, $p_\text{T}(\ell)$, $E(\ell^+) + E(\ell^-)$, $m(\ell^+\ell^-)$, bruges til at ekstrahere top kvarken polmassen på grund af deres følsomhed over for top kvark massen. Målingerne udføres ved at sammenligne de målte fordelinger med Monte Carlo skabeloner ved forskellige top masse værdier. Resultaterne viser, at usikkerheden på top polmassen kan reduceres sammenlignet med tidligere målinger takket være den lavere usikkerhed på de normaliserede differentielle tværsnitsfordelinger, men skabelonerne, der er brugt i denne afhandling, er ikke tilstrækkelige og mere korrekte skabeloner, der inkluderer korrektion af top p_T spektrum og NNLO processer, ville forbedre resultaterne.

ACKNOWLEDGEMENTS

I want to thank first and foremost my supervisor Prof. Peter H. Hansen, for following me during these three years and helping me in achieving my goals. I also would like to thank very deeply Richard Hawkings, for always answering my questions and for giving me excellent advice and physics insight.
I would like to thank the high energy physics group at NBI and all the people in it (students, Post. Docs and Professors), for inspiring me in my work and for always being ready for a quick or long discussion, both about physics and about personal matters. I will very much miss their company and their support.
A special thanks goes to Luca Martinelli and Giuseppe Salamanna, for joining me in the analysis team, making it possible for us to achieve very good and sound results.
I am also grateful for all the people I have met at CERN and in ATLAS, in the Top Mass and Properties and in the Top Cross Section groups, but also all the other passionate people at workshops and schools.
A big thank goes to my family, especially my mum and dad, for always listening to me and encouraging me. But there is a person without which all this would not have been possible at all, a person who has supported me, sustained me and, at times, tolerated me through all the steps of this journey, both when I have been abroad or at home, my husband Jonathan. Thank you, Jonathan.

CONTENTS

CHAPTER 1

INTRODUCTION

The top quark is one of the fundamental particles in the Standard Model [1] and it was discovered in 1995 at the Tevatron [2, 3]. The mass of the top quark, which is around 173 GeV [1], is the largest particle mass in the entire Standard Model, and is furthermore comparable with the Higgs field vacuum expectation value of 246 GeV [4]. This suggests that the top quark could couple stronger than other Standard Model particles to fields beyond the Standard Model, which makes the top quark properties, mass and production cross sections especially interesting to observe, because they could be the key to unveiling a theoretical framework beyond the Standard Model [5, 6]. The total inclusive production cross section of $t\bar{t}$ pairs, which can be predicted to NNLO level within the Standard Model [7–11], can be measured and compared to the theoretically predicted value, to check if the measured value is in accordance with its prediction. The mass of the top quark, which is a free parameter in the Standard Model, is one of the central variables used to check the validity of the Standard Model and it is included in a global fit, together with other experimental parameters, to assess what the probability is, that the Standard Model is consistent with the observed data [12]. The more precise the mass measurement is (as well as all the other measurements of the other parameters), the more accurately can we know if the Standard Model is indeed the complete description of particle physics, or if it is only a part of a more comprehensive theory.

This thesis outlines a way to measure the production cross section of $t\bar{t}$ pairs and the top quark mass using the measured fiducial differential cross section distributions fitted to theoretical templates. The first part of the thesis presents the measurement of the total and differential production cross sections of $t\bar{t}$ events measured using the full dataset collected during the Run 2 period $(2015-2018)$ at a center of mass energy of $\sqrt{s} = 13$ TeV in the ATLAS experiment with an integrated luminosity of $139\,\text{fb}^{-1}$, while at the end the mass extraction method is outlined.

The fiducial production cross section measurement of $t\bar{t}$ events is performed in the dilepton channel of the $t\bar{t}$ decay, where the top pair decays to two W bosons and two b-jets, $t\bar{t} \to W^+W^-b\bar{b}$, and the W bosons both decay to leptons and corresponding neutrinos. In order to select the cleanest channel, only the events where one W decays to an electron and the other to a muon and the two leptons have opposite sign are taken into consideration as signal events. The events are furthermore required to contain either exactly one or exactly two b-tagged jets in order to finally extract the cross section.

Previous ATLAS measurements of the total inclusive and fiducial $t\bar{t}$ production cross section with the same method as used in this thesis include the measurements at $\sqrt{s} = 7$ TeV, at $\sqrt{s} = 8$ TeV and at $\sqrt{s} = 13$ TeV [13–15], where the measurement of the total inclusive cross section reached a precision of 3.9%, 3.6% and 4.4% total relative uncertainty. The measurement at $\sqrt{s} = 13$ TeV was performed only with the data collected in 2015 (3.2 fb^{-1}). Another more recent measurement at $\sqrt{s} = 13$ TeV, also with the same method as the one used in this thesis, with the data from the 2015 – 2016 period (36.2 fb^{-1}) shows a precision on the total inclusive cross section of 2.4% (and on the total fiducial cross section of 2.36%) [16]. A measurement of the fiducial differential cross section was performed at $\sqrt{s} = 8$ TeV in [17, 18] and at $\sqrt{s} = 13$ TeV in [16] and the distributions were used to extract the pole mass in [17, 18]. The differential distributions in [16] have the same range and binning of [17, 18], but a lower uncertainty on each bin.

The analysis presented in this thesis includes the total fiducial and inclusive cross section and the differential (absolute and normalised) cross section for 7 different leptonic variables, $p_\mathrm{T}(\ell^+\ell^-)$, $p_\mathrm{T}(\ell^+) + p_\mathrm{T}(\ell^-)$, $p_\mathrm{T}(\ell)$, $E(\ell^+) + E(\ell^-)$, $m(\ell^+\ell^-)$, $|\eta(\ell)|$ and $\Delta\phi(\ell^+\ell^-)$. Using leptonic kinematic variables has the advantage that it does not require the $t\bar{t}$ system to be reconstructed.

Compared to the previous mentioned analysis, due to the high statistics of the Run 2 dataset and the improvements in the modelling of the detector and of the $t\bar{t}$ system [19], this analysis aims to reach a lower uncertainty on the total cross section and differential cross section than previously obtained, also the granularity and range of the differential distributions as a function of the leptonic variables have been extended as compared with [17] and [16]. The finer granularity and the lower uncertainty could be helpful in the future both for a mass estimation, but also for the tuning of Monte Carlo generators and for checking the theoretical modelling of $t\bar{t}$ processes [20–23].

Finally the normalised differential cross sections for five of the seven variables, $p_\mathrm{T}(\ell^+\ell^-)$, $p_\mathrm{T}(\ell^+) + p_\mathrm{T}(\ell^-)$, $p_\mathrm{T}(\ell)$, $E(\ell^+) + E(\ell^-)$, $m(\ell^+\ell^-)$, as suggested by [24] are used to outline a method to extract the top pole mass, where the extracted distributions are compared to Monte Carlo templates at different top mass values to extract a χ^2 distribution per variable. The results found for each distribution are then used to find a combined estimate using the BLUE method, as in [17]. The limitations of this method to extract the top pole mass are discussed.

The thesis is structured as such: Chapter 2 outlines the theory behind the Standard Model and presents the top quark within the Standard Model framework, Chapter 3 describes the ATLAS detector, Chapter 4 contains a description of the data and simulation samples, in Chapter 5 the object and event selections used in this analysis are outlined, in Chapter 6 the modelling of the fake lepton and the $Z \to \tau\tau +$ jets backgrounds are described, in Chapter 7 the analysis technique is explained and the validation tests presented, in Chapter 8 the different systematic uncertainties are described, together with an explanation on how they are evaluated, in Chapter 9 the results of the total and differential cross section are presented, and finally in Chapter 10 the top mass extraction method is presented.

CHAPTER 2

THE STANDARD MODEL OF PARTICLE PHYSICS

The journey to the current particle physics theories started with Democritus in 400 B.C., he was the first to postulate the existence of small indivisible entities that make up all the space, and he called those entities “atomi” (from Greek, indivisible). This idea was kept alive by alchemists, who were studying chemical reactions, in particular J. Dalton postulated in the first half of the 19th century, that different materials are composed by small particles, which are all the same for one material, and he based this on the observation that different materials react with each other in chemical reactions in very precise ratios. The last sceptics of this theory (that “molecules” are the smallest constituent of any substance) were convinced by Einstein’s explanation of observations on Brownian motion [25].

In the course of the 19th century, the discoveries of the electron, X-rays, radioactivity and line-spectra paved the way for the notion of structure in the “atomic” constituents of molecules. It was finally Rutherford’s scattering experiment that led Bohr to suggest the atomic model with a small nucleus of positive electric charge surrounded by a cloud of negative electrons in different discrete orbits [26].

With the birth of quantum mechanics, relativity and the technological ad-

vancement, physicists realised that the nucleus was not indivisible, but it was a collection of other fundamental particles. In 1932 Chadwick discovered the neutron [27], and the same year also saw the first "split atom" when Cockcroft and Walton turned a Lithium nucleus into two Helium nuclei [28]. This was accomplished with one of the first "accelerators", a device that can produce high energy beams of particles. Years later scientists realised that protons and neutrons have a substructure of point like constituents. This was proven thanks to the developments of accelerator technology, in particular the 5 km long linear electron accelerator at Stanford could in 1969 show the "grainy" substructure of protons [29, 30]. These point like constituents were shown to have the properties of the "quarks" that had been earlier suggested on the basis of symmetry patterns in observed hadron states.
A theory, now called the Standard Model of particle physics, had at that time already taken shape and it would eventually explain all the observations done in accelerator experiments. It had been primarily developed by S. Glashow, S. Weinberg and A. Salam in the 1970s and it could explain the known particles and their interactions through three of the four fundamental forces, electromagnetism, the weak force and the strong force [31, 32].

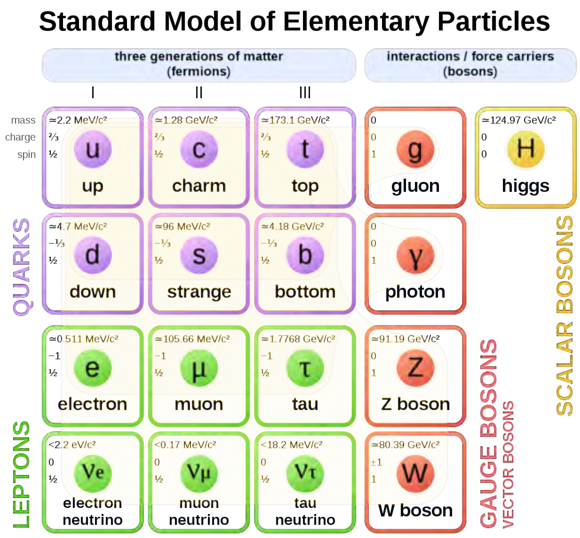

Figure 2.1: Particles in the Standard Model of particle physics [33].

The fundamental particles and forces included in the Standard Model are shown in Fig. 2.1, which includes the leptons and quarks as the fundamental fermions and the force carriers as fundamental bosons [4]. This theory was postulated when not all the particles were found, so many of them were theorized and then searched in particle accelerators. For example the Z and W were first discovered in 1983 at CERN [34–37], the top quark was measured for the first time at the Tevatron in 1995 [2, 3] and the Higgs boson was the last particle to be measured at CERN in 2012 [38, 39]. On the other hand, the discoveries of the muon in cosmic rays in 1937 [40], the discovery of the charmed quark in 1974 at SLAC and BNL [41, 42] and of the tau-lepton at SLAC in 1975 [43] were more of an experimental surprise.

2.1 Electroweak Standard Model and the Higgs mechanism

The Standard Model of particle physics is a theory within the Quantum Field Theory (QFT) formulation, where the quantum mechanical and relativistic properties of particles and fields are united in a unified formulation. In particular the Standard Model is a unification of quantum electrodynamics (QED), of the weak interaction and of the quantum chromodynamics (QCD) theories [4].
The QED describes the electromagnetic interactions, which happen with the exchange of the field boson, in this case the massless photon, the weak interaction describes the weak force, which is responsible for radioactive decay, for example, and proceed via the exchange of a massive W or Z, and the QCD describes the interactions between the quarks and their boson field, the massless gluon. Each theory is internally gauge symmetric[1] and they respect the $\mathrm{U}(1)_Y$, $\mathrm{SU}(2)_L$ and the $\mathrm{SU}(3)_C$ gauge symmetries respectively [4].
For the Standard Model to have internal consistency there needs to be an internal gauge symmetry in the unified theory, but this is not possible by just unifying the three theories above, as the gauge symmetry in the Standard Model in this form is broken by the masses of the particles in the electroweak sector, in particular by the masses of the W and Z. This can though be resolved by introducing the Higgs mechanism, which preserves the symmetry of the underlying model, but breaks it spontaneously by the vacuum choosing a certain state to be in. This is done by introducing a field ϕ, with potential

$$V(\phi) = \frac{1}{2}\mu^2\phi^2 + \frac{1}{4}\lambda\phi^4 \tag{2.1}$$

with $\lambda > 0$ and $\mu^2 < 0$. The constraints on λ and μ are there to assure that the potential has a minimum, also called vacuum expectation value v, and this exists first if $\lambda > 0$, if $\mu^2 > 0$ the vacuum expectation value is zero, while if $\mu^2 < 0$ the vacuum expectation value is

$$v = \sqrt{\frac{-\mu^2}{\lambda}}. \tag{2.2}$$

Since the potential has minima at field values different from zero, the symmetry is broken, because we need to choose one value for the vacuum and this is called spontaneous symmetry breaking [4].
When the above mentioned Higgs field is introduced, in a gauge invariant way, in the electroweak sector of the Standard Model, it generates the masses of the W^+, the W^- and the Z, as well as a boson corresponding to the excitation

[1] A theory is gauge invariant when it is invariant under local phase transformation in the space of the internal degrees of freedom of the theory [4].

of the Higgs field introduced to ensure gauge symmetry [4]. In this case the Higgs scalar field is chosen as [4]:

$$\phi(x) = \begin{bmatrix} 0 \\ v + h(x) \end{bmatrix} \tag{2.3}$$

and the free field is introduced in the Lagrangian for this field, which has the form [4]:

$$\mathcal{L} = (\partial_\mu \phi)^\dagger (\partial^\mu \phi) - V(\phi). \tag{2.4}$$

In the framework of the Standard Model, the derivative is replaced with the covariant derivative ($\partial_\mu \to D_\mu$) with the coupling constants of the SU(2) and U(1) symmetries and the generators and gauge fields of the symmetries as well. When the covariant derivative acts on the Higgs doublet in Eq. 2.3 the mass terms of the electroweak bosons come out as $m_W = \frac{1}{2} g_W v$, $m_A = 0$ and $m_Z = \frac{1}{2} v \sqrt{g_W^2 + g'^2}$, where m_W is the mass of the W, m_Z is the mass of the Z and m_A is the mass of the photon, g_W is the coupling constant of the $\mathrm{SU}(2)_L$ and g' is the coupling constant of the $\mathrm{U}(1)_Y$.
The fermion masses need to be addressed as well. This is done by introducing the Yukawa coupling to the Higgs field, and from the Yukawa interaction Lagrangian the mass terms for the different fermions can be extracted as $g_f = \sqrt{2} \frac{m_f}{v}$ [4]. The values of the Yukawa couplings are not predicted in the Standard Model, as well as the value of the masses of the fermions, they are purely found by experiments.

2.2 Top quark

In 1977 the bottom quark was discovered [44] with a charge of $-1/3$ and in the Standard Model each quark needs a charge partner, in this case the top quark with charge $+2/3$. The W propagator of the electroweak force, which in the low energy limit is measured by the Fermi constant, contains loops of top-bottom pairs [4], therefore it was suggested already in the 1980s that the top quark would have a significant mass due to the experimental measurement of the Fermi constant, of the W mass and the electroweak mixing angle [4].
The top quark was first observed in 1995 at the CDF and D0 experiments at the Fermilab Tevatron [2, 3] and since then several experiments have attempted to measure the top quark and its properties as the production cross section or its mass, both at the Tevatron and since also at the LHC [5].
As expected, the top quark was found to be massive, the heaviest fundamental particle in the Standard Model. Remarkably, the mass of the top quark is comparable to the electroweak scale given by the vacuum value of 246 GeV [4]. This could mean, that the top quark might play a special role in a framework more comprehensive than the Standard Model [5, 6].
In the following sections, an overview will be given on the production mechanisms and on the properties of the top quark.

2.2.1 Production mechanism and decay channels

The top quark decays with almost a 100% branching ratio to a W boson and to a b-quark [1]. The type of decays of the top quark are then defined mainly from the different decays of the W boson, which can decay to an electron, muon or τ and their corresponding neutrino with a $\sim 11\%$ branching ratio each or to a quark and antiquark pair (the sum of the charge of the two quarks have to be either $+1$ or -1, depending on whether it is a W^+ or a W^- decaying) with a total branching ratio of $\sim 67\%$ [1, 45].

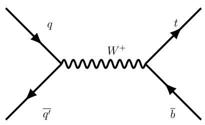

(a)

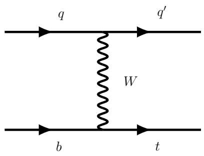

(b)

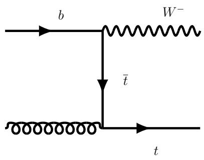

(c)

Figure 2.2: Single top s-channel in 2.2(a) and t-channel production in 2.2(b) and 2.2(c).

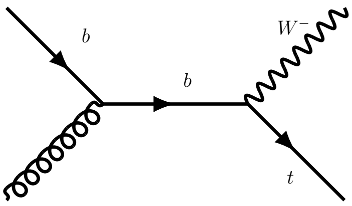

Figure 2.3: Single top Wt channel production.

The top quark is produced either in a $t\bar{t}$ pair or in single top processes, which means alone together with other particles. There are three different types of single top processes, the s-channel one, the t-channel one and the Wt production channel [1, 46], which can be seen in Fig. 2.2(a), Fig. 2.2(b) and 2.2(c) and in Fig. 2.3 respectively.
The $t\bar{t}$ production modes can have 3 different decay channels: the fully leptonic channel, where both W bosons decay to leptons, see Fig. 2.5, with a branching ratio of $\sim 10\%$, see Fig. 2.4, the lepton + jets channel, where one W decays leptonically and the other hadronically with a branching ratio of $\sim 45\%$, and the fully hadronic channel, where both W bosons decay hadronically with a total branching ratio of $\sim 46\%$ [1]. The precise branching ratios of the different decay channels depend on which values of the W boson decay branching fractions are used, as they are both theoretically predicted and experimentally measured and those values are not exactly the same [45].
In the cases of the Wt channel, the top quark decays to a W boson as well and this can result in the same final states as the in the $t\bar{t}$ production, giving an interference between the two production mechanisms. This interference needs to be resolved in order to produce Monte Carlo samples for $t\bar{t}$ and Wt decays

separately and for this two different ways of taking care of this interference are devised, the diagram removal (DR) and the diagram subtraction (DS) schemes [46, 47]. In the DR case the interference term and the term describing any $t\bar{t}$ contributions are removed from the total amplitude, leaving only the pure Wt signal, while in the DS case the cross section of the Wt signal is corrected in order to remove all $t\bar{t}$ contributions (leaving though the interference contribution) [47]. Effectively, by taking the difference between the DR and the DS schemes, the effect of the interference between Wt and $t\bar{t}$ can be measured [47].

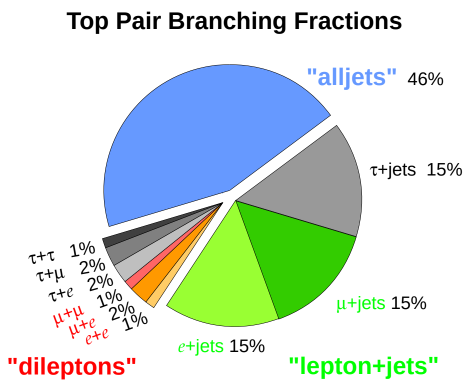

Figure 2.4: $t\bar{t}$ production decay channels [48].

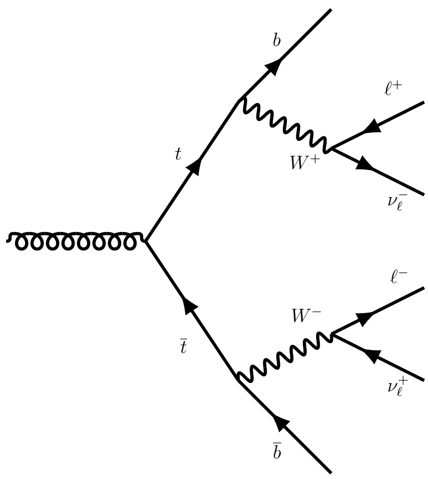

Figure 2.5: $t\bar{t}$ production in the fully leptonic channel.

2.2.2 Properties

The charge of the top quark is 2/3 of the elementary charge and it has a lifetime of $\sim 10^{-24}$ s [5]. Given that the lifetime of the quark is so short, the top quark cannot form bound states before decaying, as all the other quarks, giving researchers the opportunity of studying its properties without having

to untangle bound states [5].
The current world average of the top mass is 173.34±0.76 GeV [49], see Fig. 2.6, making the top quark the heaviest particle so far known in the Standard Model. The high mass introduces significant electroweak loop corrections to the mass of the Higgs, which helped in constraining the mass interval where the Higgs could be found before its discovery in 2012 [4]. The Yukawa coupling to the Higgs field for the top quark is correspondingly big [5], and therefore the top quark could help in understanding the electroweak symmetry breaking process better.

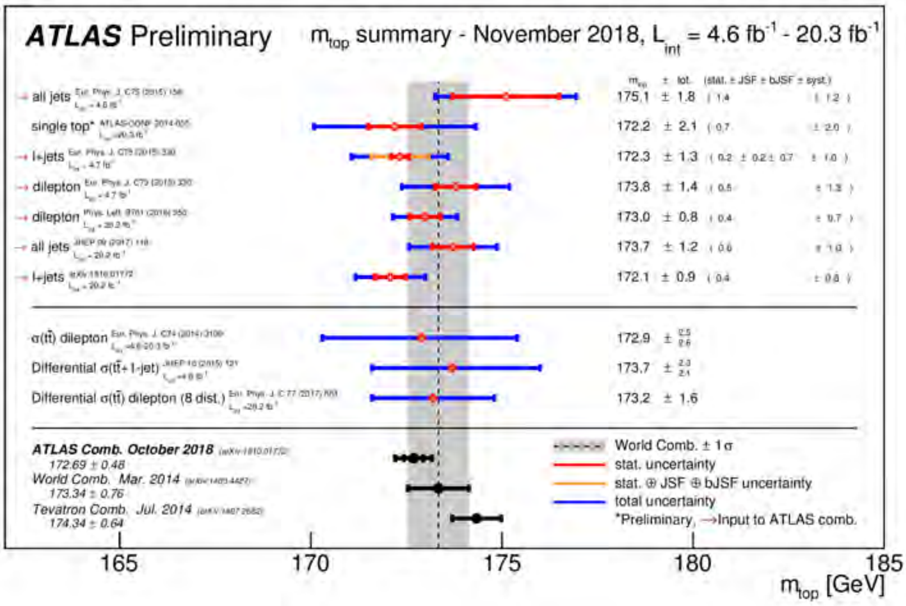

Figure 2.6: Top quark mass measurements in the ATLAS experiment from [50].

The measurement of the top mass is rather significant, because it is one of the free parameters of the Standard Model and the more precisely we know the mass value, the better we can constrain other parameters, such as the mass of the Higgs and the mass of the W, and the better we can perform a fit to the Standard Model see Fig. 2.7(a), to see how well these parameters coincide with the current Standard Model formulation [12]. The fit to these parameters, shown in Fig. 2.7(a), thus provide a powerful test of the Standard Model. In particular the efforts to improve the measurement of the top quark mass is motivated by the special role of the top in Standard Model loop-corrections. Within the Standard Model, the loop-corrections to the W propagator precisely relate the top quark mass to the W mass for a given value of the Higgs mass. Also, the top mass, together with the Higgs mass can be used to calculate the stability of the vacuum of the Standard Model, and following current calculations it seems that the vacuum is in a metastability state [51], see Fig. 2.7(b).
Two types of techniques are used to extract the top mass, direct reconstruction or inference from total fiducial or differential cross section methods (also

called indirect methods). The first technique forms the invariant mass of the top quark from the reconstructed four-momenta of the top decay products. It can be performed in all decay channels, where each channel has its own challenges. In the dilepton channel the reconstruction is made difficult from the presence of two undetected neutrinos, therefore a series of equations needs to be solved to constrain the energy of the neutrinos to finally extract the top mass. In the lepton + jets and the fully hadronic channels the reconstruction is easier, though the measurement suffers from the uncertainties on the modelling of jets. Examples of analysis using the reconstructed four-momenta can be seen in the upper part of Fig. 2.6. The other method infers the top mass value either from the total $t\bar{t}$ production cross section, or from comparing the shapes of differential cross section distributions with theoretical templates calculated at different values of the top quark mass. This method results in a higher uncertainty, see Fig. 2.6, but helps in validating QCD calculations at NLO level. Examples of analysis using the indirect method can be seen in the middle part of Fig. 2.6. With the indirect method the mass extracted is the $m_{\text{top}}^{\text{pole}}$, the pole mass, which is the mass of the free particle. So far there are two definitions of the top mass, the pole mass and the direct mass, where the direct mass, as it is measured, is the same as a parameter in the Monte Carlo generator, which makes it vulnerable towards uncalculated soft QCD effects, and the pole mass is the mass in a theoretically defined renormalisation scheme. From a theoretical point of view, the pole mass is more interesting, even if it is less precise than the direct mass, as it is found in a well defined renormalisation scheme [52]. With the current level of experimental precision of around 1 GeV, there is no significant difference between these two values [1], but the more the precision is lowered on the top mass measurement, the easier it would be to see if those two values are the same or not.
As mentioned before, the high mass means that the top quark couples strongly to the Higgs field, and this manifests itself to the coupling of the top quark to the Higgs particle through associated production, observed with a significance of above 5 standard deviations in ATLAS for the first time [53].

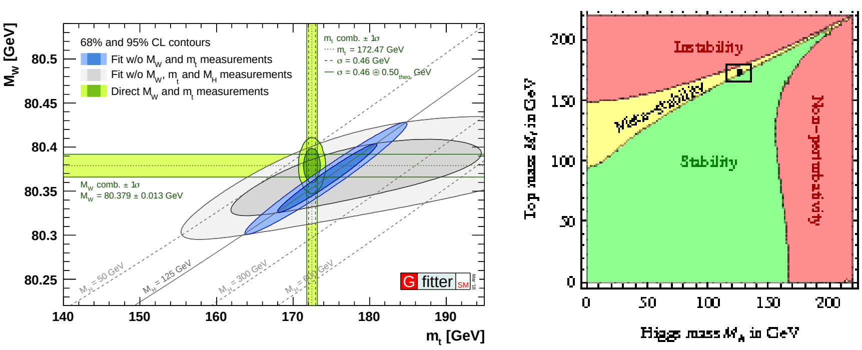

(a) (b)

Figure 2.7: Fit of the Standard Model electro-weak sector with the top mass and the W mass, from [54] and graph for the vacuum stability as a function of top mass and Higgs mass from [51]

Another property usually studied is the production cross section, both for the single top production channels and in the $t\bar{t}$ production channels. In fact the production cross section can be theoretically calculated for different center of mass energies [7–11] and by comparing the measured values with the calculated ones, the Standard Model predictions can be verified. One example can be seen in Fig. 2.8, where the $t\bar{t}$ production cross section theoretical values are compared to the measured values at the ATLAS and CMS experiments [7]. In case the predictions and the measurements were not compatible, an eventual difference would imply the existence of other production mechanisms that are not included in the Standard Model, opening the door to new physics.
Another property that has been studied at the LHC and Tevatron thanks to the high quantity of top quarks produced, is the spin correlation between the two top quarks. Due to the short lifetime, the spin of the top quark has not enough time to decouple and hence it is transmitted directly to its decay products, in particular it is known from the Standard Model, that the spin of the two quarks are correlated and the correlation will be visible in the decay products as well [57]. A way to measure this spin correlation is to find the difference in azimuthal angle between the decay products of the two quarks, and it has been done in ATLAS in the $e\mu$ opposite sign channel [58], for example.

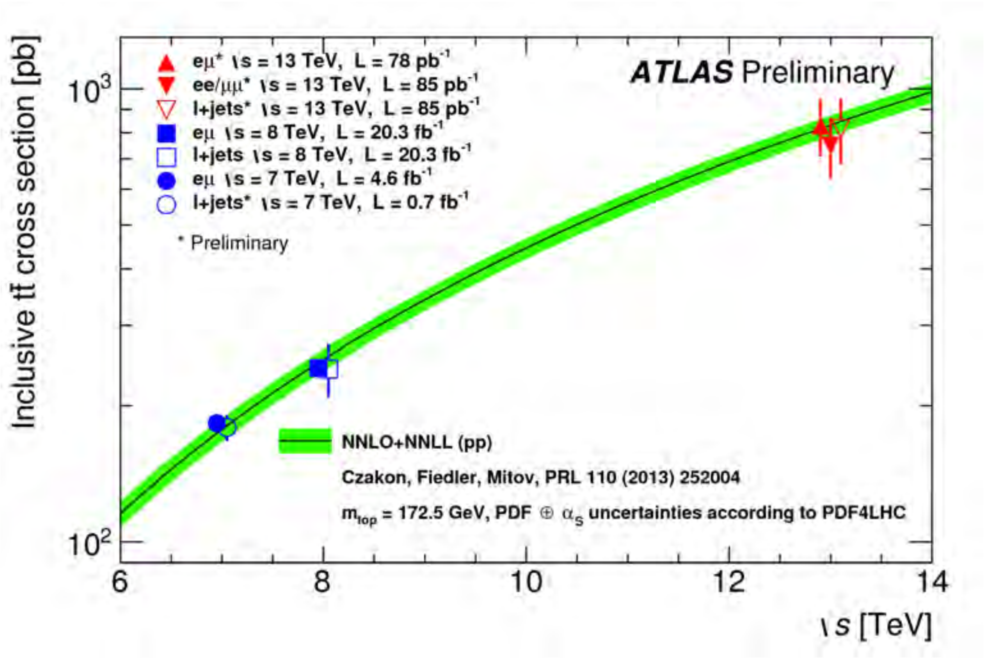

(a)

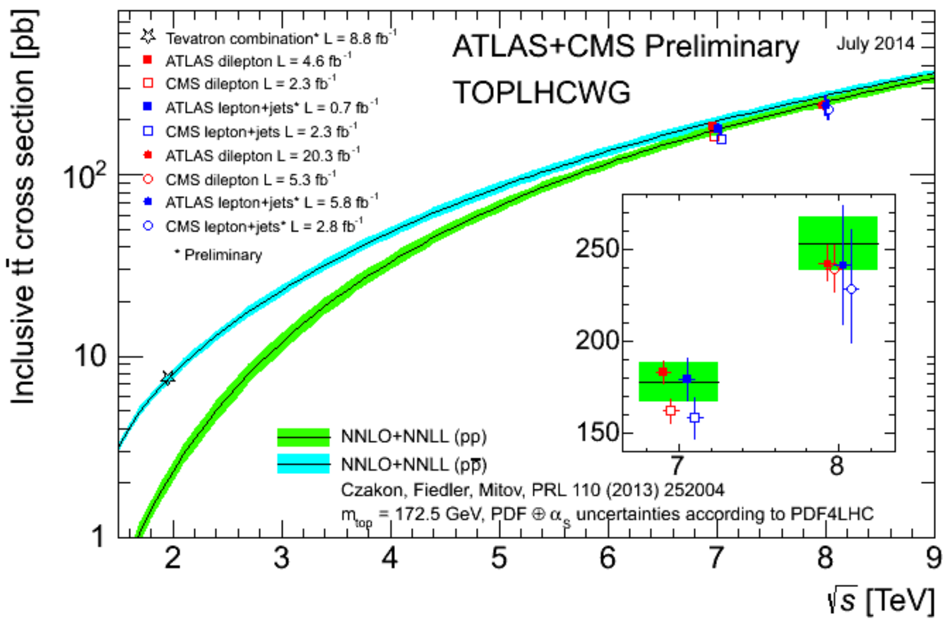

(b)

Figure 2.8: $t\bar{t}$ production cross section for ATLAS [55] and for CMS, ATLAS and Tevatron from [56].

CHAPTER 3

THE ATLAS EXPERIMENT

The A Toroidal LHC ApparatuS (ATLAS) detector, one of the Large Hadron Collider (LHC) detectors, is a multi-purpose particle detector composed of several different layers, the inner detector as the innermost layer, the electromagnetic calorimeter, the hadronic calorimeter and the muon system. The Inner Detector system is enclosed in a solenoid magnet, that provides a 2 T magnetic field in the direction parallel to the beam, the muon system and calorimeters are enclosed in a toroidal magnetic system [59].

3.1 Coordinate system

The ATLAS coordinate system follows the LHC convention, where the z-axis is along the beam axis, the x-axis points to the LHC center and the y-axis

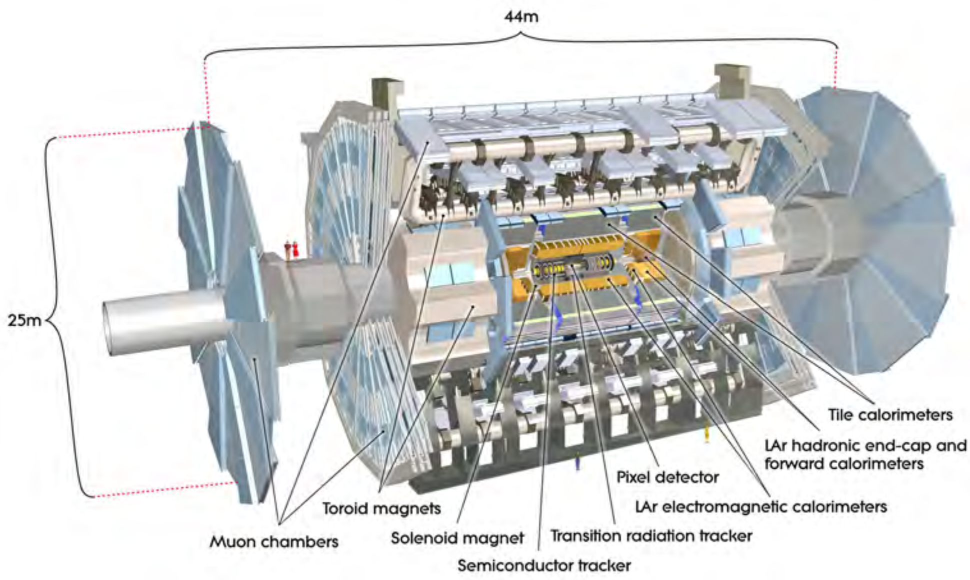

Figure 3.1: Scheme of the ATLAS detector and its subdetectors, taken from [59].

points up. The origin of the coordinate system is in the center of the detector, also called the interaction point, since it is here the bunches of particles collide. The Cartesian coordinate system is not often used in the physics and analysis of the data and due to the cylindrical geometry of the detector, instead the cylindrical coordinate system is preferred. The z-axis, or beam axis, is in the same direction, the ϕ angle goes around the beam axis (with $\phi = 0$ along the x-axis) and the θ angle starts from the beam axis (goes from zero along the positive z-axis to π along the negative z-axis). When describing the position of a particle in the detector, we do not use the polar angle θ, but we use instead the pseudorapidity η, where $\eta = -\ln(\tan(\theta/2))$, or the rapidity y, where $y = 1/2\ln[(E + p_z)/(E - p_z)]$ (E is the energy of a particle, while p_z is the z-component of the 4-momentum of a particle) [59]. These variables are convenient since an interval of rapidity is a Lorentz-invariant and the particle density is approximately constant in rapidity. The two variables are the same for highly relativistic particles and hence the more convenient pseudo-rapidity is used. The Cartesian and the corresponding cylindrical coordinate systems are sketched in Fig. 3.2.

3.2 The Inner Detector

The Inner Detector (ID) covers the pseudo-rapidity region of $|\eta| < 2.5$, a ϕ-slice of it is shown in Fig. 3.3. The purpose of the ID is to measure the tracks of charged particles, to identify charged particles (especially electrons) and to find and locate the vertices of the primary interactions as well as the vertices from secondary particle decays, useful for b-physics and τ identification [59]. These tasks are achieved by having a high granularity in the detector,

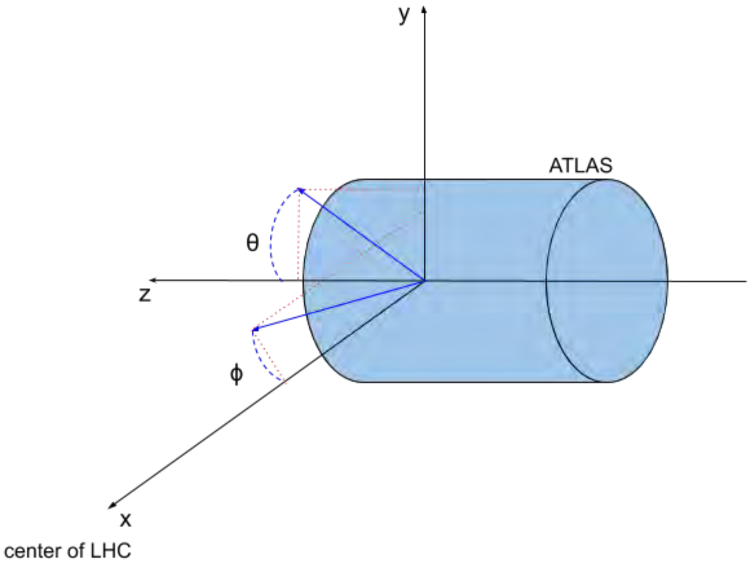

Figure 3.2: Scheme of the ATLAS coordinate system.

especially close to the interaction point, and by providing sufficient redundancy with many detector layers each measuring a track coordinate as shown in Fig. 3.3. The high granularity helps also in discerning different trajectories from each other in the presence of a high density of particles. The track density is very high because of the high luminosity of the LHC. The LHC bunches collide every 25 ns and in each bunch-crossing up to 70 simultaneous inelastic proton collisions take place. If a bunch-crossing is flagged interesting enough to be read out, the interesting collision will thus be accompanied by the tracks from up to 70 other collisions. These tracks are called *pileup* tracks. Since the particles of interest can have hundreds of GeV in momentum, the momentum resolution needs to be very high. On the other hand, the detector must also be able to reconstruct tracks with transverse momenta as low as 500 GeV, and even as low as 200 MeV [59]. To obtain a precise momentum measurement, the ID is immersed in a uniform magnetic field of 2 T in the beam axis direction, provided by a superconducting solenoid encompassing the detector.

The sensors of the ID are of different technologies, but they all register the position of the cloud of ionization electrons and ions created in the sensor material by the passing of a charged particle. It is important that the sensors represent a minimum of material to accomplish this, because any material in the way of the charged particle also produces multiple scattering which reduces the momentum resolution.

The ID is subdivided in three main subdetectors, the Pixel detector, the Semi-Conductor Tracker (SCT) detector and the Transition Radiation Tracker (TRT) detector, see Fig. 3.3. Each subsystem is subdivided in a barrel section, concentric to the beam, and an endcap section, perpendicular to the beam.

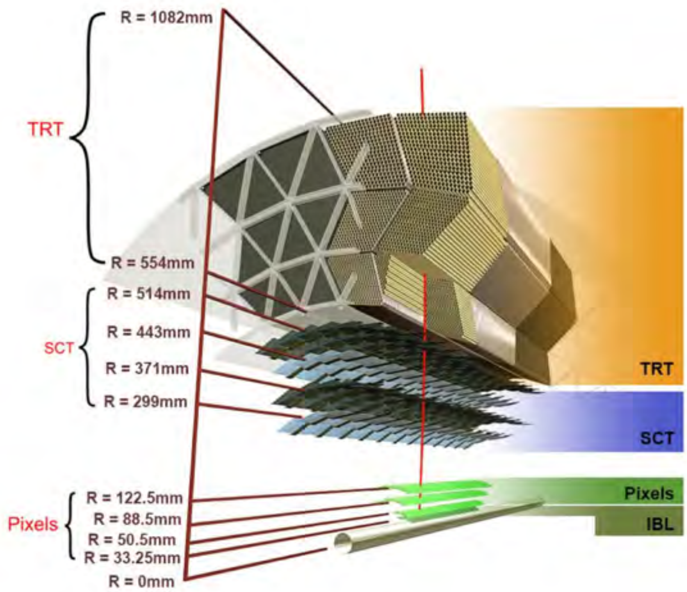

Figure 3.3: Scheme of the ATLAS barrel ID passed by a track, taken from [59].

3.2.1 The Pixel Detector

The Pixel detector is the detector closest to the interaction point and is extremely important for identifying vertices and for precise measurements of tracks. This precision is achieved with a very fine granularity of pixel modules, which are oxigenated semiconductor (Silicon) n-type wafers, which have a nominal size of 50 μm$\times$400 μm and 250 μm in thickness and are arranged in three layers in the barrel and in three disk layers in each endcap, giving 3 high precision points [59, 60]. There are approximately 80 million readout channels in this part of the detector. The resolution in the barrel is of 10 μm in the $R-\phi$ direction ($R-\phi$ is the azimuthal direction) and of 115 μm in the z-direction, the resolution in the endcap is the same in the $R-\phi$ direction and it is 115 μm in the R direction [59].
The Insertable B-Layer, also visible in Fig. 3.3, was introduced first after Run-1 as the innermost layer of the Pixel detector.
Since the pixel modules are so close to the collisions, the distance from the beam to the Insertable B-Layer is just above 3 cm, see Fig. 3.3, the modules were designed to tolerate radiations, though this part of the detector needs to be operated at a lower temperature ($\sim 5^{\circ} - 10^{\circ}$ C), in order to avoid temperature dependent changes induced by the large amount of radiations [59, 60].

3.2.2 The Semi-Conductor Tracker

The SCT consists of 4 cylindric barrel layers and 9 perpendicular endcap disk layers of double-sided p-on-n-type semiconductor (Silicon) strips, that provide

four 3-dimensional points on the track. Since the highest precision is needed in the magnetic bending direction, the strips on one side of the wafer are oriented along the z-axis. In order to also provide a coordinate in the z-direction, the strips on the other side are tilted by a 40 mrad stereo angle. The wafer is 285 μm thick and the strip pitch is approximately 80 mm.
The resolution in the barrel is of 17 μm in the $R - \phi$ direction and of 580 μm in the z-direction, the resolution in the endcap is the same in the $R - \phi$ direction and it is 580 μm in the R direction [59, 61].
There are around 6.3 million readouts from this detector [59, 61]. The detector is operated at a low temperature by the same system that cools the pixel detector, making the operation temperature $\sim 5^{\circ} - 10^{\circ}$ C, again to improve the silicon properties and to minimise radiation damage.

3.2.3 The Transition Radiation Tracker

The TRT in the ATLAS experiment is a tracking gaseous detector, composed of straw tubes. These tubes are 4 mm in diameter and are filled with either Xenon or Argon gas and contain a gold-plated tungsten wire in the middle. There are concentric layers of straws parallel to the beam axis in the barrel and 160 straw planes perpendicular to the beam axis in the endcap, giving in total around $\sim$ 300.000 readout channels [59, 62]. This detector covers a region with $|\eta| < 2$. Each track passes 36 straws at least (this is though not true in the region between the barrel and the endcap) and creates here ionization electrons that drift towards the central wire. At arrival at the 30 μm thin wire, which is placed at a +1530 V potential relative to the straw wall, an ionization avalance provides a gas gain of 25000, thus removing the need for preamplification. The drift-time needed to reach to the wire provides a tracking coordinate in the R-phi direction with a resolution of about 130 μm [59, 62]. The large amount of possible track interaction points allows continuous tracking.
Interspersed between the straw layers are polymer fibers with a refractive index slightly above air. Charged particles with a Lorentz gamma exceeding 10^4 will produce transition radiation X-ray quanta when passing the fibers. Especially the Xenon gas has a high cross section for absorbing such a quantum and produce a large number of ions in the gas. By detecting such large signals, traversing electrons can be distinguished from heavier particles even down to a momentum of 5 GeV.

3.2.4 Inner Detector Tracking

The ionisation signals from the silicon detectors are collected into clusters and converted into very accurate space-points on the tracks traversing the detectors. The measured space-points are used to determine the particle tracks and estimate its p_{T} and their association is performed by a combinatorial Kalman filter. The fit combines seeds (a collection of three space-points) both from the SCT and Pixel detectors (independently and together) to find the most likely particle tracks and it iteratively corrects space-points, splits clusters and it resolves ambiguities in hit assignments while finding the tracks.

Subsequently the fit is carried out with the chosen seeds and further space-points in the Pixel and SCT detectors are included [63]. The tracks that fulfil certain quality criteria are extended into the TRT, where they are associated to 36 driftcircles. The TRT hits associated to the tracks are then included in the final global χ^2 fit of the track parameters, where the extra coordinate information from the TRT are responsible for half of the momentum resolution power at high momenta. Following the inside-out tracking, which has the main goal of finding the tracks of primary particles, a back-tracking is performed, where the tracking algorithms starts from the outmost layer of driftcircles in the TRT and continues inwards. This has the goal of finding mainly secondary particles. [64]

3.3 Calorimetry

After tracking charged particles, both electromagnetically interacting particles and hadrons need to be measured and to this purpose calorimeters are used. Calorimeters are designed to measure the energy of particles by destroying them and stopping them before they go into the muon system. In the ATLAS experiment there are two calorimeters, an electromagnetic and a hadronic calorimeter. These are great to measure the energy of photons, electrons and hadronic particles. The energy resolution of a calorimeter is one of the most important design parameters and it is optimized in order to have high sensitivity in specific analysis channels, as the $H \to \gamma\gamma$. The expression that dictates the resolution of a calorimeter is [59, 65]:

$$\frac{\sigma(E)}{E} = \frac{a}{\sqrt{E}} \oplus \frac{b}{E} \oplus c \tag{3.1}$$

where the resolution is $\sigma(E)/E$, a is a stochastic term that expresses the fluctuations in energy depositions, b is a noise term, which is dictated both by electronic noise and by pileup noise, and c is a constant term that takes eventual calibration inhomogeneities and calibration issues into consideration.
In Fig. 3.4 the calorimeters in the ATLAS experiment are pictured, the electromagnetic calorimeter is closest to the ID, while the hadronic calorimeter is placed right after the electromagnetic calorimeter and they together cover up to $|\eta| < 4.9$.

3.3.1 The Electromagnetic Calorimeter

The purpose of the electromagnetic calorimeter is to precisely measure the energy of electromagnetic interaction particles, in particular of electrons and photons. The granularity of this detector is finer in the region closest to the ID, in order to get good information about the particles, in particular about their pseudorapidity, to measure their energy quite precisely when they disintegrate, to identify electrons and photons and to distinguish photons coming from a π° decay from other photons, as from a $H \to \gamma\gamma$ decay. In the outer part of the detector the granularity is coarser, but still enough to collect the

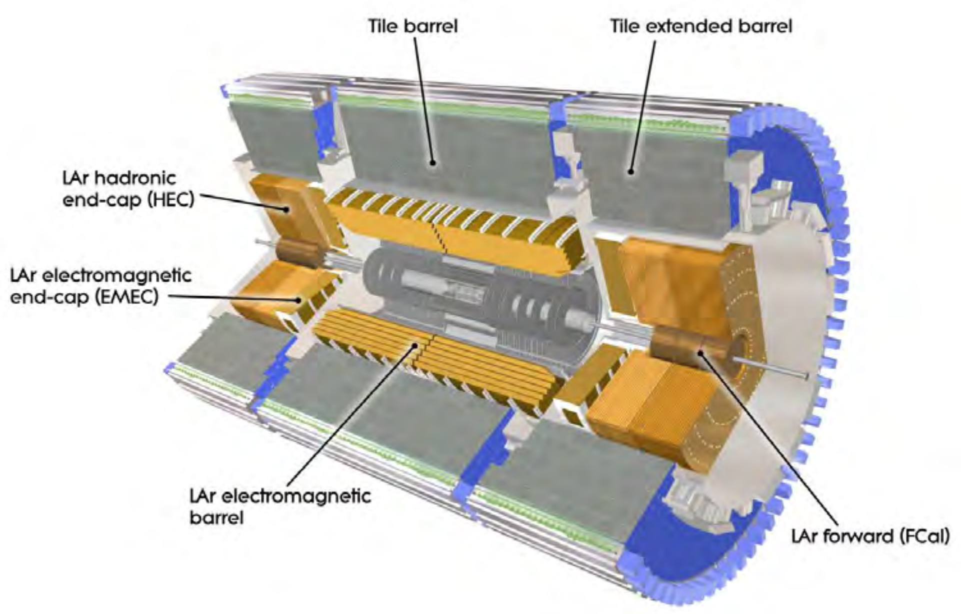

Figure 3.4: Scheme of the ATLAS calorimeter system, taken from [59].

remaining energies and to measure jets from other electromagnetically interacting particles, as π°.
The electromagnetic calorimeter has an $|\eta|$ range up to 3.2 and it is also divided in a barrel and an endcap part, it is made with lead as the passive material and liquid argon as the active material (lead-LAr). An impinging electron or photon on the passive material creates an electromagnetic shower. The ionization electrons created by the shower-electrons in the active material are picked up by accordion shaped copper-on-kapton electrodes whose geometry ensures that there are no cracks at any azimuthal angle, where an incoming particle can escape detection [59, 65]. The choice of LAr was dictated by the linear behaviour of the material, by the stability of its response and by its radiation hardness, while the choice of lead was dictated by the fact that the radiation length of a photon in the lead is very short, permitting to decrease the size the calorimeter. Before the electromagnetic calorimeter a presampler is placed at $0 < |\eta| < 1.8$ in the barrel and at $1.5 < |\eta| < 1.8$ in the endcap, in order to measure the energy of the particles coming right out of the ID and correct the energy measurement for any loss that happened before the calorimeter [59, 65].
The electromagnetic calorimeter is made of three layers in the $0 < |\eta| < 2.5$ region, in order to complement the ID measurement, and of two layers in the $2.5 < |\eta| < 3.2$ region and the granularity of the calorimeter towers changes with the layer, where the first layer has a cell size of $\Delta\eta \times \Delta\phi = 0.0031 \times 0.1$, the second layer of $\Delta\eta \times \Delta\phi = 0.025 \times 0.025$ and the third layer of $\Delta\eta \times \Delta\phi = 0.05 \times 0.025$ [59].
The overall energy resolution of the electromagnetic calorimeter is of $\sigma(E)/E = 10\%/\sqrt{E} \oplus 0.7\%$ [59, 65].

3.3.2 The Hadronic Calorimeter

The point of an hadronic calorimeter is to detect hadrons, in particular the neutral ones that have no momentum measurement in the ID, and in particular jets of hadrons from the fragmentation of high p_{T} partons from a hard scattering process. Hadrons interact with the nuclei through elastic and inelastic scattering and produce jets of particles from these interactions. Together with information gathered from other subsystems, the hadronic calorimeter contributes to the precise measurement of jets and $E_{T,miss}$, which is minus the vector sum of all the measured transverse momenta in the detector.
Since a nuclear interaction length is much larger than a radiation length, the hadronic calorimeter needs to be much deeper than the electromagnetic calorimeter. In fact the ATLAS tile calorimeter (TileCal) (see below) has ≈ 150 cm of steel which is enough to contain 99% of an 100 GeV hadron. Muons, on the other hand, generally sail though both calorimeters depositing only minimum ionizing energy (≈ 2 MeV per gram traversed material).
The hadronic calorimeter system in ATLAS is divided in three different parts with varied materials and designs, in order to adjust its purpose to the different η regions. The first component is the TileCal, placed in the $0 < |\eta| < 1.7$ region; this detector is composed of scintillating tiles with steel as absorbing material. The scintillator tiles are arranged radially and perpendicular to the beam axis, in order to insure almost perfect ϕ coverage [59, 66]. The geometry of the tiles is guided by the desire to have an e/h ratio (electromagnetic vs hadronic response ratio) as close to one as possible. In the nuclear interactions in the calorimeter, fluctuating numbers of charged and neutral hadrons are created, and they dissipate their energy very differently, for example the charged pions via new nuclear interactions and the neutral ones via electromagnetic showers. An e/h ratio of one ensures that the calorimeter response is the same for the two components.
The energy resolution of the tile calorimeter is $\sigma(E)/E = 50\%/\sqrt{E} \oplus 3\%$ [66]. Further in η there is the hadronic endcap calorimeter, HEC, placed at $1.5 < |\eta| < 3.2$, which consists of two wheels per endcap. The HEC also uses copper and LAr as sampling mediums. Finally, furthest in η there is the forward calorimeter, FCal, that spans in the $3.1 < |\eta| < 4.9$ region and is used to ensure full coverage for energy measurements and stops most of the radiations from going into the muon detector using modules of copper and tungsten [59, 65].
The ATLAS experiment focuses on hard reactions between proton constituents and hence the measurement of jets of hadrons from parton fragmentation is an important responsibility of the calorimeters. Since the jets comprise both π^0 and charged hadrons, both the electromagnetic and hadronic calorimeter must be combined for the jet energy measurement. The calorimeters are also used to estimate the amount of energy from pileup tracks that must be subtracted from the jet energy. Finally, the track momenta measured in the ID can be used to refine the jet energy estimate. This estimate is calibrated *in situ*, for example by measuring the jets recoiling from a precisely measured photon or Z boson.

3.4 The Muon Spectrometer

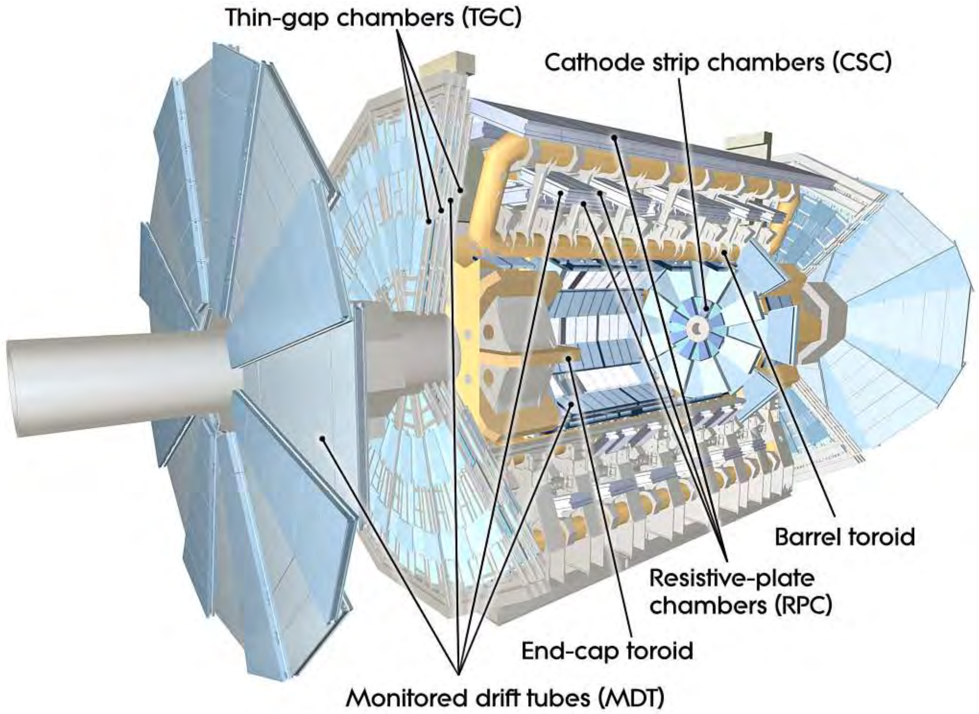

Figure 3.5: Scheme of the ATLAS muon spectrometer, taken from [59].

The last layer of the ATLAS detector is the muon spectrometer, especially designed to measure the tracks of the muons produced in the interactions. Muons are particles that do not interact much with matter and they have a rather long lifetime, which means that they can travel through the inner layers of the ATLAS detector leaving only their own ionization signal in the detector elements. Only very rarely can other charged particles penetrate the calorimeters (called *punch-trough* particles). In order to measure muons precisely, a layer after the hadronic calorimeter has been introduced and thanks to the magnetic field from the toroid magnets, the momentum of the muons can be measured from the track deflection in the plane perpendicular to the magnetic field.
In the $|\eta| < 2.0$ region this detector consists of Monitored Drift Tubes, which are gas filled tubes that permit to measure the passage of a particle thanks to the gas ionization, measured by a tungsten wire in the middle, in the same way as for the TRT straws. The resolution for one tube is of 80 μm [59] (The drift tubes are operated at high pressure and hence the resolution is better than in the TRT). In the higher region of $2.0 < |\eta| < 2.7$ Cathode Strip Chambers are used instead, which are multiwire proportional chambers with cathodes divided in strips, that measure the ionization charge from a passing particle [59]. There are also dedicated trigger chambers with good time resolution to trigger whenever a muon is detected. The trigger chamber in the barrel ($|\eta| < 1.05$) consists of Resistive Plate Chambers and in the endcap ($1.05 < |\eta| < 2.4$) of

this Gap Chambers and they are able to measure two coordinates of a track, η and ϕ, and perform rejection based on the momentum of the muon [59].
The design momentum resolution of the muon spectrometer is of 10% for 1 TeV tracks with the possibility to measure tracks down to 3 GeV, but in order to have this resolution it is crucial that all the parts of the muon spectrometer are correctly aligned (with a 30 μm precision) and the magnetic field calibrated [59].

3.5 The Trigger System

Since we cannot keep all the events generated from the collisions, we need to make quick and informed decisions about which events are most relevant and interesting for physics analysis. This job is done by the Trigger and Data AcQuisition system (TDAQ), which reduces the rate of the events written to tape significantly.
The trigger system is divided into three steps, the Level-1 trigger (L1), the Level-2 trigger (L2) and the event filter. Together the L2 and event filter constitute the High-Level Trigger (HLT) [59, 67]. Each step of the trigger system refines the decision taken from the previous step, before writing the data to storage. The L1 trigger is the first trigger and it finds interesting events containing high p_{T} electrons, muons, jets, photons and τ's or events with a large $E_{T,miss}$ based on information from the muon trigger system and the calorimeter system (both the electromagnetic and the hadronic calorimeters), though with a coarser granularity than the entire system. The decision is taken within 2.5 μs and it reduces the rate to 75 kHz. Since the bunch crossings are every 25 ns and the L1 trigger does not take instantaneous decisions, there is a pipeline of bunch crossings in memory, before a decision is taken. When the L1 trigger has identified the desired events, it computes also regions of interest (RoI), regions in the $\eta - \phi$ planes, where the interesting events have happened. These RoI are fed to the L2 trigger, which uses the information from the entire detector in those regions to select or reject more events. The decision is taken within 40 ms and the rate is brought down to 3.5 kHz. Finally the event selection brings down the rate to 200 Hz by an offline selection that takes 4 s per event and those events are finally written to tape [59, 67].

CHAPTER 4

DATA AND SIMULATION SAMPLES

The analysis is performed with the full dataset collected during the Run 2 period (2015 − 2018) at a center of mass energy of $\sqrt{s} = 13\,\text{TeV}$ in the ATLAS experiment with an integrated luminosity of $139\,\text{fb}^{-1}$. To develop the analysis, Monte Carlo samples were used from the mc16 simulation campaign (with format DAOD_TOPQ1). The mc16 campaign is divided in three sub-campaigns, mc16*a*, mc16*d* and mc16*e*, each used for a different data taking period: mc16*a* simulates the experimental conditions of the 2015 and 2016 period, mc16*d* simulates the experimental conditions of the 2017 period and mc16*e* simulates the experimental conditions of the 2018 data taking period. The three campaigns take into account the different signal and background efficiencies in the three different periods. Each Monte Carlo mc16 sub-campaign is reweighted according to the average number of interactions per crossing (pileup) distribution of the corresponding data taking period, see Fig. 4.1(b). In order to check the stability and the internal consistency of the analysis within each Monte Carlo campaign, the data is subdivided as well into three periods, the first period includes data collected in 2015 and 2016, with an integrated luminosity of 36.2 fb^{-1} (and an uncertainty on the integrated luminosity of 2.1%), the second period includes data collected in 2017 with an integrated luminosity of 44.3 fb^{-1} (and an uncertainty on the integrated lu-

minosity of 2.4%) and the third period includes data collected in 2018 with an integrated luminosity of 59.9 fb^{-1} (and an uncertainty of 2.0% on the integrated luminosity) [68]. The final luminosity of the full Run 2 is 138.9 fb^{-1} with an uncertainty of 1.7% on the integrated luminosity [68]. The quoted luminosities correspond to events included in the "Good Run List" of runs and portions of runs suited for physics analysis [69], see Fig. 4.1(a).
Most of the Monte Carlo samples used for the analysis are simulated using the full ATLAS detector simulation (FullSim), while a few samples, in particular samples used for evaluating systematic uncertainties, are simulated with a faster ATLAS detector simulation, AtlasFast 2 (AFII) [70].
Both the data and Monte Carlo samples were reconstructed using the ATLAS reconstruction software `Athena`, release 21. The reconstructed events in both the data and Monte Carlo samples in DAOD_TOPQ1 format are then processed using the `AnalysisTop` packages, which selects the data and Monte Carlo events needed for the analysis and calculates the efficiencies and scale factors for object working points needed to compare data and Monte Carlo in each sub-period. In particular the data and Monte Carlo samples used here are processed with `AnalysisTop-21.2.65`.
Each event needs to pass the "All Good" requirements included in the Good Run List (GRL), the LAr and Tile working requirements and the primary vertex presence requirements. Once these requirements are passed, the events need to pass at least one of the single lepton trigger chains[1] listed in Table 4.1 with a p_{T} of at least 27 GeV (25 GeV for events from the 2015 data taking year) before they can be used in the analysis.

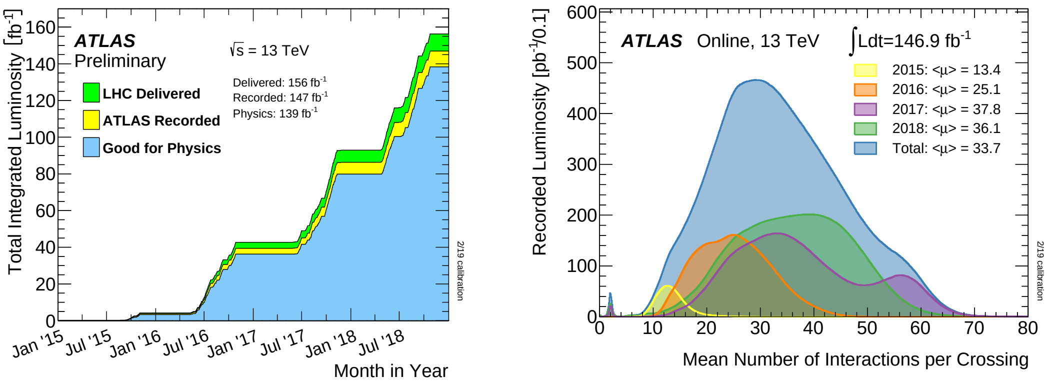

(a) (b)

Figure 4.1: Luminosity collected by ATLAS in Run 2 and number of interactions per crossing in each year of Run 2.

[1]The naming of the triggers is as such HLT refers to the High Level Trigger, eXX or muXX refer to the threshold E_T =XX GeV for electrons and muons respectively, *ltight*, *lhloose* and *lhmedium* refer to the electron identification applied and it can come with modifiers as *nod0*, *ivarmedium*, *iloose* and *ivarloose* refer to the isolation applied, *L1EM20VH* and *L1MU15* refer to the L1 seed used, in case this is not the default one.

Table 4.1: List of trigger chains used for each data taking period during the Run 2.

Year	Electron triggers	Muon triggers	lepton p_T requirement
2015	HLT_e24_lhmedium_L1EM20VH HLT_e120_lhloose HLT_e60_lhmedium	HLT_mu20_iloose_L1MU15 HLT_mu50	25 GeV
2016	HLT_e26_lhtight_nod0_ivarloose HLT_e60_lhmedium_nod0 HLT_e140_lhloose_nod0	HLT_mu26_ivarmedium HLT_mu50	27 GeV
2017	HLT_e26_lhtight_nod0_ivarloose HLT_e60_lhmedium_nod0 HLT_e140_lhloose_nod0	HLT_mu26_ivarmedium HLT_mu50	27 GeV
2018	HLT_e26_lhtight_nod0_ivarloose HLT_e60_lhmedium_nod0 HLT_e140_lhloose_nod0	HLT_mu26_ivarmedium HLT_mu50	27 GeV

4.1 Signal samples

The nominal Monte Carlo $t\bar{t}$ sample used in this analysis is produced with Powheg-Box [71–73] for the matrix elements events with PDF NNPDF3.0 [74] at NLO and Pythia 8 [75, 76] for the underlying event, parton shower and fragmentation and it is simulated with the A14 [77] tune with PDF NNPDF23 at LO [78]. The h_{damp} parameter is set to $1.5 \cdot m_{\text{top}}$ and a dilepton filter is applied to the sample generator, to select only ee, $\mu\mu$ and $e\mu$ events (including events coming from τ decays). The same sample with a non all hadronic filter (including ℓ + jets and dilepton events) instead of the dilepton filter is used to estimate the fake lepton contribution from signal events. After the event simulation, the events are run through a full simulation of the ATLAS detector based on Geant 4 [79]. To estimate the initial state radiation (ISR) systematic uncertainty another Powheg+Pythia 8 sample is used, this time with a higher h_{damp} of $3 \cdot m_{\text{top}}$ and run through the AtlasFast-II detector simulation. This sample is then reweighted with the internal 'var3cup' weight to select a high ISR scenario, while the nominal sample is weighted to the 'var3cdown' weight to select a low ISR scenario [19]. The nominal sample is also used to calculate the PDF systematic uncertainties and the final state radiation (FSR) systematic uncertainty by reweighing it with an internal set of generator weights, similarly as for the low ISR systematic uncertainty. A set of samples with the same set-up as the nominal but with different top masses is generated and used to make stress tests and for the mass estimation, the complete list can be seen in Table 4.2. To estimate the systematic uncertainty coming from the fragmentation model and parton shower settings, an alternative $t\bar{t}$ sample was simulated with Powheg-Box for the underlying simulation with PDF NNPDF3.0, interfaced with Herwig 7 [80] for the fragmentation model and parton shower [19]. The tune used is H7UE [81] and the sample is simulated with $h_{damp} = 1.5 \cdot m_{\text{top}}$. The detector simulation of the events is performed with the AtlasFast-II [82] package, that uses parametrized shower shapes in the calorimeters to speed up the detector response simulation process. To calculate the systematic uncertainty related to hard scattering, a sample simulated with

MadGraph5_aMC@NLO [83] interfaced with Pythia 8 with the A14 tune is generated and run through the AtlasFast-II detector simulation [19].
A detailed list of signal samples and their DSIDs can be seen in Table 4.2. A detailed list of each sample cross section, k-factor and filter efficiency is listed in Appendix A in Table 1 and Table 2.

4.2 Background samples

The major background in this analysis comes from the single top Wt channel and the samples (one for the Wt and one for the $W\bar{t}$ channel) used to describe it are produced with Powheg-Box with PDF NNPDF3.0 at NLO and $h_{damp} = 1.5 \cdot m_{\text{top}}$ interfaced with Pythia 8 with the A14 tune and PDF NNPDF2.3 at LO and with a dilepton filter. The interference between the $t\bar{t}$ and Wt is modelled using the diagram removal scheme [46, 84]. The samples are run through the full ATLAS simulation. The same samples, produced with the non all hadronic filter, is used for the fake lepton background estimation. To estimate the systematic uncertainties coming from the modelling of the interference between $t\bar{t}$ and Wt an alternative set of samples with the same setup as the nominal Wt samples is used, where the interference is modelled with the diagram subtraction scheme instead [46]. To estimate the fragmentation systematic uncertainty in the single top background, samples produced with Powheg-Box for the underlying simulation with PDF NNPDF3.0, interfaced with Herwig 7 [80] for the fragmentation model and parton shower are used. The tune used is H7UE [81] and the sample is simulated with $h_{damp} = 1.5 \cdot m_{\text{top}}$. To estimate the hard scattering systematic uncertainty a sample simulated with MadGraph5_aMC@NLO [83] interfaced with Pythia 8 with the A14 tune is generated. Both the sample for the hard scattering and for the fragmentation uncertainty are simulated with a dilepton filter and are run through the AtlasFast-II detector simulation. A set of samples with the same set-up as the nominal Powheg+Pythia 8 Wt samples with dilepton filter but with varied top masses is generated and used to estimate the top mass uncertainty on the cross section. A minor contribution to the single top background comes from the t-channel, which is simulated with Powheg with PDF NNPDF3.04f at NLO interfaced with Pythia 8 with the A14 tune and PDF NNPDF2.3 at LO.
The background generated from diboson events (WW, WZ and ZZ) is simulated using Sherpa v. 2.2.2 with PDF NNPDF3.0 at NNLO and run through the ATLAS full simulation. Three diboson samples are included for processes where two gluons produce four leptons via intermediate vector bosons [85]. Diboson samples generated with Sherpa v. 2.2.1 with PDF NNPDF3.0 at NNLO are used to include final states where one of the leptons is misidentified.
Another background contribution comes from the Z boson decaying to two τ, which then decay to an e and a μ, and jets. Those samples are simulated with Sherpa v. 2.2.1 with PDF NNPDF3.0 at NNLO in p_{T} slices of the Z boson and run through the full ATLAS simulation. Additional $Z \to ee$ + jets and $Z \to \mu\mu$ + jets samples are used to extract a factor to scale the $Z \to \tau\tau$ +

jets background to data, see Section 6.2. To compare the Z + jets modelling, alternative Z + jets samples are generated with POWHEG + PYTHIA 8.
The background coming from $t\bar{t}V$ are described by samples simulated with MADGRAPH + aMC@NLO interfaced with PYTHIA 8 with the A14 tune and PDF NNPDF2.3 at LO and run through the full ATLAS simulation. The background coming from $t\bar{t}H$ is also included and is simulated with MADGRAPH + aMC@NLO and with the AtlasFast-II simulation software.
The fake lepton background is estimated with the samples used for constructing both signal and background ($t\bar{t}$ and single top both leptonic and semileptonic decays, diboson, $Z \to \tau\tau$ + jets, $t\bar{t}V$, $t\bar{t}WW$, $t\bar{t}\gamma$ and $t\bar{t}H$) as well as W+ jets samples (simulated with SHERPA v.2.2.1 with with PDF NNPDF3.0 at NNLO and with the ATLAS Full Simulation) and it is evaluated using the same sign eμ events with a combination of simulation and data. For more information on the estimation of the fake lepton background, see Section 6.1.

4.3 Error in MadGraph5_aMC@NLO samples

Some of the samples simulated with MADGRAPH5_aMC@NLO + PYTHIA 8 were simulated with the wrong W branching fractions, in particular, $BR(W \to ud)$ and $BR(W \to cs)$ were set to 33.37% instead of the correct 33.77%. This means that the total branching fraction in those simulation samples was not one, but somewhat below (0.992) and this affected the production of all decay channels. In the $t\bar{t}$ MADGRAPH5_aMC@NLO + PYTHIA 8 sample, which contains only dilepton events, this can be seen because of a slightly higher filter efficiency than other $t\bar{t}$ samples (0.107 compared to 0.105, see Appendix A). Since this sample contains only dilepton events, a correction factor of 0.984 (0.992^2) can be applied to correct the filter efficiency. The same error is present in the $t\bar{t}W$ sample, but since all decay channels are simulated within the same sample, there is no easy fix, as a correction factor would have to be applied per event. In the analysis presented here, no correction was applied to the $t\bar{t}W$ sample.

Table 4.2: List of DSID for the TOPQ1 Monte Carlo samples used in this analysis.

Process	DSID	Generator, parton shower, simulation	PDF
$t\bar{t}$ (nominal, PP8, dilepton)	410472	Powheg + Pythia 8, $hdamp = 1.5 * m_{\mathrm{top}}$, FullSim	NNPDF3.0 NLO
$t\bar{t}$ (nominal, PP8, non all hadronic)	410470	Powheg + Pythia 8, $hdamp = 1.5 * m_{\mathrm{top}}$, FullSim	NNPDF3.0 NLO
$t\bar{t}$ (PP8, higher $hdamp$, dilepton)	410482	Powheg + Pythia 8, $hdamp = 3.0 * m_{\mathrm{top}}$, AFII	NNPDF3.0 NLO
$t\bar{t}$ (PH7, dilepton)	410558	Powheg + Herwig 7, $hdamp = 1.5 * m_{\mathrm{top}}$, AFII	NNPDF3.0 NLO
$t\bar{t}$ (MCatNLO, dilepton)	410465	MadGraph5_aMC@NLO + Pythia 8, AFII	
$t\bar{t}$ (PP8, $m_{\mathrm{top}} = 169$GeV, dilepton)	411052	Powheg + Pythia 8, $hdamp = 1.5 * m_{\mathrm{top}}$, AFII	NNPDF3.0 NLO
$t\bar{t}$ (PP8, $m_{\mathrm{top}} = 171$GeV, dilepton)	411053	Powheg + Pythia 8, $hdamp = 1.5 * m_{\mathrm{top}}$, AFII	NNPDF3.0 NLO
$t\bar{t}$ (PP8, $m_{\mathrm{top}} = 172$GeV, dilepton)	411054	Powheg + Pythia 8, $hdamp = 1.5 * m_{\mathrm{top}}$, AFII	NNPDF3.0 NLO
$t\bar{t}$ (PP8, $m_{\mathrm{top}} = 172.25$GeV, dilepton)	411055	Powheg + Pythia 8, $hdamp = 1.5 * m_{\mathrm{top}}$, AFII	NNPDF3.0 NLO
$t\bar{t}$ (PP8, $m_{\mathrm{top}} = 172.75$GeV, dilepton)	411056	Powheg + Pythia 8, $hdamp = 1.5 * m_{\mathrm{top}}$, AFII	NNPDF3.0 NLO
$t\bar{t}$ (PP8, $m_{\mathrm{top}} = 173$GeV, dilepton)	411057	Powheg + Pythia 8, $hdamp = 1.5 * m_{\mathrm{top}}$, AFII	NNPDF3.0 NLO
$t\bar{t}$ (PP8, $m_{\mathrm{top}} = 174$GeV, dilepton)	411058	Powheg + Pythia 8, $hdamp = 1.5 * m_{\mathrm{top}}$, AFII	NNPDF3.0 NLO
$t\bar{t}$ (PP8, $m_{\mathrm{top}} = 176$GeV, dilepton)	411059	Powheg + Pythia 8, $hdamp = 1.5 * m_{\mathrm{top}}$, AFII	NNPDF3.0 NLO
single top Wt (top, DR, dilepton)	410648	Powheg + Pythia 8, $hdamp = 1.5 * m_{\mathrm{top}}$, FullSim	NNPDF3.0 NLO
single top Wt (antitop, DR, dilepton)	410649	Powheg + Pythia 8, $hdamp = 1.5 * m_{\mathrm{top}}$, FullSim	NNPDF3.0 NLO
single top Wt (top, DR, non all hadronic)	410646	Powheg + Pythia 8, $hdamp = 1.5 * m_{\mathrm{top}}$, FullSim	NNPDF3.0 NLO
single top Wt (antitop, DR, non all hadronic)	410647	Powheg + Pythia 8, $hdamp = 1.5 * m_{\mathrm{top}}$, FullSim	NNPDF3.0 NLO
single top Wt (top, DS, dilepton)	410656	Powheg + Pythia 8, $hdamp = 1.5 * m_{\mathrm{top}}$, FullSim	NNPDF3.0 NLO
single top Wt (antitip, DS, dilepton)	410657	Powheg + Pythia 8, $hdamp = 1.5 * m_{\mathrm{top}}$, FullSim	NNPDF3.0 NLO
single top Wt (top, DR, dilepton)	411038	Powheg + Herwig 7, $hdamp = 1.5 * m_{\mathrm{top}}$, AFII	NNPDF3.0 NLO
single top Wt (antitop, DR, dilepton)	411039	Powheg + Herwig 7, $hdamp = 1.5 * m_{\mathrm{top}}$, AFII	NNPDF3.0 NLO
single top Wt (top+antitop, DR, dilepton)	412003	MadGraph5_aMC@NLO + Pythia 8, AFII	
single top Wt (top, antitop, DR, $m_{\mathrm{top}} = 169$GeV, dilepton)	411107, 411108	Powheg + Pythia 8, $hdamp = 1.5 * m_{\mathrm{top}}$, AFII	NNPDF3.0 NLO
single top Wt (top, antitop, DR, $m_{\mathrm{top}} = 171$GeV, dilepton)	411109, 411110	Powheg + Pythia 8, $hdamp = 1.5 * m_{\mathrm{top}}$, AFII	NNPDF3.0 NLO
single top Wt (top, antitop, DR, $m_{\mathrm{top}} = 172$GeV, dilepton)	411111, 411112	Powheg + Pythia 8, $hdamp = 1.5 * m_{\mathrm{top}}$, AFII	NNPDF3.0 NLO
single top Wt (top, antitop, DR, $m_{\mathrm{top}} = 172.25$GeV, dilepton)	411113, 411114	Powheg + Pythia 8, $hdamp = 1.5 * m_{\mathrm{top}}$, AFII	NNPDF3.0 NLO
single top Wt (top, antitop, DR, $m_{\mathrm{top}} = 172.75$GeV, dilepton)	411115, 411116	Powheg + Pythia 8, $hdamp = 1.5 * m_{\mathrm{top}}$, AFII	NNPDF3.0 NLO
single top Wt (top, antitop, DR, $m_{\mathrm{top}} = 173$GeV, dilepton)	411117, 411118	Powheg + Pythia 8, $hdamp = 1.5 * m_{\mathrm{top}}$, AFII	NNPDF3.0 NLO
single top Wt (top, antitop, DR, $m_{\mathrm{top}} = 174$GeV, dilepton)	411119, 411120	Powheg + Pythia 8, $hdamp = 1.5 * m_{\mathrm{top}}$, AFII	NNPDF3.0 NLO
single top Wt (top, antitop, DR, $m_{\mathrm{top}} = 176$GeV, dilepton)	411121, 411122	Powheg + Pythia 8, $hdamp = 1.5 * m_{\mathrm{top}}$, AFII	NNPDF3.0 NLO
single top $t-$channel (top)	410658	Powheg + Pythia 8, FullSim	NNPDF3.04f NLO
single top $t-$channel (antitop)	410659	Powheg + Pythia 8, FullSim	NNPDF3.04f NLO
W+jets	364156 - 364197	Sherpa 2.2.1, FullSim	NNPDF3.0 NNLO
Z+jets	364100 - 364141	Sherpa 2.2.1, FullSim	NNPDF3.0 NNLO
Z+jets (10 GeV < $M(\ell\ell)$ < 40 GeV)	364198 - 364215	Sherpa 2.2.1, FullSim	NNPDF3.0 NNLO
Z+jets	361106 - 361108	Powheg + Pythia 8 , FullSim	
Diboson $W\ W$, $W\ Z$, $Z\ Z \to \ell\ell\ell\ell$	364250	Sherpa 2.2.2, FullSim	NNPDF3.0 NNLO
Diboson $W\ W$, $W\ Z$, $Z\ Z \to \ell\ell\ell\nu$	364253	Sherpa 2.2.2, FullSim	NNPDF3.0 NNLO
Diboson $W\ W$, $W\ Z$, $Z\ Z \to \ell\ell\nu\nu$	364254	Sherpa 2.2.2, FullSim	NNPDF3.0 NNLO
Diboson $W\ W$, $W\ Z$, $Z\ Z \to \ell\nu\nu\nu$	364255	Sherpa 2.2.2, FullSim	NNPDF3.0 NNLO
Diboson $W\ W$, $W\ Z$, $Z\ Z \to \ell\ell\ell\ell jj$, EW	364283	Sherpa 2.2.2, FullSim	NNPDF3.0 NNLO
Diboson $W\ W$, $W\ Z$, $Z\ Z \to \ell\ell\ell\nu$ jj, EW	364284	Sherpa 2.2.2, FullSim	NNPDF3.0 NNLO
Diboson $W\ W$, $W\ Z$, $Z\ Z \to \ell\ell\nu\nu jj$, EW, OS	364285	Sherpa 2.2.2, FullSim	NNPDF3.0 NNLO
Diboson $W\ W$, $W\ Z$, $Z\ Z \to \ell\ell\nu\nu jj$, EW, SS	364287	Sherpa 2.2.2, FullSim	NNPDF3.0 NNLO
Diboson $W\ W$, $W\ Z$, $Z\ Z \to \ell\ell\ell\ell$, low $M(\ell\ell)$ and p_{T}	364288	Sherpa 2.2.2, FullSim	NNPDF3.0 NNLO
Diboson $W\ W$, $W\ Z$, $Z\ Z \to \ell\ell\ell\nu$, low $M(\ell\ell)$ and p_{T}	364289	Sherpa 2.2.2, FullSim	NNPDF3.0 NNLO
Diboson $W\ W$, $W\ Z$, $Z\ Z \to \ell\ell\nu\nu$, low $M(\ell\ell)$ and p_{T}	364290	Sherpa 2.2.2, FullSim	NNPDF3.0 NNLO
Diboson $W\ W$, $W\ Z$, $Z\ Z \to gg\ell\ell\ell\ell$, $M(\ell\ell\ell\ell) < 130$	345705	Sherpa 2.2.2 + OpenLoops, FullSim	NNPDF3.0 NNLO
Diboson $W\ W$, $W\ Z$, $Z\ Z \to gg\ell\ell\ell\ell$, $M(\ell\ell\ell\ell) > 130$	345706	Sherpa 2.2.2 + OpenLoops, AFII	NNPDF3.0 NNLO
Diboson $W\ W$, $W\ Z$, $Z\ Z \to gg\ell\ell\nu\nu ZZ$	345723	Sherpa 2.2.2 + OpenLoops, FullSim	NNPDF3.0 NNLO
Diboson $Z \to qq\ Z \to \nu\nu$	363355	Sherpa 2.2.1, FullSim	NNPDF3.0 NNLO
Diboson $Z \to qq\ Z \to \ell\ell$	363356	Sherpa 2.2.1, FullSim	NNPDF3.0 NNLO
Diboson $W \to qq\ Z \to \nu\nu$	363357	Sherpa 2.2.1, FullSim	NNPDF3.0 NNLO
Diboson $W \to qq\ Z \to \ell\ell$	363358	Sherpa 2.2.1, FullSim	NNPDF3.0 NNLO
Diboson $W^{+} \to qq\ W^{-} \to \ell\nu$	363359	Sherpa 2.2.1, FullSim	NNPDF3.0 NNLO
Diboson $W^{+} \to \ell\nu\ W^{-} \to qq$	363360	Sherpa 2.2.1, FullSim	NNPDF3.0 NNLO
Diboson $W \to \ell\nu\ Z \to qq$	363389	Sherpa 2.2.1, FullSim	NNPDF3.0 NNLO
Diboson $\nu\nu\nu\nu$	363394	Sherpa 2.2.1, FullSim	NNPDF3.0 NNLO
$t\bar{t}\ W$	410155	MadGraph + aMC@NLO + Pythia 8, FullSim	
$t\bar{t}\ Z\ \nu\bar{\nu}$	410156	MadGraph + aMC@NLO + Pythia 8, FullSim	
$t\bar{t}\ Z\ q\bar{q}$	410157	MadGraph + aMC@NLO + Pythia 8, FullSim	
$t\bar{t}\ e^{+}e^{-}$	410218	MadGraph + aMC@NLO + Pythia 8, FullSim	
$t\bar{t}\ \mu^{+}\mu^{-}$	410219	MadGraph + aMC@NLO + Pythia 8, FullSim	
$t\bar{t}\ \tau^{+}\tau^{-}$	410220	MadGraph + aMC@NLO + Pythia 8, FullSim	
$t\bar{t}$ H	345940	MadGraph + aMC@NLO, AFII	

CHAPTER 5

OBJECT AND EVENT SELECTION

5.1 Object identification

The objects selected in this analysis, as muons, electrons, jets and *b*-jets, are the default objects selected using `AnalysisTop-21.2.65`. The objects collected in these containers need to pass certain requirements before being taken into consideration for further analysis.

5.1.1 Electrons

Electrons are identified in the ATLAS detector using both tracking information from the inner detector and energy deposits in the electromagnetic calorimeter [86]. The electrons required in this analysis need to pass the reconstruction identification 'TightLH' quality requirements. The reconstruction identification combines a series of tracking and calorimetric variables to reconstruct the electron off-line and to identify it as an electron. The 'TightLH' requirement selects a high purity electron sample [86]. In particular each reconstructed electron needs to come from a primary interaction vertex, which is ensured by requiring $|d_0/\sigma_{d_0}| < 5$ and $|\Delta z_0 sin\theta| < 0.5$ mm, where $|d_0/\sigma_{d_0}|$ is the significance of the distance of closest approach from the track to the beam-line, while the z_0 coordinate is the distance from d_0 to the beam axis (point of closest approach) and θ is the polar angle of the track [86]. Each electron is required to fulfil the 'Gradient' isolation requirements (the tight version), in order to minimize the amount of non-prompt electrons in the selected events by requiring that the total energy of particles measured in the vicinity of the electron does not exceed a certain fraction of the electron energy [86]. The isolation requirement allows 90% of the electrons with $p_{\mathrm{T}} > 25$ GeV to pass. To avoid double counting, overlap removal is applied first between electrons and muons that share a track (the electron is thrown away if the two objects have a shared track), then between electrons and jets, removing jets within $\Delta R < 0.2$ from an electron, and afterwards, electrons that find themselves in a $\Delta R < 0.4$ from remaining jets are removed. Finally, each electron needs to have a p_{T} of at least 25 GeV and needs to be in a η region of $|\eta| < 2.5$ with exclusion of the transition region in $1.37 < |\eta| < 1.52$ between the barrel and endcap calorimeters.

5.1.2 Muons

Muons are identified in the ATLAS detector using the tracking information from the muon detector and the inner detector. The muons required in this analysis need to pass the reconstruction identification 'Medium' quality requirements, that reduces the fake muon rate to a few per mille. As well as the electrons, muons are required to come from a primary vertex, which is ensured by requesting that $d_0/\sigma_{d_0} < 3$ and $\Delta z_0 sin\theta < 0.5$ mm. Each muon is also required to fulfil the 'Gradient' isolation requirement [87]. An overlap removal procedure starts with removing electron candidates that share a track with a muon candidate. Then jets that are within $\Delta R < 0.2$ from a muon candidate are removed, and finally muons within $\Delta R < 0.4$ from any remaining jet are discarded. Just as for electrons, muons must have a minimum p_{T} of 25 GeV and an $|\eta|$ fiducial acceptance of $|\eta| < 2.5$.

5.1.3 Jets

Jets are reconstructed from energy deposits in the electromagnetic and hadronic calorimeter using the anti-k_T algorithm [88] with a radius of $R = 0.4$. The constituents of the jets are connected energy deposits in calorimeter cells, called topological clusters. These clusters are calibrated to the electromagnetic scale, meaning that the cluster energy is the expectation value of the energy of an electron, given the measured signals in the cells. After the reconstruction of the jet, its energy is recalibrated to the jet energy scale (JES), meaning the energy of the matching jet reconstructed from truth particle constituents [89, 90]. In order to minimize the number of jets coming from pileup collisions, a further requirement applied is that jets with a p_{T} lower than 120 GeV and

$|\eta| < 2.4$ have to come from a primary vertex. A primary vertex is defined as the reconstructed vertex with the highest summed p_T of the participating charged tracks. We reduce the number of jets from pileup vertices by requiring the fraction of the charged tracks in the jet being associated with the primary vertex (JVT) to be larger than 0.59 ('Medium' working point) [91]. The JVT cut is also applied for jets with a p_T lower than 120 GeV and $2.4 < |\eta| < 2.5$ where the JVT threshold is 0.11 instead (also part of the 'Medium' working point). Finally events with jets coming from other sources than collisions are rejected (LooseBad). Finally, the reconstructed jets are required to have a p_T exceeding 25 GeV and $|\eta| < 2.5$.

5.1.4 b-jets

To assess whether a jet comes from a $b-$hadron, the MV2c10 algorithm is used. This algorithm takes a series of jet and track observables, all sensitive to $b-$ and $c-$hadron lifetime, and returns a variable, used to choose the efficiency working point [92]. In this analysis we have chosen a 70% working point, which means that the efficiency for retaining b-jets is 70% in nominal $t\bar{t}$ Monte Carlo events integrated over p_T [92, 93]. In this case the MV2c10 output variable needs to be greater than 0.83 for the jet to be tagged as a b-jet.

5.1.5 Particle level electrons and muons

Particle level electrons and muons are stable particles after parton shower, but they have not gone through the ATLAS detector simulation. Their 4-momentum is dressed with the 4-momentum of photons in a $\Delta R = 0.1$ cone [94]. They are chosen in a fiducial region of $p_T > 25$ GeV and $|\eta| < 2.5$.

5.2 Event selection

Before taking an event and its objects into consideration, the event has to pass first the "Good Run List", then the calorimeter had to work properly during data taking of this event, there needs to be at least one primary vertex in the event and at least one of the leptons needs to be trigger-matched (the list of triggers used for the different data taking years can be found in Table 4.1). Of the events that pass these requirements, the events used for this analysis are the ones containing exactly one electron and one muon with a p_T of at least 25 GeV each. These events are then categorised as same sign (SS) or opposite sign (OS) events, depending on the relative charge of one lepton to the other one, and for each category, further two subsamples are created, one where the events have one associated b-jet and the other where the events have two associated b-jets. The event count for the full Run 2 dataset is presented in Table 5.1, where N_1 is the number of $e\mu$ events with one b-jet, N_2 is the number of $e\mu$ events with two b-jets and $N_{e\mu}$ is number of all $e\mu$ events (without any b-jet requirement). The Monte Carlo contribution has been normalised to the same integrated luminosity as the data and corrected with the appropriate lepton, pileup, b-tagging and JVT scale factors. The misidentified lepton background is derived using the technique explained in Section 6.1 and

the event count of the Z + jets background is evaluated using the technique explained in Section 6.2. The number of events for different b-jet multiplicities can also be seen in Fig. 5.1.
The kinematic variables derived with the selected $e\mu$ events with either one or two b-jets are shown in Fig. 5.2, 5.3, 5.4, 5.5. In all these figures, but for the η and $\Delta\phi$ distributions, the last bin contains the overflow events. In all distributions the grey shaded area both in the histogram and in the ratio plot is an uncertainty band that contains the detector, background and luminosity uncertainties, but not the $t\bar{t}$ modelling uncertainties. Some of the alternative $t\bar{t}$ samples are also plotted, such as the hard scattering sample simulated with MadGraph5_aMC@NLO + Pythia 8, the fragmentation sample simulated with Powheg + Herwig 7 and the nominal sample (or the nominal with a higher h_{damp}) with more or less initial state radiation.
The backgrounds included in the figures are the ones from Wt and t-channel single top events in blue, from diboson events in green, from $Z \rightarrow \tau\tau$ + jets events in purple, from misidentified leptons in light blue and from $t\bar{t}V$ and $t\bar{t}H$ events in orange and brown respectively.
The ratio plots show the data/MC ratio for the nominal $t\bar{t}$ Powheg+Pythia 8 plus background in black points and the data/MC ratio for the alternative $t\bar{t}$ samples plus background in the same colours as for the plot above.

Table 5.1: Event counts for the full Run 2 dataset

	OS			SS		
Run 2	N_1	N_2	$N_{e\mu}$	N_1	N_2	$N_{e\mu}$
$t\bar{t}$	387770	217955	782959	0.7	0.1	1.3
Single top	39763.8	6774.2	75717.8	0	0	0.7
Z + jets	1427.3	88.1	82769.4	0	0	0
Diboson	1494.8	52.7	96416.1	246.2	10.9	9059.1
mis-ID leptons	4547.32	1877.5	24886.7	3120.4	1172.9	8616.9
$t\bar{t}V$ + $t\bar{t}H$	1122.1	744.9	2520.17	389.2	221.5	801.9
Total	436125	227492	1.06527e+06	3756.6	1405.5	18479.8
Data	439090	232610	1.07995e+06	3760	1418	25821
Data/MC	1.007	1.02	1.01	1.001	1.009	1.4

From Fig. 5.1 it is seen, that in the $e\mu$ OS region, the data/Monte Carlo agreement is good, while in the SS region, the agreement is good, except in the first bin, for the $e\mu$ events with zero associated b-jets. This is caused by Monte Carlo mismodelling of some of the contributions, where the diboson one is the biggest, due to uncertainties in the modelling of the diboson signal with additional jets, also seen in [14]. In the rest of the kinematic variables in Fig. 5.2 and 5.4 the mismodelling of the lepton p_{T} is clear, and it comes from the mismodelling of the p_{T} of the top quark by the current Monte Carlo generators due to missing NNLO QCD effects in $t\bar{t}$ pair production [19, 20, 95].

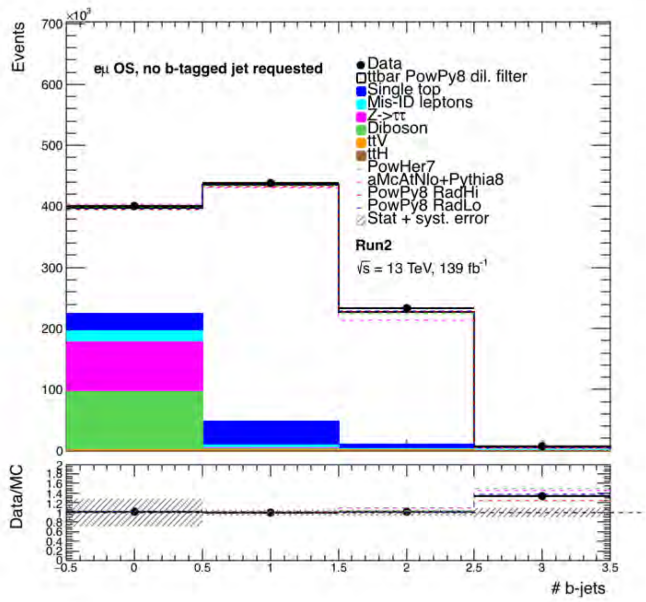

(a)

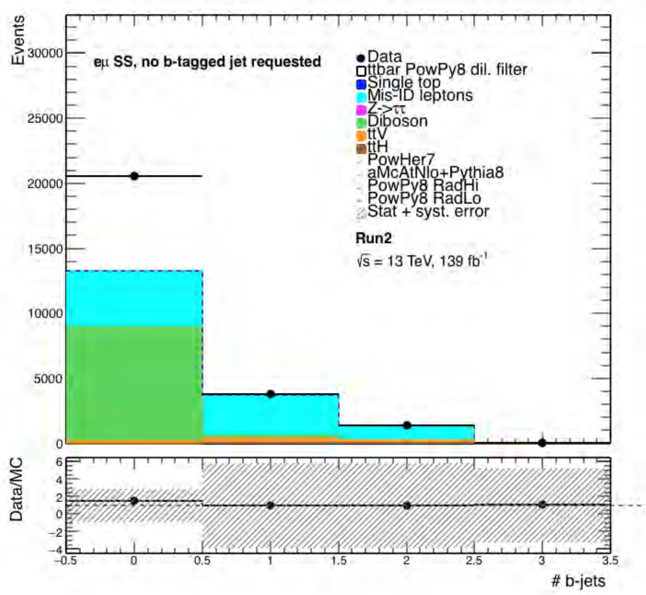

(b)

Figure 5.1: Event count for different b-jet multiplicities in the $e\mu$ OS and SS regions. The uncertainty band contains the statistical uncertainty and all the experimental and background uncertainties, but no $t\bar{t}$ uncertainties. The blue background comes from single top (Wt and t-channel), the light blue from the misidentified leptons, the purple from the $Z \to \tau\tau$ + jets, the green from diboson events, the orange from $t\bar{t}V$ and the brown from $t\bar{t}H$. Alternative $t\bar{t}$ samples are plotted as well, as the POWHEG-BOX + HERWIG 7 sample, the MADGRAPH5_aMC@NLO + PYTHIA 8 sample and the POWHEG + PYTHIA 8 with more or less ISR. The lower plot shows the ratio between the data count and the predicted counts from Monte Carlo.

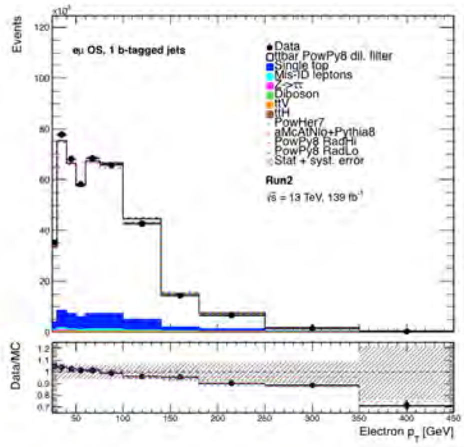

(a)

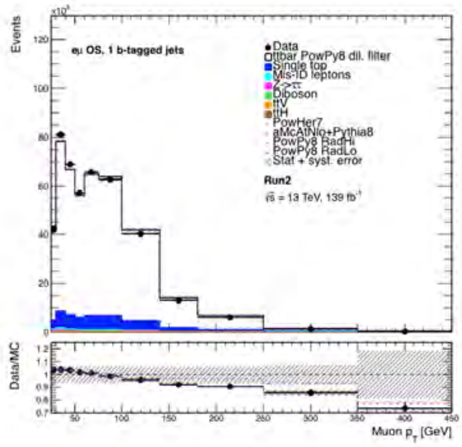

(b)

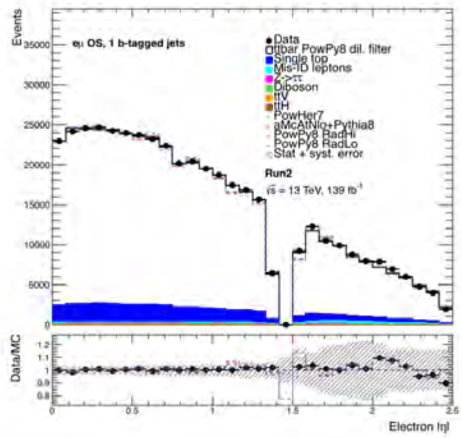

(c)

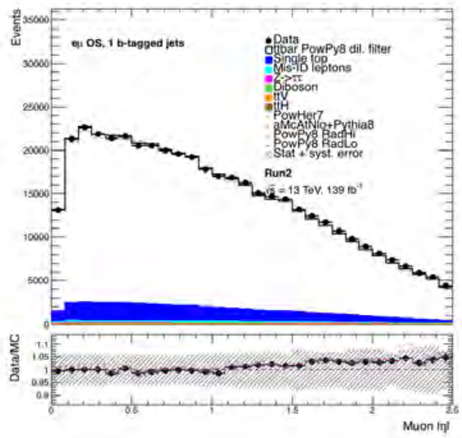

(d)

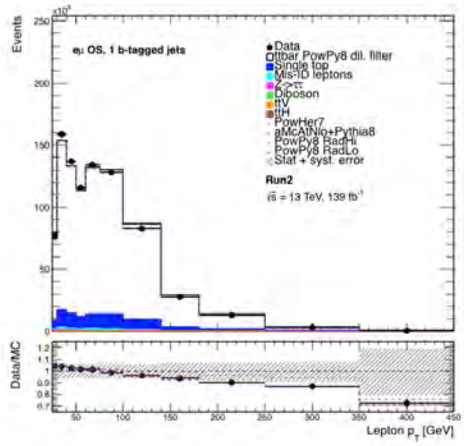

(e)

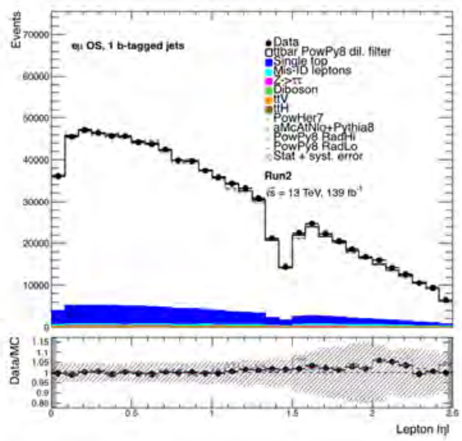

(f)

Figure 5.2: Kinematic variables for $e\mu$ events with one b-jet.

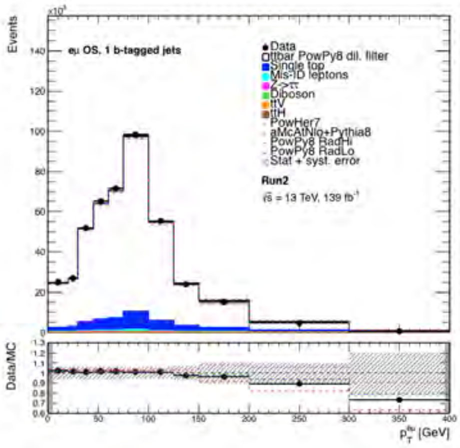

(a)

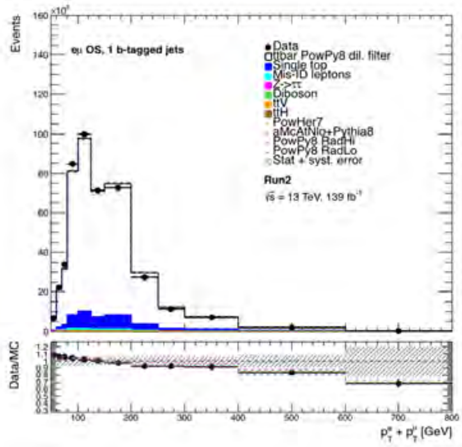

(b)

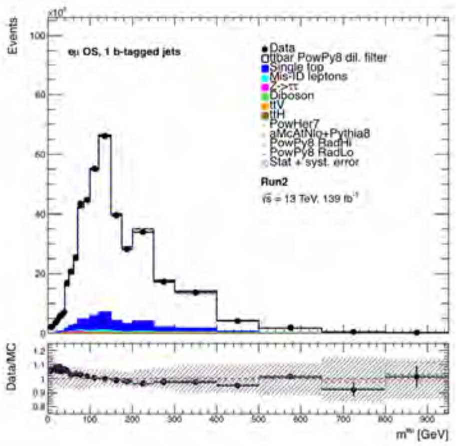

(c)

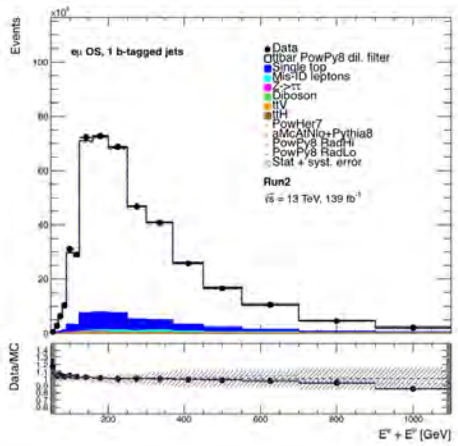

(d)

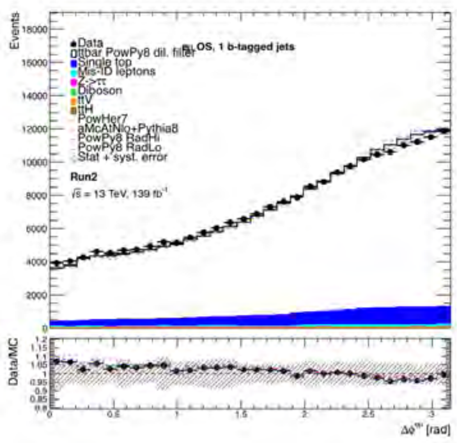

(e)

Figure 5.3: Kinematic variables for $e\mu$ events with one b-jet.

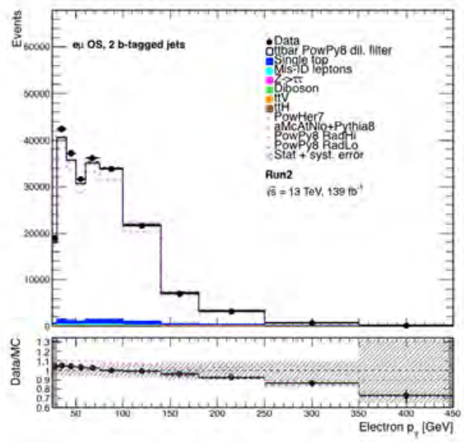

(a)

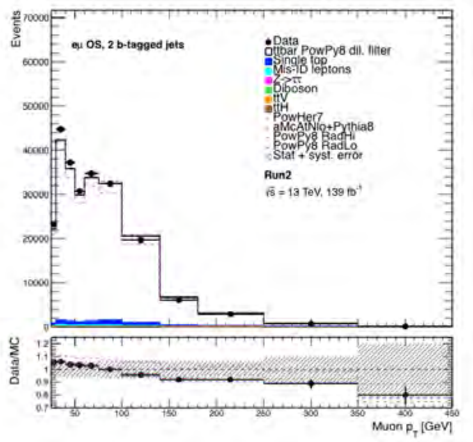

(b)

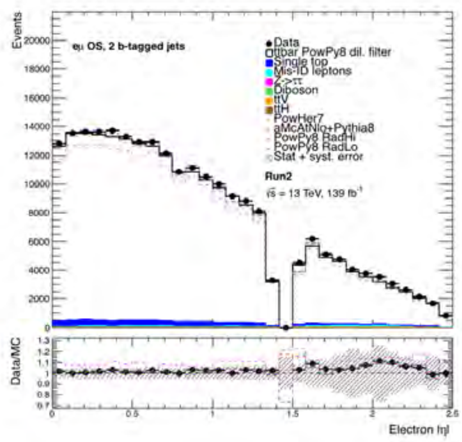

(c)

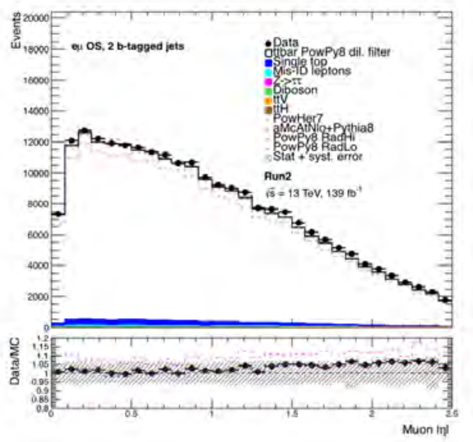

(d)

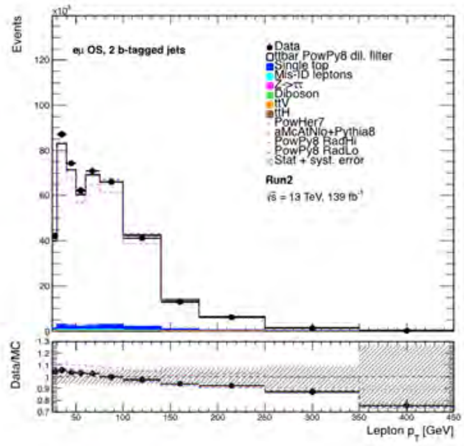

(e)

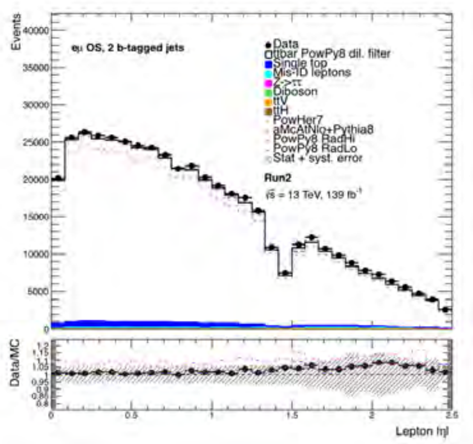

(f)

Figure 5.4: Kinematic variables for $e\mu$ events with two b-jets.

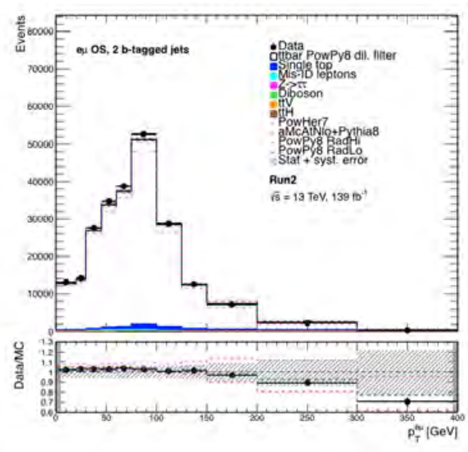

(a)

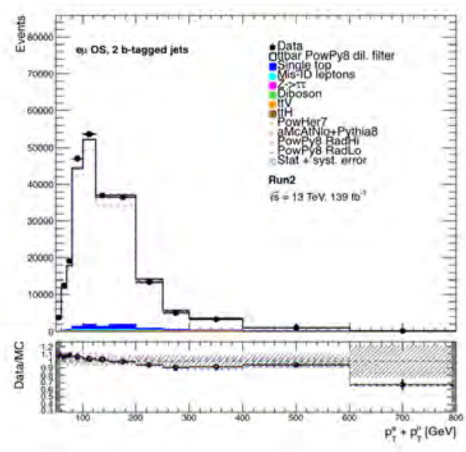

(b)

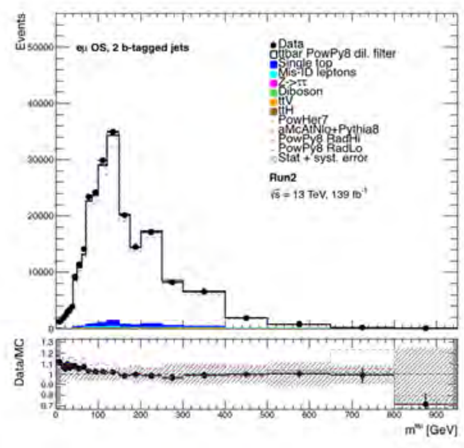

(c)

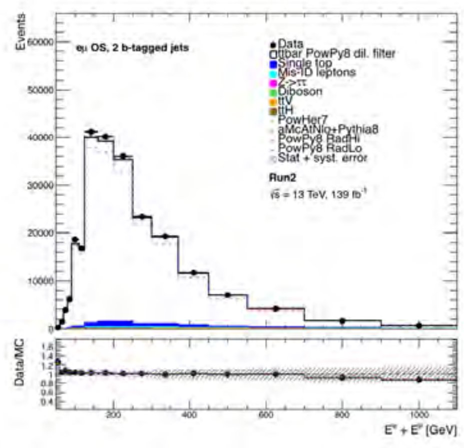

(d)

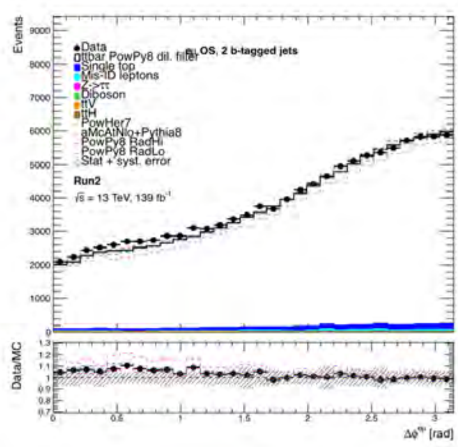

(e)

Figure 5.5: Kinematic variables for $e\mu$ events with two b-jets.

CHAPTER 6

BACKGROUND MODELLING

Not all backgrounds can be safely taken from Monte Carlo predictions, in some cases Monte Carlo predicts a background which does not match the data correctly. This is why predictions need to be compared to data in a region where such backgrounds dominate, in order to correct the size of the background to the data, making this method of background estimation partially data driven. For this analysis this is done for the misidentified lepton background, which is studied in the $e\mu$ same sign (SS) channel, that is enriched with fake lepton events, and for the $Z \to \tau\tau$ + jets background, to which a correction factor extracted from the $Z \to ee$ + jets and $Z \to \mu\mu$ + jets control regions needs to be applied.

6.1 Fake lepton background

The misidentified lepton background is estimated with a partially data-driven technique and using the $e\mu$ SS control region, since the majority of the events in this region are fakes. For almost all of the cases, only one of the leptons is misidentified or comes from another source than the top quark, while only in very few events both leptons are misidentified. Each Monte Carlo SS and OS $e\mu$ event is categorized depending on the type of the leptons (from the `true_type` variable derived from the `MCTruthCassifier` package) in one of those six categories:

prompt RS (right sign) (electron `true_type` is 2 and muon `true_type` is 6), both leptons are prompt and both are reconstructed with the correct charge (which is checked by looking at the sign of truth pdgID of the leptons).

prompt WS (wrong sign) (electron `true_type` is 2 and muon `true_type` is 6), both leptons are prompt, but the electron was reconstructed with the wrong charge (again checked against the truth pdgID of the truth electron). This happens mostly for very high-p_T electrons, as the tracks are so straight, that the curvature is not easily discernible.

photon conversion e (electron `true_type` is 4 and muon `true_type` is 6), where the muon is prompt, while the electron comes from a photon conversion, which can both originate from a photon emitted by the electron from the top quark ($t \to e \to \gamma \to e$) or from a background conversion.

heavy-flavour e (electron `true_type` is 3 and muon `true_type` is 6), where the muon is prompt, while the electron either comes from a jet or a heavy-flavour deposit in the calorimeter reconstructed as an electron.

heavy-flavour μ (electron `true_type` is 2 and muon `true_type` is 7), where the electron is prompt, while the muon comes from a jet or a heavy flavour deposit reconstructed as a muon.

other, which includes all the other cases: the electron is prompt and the muon is a background muon, coming from an in-flight decay of a pion or kaon (electron type is 2 and muon `true_type` is 8); the electron is prompt and the muon is not prompt but the source is unknown (electron `true_type` is 2 and muon `true_type` is 5); the muon is prompt while the electron is non prompt but the source is unknown (electron `true_type` is 1 and muon `true_type` is 6); both leptons are non prompt.

Table 6.1: Event counts divided into misidentified lepton categories for the full Run 2 dataset

	OS			SS		
Run 2	N_1	N_2	$N_{e\mu}$	N_1	N_2	$N_{e\mu}$
Prompt RS	431119	225172	1.03953e+06	636.8	232.5	9864.0
Prompt WS	1.9	0.6	29.2	789.7	335.6	1895.2
Conversion	3402.5	1565.2	8556.8	1702.2	774.2	4914.5
Heavy flavour e	423.6	43.5	1190.8	382.5	23.3	852.9
Heavy flavour μ	262.1	44.9	918.7	163.0	10.2	400.3
Other	453.2	203.4	2743.5	83.0	29.6	553.9
Total	435663	227030	1.05297e+06	3757.2	1405.3	18480.9
Data	439090	232610	1.07995e+06	3760	1418	25821
Data/MC	1.008	1.02	1.03	1.001	1.009	1.4

When all the events are categorized, the different lepton pair contributions are summed for all the signal and background samples for both the OS and

SS channels and they are plotted again the data collected in those same channels. The different contributions in the OS and SS regions can be seen in Table 6.1, where N_1 is the number of $e\mu$ events with one b-jet, N_2 is the number of $e\mu$ events with two b-jets and $N_{e\mu}$ is number of all $e\mu$ events, and in Fig. 6.1, 6.2, 6.3 and 6.4 for one and two b-jets selections. The signal and background samples used are those mentioned in Chapter 4, in particular it is noteworthy, that instead of using the dilepton filtered samples for $t\bar{t}$ and Wt, the all inclusive samples are used. This is done in order to include the events from the lepton + jets channel, where the jet might be mistakenly reconstructed as a lepton or where the event is reconstructed as a dilepton event due to another (fake) lepton being involved.

It can be noticed that in the SS channel the majority of the events have one fake lepton, as mentioned before, while in the OS channel only few events have one misidentified lepton. The biggest contribution to the misidentified leptons in the SS channel comes from the events with a misidentified electron, in particular from events where the electron comes from a conversion process or the charge of the electron has been misidentified. Another thing to note, is that the heavy flavour contribution to the misidentified lepton background lies mostly in a low p_{T} region, due to either low energetic deposits in the calorimeter that are reconstructed as leptons, or due to low energetic semileptonic b-decays, for example.

The number of misidentified lepton events in the OS channel can be computed as:

$$N_b^{i,mis-ID,OS} = R_b^i \cdot \left(N_b^{i,data,SS} - N_b^{i,promptRS,SS}\right) \tag{6.1}$$

with

$$R_b^i = \frac{N_b^{i,mis-ID,OS}}{N_b^{i,mis-ID,SS}} \tag{6.2}$$

where b is the number of b-jets used in the selection, i is the bin number, $N_b^{i,mis-ID,OS}$ is the number of estimated fake lepton events from Monte Carlo and data in the OS channel for a b-jet selection in bin i, $N_b^{i,data,SS}$ is the number of data events in the SS channel with b-jet selection b, $N_b^{i,promptRS,SS}$ is the number of prompt RS lepton pairs from Monte Carlo in the SS channel for a b-jet selection and R_b^i is the ratio between the number of misidentified leptons in the OS and SS channels, as derived from Monte Carlo.

Using the above equations, the misidentified lepton background can be computed for each bin of each distribution as seen in Fig. 5.1, 5.2, 5.3, 5.4, 5.5 and Table 5.1. The R_b^i factor for the 1 and 2 b-jet distributions and for the distributions with no b-jet requirements can be seen in Fig. 6.5 and 6.6, where it is seen that the factor is above one for all distributions and generally around 1.5, indicating, that generally in Monte Carlo there are more misidentified lepton events predicted in the OS channel than in the SS channel. This is independent on the number of events, as this seems to be the same whether we consider the distributions with one, two or no b-jet requirements.

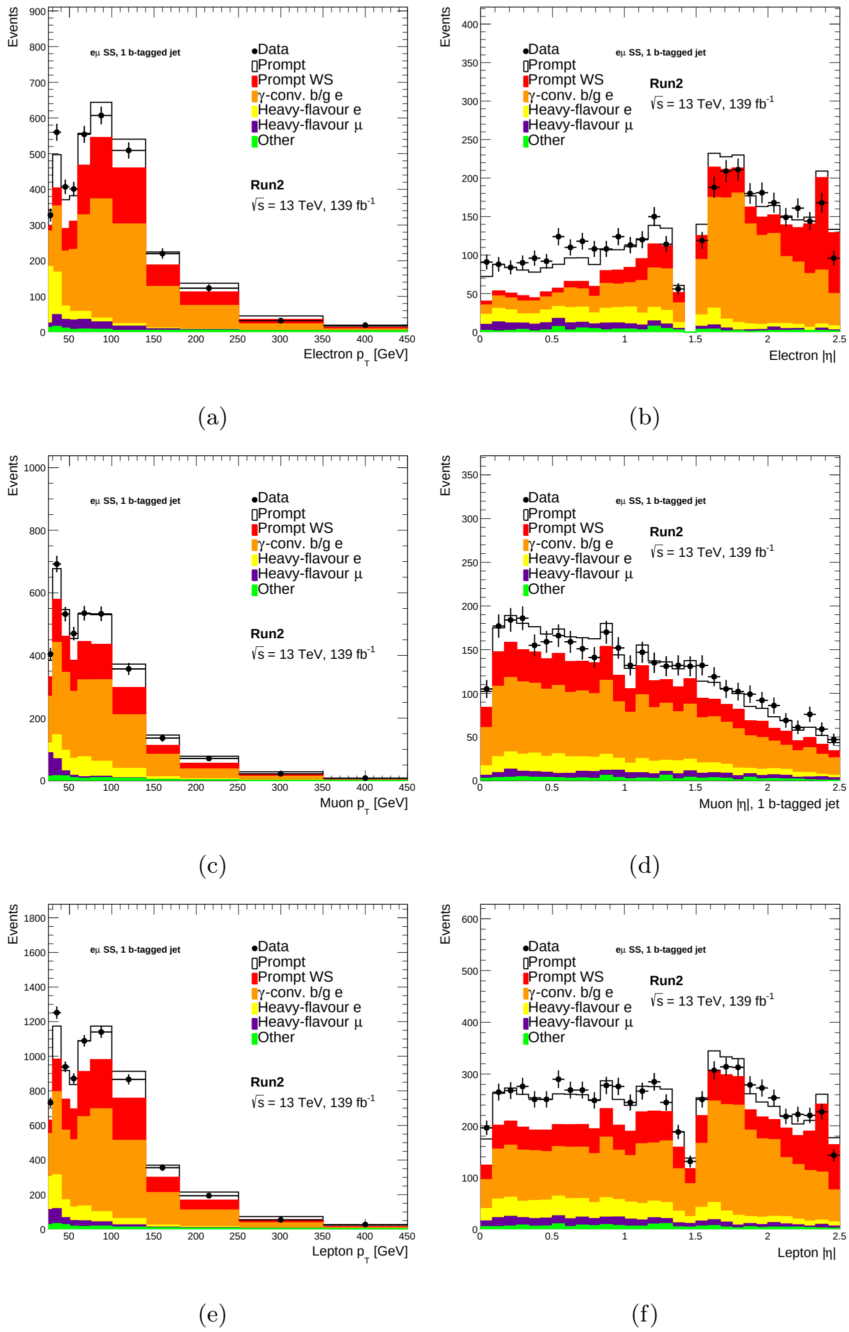

Figure 6.1: Kinematic variables for $e\mu$ SS events with one b-jet divided into the different fake lepton contributions. The last bin of the p_{T} distributions contains the overflow events.

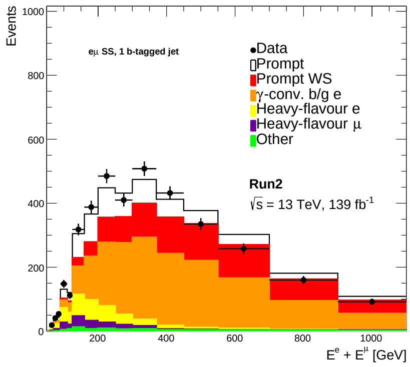

(a)

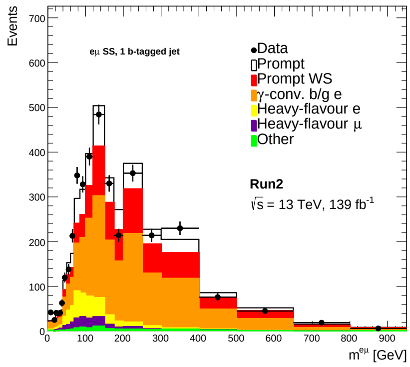

(b)

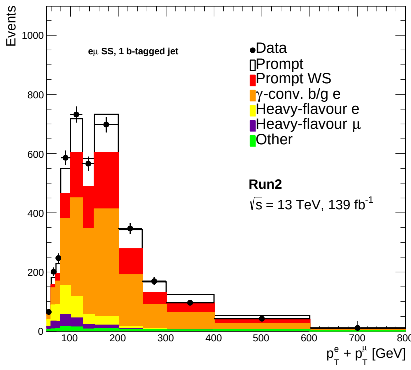

(c)

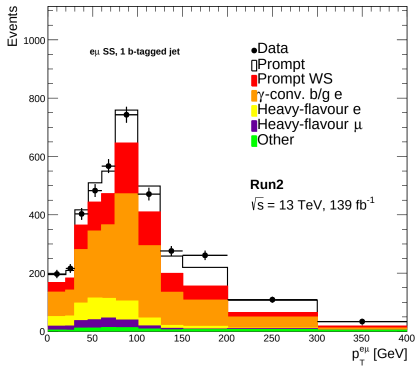

(d)

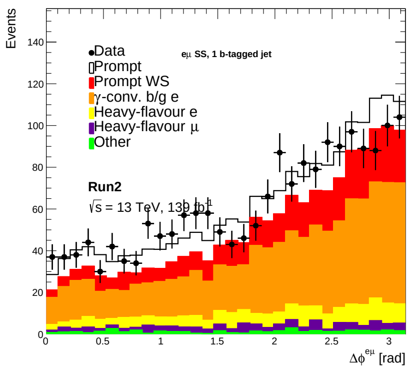

(e)

Figure 6.2: Kinematic variables for $e\mu$ SS events with one b-jet divided into the different fake lepton contributions. The last bin contains the overflow events, apart in (e).

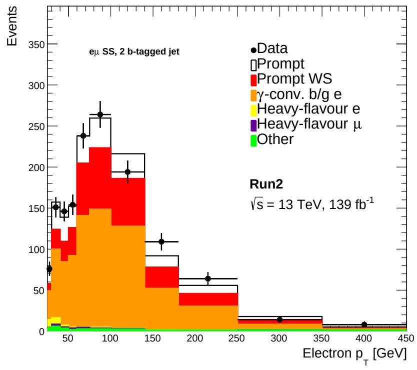

(a)

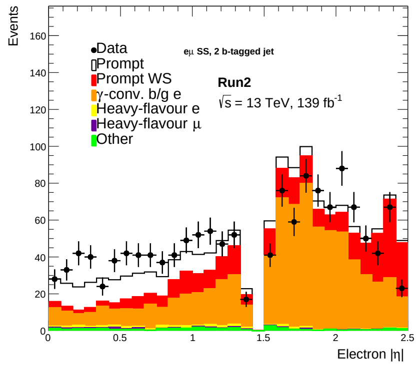

(b)

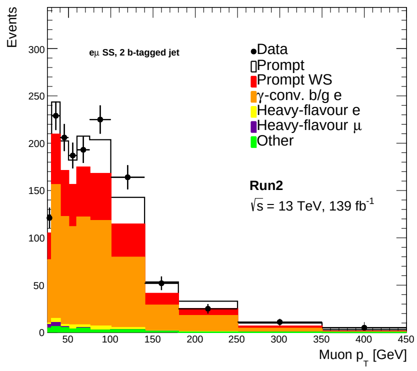

(c)

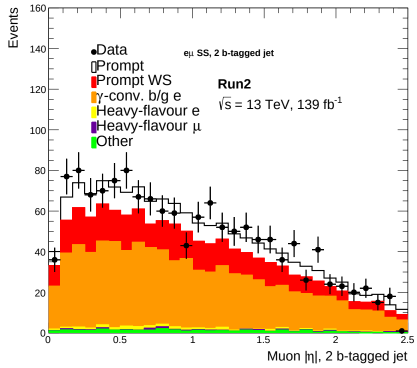

(d)

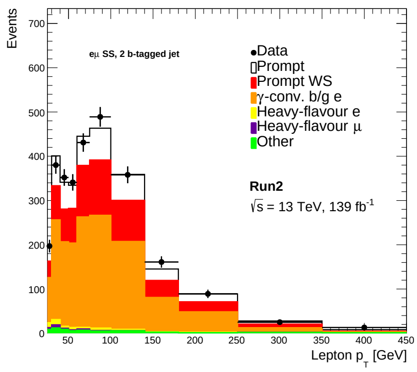

(e)

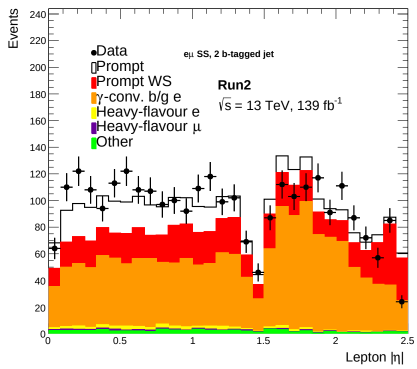

(f)

Figure 6.3: Kinematic variables for $e\mu$ SS events with two b-jets divided into the different fake lepton contributions. The last bin of the p_{T} distributions contains the overflow events.

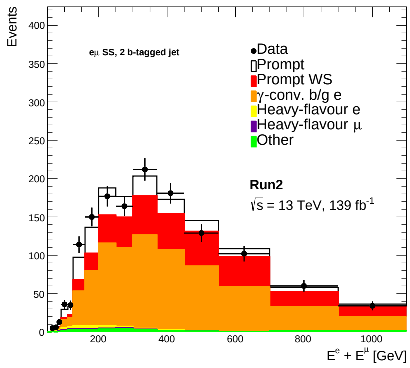

(a)

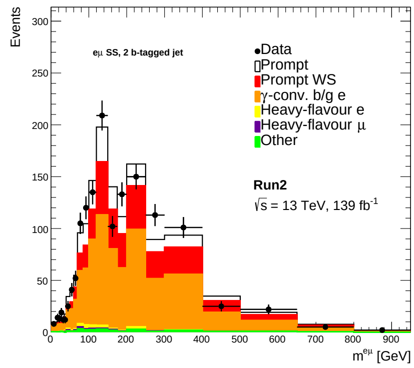

(b)

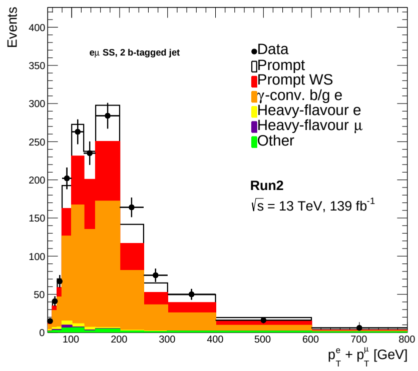

(c)

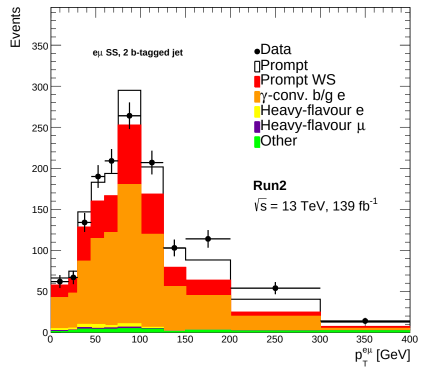

(d)

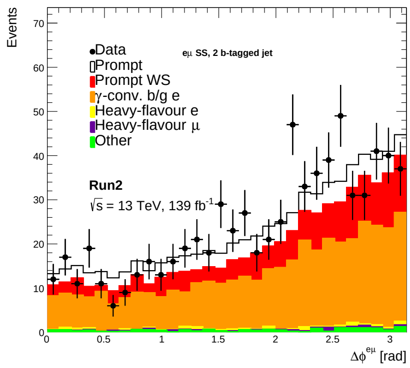

(e)

Figure 6.4: Kinematic variables for $e\mu$ SS events with two b-jets divided into the different fake lepton contributions. The last bin contains the overflow events, apart in (e).

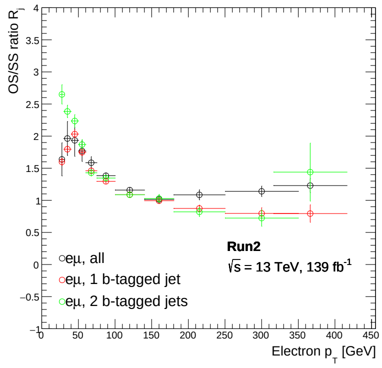

(a)

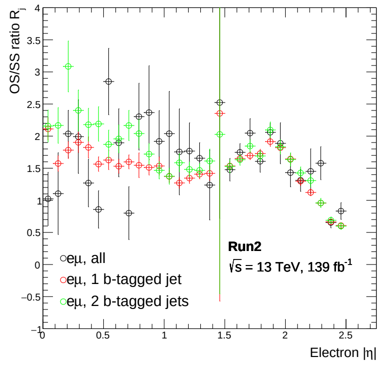

(b)

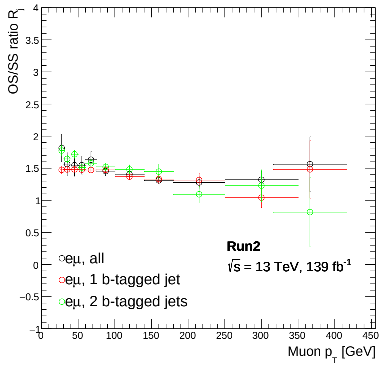

(c)

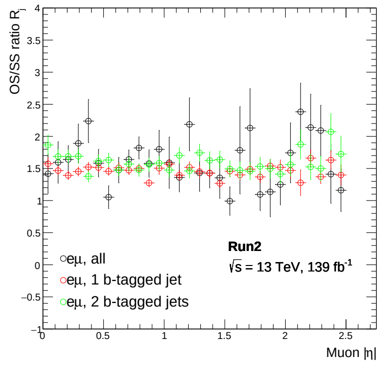

(d)

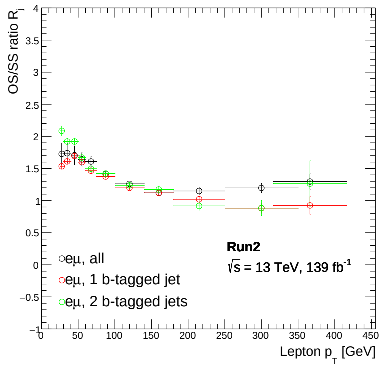

(e)

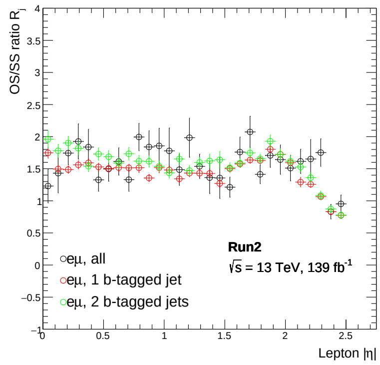

(f)

Figure 6.5: R factor from Eq. 6.2 for each bin of each leptonic kinematic variables for different selections.

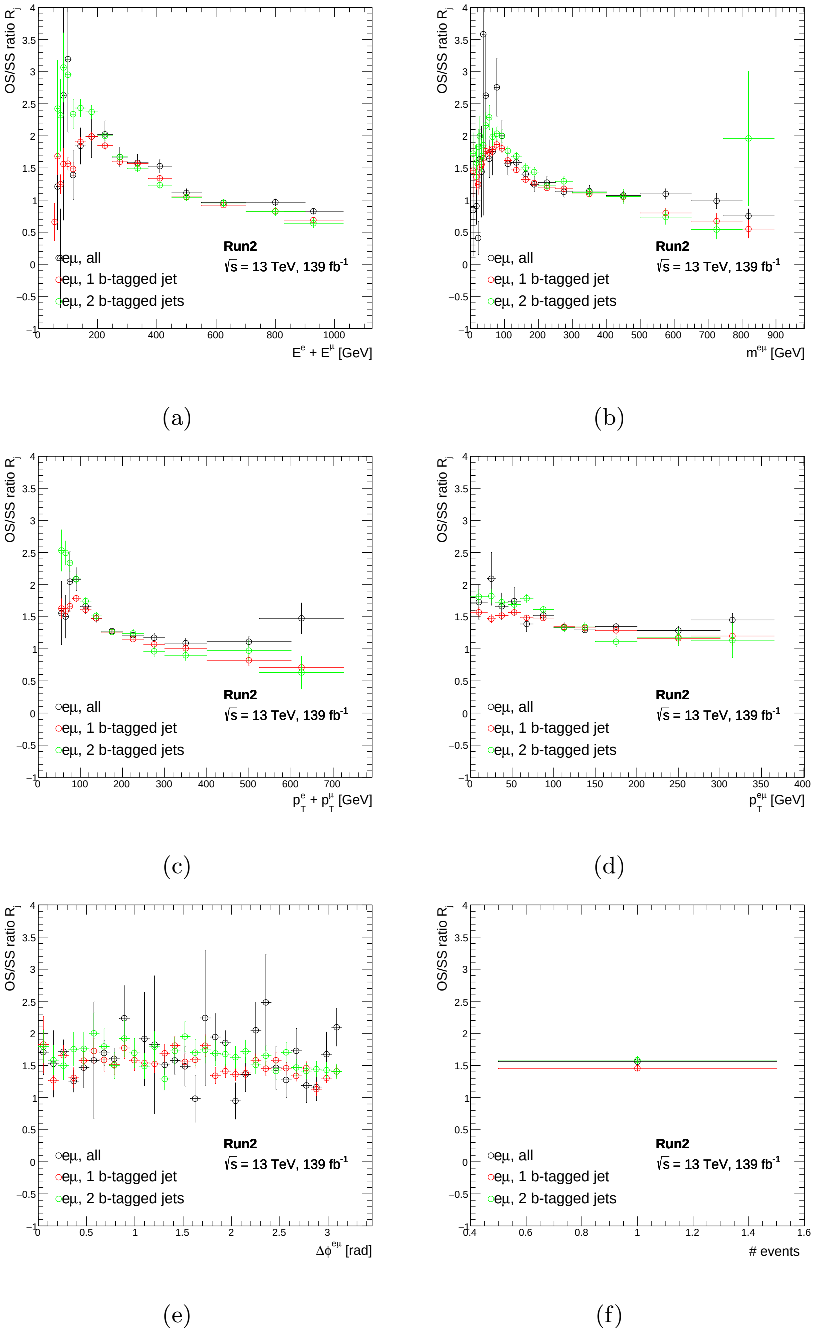

Figure 6.6: R factor from Eq. 6.2 for each bin of each leptonic kinematic variables and for the total number of events for different selections.

6.2 $Z \to \tau\tau$ + jets background

The $Z \to \tau\tau$ + jets background is simulated with Sherpa 2.2.1, but the evaluation of this background suffers from mismodelling due to its cross section's theoretical QCD uncertainties [96] used to generate the Monte Carlo samples. In order to correct for this mismodelling, the inconsistencies between the Z + jets background and the data is measured in two control regions and a correction factor is derived from this procedure and applied then to the $Z \to \tau\tau$ + jets background in the signal region, assuming lepton universality. The two control regions are the $Z \to ee$ + jets and the $Z \to \mu\mu$ + jets channels around the Z pole mass and the factors are derived separately for events with 1 and 2 b-jets.

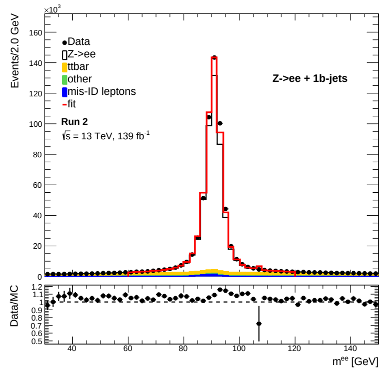

(a)

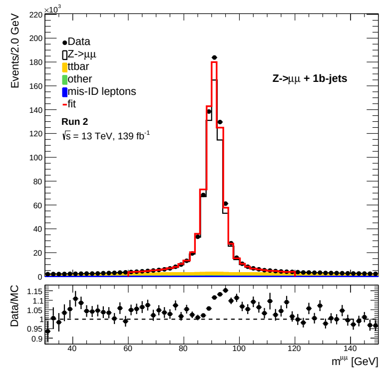

(b)

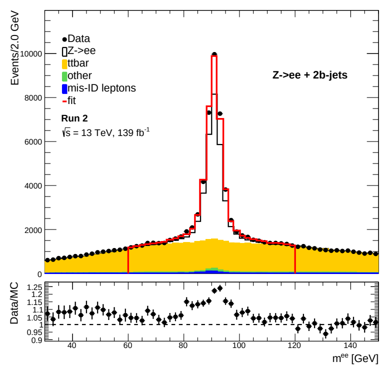

(c)

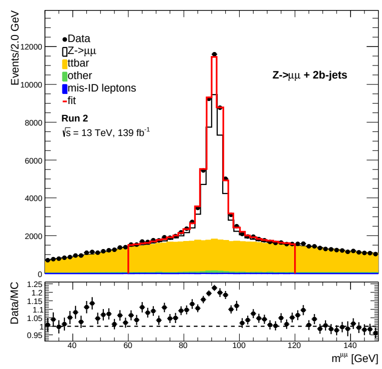

(d)

Figure 6.7: Control regions to extract the Z-factor that normalises the Sherpa simulated samples to data. Different components, as $t\bar{t}$, diboson and misidentified leptons are also included as part of the background. The fit to extract the Z-factor is performed between 60 GeVand 120 GeV.

In order to derive the correction factors, the invariant mass of the two leptons, $m(\ell^+\ell^-)$ is calculated for each event in the control regions, both for the $Z \to \ell\ell$ + jets samples and for the background samples ($t\bar{t}$, $t\bar{t}V$, single top, diboson). The fake lepton contribution is in this case taken directly from Monte Carlo, by categorizing each dilepton event as either prompt or fake in the same way

Table 6.2: Event counts for $Z \to ee$ + jets and the $Z \to \mu\mu$ + jets the full Run 2 dataset

Run 2 OS	ee + 1 b-jet	mumu + 1 b-jet	ee + 2 b-jets	mumu + 2 b-jets
$t\bar{t}$	110592	135882	63649.3	78354.2
Other	13556.8	16504.4	2362.2	2818.9
mis-ID leptons	9208.8	387.9	1229.4	72.6
Z+jets	498424	672873	25038.6	32500.3
Total	631782	825648	92279.4	113746
Data	678308	888862	100952	124439
Data/MC	1.07	1.08	1.09	1.09

as in Section 6.1. The invariant mass of the leptons is then plotted for all the contributions around the Z-peak value, which is clearly visible both in data and in Monte Carlo around 90 GeV. The difference between data and Monte Carlo is clear from Fig. 6.7, where there is an excess of data events compared to Monte Carlo events. The event counts for the plots can be seen in Table 6.2, where it is shown that the data excess is between $7-9\%$.
The correction scale factors for each region are extracted by fitting the Monte Carlo $Z \to \ell\ell$ + jets contribution and background contributions to the data. The fitting function contains two normalisation factors, one for the $Z \to \ell\ell$ + jets contribution and one for the total background contributions. Those two normalisation parameters are fitted, so that the entire Monte Carlo $Z \to \ell\ell$ + jets + background contribution is fitted to the data. The function fitted to data is:

$$f = n_Z \cdot \text{hist}(Z \to \ell\ell) + n_{bkg} \cdot \text{hist}(\text{bkg}) \tag{6.3}$$

where f is the fitting function, n_Z and n_{bkg} are the fitted normalisation parameters for the Monte Carlo $Z \to \ell\ell$ contribution and for the background contribution respectively, while hist$(Z \to \ell\ell)$ and hist(bkg) are the Monte Carlo $Z \to \ell\ell$ and background histogram contributions. The fit is performed with a log likelihood in a range between 60 GeV and 120 GeV. The normalisation factor of the $Z \to \ell\ell$ contribution is then taken as the scale factor for that specific control region. The normalisation factor for the background contribution is less than 1.06 for every region, without any need to constrain this parameter, meaning that the background contribution is well simulated within 6%. After this procedure, four scale factors are found in total, two for each signal region, both for the events with one b-tagged jet and for the events with two b-tagged jets. The results can be seen in Table 6.3. A total scale factor for the $Z \to \tau\tau$ + jets background for the 1-b-jet and 2-b-jet sub-samples are found by taking the weighted average of the two scale factors derived from the $Z \to ee$ + jets and from the $Z \to \mu\mu$ + jets regions, since we are assuming, that the two regions are uncorrelated from each other. The final results can be seen also in Table 6.3.

Table 6.3: Factors extracted from the $Z \to ee$ + jets and the $Z \to \mu\mu$ + jets control regions.

Selection/number of b-jets	1 b-jet	2 b-jets
$Z \to ee$ + jets	1.093 ± 0.002	1.25 ± 0.01
$Z \to \mu\mu$ + jets	1.093 ± 0.002	1.251 ± 0.009
Total	1.093 ± 0.001	1.252 ± 0.006

CHAPTER 7

ANALYSIS STRATEGY

In the following chapter the method to extract the total and the differential cross section is outlined. The fit to extract the cross section is also tested with various validation techniques, to assess its stability and its possible bias.
The total and differential $t\bar{t}$ production cross sections are measured in the dilepton channel of the $t\bar{t}$ decay, where $t\bar{t} \to W^+W^-b\bar{b}$ and one W boson decays to an electron and the other to a muon and the two leptons have opposite sign. This also removes the need to exclude the Z peak region in the $ee-$ and $\mu\mu-$channels using cuts on the dilepton mass. The total branching ratio of the top quark to a W boson and a bottom quark is nearly 100%, which means that the branching ratio of the $t\bar{t}$ system to an electron and a muon are dictated by the branching ratio of the decays of the W. The branching ratio of the $t\bar{t}$ system to an electron and a muon can be calculated to approximately 2.4% [97]. In this analysis though, the events where $W \to \tau\nu_\tau \to e\bar{\nu}_e\nu_\tau\nu_\tau$ or $W \to \tau\nu_\tau \to \mu\bar{\nu}_\mu\nu_\tau\nu_\tau$ are included as well, which makes the total branching ratio of the signal events increase slightly. This can be calculated by taking into account that the branching ratio of a τ to an electron

or a muon with their corresponding neutrino and a tau neutrino is roughly 17%. The resulting branching ratio of the $t\bar{t}$ signal taken into consideration in this analysis becomes $\sim 3.2\%$. The events are furthermore required to contain either exactly one or exactly two b-tagged jets in order to finally extract the cross section.
The fiducial cross section (both total and differential) are extracted to particle level.

7.1 Total fiducial cross section

The total fiducial cross section is found experimentally using an event count technique. Said technique, also called the double tagging technique, subdivides the selected $e\mu$ OS events into events with one b-jet and events with two b-jets. The double tagging technique equations can be derived starting from the definition of the cross section:

$$\sigma_{t\bar{t}} = \frac{N}{\mathcal{L} \cdot A \cdot \epsilon \cdot Br} \tag{7.1}$$

where $\sigma_{t\bar{t}}$ is the cross section, N is the number of events after background subtraction (the number of signal events), $\mathcal{L}$ is the dataset integrated luminosity, A is the detector acceptance, ϵ is the efficiency and Br is the branching ratio of the process used to calculate the cross section.
From this equation we can write the total inclusive cross section as:

$$N = \sigma_{t\bar{t}} \cdot \mathcal{L} \cdot A \cdot \epsilon \cdot Br \tag{7.2}$$

where the number of signal events is $N = N_{tot} - N_{bkg}$. To measure the fiducial cross section we can use the fact that

$$\sigma_{t\bar{t}} \cdot A \cdot Br = \sigma_{t\bar{t}}^{fid} \tag{7.3}$$

and the above equation becomes:

$$N_{tot} = \sigma_{t\bar{t}}^{fid} \cdot \mathcal{L} \cdot \epsilon - N_{bkg}. \tag{7.4}$$

Since $e\mu$ OS events are selected with either one or two b-jets, two different equations can be set up, where the cross section can be extracted from the number of $e\mu$ OS events with one b-jet and in the other with two b-jets. By doing so, we have to introduce the b-tagging efficiency in both equations. The correlation between the two b-tagged jets needs to be accounted for in both equations, so a coefficient is introduced for that. Apart from the b-tagging efficiency, we need to consider the reconstruction efficiency, that is a measure of how many $e\mu$ OS events were reconstructed in the detector out of the entire true $e\mu$ OS events generated. This value, as well as the b-tagging correlation coefficient, are entirely evaluated from Monte Carlo simulation samples. By putting together all these elements, the double tagging equations are derived:

$$\begin{aligned} N_1 &= \mathcal{L}\sigma_{t\bar{t}}^{fid} G_{e\mu} 2\epsilon_b(1 - \epsilon_b C_b) + N_{1,bkg} \\ N_2 &= \mathcal{L}\sigma_{t\bar{t}}^{fid} G_{e\mu} (\epsilon_b)^2 C_b + N_{2,bkg} \end{aligned} \tag{7.5}$$

where N_1 and N_2 are the number of data events with either one b-jet or two b-jets, $\mathcal{L}$ is the integrated luminosity of the dataset used for the analysis, $\sigma_{t\bar{t}}^{fid}$ is the total fiducial cross section, $G_{e\mu}$ is the reconstruction efficiency for the $e\mu$ events taken from simulation, ϵ_b is the b-tagging efficiency, while C_b is the b-tagging correlation coefficient, also taken from simulation, and finally $N_{2,bkg}$ and $N_{1,bkg}$ are the number of background events with either one or two b-jets, calculated using simulation samples and, in some cases, by applying data driven techniques together with the estimates from simulations, as explained in Chapter 6. The two unknowns in these equations, the cross section and the b-tagging efficiency can be found by applying the log-likelihood method to these two equations.

The b-tagging efficiency, ϵ_b, in this equation is not the same as the b-tagging working point efficiency used to tag jets as b-jets, as explained in Section 5.1.4, this parameter expresses the efficiency that a jet is reconstructed in the fiducial region chosen (both regarding η and p_{T} cut), passes the JVT cut and is also tagged as a b-jet. This efficiency will therefore be lower than the b-tagging working point efficiency chosen. The ϵ_b values could be taken by simulation, this would though probably introduce higher uncertainties related to jets and b-jets, therefore this value is fitted together with the cross section.

The reconstruction efficiency $G_{e\mu}$ is defined as the ratio between the number of reconstructed $e\mu$ OS events from $t\bar{t}$ and the number of true $e\mu$ OS events from $t\bar{t}$ at particle level, where particle level refers to the true stable particles, present after the parton shower (but which have not been put through the detector simulation, see Section 5.1.5) [94]:

$$G_{e\mu} = \frac{N_{e\mu,all}^{t\bar{t},reco}}{N_{e\mu,all}^{t\bar{t},particle}} \tag{7.6}$$

where *all* means that all $e\mu$ OS events in the $t\bar{t}$ signal sample are taken into account, without subdividing them according to how many b-tagged jets they have. When calculating $t\bar{t}$ related systematic uncertainties, the reconstruction efficiency is calculated using a different $t\bar{t}$ samples or reweighted $t\bar{t}$ samples, see Section 8.2. The nominal value of the reconstruction efficiency with the nominal $t\bar{t}$ POWHEG + PYTHIA 8 dilepton sample is $53.26\% \pm 0.02\%$.

The b-tagging correlation coefficient C_b takes into consideration the correlation between between the two b-tagged jets and provides a correction to the b-tagging efficiency and is:

$$C_b = \frac{\epsilon_{bb}}{(\epsilon_b)^2} \tag{7.7}$$

where ϵ_{bb} is the product of the efficiency of tagging the first b-jet and the second b-jet, where the two efficiencies are not equal, and $(\epsilon_b)^2$ is again the product of the efficiency of tagging the first b-jet and the second b-jet, where the two efficiencies are the same. The correlations arises from the fact, that the second b-jet has a non-independent probability of being tagged as a b-jet, when a first b-jet as already been tagged, due to the two jets having the same common primary vertex. By isolating the C_b term in Eq. 7.5, it can be derived that:

$$C_b = \frac{4 \cdot N^{t\bar{t}}_{e\mu,all} \cdot N^{t\bar{t}}_{e\mu,2}}{(N^{t\bar{t}}_{e\mu,1} + 2N^{t\bar{t}}_{e\mu,2})^2} \tag{7.8}$$

where $N^{t\bar{t}}_{e\mu,all}$ is the total number of reconstructed $e\mu$ OS events from $t\bar{t}$ while $N^{t\bar{t}}_{e\mu,1}$ and $N^{t\bar{t}}_{e\mu,2}$ are the number of reconstructed $e\mu$ OS events from $t\bar{t}$ with either one or two b-tagged jets. When estimating the $t\bar{t}$ systematic uncertainties, the values are calculated with the appropriate samples, see Section 8.2. The nominal value of the b-tagging correlation coefficient with the nominal $t\bar{t}$ Powheg + Pythia 8 dilepton sample is 1.0061 ± 0.0006.
When the reconstruction efficiency, the b-tagging correlation coefficient and the number of background events are calculated, the minimization of the negative log-likelihood of Eq. 7.5 can be performed.
The probability to observe N signal events in a collection of signal and background events is by definition Poissonian and can therefore be written as:

$$p(N|s,b) = \frac{(s+b)^N e^{-(s+b)}}{N!} \tag{7.9}$$

where $p(N|s,b)$ is the probability of observing N data events given signal prediction s and background prediction b. In case we have two different observations N_1 and N_2, the probability (or likelihood) of observing them both is the product of the single probabilities. If the signal and background models contain parameters, those can then be found by minimizing the negative log of the likelihood:

$$\frac{\partial(-ln(L(N|s,b)))}{\partial(s,b)} = 0. \tag{7.10}$$

In the case of the double tagging techinique, the likelihood becomes:

$$L = p(N_1^{obs}|N_1) \cdot p(N_2^{obs}|N_2) \tag{7.11}$$

where L is the likelihood, N_1^{obs} and N_2^{obs} are the number of observed $e\mu$ OS events with one or two b-jets in data while N_1 and N_2 is the predicted number of events with one or two b-jets from Eq. 7.5. The negative log-likelihood takes this form:

$$-ln(L) = N_1 + N_2 - N_1^{obs} ln(N_1) - N_2^{obs} ln(N_2) \tag{7.12}$$

and by substituting the double tagging equations from Eq. 7.5 in Eq. 7.12, the cross section $\sigma_{t\bar{t}}$ and the b-tagging efficiency ϵ_b can be found by minimization. Note that in Eq. 7.12 the factorial of N_1^{obs} and N_2^{obs} have been removed since they are constants and they would not affect the final minimisation result. In order to carry this out, the TMinuit ROOT class was used with the MINOS minimizer algorithm [98]. This algorithm also yields uncertainties on the parameters of interest, but these uncertainties will be recalculated from toy-experiments as described in Section 7.4.
The results for the b-tagging efficiency are shown in Fig. 1 in Appendix B, while the results for the total fiducial cross section are discussed in Section 9.1.

7.2 Total inclusive cross section

The total inclusive cross section can be found in the same manner as the total fiducial cross section, though with the addition of a factor that takes into account the acceptance between the entirety of the $t\bar{t}$ pair produced in all channels and those chosen in the fiducial region, as shown in Eq. 7.3.
In this case the reconstruction efficiency is substituted with the preselection efficiency $E_{e\mu} = A_{e\mu} \cdot G_{e\mu}$, where $A_{e\mu}$ is defined as such:

$$A_{e\mu} = \frac{N^{t\bar{t},particle}_{e\mu,all}}{N^{t\bar{t}}_{all}} \tag{7.13}$$

where $N^{t\bar{t},particle}_{e\mu,all}$ is the number of all particle level $e\mu$ OS events (not subdivided according to the number of b-jets), while $N^{t\bar{t}}_{all}$ is the total number of $t\bar{t}$ pairs produced in the Monte Carlo sample used. The acceptance factor comes purely from Monte Carlo $t\bar{t}$ samples (the same sample used to calculate the reconstruction efficiency should be used to calculate the acceptance). However, since the nominal sample and the alternative $t\bar{t}$ samples used in this analysis are produced with a dilepton filter, it means that $N^{t\bar{t}}_{all}$ is in reality $N^{t\bar{t}}_{dilepton}$. This needs to be corrected with the branching ratio to obtain the proper $N^{t\bar{t}}_{all}$. The branching ratio for $t\bar{t}$ events to dilepton used in this analysis is 10.537%, which is calculated using the Standard Model predicted branching ratio, $BR(W \to \ell\nu) = 10.82\%$ [99, 100]. The nominal value of $E_{e\mu}$ (including the branching ratio of $t\bar{t}$ pairs to dilepton events) with the nominal $t\bar{t}$ POWHEG + PYTHIA 8 dilepton sample is $0.6768\% \pm 0.0003$, while the value of the acceptance $A_{e\mu}$ also calculated with the nominal $t\bar{t}$ POWHEG + PYTHIA 8 dilepton sample is $1.2708\% \pm 0.0004\%$.
When extracting the total inclusive cross section the double tagging equations become:

$$\begin{aligned} N_1 &= \mathcal{L}\sigma^{fid}_{t\bar{t}} E_{e\mu} 2\epsilon_b(1 - \epsilon_b C_b) + N_{1,bkg} \\ N_2 &= \mathcal{L}\sigma^{fid}_{t\bar{t}} E_{e\mu} (\epsilon_b)^2 C_b + N_{2,bkg} \end{aligned} \tag{7.14}$$

7.3 Fiducial differential cross section

Seven leptonic differential distributions are taken into consideration in this analysis: $p_{\mathrm{T}}(\ell^+\ell^-)$, $p_{\mathrm{T}}(\ell^+)+p_{\mathrm{T}}(\ell^-)$, $p_{\mathrm{T}}(\ell)$, $E(\ell^+)+E(\ell^-)$, $m(\ell^+\ell^-)$, $|\eta(\ell)|$ and $\Delta\phi(\ell^+\ell^-)$. Each distribution is unfolded to particle level in the fiducial region by applying the double tagging technique on each bin of each distribution, as earlier done in [13, 15, 17, 18]. The double tagging equations for the differential measurements are as follows:

$$\begin{aligned} N^i_1 &= \mathcal{L}\sigma^i_{t\bar{t}} G^i_{e\mu} 2\epsilon^i_b(1 - \epsilon^i_b C^i_b) + N^i_{1,bkg} \\ N^i_2 &= \mathcal{L}\sigma^i_{t\bar{t}} G^i_{e\mu} (\epsilon^i_b)^2 C^i_b + N^i_{2,bkg} \end{aligned} \tag{7.15}$$

where N^i_1 and N^i_2 are the number of data events with either one b-jet or two b-jets in bin i, $\mathcal{L}$ is the integrated luminosity of the dataset used for the

analysis, $\sigma^i_{t\bar{t}}$ is the fiducial cross section in bin i, $G^i_{e\mu}$ is the reconstruction efficiency for $e\mu$ OS events taken from simulation, ϵ^i_b is the b-tagging efficiency in bin i, while C^i_b is the b-tagging correlation coefficient in bin i also taken from simulation and finally $N^i_{2,bkg}$ and $N^i_{1,bkg}$ are the number of background events in bin i with either one or two b-jets, calculated using simulation samples and, in some cases, by applying data driven techniques together with the estimates from simulations, as explained in Chapter 6. The two unknowns in these equations, the cross section and the b-tagging efficiency, can be found by applying the log-likelihood method to these two equations.
The reconstruction efficiency $G^i_{e\mu}$ is defined as above, though one value per bin i per distribution is found:

$$G^i_{e\mu} = \frac{N^{i,t\bar{t},reco}_{e\mu,all}}{N^{i,t\bar{t},particle}_{e\mu,all}} \tag{7.16}$$

where *all* means that all $e\mu$ OS events from $t\bar{t}$ events are taken into account, without subdividing them according to how many b-tagged jets they have. The $N^{i,t\bar{t},reco}_{e\mu,all}$ and $N^{i,t\bar{t},particle}_{e\mu,all}$ in the last bin of each distribution contain the overflow events as well. This value is calculated for each bin in each distribution using the nominal $t\bar{t}$ Powheg + Pythia 8 sample and the results can be seen in Fig. 7.1. It is important to note, that in Fig. 7.1(a) and 7.1(b) both leptons in the event are entered, meaning that there are two entries per event. When calculating $t\bar{t}$ related systematic uncertainties, the reconstruction efficiency is calculated using a different $t\bar{t}$ sample or a reweighted $t\bar{t}$ sample, see Section 8.2.
As in Eq. 7.8, the b-tagging correlation coefficient C^i_b takes into consideration the correlation between between the two b-tagged jets for each bin i of each distribution and provides a correction to the b-tagging efficiency and is:

$$C^i_b = \frac{4N^i_{e\mu,all}N^i_{e\mu,2}}{(N^i_{e\mu,1} + 2N^i_{e\mu,2})^2} \tag{7.17}$$

where N^i_{all} is the total number of $e\mu$ OS events while N^i_1 and N^i_2 are the number of $e\mu$ OS events with either one or two b-tagged jets. The overflow events are added to the counts of the last bin in each distribution. The correlation coefficient is calculated using the nominal $t\bar{t}$ Powheg + Pythia 8 simulation sample, as for the reconstruction efficiency, and when estimating the $t\bar{t}$ systematic uncertainties, the values are calculated with the appropriate samples, see Section 8.2. The results for the nominal $t\bar{t}$ Powheg + Pythia 8 simulation sample can be seen in Fig. 7.2.
In order to ensure, that the double tagging technique, which is a bin-by-bin unfolding technique, is valid and works, the data needs to be binned such that most of the reconstructed $e\mu$ OS events are in the same bin as the corresponding particle level events. To check for this, migration matrices have been built to check that around 90% of the events lie in the diagonal. In fact, in a bin-by-bin unfolding from reconstruction level to particle level, the unfolding itself is just a correction factor applied to every bin, and this can only be done if the migration from particle level bins to reconstruction level bins does

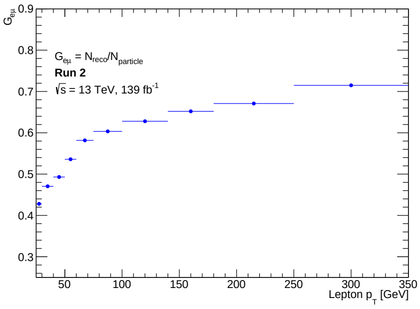

(a)

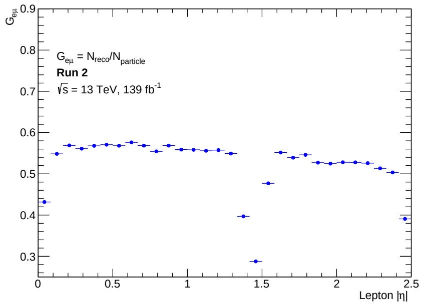

(b)

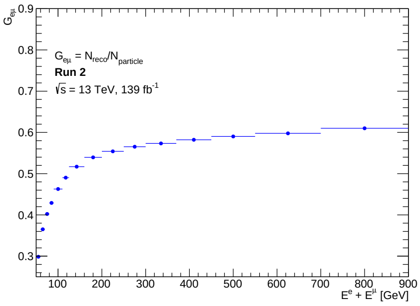

(c)

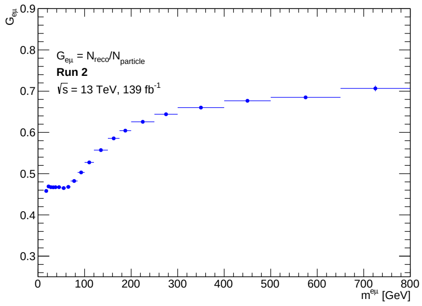

(d)

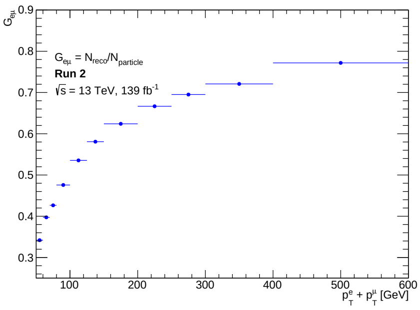

(e)

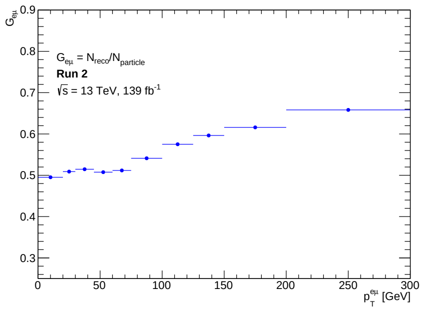

(f)

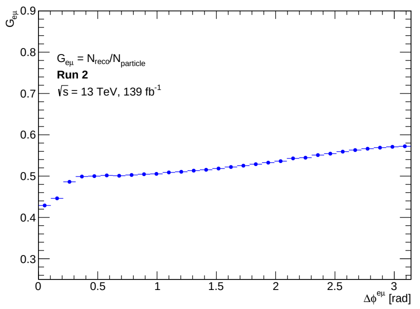

(g)

Figure 7.1: Reconstruction efficiency for each bin of each distributions calculated using Eq. 7.16 with the baseline dilepton POWHEG + PYTHIA 8 sample.

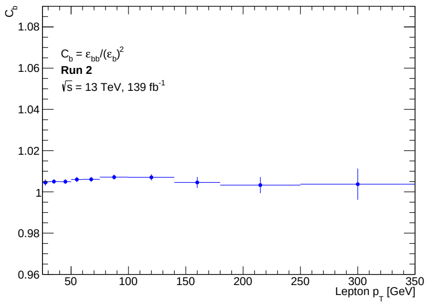

(a)

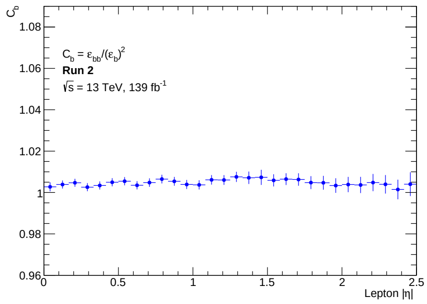

(b)

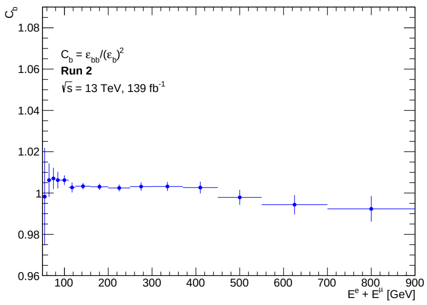

(c)

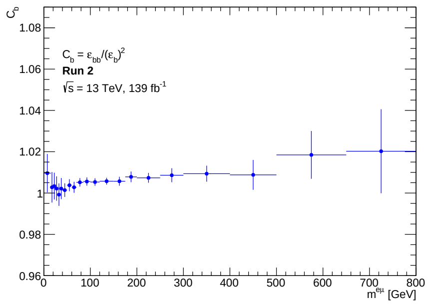

(d)

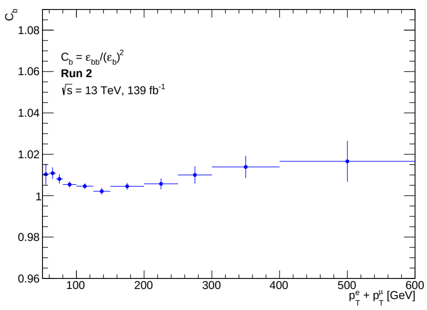

(e)

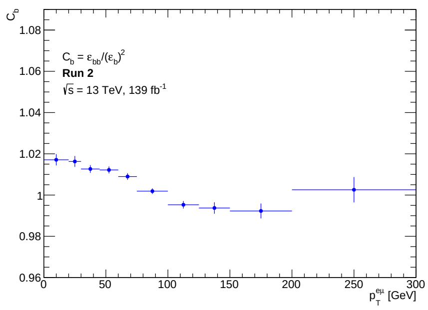

(f)

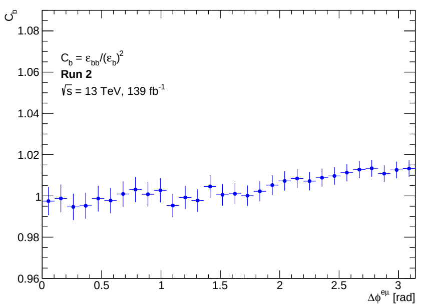

(g)

Figure 7.2: b-tagging correlation coefficient for each bin of each distributions calculated using Eq. 7.17 with the baseline dilepton POWHEG + PYTHIA 8 sample.

not branch to too many bins. The migration matrices for the seven variables, calculated with the nominal $t\bar{t}$ POWHEG + PYTHIA 8 dilepton sample, are seen in Fig. 7.3 and they are obtained by matching the reconstructed $e\mu$ OS events with the corresponding $e\mu$ OS events at particle level and plotting the variables at reconstruction and particle level in a 2D histogram.

Once the binning is set in place and the reconstruction efficiency, b-tagging correlation coefficient and the number of background events are calculated, the b-tagging equations can be minimized for each bin in each distribution adapting the negative log-likelihood from Eq. 7.12 to the following:

$$-\,ln(L) = N_1^i + N_2^i - N_1^{i,obs} ln(N_1^i) - N_2^{i,obs} ln(N_2^i) \tag{7.18}$$

where again the factorial of N_1^{obs} and N_2^{obs} are not included. The overflow events in each distribution are added to the last bin of each distribution, both for $G_{e\mu}^i$, C_b^i, $N_1^{i,obs}$ and $N_2^{i,obs}$, but also for $N_{1,bkg}^i$ and $N_{2,bkg}^i$. Finally, in order to present the results in standard units, the differential cross section from bin i is divided by the width of the same bin i.

The normalised differential cross section can be found by normalising the absolute differential cross section. The normalised differential cross section for bin i is therefore:

$$\sigma_{t\bar{t},norm}^i = \frac{\sigma_{t\bar{t}}^i}{\sum_j \sigma_{t\bar{t}}^j} \tag{7.19}$$

The normalisation is applied before dividing the cross section with the bin width. The normalisation condition introduces bin-to-bin correlations in the normalised differential cross section and those will be found by bootstrapping experiments, as explained in Section 7.4.4. The results for the b-tagging efficiency are shown in Fig. 2 in Appendix B, while the results for the differential cross section are discussed in Section 9.3.

7.4 Analysis strategy validation

In order to make sure that the analysis technique is not biased, validations have been carried out using different strategies based on toy experiments, seeded with both Monte Carlo and data outcomes. These are done in order to check for systematic biases in the analysis and to estimate the covariance matrix for all the measured variables.

Four different validation tests are performed:

- Internal bias tests, to measure the bias of the fit using the nominal $t\bar{t}$ POWHEG + PYTHIA 8 sample both to calculate the parameters of the fit (reconstruction efficiency and b-tagging correlation coefficient), and as signal sample to construct the pseudo-data;

- Stress tests, to measure the bias of the fit when using the nominal $t\bar{t}$ POWHEG + PYTHIA 8 sample to calculate the parameters of the fit (reconstruction efficiency and b-tagging correlation coefficient), but a sample with a different underlying truth distribution to construct the pseudo-data (for example with a different top mass);

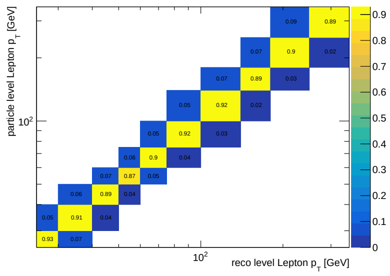

(a)

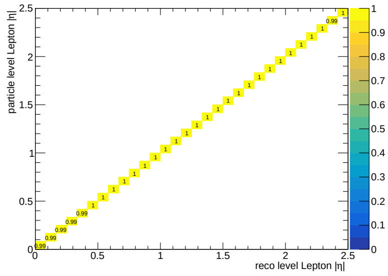

(b)

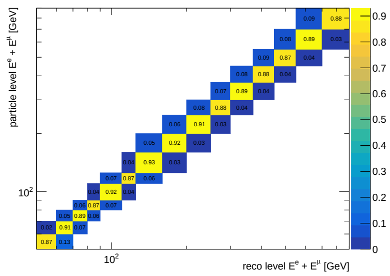

(c)

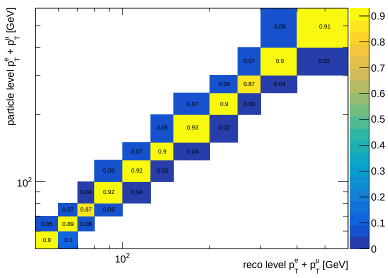

(d)

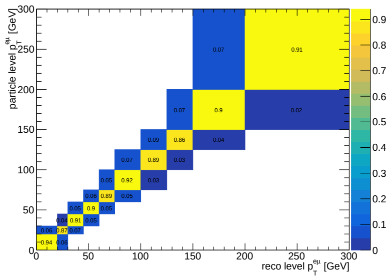

(e)

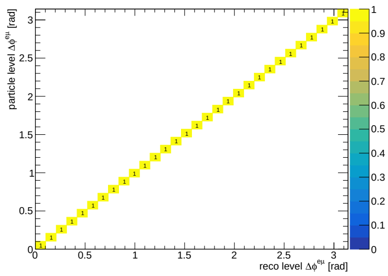

(f)

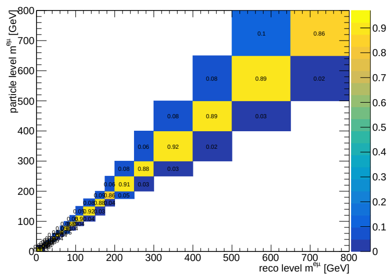

(g)

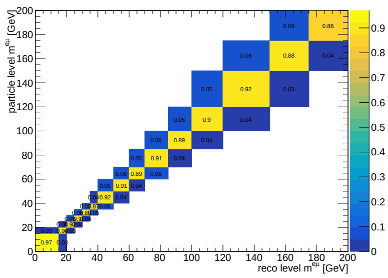

(h)

Figure 7.3: Migration matrices for each distributions calculated with the baseline dilepton POWHEG + PYTHIA 8 sample. The $m(\ell^+\ell^-)$ distribution is plotted for the total range and for a portion of the range, due to the high granularity at low values.

- Closure tests, to measure the the bias of the fit when using half of the nominal $t\bar{t}$ Powheg + Pythia 8 sample to calculate the parameters of the fit (reconstruction efficiency and b-tagging correlation coefficient) and the other half as signal sample to construct the pseudo-data;

- Bootstrapping tests, to measure the statistical covariance matrix for each variable and the statistical correlations between bins of one variable and of bins of different variables.

7.4.1 Internal bias tests

The first validation was carried out using toy Monte Carlo samples as pseudo-data, which were constructed by using the nominal $t\bar{t}$ Powheg + Pythia 8 sample as signal and the nominal estimated background as background. The values of the reconstruction efficiency and b-tagging correlation coefficient where also taken from the nominal $t\bar{t}$ sample. The N_1^i and N_2^i in Eq. 7.5 or in Eq. 7.15, derived in this case from the Monte Carlo pseudo-data, were fluctuated 1000 times, with the fluctuations being generated as a random number extracted from a Poissonian distribution with N_1^i or N_2^i as mean values. This was done for the total fiducial cross section and repeated for each bin in each differential distribution and the double tagging fit was performed on all 1000 variations of each bin independently and the results for one of the variables are shown in Fig. 7.4, where the results are plotted for each bin in each distribution and they show the normalised residuals $(\sigma_j^i - \sigma_{true}^i)/\sigma_{true}^i$ of the results, where σ_j^i is the cross section in bin i for pseudo-experiment j, while σ_{true}^i is the true cross section evaluated using true $t\bar{t} \to e\mu$ events in bin i. The normalised residuals are then each fitted to a gaussian, to extract the mean and standard deviation of each bin, which are then plotted in Fig. 7.5(a)-7.5(g) for the absolute differential cross section distributions and in Fig. 7.5(h) for the total fiducial cross section to check for internal bias. In this case a bias would be visible if the mean of the residuals of the pseudo-experiments for each bin would be different from zero and the difference would be much bigger than the standard deviation of the residuals of the same pseudo-experiments. This would mean that the cross section extracted from the pseudo-data is very different from the truth cross section predicted by the same signal sample used, leading to the conclusion that a bias is introduced most likely by the fit. As it is seen in Fig. 7.5, there are very small deviations of the mean from zero, but those deviations are well within the standard deviations, hence the results show that the double tagging technique is not internally biased. The corresponding results for the normalised differential distributions are in Fig. 3 in Appendix C.

7.4.2 Stress tests

Stress tests are performed in the same manner as for the internal bias tests, but instead of using the nominal $t\bar{t}$ Powheg + Pythia 8 sample as signal sample, a sample with a different underlying truth distribution was used, in this case we changed the underlying truth by changing the mass of the top

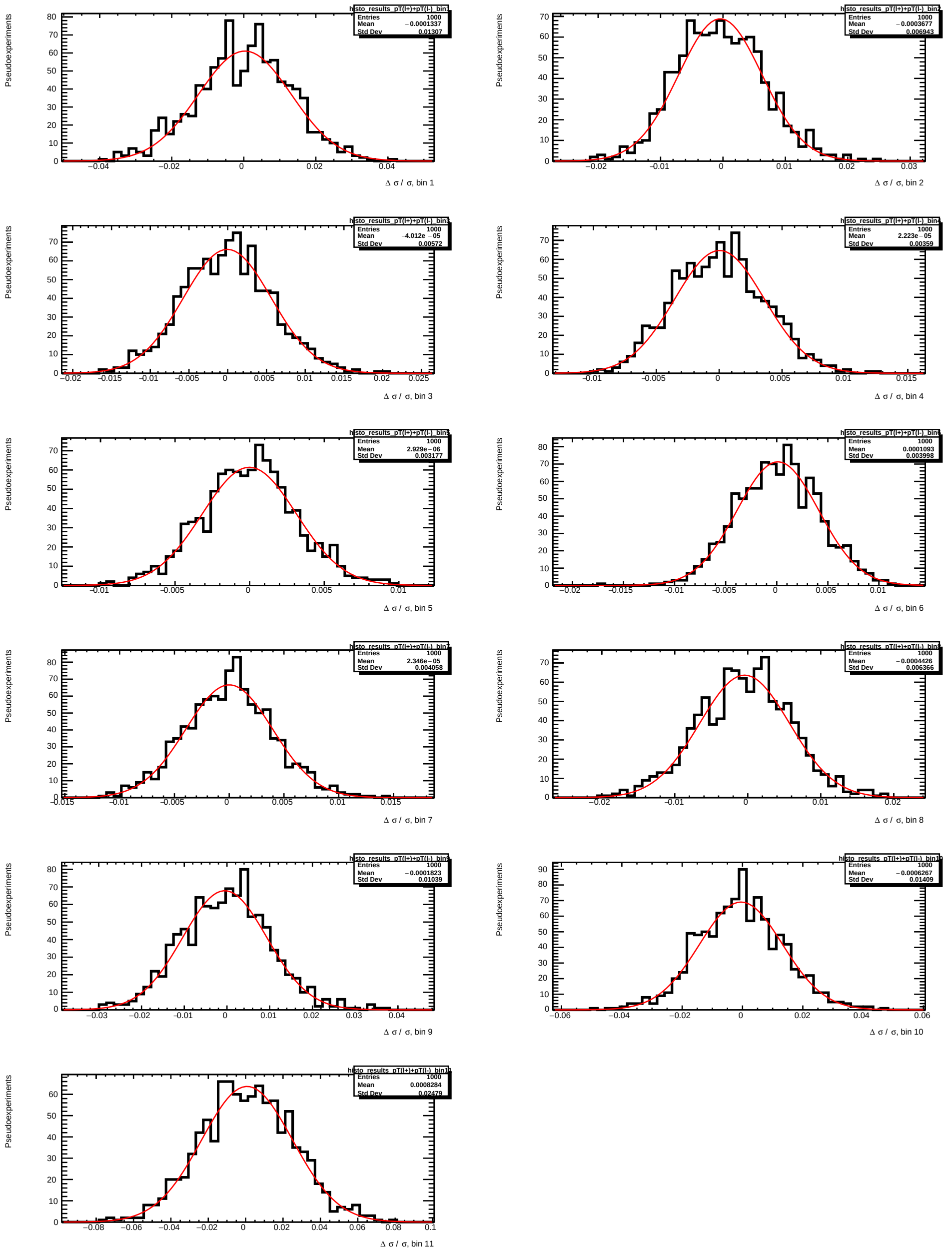

Figure 7.4: Results of the 1000 internal bias tests pseudo-experiments per bin for the $p_{\mathrm{T}}(\ell^{+}) + p_{\mathrm{T}}(\ell^{-})$ distribution, where the Monte Carlo pseudo-data bin content was fluctuated 1000 times per bin. The normalised residuals, $(\sigma^{i}_{j} - \sigma^{i}_{true})/\sigma^{i}_{true}$, are plotted for each experiment and the final results are fitted with a gaussian function.

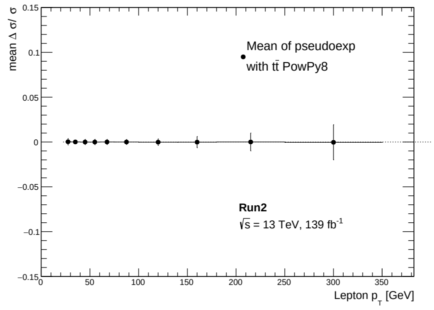

(a)

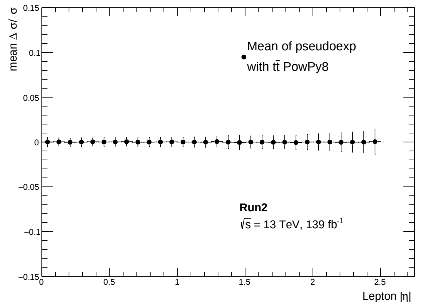

(b)

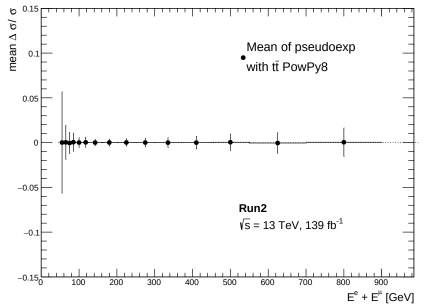

(c)

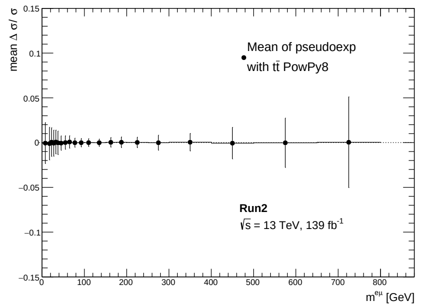

(d)

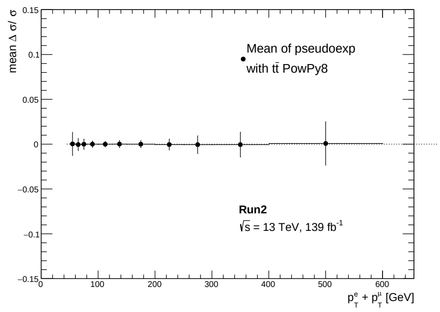

(e)

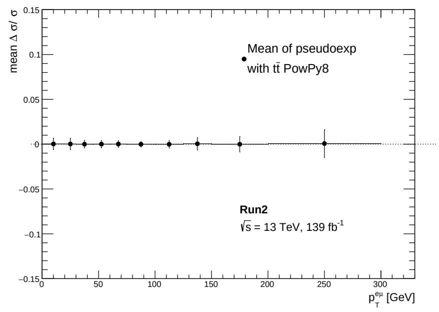

(f)

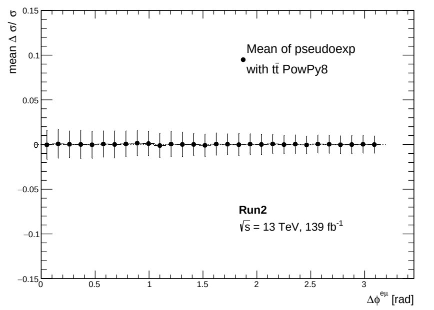

(g)

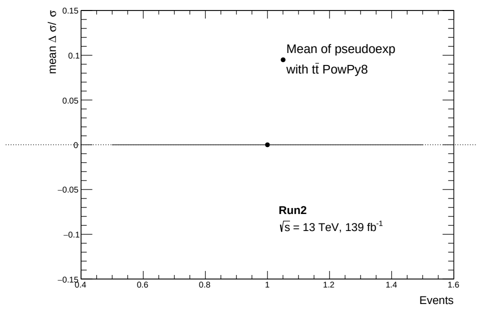

(h)

Figure 7.5: Mean and standard deviations extracted from the gaussian functions fitted to the 1000 internal bias tests pseudo-experiments results for each bin in each absolute differential distribution in (a)-(g) and for the total fiducial cross section in (h). The mean is in all cases consistent with zero within the standard deviation, demonstrating that the double tagging technique has no internal bias.

quark. The aim of these tests is to assess the stability of the double tagging fit by changing the underlying truth distribution of the pseudo-data N_1^i and N_2^i counts, to see if the fit converges towards the truth even when using different samples/underlying distributions. The only values changed are therefore the N_1^i and N_2^i, while the rest of the parameters remain unchanged and are taken from the nominal values. In particular the tests were performed with two samples with varied top mass, one with $m_{\text{top}} = 169$ GeV and another with $m_{\text{top}} = 176$ GeV. The background used is the same as the nominal background. The reconstruction efficiency and b-tagging correlation coefficient are taken from the nominal $t\bar{t}$ POWHEG + PYTHIA 8 sample with $m_{\text{top}} = 172.5$ GeV. These tests are called stress tests, since they change the underlying distribution to be tested, without changing the parameters used to unfold to the particle level true cross section, and their aim is to assess whether the technique works even if there are unexpected behaviours in the data.
The true cross section is evaluated using the true $t\bar{t} \to e\mu$ events from the alternative top mass samples as well. For both samples, 1000 pseudo-experiments were carried out, the $(\sigma_j^i - \sigma_{true}^i)/\sigma_{true}^i$ distributions of the pseudo-experiments were fitted with gaussians and the result of the these are seen in Fig. 7.6(a)-7.6(g) and Fig. 7.7(a)-7.7(g) for the absolute differential cross section distributions and in Fig. 7.6(h) and Fig. 7.7(h) for the total fiducial cross section, where the points are the mean of the gaussian distributions and the error bars are the corresponding standard deviations. For the stress tests with $m_{\text{top}} = 176$ GeV, it can be seen that the fitting is quite stable, with the bias being small compared to the error bars. On the other hand, the stress tests with $m_{\text{top}} = 169$ GeV show a bit more bias in the results, especially for the $m(\ell^+\ell^-)$ and the p_{T} (ℓ) distributions. This is not surprising since a smaller assumed m_{top} will lead to a smaller $G_{e\mu}$ at small total top quark transverse momenta. All biases are though within a few standard deviations. The corresponding results for the normalised differential distributions are in Fig. 4 and Fig. 5 in Appendix C.

7.4.3 Closure tests

Closure tests were performed to assess the ability of the double tagging fit to converge on the correct answer within the computed uncertainty, using only a part of the Monte Carlo events available. The aim of the closure tests is to assess whether the technique works even if there is a smaller statistics than expected. The $t\bar{t}$ and background samples were divided into two independent parts by using the Monte Carlo event number, events with an even event number went to one subsample and events with an odd event number to the other. One part was used to calculate the $G_{e\mu}^i$, C_b^i, $N_{1,bkg}^i$ and $N_{2,bkg}^i$, while the other was used to calculate the pseudo-data N_1^i and N_2^i values, which were fluctuated 1000 times using a Poissonian with N_1^i and N_2^i as mean. This was done in order to ensure statistical independence between the pseudo-data counts and the other elements of the double tagging technique. The cross section extracted from each pseudo-experiment was compared to the true cross section evaluated using true $t\bar{t} \to e\mu$ events. The results are shown in Fig. 7.8(a)-7.8(g) for the absolute differential cross section distributions

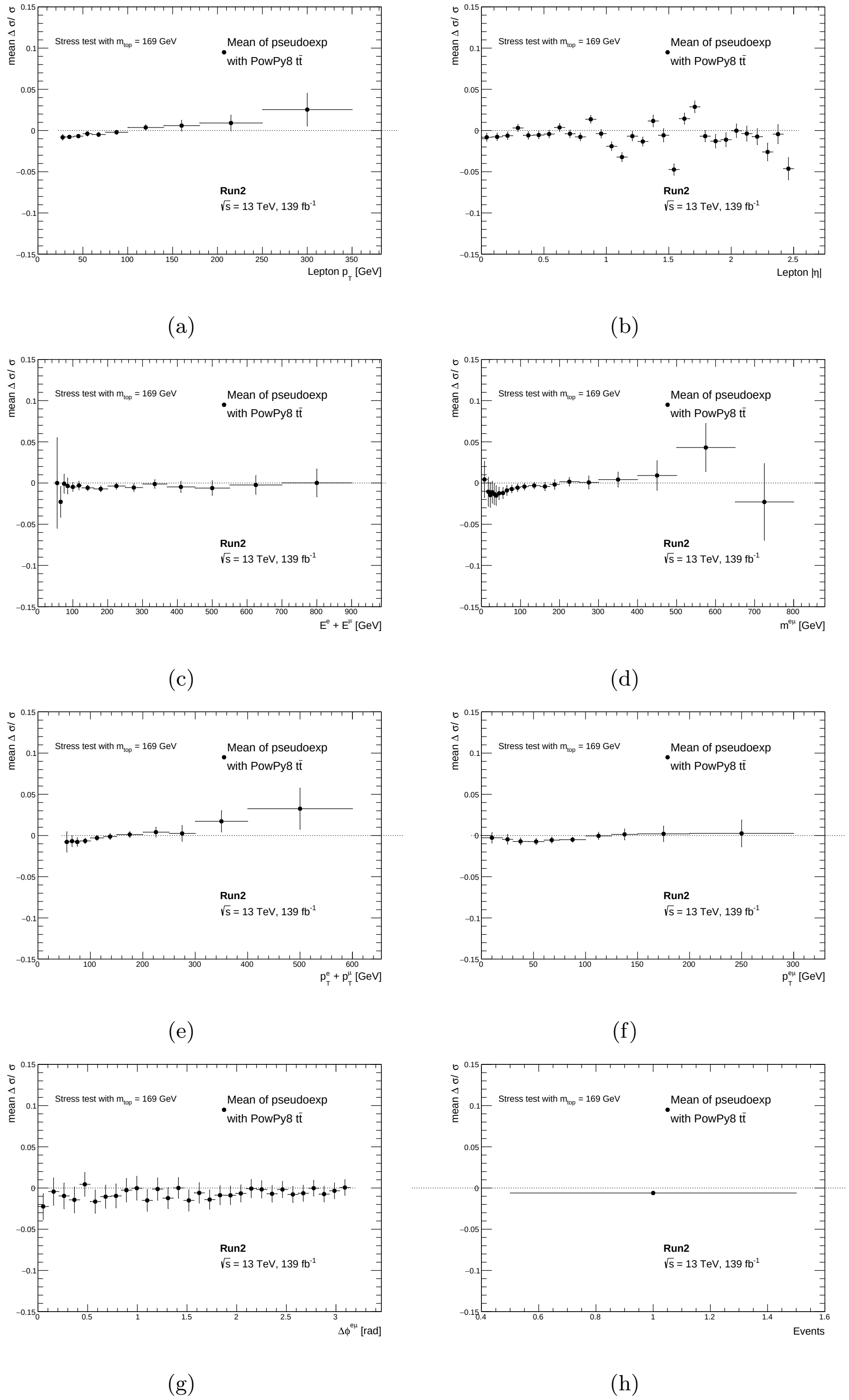

(a) (b) (c) (d) (e) (f) (g) (h)

Figure 7.6: Mean and standard deviations extracted from the gaussian functions fitted to the 1000 stress test pseudo-experiments results for each bin in each absolute differential distribution in (a)-(g) and for the total fiducial cross section in (h) using the $t\bar{t}$ Powheg + Pythia 8 sample with $m_{\text{top}} = 169$ GeV as signal sample to construct the pseudo-data.

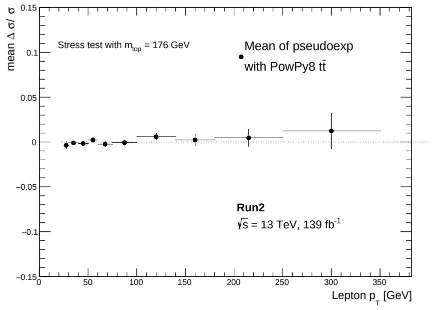

(a)

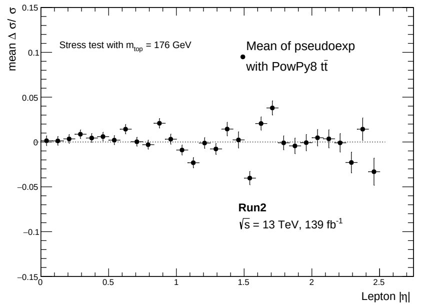

(b)

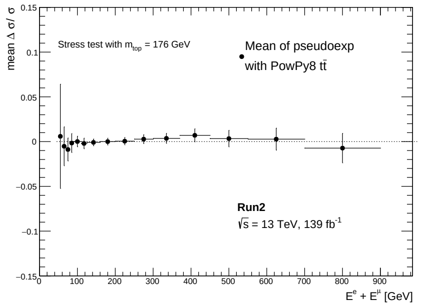

(c)

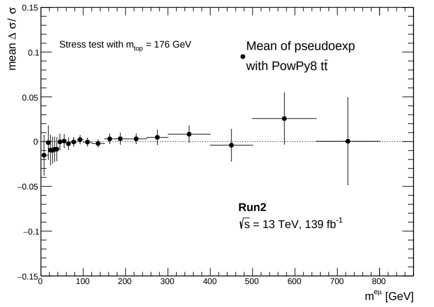

(d)

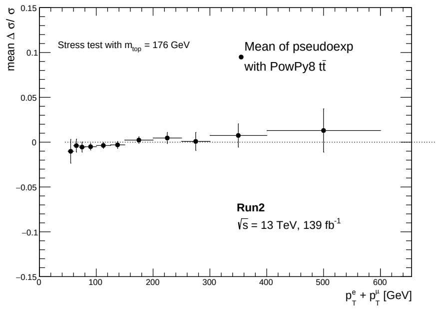

(e)

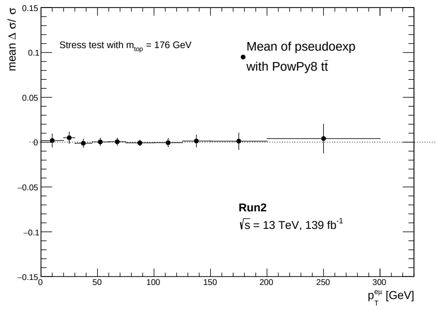

(f)

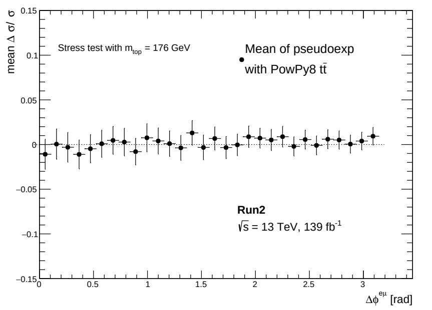

(g)

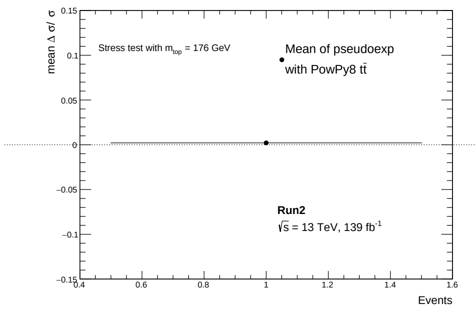

(h)

Figure 7.7: Mean and standard deviations extracted from the gaussian functions fitted to the 1000 stress test pseudo-experiments results for each bin in each absolute differential distribution in (a)-(g) and for the total fiducial cross section in (h) using the $t\bar{t}$ Powheg + Pythia 8 sample with $m_{\text{top}} = 176$ GeV as signal sample to construct the pseudo-data.

and in Fig. 7.8(h) for the total fiducial cross section and, even with a partial dataset, the double tagging technique performs well, since the mean of the normalised residuals of the pseudo-experiments is close to zero, within the standard deviation of the experiments. The corresponding results for the normalised differential distributions are in Fig. 6 in Appendix C.

7.4.4 Bootstrapping tests

Another validation technique used is bootstrapping, which is a re-sampling technique that makes it possible to evaluate statistical uncertainties as well as to uncover correlations between bins of the same and of different distributions [101, 102]. In order to create toy experiments with bootstrapping, each event used in the analysis (this applies both to data and Monte Carlo events) is assigned a series of weights, each of which is drawn from a Poissonian distribution with mean 1 (the most popular weights are then 0, 1, 2, 3 and 4). The event is then filled in the nominal histogram and in a series of replica histograms, where for each replica the event weight is multiplied by the corresponding poissonian weight for that replica. To make sure, that each event has an unique set of Poissonian weights, the seed used to generate the weights is changed for every event (for Monte Carlo events it is eventNumber +100·mcChannelNumber while for data events it is eventNumber +100·runNumber).
The first bootstrapping validation test was performed using the bootstrapped data events with 1000 replicas, meaning that for each bin in each distributions the double tagging technique was solved 1000 times, each time with a bootstrapped number of data events N_1^i and N_2^i. The reconstruction efficiency and b-tagging correlation coefficient were taken from the nominal $t\bar{t}$ POWHEG + PYTHIA 8 sample, while the number of background events are taken from the nominal background estimates (and are not bootstrapped). The 1000 replicas are then used to find the covariance matrix, which contains information about the bin-to-bin correlation within one variable and amongst bins of different variables and, in the diagonal elements, contains the data statistical uncertainty. The correlation matrix can be extracted and it is shown in Fig. 7.9 for both the absolute and normalised differential cross section.
The correlation matrix for the absolute differential cross section shows that there are almost no correlations between bins of one distribution as expected, since each bin is filled independently from the other bins in the same distribution, with the exception of the $p_{\mathrm{T}}(\ell)$ variable, since this is filled twice per event, once for the electron and once for the muon (if the electron has a low p_{T}, the muon has a high probability of having a low p_{T} as well). There are instead correlations between bins of different distributions and those are mostly positive, especially for $p_{\mathrm{T}}(\ell^+\ell^-)$, $p_{\mathrm{T}}(\ell^+)+p_{\mathrm{T}}(\ell^-)$, $p_{\mathrm{T}}(\ell)$, $E(\ell^+)+E(\ell^-)$, $m(\ell^+\ell^-)$, because, for example, an event with high p_{T} leptons will likely have a high $p_{\mathrm{T}}(\ell^+\ell-)$, $p_{\mathrm{T}}(\ell^+) + p_{\mathrm{T}}(\ell^-)$, $E(\ell^+) + E(\ell^-)$ and $m(\ell^+\ell^-)$. $|\eta(\ell)|$ and $\Delta\phi(\ell^+\ell^-)$ are not as strongly correlated with other variables. When looking at the correlation matrix for the normalised differential cross section the positive correlations between bins of different distributions are still there, and new negative correlations arise between the bins of one distribution, due to the normalisation condition, where all bins are shifted.

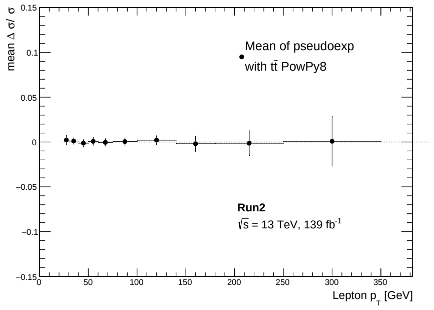

(a)

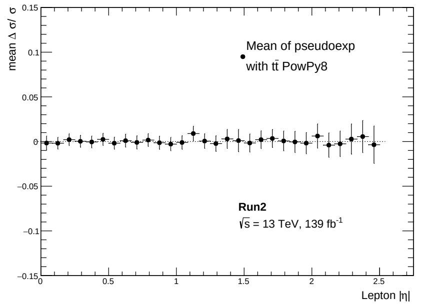

(b)

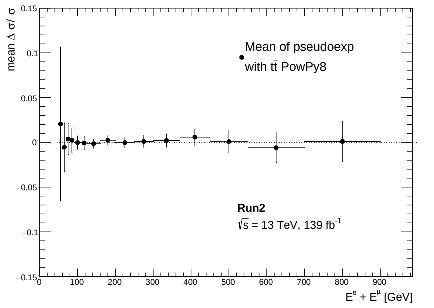

(c)

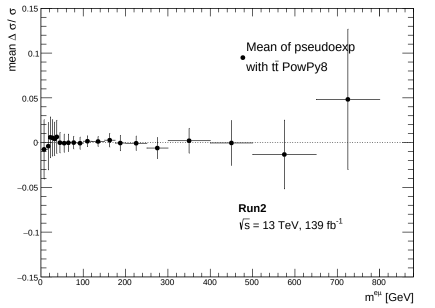

(d)

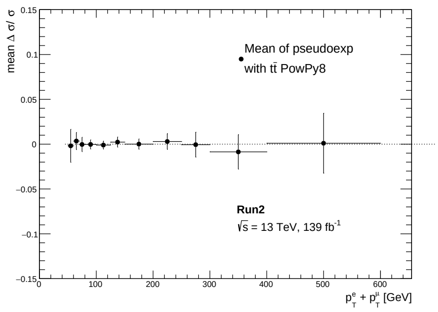

(e)

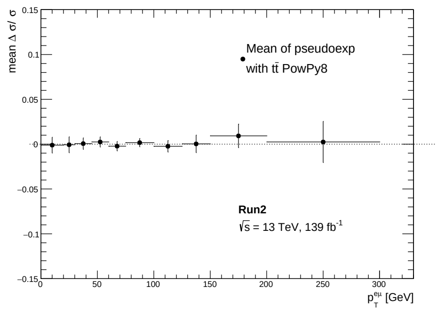

(f)

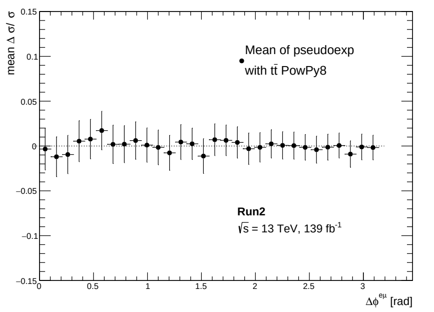

(g)

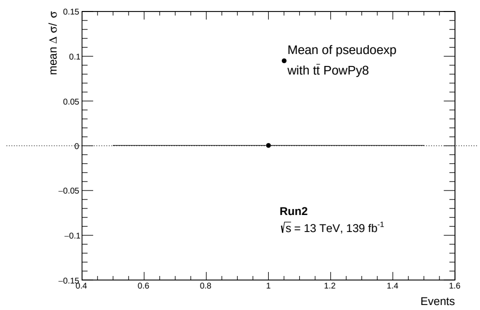

(h)

Figure 7.8: Mean and standard deviations extracted from the gaussian functions fitted to the 1000 pseudo-experiments results for each bin in each absolute differential distribution in (a)-(g) and for the total fiducial cross section in (h) performed on a subpart of the total nominal $t\bar{t}$ POWHEG + PYTHIA 8 sample sample for closure tests. The mean is in all cases consistent with zero within the standard deviation, demonstrating that the double tagging technique works with lower statistics than expected.

The second bootstrapping validation test was performed using Monte Carlo events as pseudo-data, where the Monte Carlo events are bootstrapped instead of data. Again 1000 pseudo-data toy Monte Carlo replicas were generated using the bootstrapping replica histograms from the nominal $t\bar{t}$ POWHEG + PYTHIA 8 sample as signal plus background from the bootstrapping replicas of the nominal background samples. The sum of the signal and background bootstrapped counts were used as pseudo-data in the double tagging technique's N_1^i and N_2^i. In this case, the fake lepton background was not estimated as in the nominal background, but it was taken directly by Monte Carlo by adding all the bootstrapped fake lepton contributions in the OS region. The reconstruction efficiency and b-tagging correlation coefficient were taken from the nominal $t\bar{t}$ POWHEG + PYTHIA 8 sample, while the number of background was taken from the nominal samples. The double tagging equations were solved 1000 times for each bin in each differential distribution. Again the correlation matrix extracted from these experiments is seen in Fig. 7.10 for both the absolute and normalised differential cross section. The same tendencies are seen as in the data bootstrapping experiments. Again here, the diagonal elements of the covariance matrices for single differential distributions can be used as the Monte Carlo statistical uncertainty.

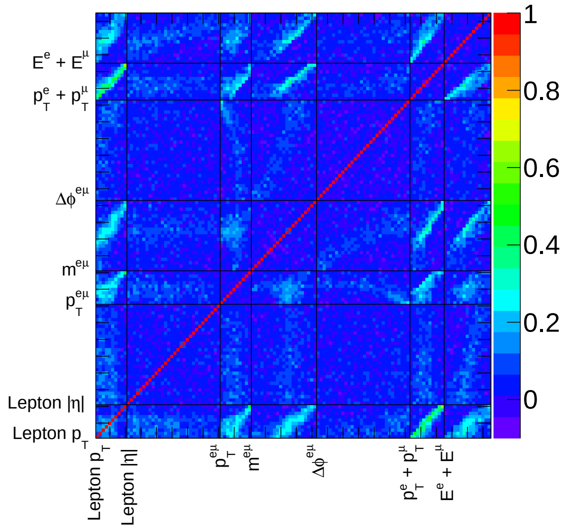

(a)

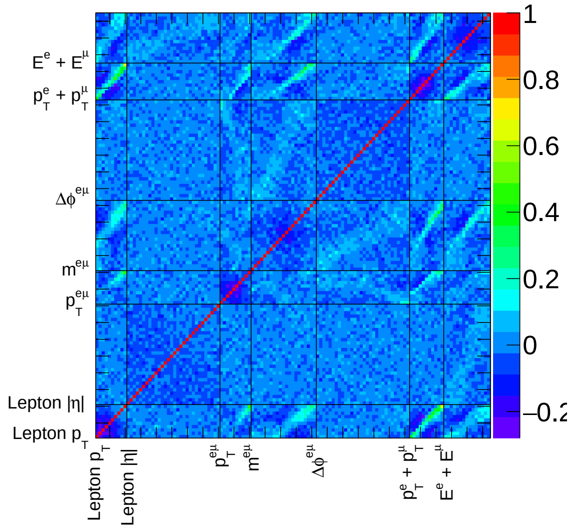

(b)

Figure 7.9: Correlation matrices for the normalised and absolute differential cross section from data bootstrapping experiments.

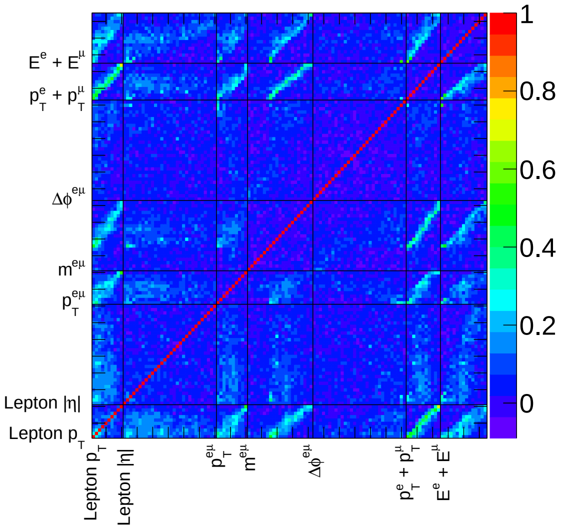

(a)

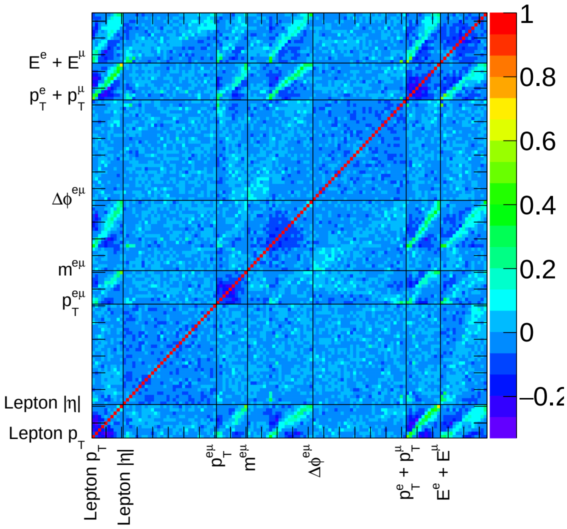

(b)

Figure 7.10: Correlation matrices for the normalised and absolute differential cross section from Monte Carlo bootstrapping experiments

CHAPTER 8

SYSTEMATIC UNCERTAINTIES

The effect of each systematic uncertainty on the total and differential cross section has been determined by recalculating each parameter of the double tagging technique with the appropriate shift, and re-solving the equations to find the shifted cross section. Depending on the systematic uncertainty though, only some of the elements of Eq. 7.5 and Eq. 7.15 need to be recalculated and therefore the systematic uncertainties have been divided into five major families:

detector and reconstructed objects systematic uncertainties: this category collects all the systematic uncertainties related to the reconstructed objects, as electrons, muons, jets, b-jets, and the systematic uncertainties related to the detector, such as the pileup. These systematic uncertainties affect all the elements of the double tagging equations.

$t\bar{t}$ **related systematic uncertainties**: this category is for all the systematic uncertainties connected to the $t\bar{t}$ production, such as ISR and FSR, PDF, matrix element generator and fragmentation. Since the $t\bar{t}$ sample is not part of the background, these systematic uncertainties affect only the reconstruction efficiency, the acceptance factor and the b-tagging correlation coefficient.

background related systematic uncertainties: this category is for the systematic uncertainties connected to the different backgrounds, which include possible variations in the cross sections used to normalise them, variations due to the modelling and estimation of data-driven backgrounds. These systematic uncertainties affect only the count of background events in Eq. 7.5 and Eq. 7.15.

integrated luminosity systematic uncertainty: this category is only for the systematic uncertainty on the integrated luminosity. This affects the value of the integrated luminosity in Eq. 7.5 and Eq. 7.15 and the number of background events.

beam energy systematic uncertainty: this category is only for the systematic uncertainty due to the uncertainty on the beam energy, which affects the value of the final cross section at 13 TeV, and changes the reconstruction efficiency and the b-tagging correlation coefficient in Eq. 7.5 and Eq. 7.15 and the acceptance factor in Eq. 7.13.

MC statistics systematic uncertainty: this category is only for the systematic uncertainty due to the limited statistics of Monte Carlo based variables and it affects all the elements of the double tagging equations.

8.1 Detector and reconstructed objects

Since the events are reconstructed in the detector, we need to take into consideration the systematic uncertainties that can arise due to features of the detector itself, as event triggering, object reconstruction (electron, muons and jets) and pileup. When selecting events with `AnalysisTop-21.2.65`, several packages are loaded to calculate the up and down variations and weights for each event in Monte Carlo, allowing for the calculation of the cross section for each systematics variation. In Table 3 in Appendix D all the variations are divided into categories.

Electron scale and resolution The energy scale and resolution of electrons are calculated using $Z \to ee$ events and $J/\Psi \to ee$ events. The uncertainties due to the electron energy scale and energy resolution are calculated by shifting the objects (electrons in this case) in energy.

Electron efficiency The trigger, reconstruction, isolation and identification efficiencies for electrons are derived with the tag-and-probe technique using $Z \to ee$ events, $J/\Psi \to ee$ events and $W \to e\nu_e$ events and using electrons with $\Delta R(e, jet) > 0.4$ in different η and p_{T} bins. Scale factors are computed to account for the difference in efficiency in Monte Carlo samples and data. The systematic uncertainties for these scale factors are calculated by shifting them up and down with $\pm 1\sigma$ variation independently. For all the efficiencies the up and down variations are

calculated by assuming that the systematic uncertainties on all η and p_T bins are fully correlated, in order to approximate the up and down variations to one single variation.
This measurement is though quite sensitive to the electron identification efficiency uncertainty and assuming 100% correlation between all η and p_T bins leads to a overestimation of this uncertainty. Therefore a more complex correlation model (called *SIMPLIFIED*), which takes into account the real correlations between bins, needs to be used [103]. In this way, only some of the bins are highly correlated, while most of the bins are uncorrelated and their contribution to the systematic uncertainty will be minimal. The η and p_T binning used to find the correlations are $|\eta| = [0.0, 1.37, 4.9]$ (effectively we use only $|\eta|$ up to 2.5) and $p_T = [4, 7, 10, 15, 20, 25, 30, 60, 80, 13000]$ GeV.
With this correlation model ~ 30 up and down variations for the identification efficiency scale factors are introduced. This model is applied to the nominal $t\bar{t}$ POWHEG + PYTHIA 8 sample using `AnalysisTop-21.2.84` and the reconstruction efficiency $G_{e\mu}$ and the b-tagging correlation coefficient C_b are recalculated for each up and down variation, while the number of background events is not recalculated (the nominal values are used), since the major contribution to this systematic uncertainty comes from the uncertainty on the reconstruction efficiency.

Muon scale and resolution scale The systematic uncertainties related to the μ scale and resolution are a $\pm 1\sigma$ variation of the momentum of the inner detector track, of the muon spectrometer track and of the momentum scale based on different techniques [87].

Muon reconstruction efficiency The scale factors to take the muon identification efficiency into account are derived from J/Ψ and $Z \to \mu\mu$ events using the tag-and-probe technique [87]. The systematic uncertainties on these scale factors are calculated by shifting the factors up and down with $\pm 1\sigma$ statistic and systematic variations, separately for the low p_T region ($p_T < 15$ GeV) and for the remaining p_T region.

Muon trigger, ISO, TTVA efficiency The scale factors to correct the Monte Carlo to data for μ trigger efficiency, isolation and track-to-vertex associations efficiencies are varied up and down with $\pm 1\sigma$ statistical and systematic variations independently [87].

JVT The jet vertex tagger efficiency scale factor weight is used to correct for the JVT efficiency and hence match Monte Carlo and data. Its systematic uncertainty is found by varying the scale factor weight with its $\pm 1\sigma$ variation, this method though affects the reconstruction efficiency in the total fiducial cross section with a 0.45% uncertainty, leading to an uncertainty on the total cross section of also 0.45%. Since the reconstruction efficiency is a purely leptonic variable and does not depend on the number of jets in each event, the uncertainty from the JVT cut on this should be zero and the total uncertainty on the cross section should be dictated by the uncertainties on the b-tagging correlation coefficient

and on the number of background events. Before putting the uncertainty from JVT on the reconstruction efficiency to zero, tests need to be done to assess whether this is a fair assumption. In particular, a factor that could contribute to the uncertainty on $G_{e\mu}$ is that JVT failing jets participate in the overlap removal of objects, but they cannot remove other objects. This could lead to a difference in the number of $e\mu$ events at reconstruction level depending on the JVT working point used, hence changing $G_{e\mu}$ with the JVT working point.
Therefore, in order to have an idea of the actual size of the JVT uncertainty, a few checks were carried out. The fraction of leptons removed by overlap removal to the total number of leptons in a event was calculated. In most of the cases the fraction of leptons removed in overlap removal is zero, only in 0.1% of the selected $e\mu$ events this is different from zero. This overlap-removed lepton fraction was multiplied to the relative difference between the JVT efficiency and its up and down variations for each jet in the event. Again, in most of the events this resulted in a zero uncertainty, while in the events where the fraction of leptons removed by overlap removal was bigger than zero, the the JVT uncertainty estimated with this method amounted in average to approximately 0.03%, as visible in Fig. 8.1.

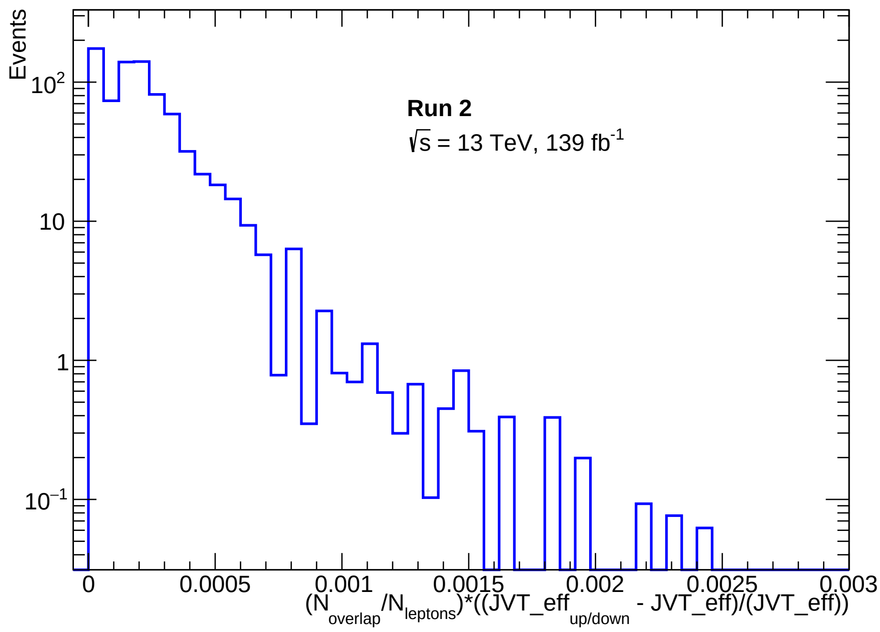

Figure 8.1: Estimation of the JVT uncertainty

Given the above tests, the error on the reconstruction efficiency in the total and differential cross section was set to zero and the JVT systematic uncertainty is calculated by varying the b-tagging correlation coefficient and number of background events with the up and down variations of the JVT scale factor uncertainty.

JES effective NPs The uncertainties in the jet energy scale are derived using Z + jet, γ + jet and multijet samples at $\sqrt{s} = 13$ TeV with data or simulation calibration corrections [104]. In total 15 nuisance parameters are varied up and down, where all variations are orthogonal to each other and are assumed uncorrelated.

JES EtaInterCalibration The η intercalibration is a way to calibrate the jet energy scale from jets in the forward region ($0.8 < |\eta| < 4.5$) from jets in the barrel ($|\eta| < 0.8$) [104]. The uncertainty due to this calibration is performed by shifting the energy of the physics objects with the up and down variations of the calibration. The systematic uncertainties components include a statistical component, a modelling component (that accounts for different Monte Carlo generators modelling of the physical objects and pileup modelling) and a non-closure component of the technique in the $2.0 < |\eta| < 2.6$ region.

JES flavour Jets contain different quark flavours and gluons, but when reconstructing the jet, uncertainties arise on their actual composition. Additionally, the jet energy scale calorimetric response poses a systematic uncertainty [104]. Both those uncertainties are found by shifting the physics objects' energy and momentum with the up and down variations of these uncertainties.

JES b-jes response The uncertainty due to the calorimetric response to b-jets is found by shifting the appropriate physics objects' energy with up and down variations [104].

JES pileup The jet energy scale pileup uncertainty comes mainly from Monte Carlo simulation modelling, in particular the number of average interactions μ, number of primary vertices N_{PV} and the modelling of the p_{T} distributions. These uncertainties are found by shifting the physics objects' energy and momentum with the up and down variations of these uncertainties.

JES PunchThrough When a jet has such a high p_{T}, that the jet is no longer contained in the calorimeter, but crosses over to the muon spectrometer, we denote it as a punch-through jet. Up and down uncertainty variations due to the correction of these jets are applied to all relevant physics objects.

JES HighPt This uncertainty is due to high p_{T} jets response in the detector and is calculated by shifting the physics objects' energy and momentum with the up and down variations of these uncertainties.

MET soft term The uncertainties related to missing energy $E_{T,miss}$ is found by data/Monte Carlo comparison of the p_{T} distribution of the missing energy components.

JER The jet energy resolution uncertainty is found by using the 7 orthogonal nuisance parameter model, where the object are recalculated for each parameter's up and down variations. Besides the 7 parameters, another uncertainty taking the data vs Monte Carlo disagreement into consideration is calculated using symmetrized variations.

***b*-tagging** The b-tagging efficiency scale factor for a specific working point is applied to Monte Carlo events through a weight and therefore the uncertainties on the b-tagging are calculated by varying this scale factor weight. The uncertainty on b-jets efficiency is found with nine eigenvectors (with up and down symmetrisation), the uncertainty on $c-$jets efficiency is found with four eigenvectors and the uncertainty on light jets efficiency is found with five eigenvectors [93].

8.2 $t\bar{t}$

The $t\bar{t}$ related uncertainties have an impact on the reconstruction efficiency and of the b-tagging correlation coefficient of the double tagging technique, see Eq. 7.5, and on the acceptance factor of Eq. 7.13. Most of these uncertainties can be calculated with alternative $t\bar{t}$ samples, others require a reweighting of the nominal sample in order to generate the variations of the parton shower. The list of $t\bar{t}$ uncertainties and an overview of how they are calculated is described here.

Hard scattering The uncertainty due to the matrix element generation of the events is determined by comparing the nominal $t\bar{t}$ POWHEG + PYTHIA 8 sample with the alternative sample generated with MADGRAPH5_aMC@NLO interfaced with PYTHIA 8 [105]. The effect of using the MADGRAPH5_aMC@NLO + PYTHIA 8 sample on $E_{e\mu}$, $G_{e\mu}$ and C_b are shown in Table 8.1.

top p_T reweighting The major impact that different matrix element generators have on a kinematic analysis is the modelling of the p_T of the top quark (at parton level). In this analysis, this is reflected in the modelling of the p_T of the leptons, which in the nominal $t\bar{t}$ POWHEG+PYTHIA 8 sample is quite evident not optimal, see Fig. 5.2, 5.3, 5.4 and 5.3 [19, 20, 95]. Therefore another way of estimating the hard scattering uncertainty is to correct the p_T of the top quark in the nominal $t\bar{t}$ POWHEG+PYTHIA 8 sample through reweighting instead of using another generator, and compare this to the nominal $t\bar{t}$ POWHEG+PYTHIA 8 sample without reweighting. The corrections are based on the NNLO QCD + NLO EW differential predictions from [106]. In order to accomplish this, for each reconstructed $e\mu$ event the corresponding truth level event is found (at parton level) and the top p_T correction is derived using the p_T of the top quark after radiation. This correction is applied to the event weight along with the Monte Carlo weight and the appropriate scale factors. The effect of the reweighting on $E_{e\mu}$, $G_{e\mu}$ and C_b for the total inclusive and fiducial cross section are shown in Table 8.1.

Fragmentation The systematic uncertainty related to the different fragmentation or hadronisation models can be assessed using a different fragmentation model than the one used in the PYTHIA samples, the Lund model. In particular the Herwig model is used as the alternative one. Therefore the nominal sample is compared to a sample using the same events, which are showered with HERWIG 7 instead of PYTHIA 8 [105]. The effect on $E_{e\mu}$, $G_{e\mu}$ and C_b of using the POWHEG + HERWIG 7 sample are shown in Table 8.1.

ISR The initial state radiation systematic uncertainty is found by reweighting, which adapts the sample to a varied renormalisation and/or factorisation scale. In Monte Carlo samples, the renormalisation scale μ_R is the energy scale at which the coupling α_S is calculated, while the factorisation scale μ_F is the energy scale at which the PDF is evaluated. The down variation is found by substituting the Monte Carlo event weight in the nominal $t\bar{t}$ POWHEG+PYTHIA 8 dilepton sample (though the AFII sample, to be consistent with the high ISR variation) with a new weight that doubles the renormalisation and factorisation scale, $\mu_{R,down} = 2.0\mu_R$ and $\mu_{F,down} = 2.0\mu_F$, which are then multiplied with the Var3cDown weight from the A14 tune, in order to adjust the α_S parameter (and the product of the weights is divided by the original Monte Carlo weight, to normalise the change of the two weights) [105]. The up variation is found using again reweighting, this time with another $t\bar{t}$ POWHEG+PYTHIA 8 AFII sample, where the h_{damp} parameter is shifted to $3 \cdot m_{\text{top}}$, see Table 4.2, in order to match the data better. Here the same reweighting procedure for the down variation is applied, though now the new weights change the renormalisation and factorisation scale to the half, $\mu_{R,up} = 0.5\mu_R$ and $\mu_{F,up} = 0./mu_F$, and the Var3cUp weight is used to adjust the A14 α_S parameter (and again the product of the weights is divided by the original Monte Carlo weight) [105]. In both cases, the resulting histograms need to be normalised with an adjusted sum of weights, that takes the above changes into consideration. The effect of using the POWHEG+PYTHIA 8 sample with more or less ISR on $E_{e\mu}$, $G_{e\mu}$ and C_b are shown in Table 8.1.

FSR The final state radiation systematic uncertainty is also found by reweighting. In this case, both the up and down variations are found by reweighting the nominal $t\bar{t}$ POWHEG+PYTHIA 8 dilepton sample, by substituting the Monte Carlo weight (and the sum of weight for normalisation) with weights that change the α_S^{FSR} parameter up and down. The effect of using the POWHEG+PYTHIA 8 sample with more or less FSR on $E_{e\mu}$, $G_{e\mu}$ and C_b are shown in Table 8.1.

PDF The PDF uncertainty is again extracted through reweighting of the nominal sample. The default PDF for the nominal sample is NNPDF3.0, which is one of the PDF's included in PDF4LHC15 as described by [107]. The same article [107] gives recipes on how to determine the uncertainty on the PDF for a cross section measurement, and these guidelines were followed. First of all the cross section is calculated with the PDF4LHC15

PDF, by reweighing the nominal sample by changing the Monte Carlo weight with the appropriate weight. The value of the cross section found is then the central value. Afterwards the cross section is calculated for each of the components of the Hessian PDF4LHC15_30 error set, where each component is orthogonal to the others, again by changing the Monte Carlo weight with the appropriate Hessian PDF4LHC15_30 weight in the nominal $t\bar{t}$ sample. When the cross section is determined both with the central value and with the error set, the PDF uncertainty is found with:

$$\delta^{PDF}\sigma = \sqrt{\sum_{k=1}^{30}(\sigma^{(k)} - \sigma^{(0)})^2} \tag{8.1}$$

where 30 is the number of the vectors of the error set, $\sigma^{(k)}$ is the cross section found with each of the error set weights and $\sigma^{(0)}$ is the cross section found with the central value. The formula is taken from [107].

Table 8.1: Difference in total b-tagging correlation coefficient, total reconstruction and total preselection efficiency between the baseline dilepton Powheg + Pythia 8 sample and $t\bar{t}$ systematics samples.

Generator difference with respect to Powheg+Pythia 8 (410472 FS)	$\Delta E_{e\mu}/E_{e\mu}$ [%]	$\Delta G_{e\mu}/G_{e\mu}$ [%]	$\Delta C_b/C_b$ [%]
Powheg + Herwig 7 (410558)	-0.47	-0.19	-0.05
MadGraph5_aMC@NLO + Pythia 8 (410465)	-1.75	-0.60	-0.15
Powheg+Pythia 8 $h_{damp} = 3 * m_{\rm top}$ more ISR (410482)	-0.63	-0.35	0.10151
Powheg+Pythia 8 less ISR (410472 AFII)	0.12	-0.12	-0.06
Powheg+Pythia 8 more FSR (410472 FS)	0.21	0.15	-0.05
Powheg+Pythia 8 less FSR (410472 FS)	-0.27	-0.22	0.11
Powheg+Pythia 8 with top $p_{\rm T}$ reweighting	-0.66	-0.27	-0.03

Top mass dependence Changing the top mass changes several values of the double tagging technique, in particular the reconstruction efficiency, the acceptance factor and the number of background events, since the major background comes from Wt, where the mass of the top quark mass plays a role. In order to estimate the affect it has on the total cross section, the dependence of the different double tagging equations' parameters on the top quark mass has been studied with samples at top mass values of 169, 171, 172, 172.25, 175.5, 172.75, 173, 174 and 176 GeV.

The plot showing the dependence of $G_{e\mu}$ for the total fiducial cross section can be seen in Fig. 8.4(a), where each point is found by $\Delta G_{e\mu}/G_{e\mu} = (G_{e\mu}(m_{\rm top}) - G_{e\mu}(172.5\,\text{GeV}))/G_{e\mu}(172.5\,\text{GeV})$ and the graph is fitted with a second order polynomial. At the top mass of 172.5 GeV, which is the value used for all the Monte Carlo samples used for this analysis, the derivative of the efficiency with respect to $m_{\rm top}$ is found in order to have an estimate of the dependence of the reconstruction efficiency on the mass of the top, and its value is $0.114 \pm 0.005\,\%/\text{GeV}$, see Table 8.2 (the uncertainty on the value is found by calculating the derivative at 173.5 and 171.5 GeV and finding the difference with the central value). In the same manner the dependence on the top mass

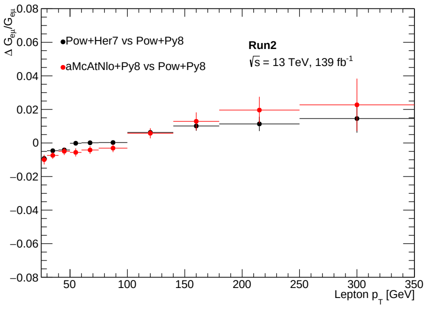

(a)

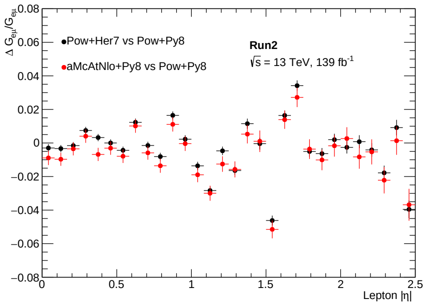

(b)

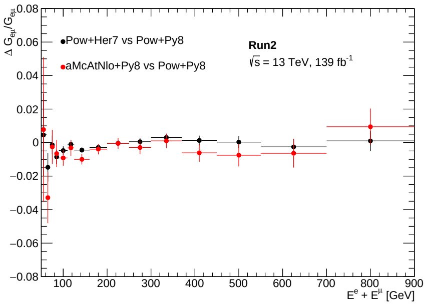

(c)

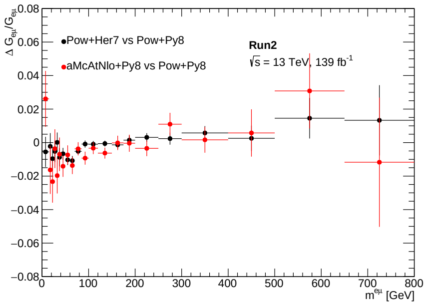

(d)

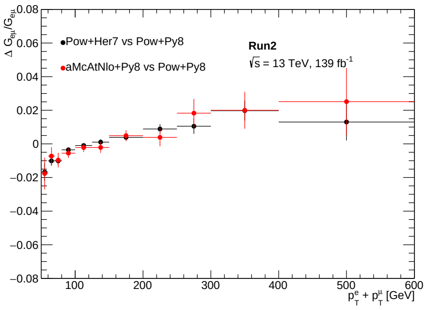

(e)

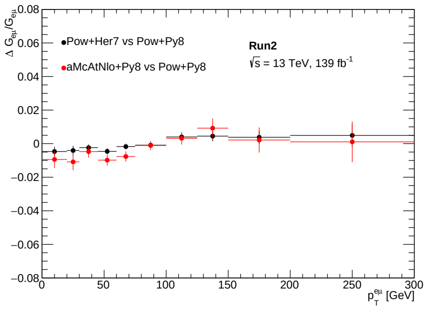

(f)

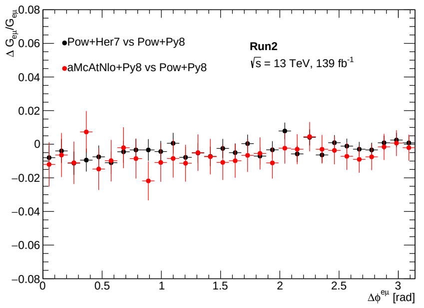

(g)

Figure 8.2: Difference in reconstruction efficiency between the baseline dilepton Powheg + Pythia 8 sample and the systematics $t\bar{t}$ samples for the hard scattering and fragmentation uncertainties for each bin of each differential distribution.

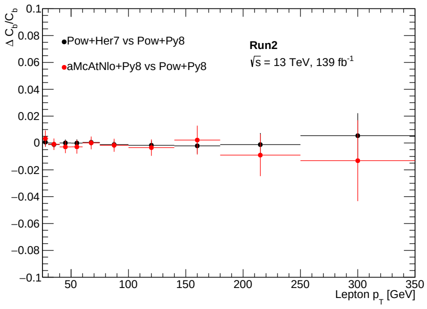

(a)

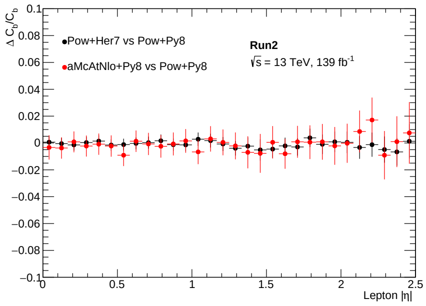

(b)

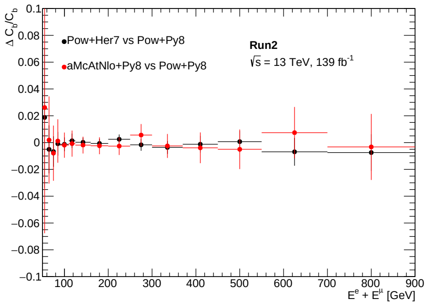

(c)

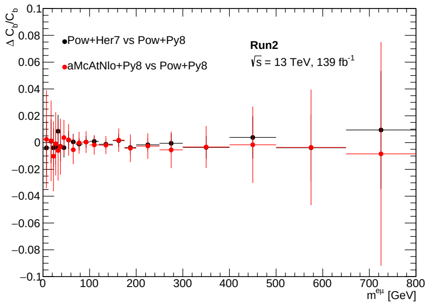

(d)

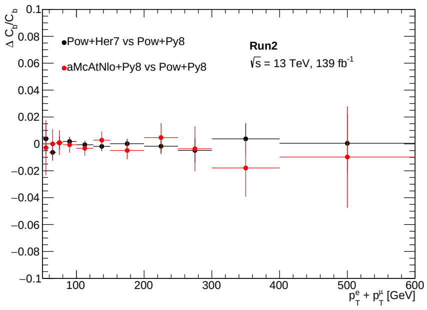

(e)

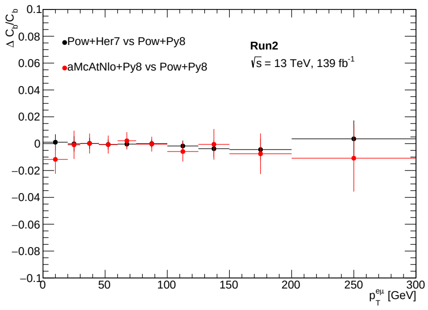

(f)

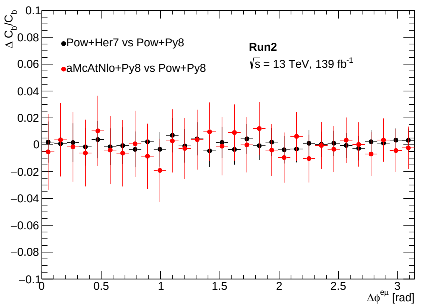

(g)

Figure 8.3: Difference in b-tagging correlation coefficient between the baseline dilepton Powheg + Pythia 8 sample and the systematics $t\bar{t}$ samples for the hard scattering and fragmentation uncertainties for each bin of each differential distribution.

for C_b is $0.0004 \pm 0.007\,\%/\mathrm{GeV}$, for the number of background events with one b-jet is $-0.76 \pm 0.02\,\%/\mathrm{GeV}$ and for the number of background events with two b-jets is $-0.58 \pm 0.04\,\%/\mathrm{GeV}$, see Table 8.2 and Fig. 8.4. The total effect of these dependencies on the total fiducial cross section amounts to $\mathrm{d}\sigma^{t\bar{t}}_{fid}/\mathrm{d}m_{\mathrm{top}} = -0.024 \pm 0.006\,\%/\mathrm{GeV}$.
The same procedure can be applied to the total inclusive cross section, where $\mathrm{d}E_{e\mu}/\mathrm{d}m_{\mathrm{top}}$ is $0.488 \pm 0.006\,\%/\mathrm{GeV}$ and its effect on the total inclusive cross section leads to $\mathrm{d}\sigma_{t\bar{t}}/\mathrm{d}m_{\mathrm{top}} = -0.399 \pm 0.008\,\%/\mathrm{GeV}$. These values are not added in Table 9.1 and Table 9.2 for the total fiducial and inclusive cross section, where the top mass uncertainty is quoted as zero. For the differential cross section the uncertainty is calculated by finding the differential cross section with the varied parameters ($G^i_{e\mu}$, C^i_b, $N^i_{1,bkg}$, $N^i_{2,bkg}$) at ± 1 GeV (from 172.5 GeV)and symmetrizing the difference between the nominal cross section and the ones with varied mass parameters. The results for the top mass uncertainty on the differential distributions are quoted in the tables in Section 9.3.

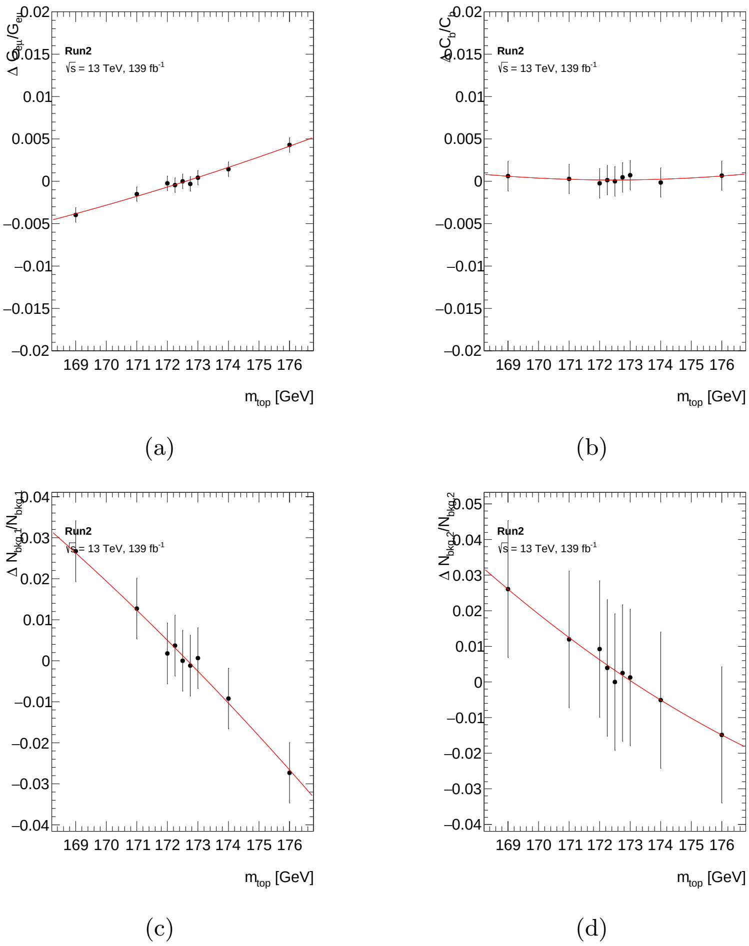

Figure 8.4: Dependence of the double tagging technique parameters on the top mass value.

Table 8.2: Derivative of the double tagging technique parameters with respect to m_{top}, evaluated at $m_{\text{top}} = 172.5$ GeV.

Quantity	Derivative [%/GeV]
$\mathrm{d}G_{e\mu}/\mathrm{d}m_{\text{top}}$	0.114 ± 0.005
$\mathrm{d}E_{e\mu}/\mathrm{d}m_{\text{top}}$	0.488 ± 0.006
$\mathrm{d}C_b/\mathrm{d}m_{\text{top}}$	0.0004 ± 0.007
$\mathrm{d}N_{bkg,1}/\mathrm{d}m_{\text{top}}$	-0.76 ± 0.02
$\mathrm{d}N_{bkg,2}/\mathrm{d}m_{\text{top}}$	-0.58 ± 0.04

8.3 Background

The background related uncertainties are calculated for each different background described in Section 4.2 independently, and they affect only the total number of background events in the double tagging technique, see Eq. 7.5. The list of background systematic uncertainties taken into consideration is described below.

Wt cross section The relative uncertainty on the Wt background theoretical cross section is 5.3% and it is calculated by [108], where the theoretical cross section uncertainty is determined in case of $\sqrt{s} = 7$ or 8 TeV. The theoretical uncertainty at $\sqrt{s} = 13$ TeV is derived with the same methods as for the $\sqrt{s} = 7$ or 8 TeV case [13–15]. The total Wt background from the top and anti-top contributions are multiplied by 1 ± 0.053 in order to find the up and down variations of this systematic uncertainty.

Wt/$t\bar{t}$ interference, DR vs DS The interference between $t\bar{t}$ and Wt is handled in the nominal samples using the diagram removal scheme. However, this is not the only choice, as another scheme has been developed, the diagram subtraction scheme, the difference between the two schemes is explained in [46] and in Section 2.2.1. The samples used to derive this systematic uncertainty are referenced in Table 4.2 and are also generated with POWHEG + PYTHIA 8 as the nominal Wt background.

Wt ISR/FSR The uncertainty due to initial and final state radiation in the Wt background is derived by reweighting of the nominal samples, in the same way as the $t\bar{t}$ samples above. The only difference is that for the ISR up variation we do not need to use a sample with a higher h_{damp}, the samples used for both the up and down variations are the nominal samples from Table 4.2.

Wt hard scattering The uncertainty in the matrix element generation is determined by comparing the nominal Wt background with the one generated using the MADGRAPH5_aMC@NLO generator interfaced with PYTHIA 8, see Table 4.2.

Wt fragmentation The systematic uncertainty due to the hadronisation or fragmentation model is assessed by comparing the nominal Wt

background to the one produced with POWHEG interfaced with HERWIG 7. The same events as in the nominal samples are generated, but they are showered with a different approach thanks to HERWIG 7 [80].

Diboson cross section The uncertainty on the diboson background theoretical cross section is 6% following [109]. The total diboson background (derived from the sum of all the sub-sample contributions) is scaled up and down with 1 ± 0.06 in order to find the up and down variations of this systematic uncertainty.

Diboson modelling The modelling uncertainty of the diboson background is assessed through reweighting of the SHERPA sample in order to change the factorisation and renormalisation scale used to generate the SHERPA samples. The seven point scale variation are changed as such: $(\mu_{R,var}, \mu_{F,var})x(0.5\mu_R, 0.5\mu_F)$, $(0.5\mu_R, 1\mu_F)$, $(1\mu_R, 0.5\mu_F)$, $(1\mu_R, 1\mu_F)$, $(1\mu_R, 2\mu_F)$, $(2\mu_R, 1\mu_F)$, $(2\mu_R, 2\mu_F)$. The uncertainty on the diboson modelling is the envelope of the scale variations.

Z+jets scale factor The scale factors derived in Section 6.2 have a statistical uncertainty due to the limited Monte Carlo events. The uncertainty from the fit amounts to less then 1%, but in order to take into consideration eventual errors due to high Monte Carlo weights or other fluctuations due to the fitting procedure, a systematic uncertainty of 5% is assigned to the derived factors, both in the one b-jet and in the two b-jet region.

Z+jets modelling The systematic uncertainty due to the modelling of the Z + jets background is derived by looking at a few alternative samples. The nominal SHERPA 2.2.1. samples are compared to POWHEG + PYTHIA 8 samples (see Table 4.2). The scaling factors are recalculated using the alternative samples and they are applied to the alternative $Z \to \tau\tau$ + jets samples, see Fig. 8.5 and Table 8.3. The POWHEG + PYTHIA 8 samples in the two b-jets selection, see Fig. 8.5(c) and 8.5(d) have a larger Monte Carlo/data discrepancy than the corresponding selection with the SHERPA 2.2.1. samples, this could be caused by the fact, that POWHEG + PYTHIA 8 does not have the matrix elements for $Z \to b\bar{b}$ production, generating the two b-jet final state only via the parton shower. This means, that the normalisation factor extracted for these samples is higher than for the SHERPA 2.2.1. samples, as shown in Table 8.3.

Table 8.3: Factors extracted from the $Z \to ee$ + jets and the $Z \to \mu\mu$ + jets control regions for the POWHEG + PYTHIA 8 samples.

Selection/number of b-jets	1 b-jet	2 b-jets
$Z \to ee$ + jets	1.270 ± 0.002	2.34 ± 0.02
$Z \to \mu\mu$ + jets	1.347 ± 0.002	2.45 ± 0.02

Fake lepton background When performing the estimate of the number of misidentified leptons in the OS region using Eq. 6.1, the R_b^i factor

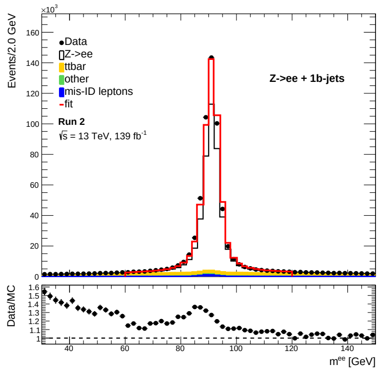

(a)

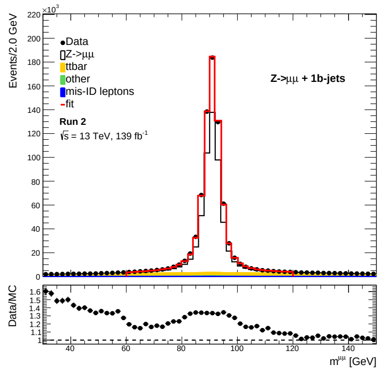

(b)

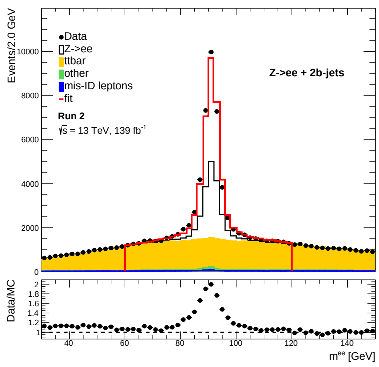

(c)

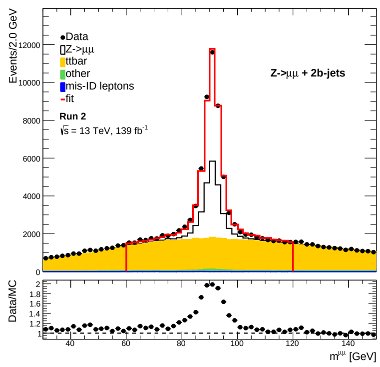

(d)

Figure 8.5: Control regions to extract the Z-factor that normalises the POWHEG + PYTHIA 8 simulated samples to data. Different components, as $t\bar{t}$, diboson and misidentified leptons are also included as part of the background. The fit to extract the Z-factor is performed between 60 GeV and 120 GeV.

derived from Monte Carlo and the $N_b^{i,promptRS,SS}$, the number of SS prompt events from Monte Carlo estimations, are affected by systematic uncertainties. The origin of these systematic uncertainties is the fact that a series of assumptions are made both on the mechanisms to produce the secondary or misidentified leptons, and on instrumental effects that result in misidentified leptons. The number of data events $N_b^{i,data,SS}$ has also a statistical uncertainty and this contribution is also included. For each detector systematic uncertainty, the values of R_b^i, $N_b^{i,prompt,SS}$ and $N_b^{i,data,SS}$ are recalculated and a new estimate of the fake lepton background is performed, while for the rest of the $t\bar{t}$ and background uncertainties, these numbers are taken as their nominal values. This does not mean though, that these values could not be affected by a different fragmentation model, for example, or by one of the background samples. For this reason, instead of recalculating the misidentified lepton background each time we change one of the signal or background samples, we apply a conservative 50% systematic uncertainty on the number of prompt RS events in the SS region, both for the one and two b-jets selections, while the R_b^i are varied up and down, with 25% for the one b-jet sample and with 50% for the two b-jet sample [13–15, 110].

$t\bar{t}V$ cross section The uncertainty on the $t\bar{t}$ V cross section is 13% following [111].

8.4 Luminosity

The integrated luminosity uncertainty affects two parts of the double tagging technique, one is the value itself of the integrated luminosity, which is included in Eq. 7.5 and in Eq. 7.15, the other is the number of background events. The reconstruction efficiency and the b-tagging correlation coefficient are not affected, as they are ratios and are hence not affected by normalisation uncertainties. The uncertainty in the combined $2015 - 2018$ integrated luminosity is 1.7% [68], obtained using the LUCID-2 detector [112].

8.5 Beam energy

The beam energy value is one of the parameters the theoretical value of the cross section depends on and therefore it needs to be taken into consideration in the systematic uncertainty evaluation. The uncertainty due to the LHC beam energy is considered as an experimental uncertainty and added to the rest of the systematic uncertainties. This uncertainty is parametrised in [7] and the recommendation for $\sqrt{s} = 13$ TeV analyses is to use an uncertainty of 0.23%. This value is used for the uncertainty on the total fiducial and inclusive cross section.

To extract the uncertainty on each bin of the normalised and absolute differential cross section, a reweighting method is used on the MadGraph5_aMC@NLO + Pythia 8 sample, using the nominal value for the uncertainty on the LHC beam energy, which is evaluated to 0.1% [113]. Each Monte Carlo event weight was reweighted with a ratio to correct the PDF for the higher or lower beam energy using the LHAPDF library [114]. The reweighting ratio is:

$$R = \frac{f(x_1^{mod}, Q^2) \cdot f(x_2^{mod}, Q^2)}{f(x_1, Q^2) \cdot f(x_2, Q^2)} \tag{8.2}$$

where x_1 and x_2 are the momentum fractions of the partons (also called Bjorken-x values), x_1^{mod} and x_2^{mod} are the shifted momentum fractions and Q^2 is the energy scale of the collision. The x_1^{mod} and x_2^{mod} are found as: $x_i^{mod} = x_i \cdot (1 \pm 0.001)$, where 0.001 comes from the LHC beam energy uncertainty of 0.1% [113]. The sum of weights used for normalisation is changed correspondingly, to take the new weights into consideration. The method to calculate the beam energy uncertainty was taken from [16, 110].
The effect of the beam energy on the differential measurements is very small and it amounts to a systematic uncertainty of $\sim 0.01\%$.

8.6 MC statistics

The Monte Carlo statistical uncertainty is derived from the diagonal elements of the Monte Carlo covariance matrix extracted by doing bootstrapping experiments explained in Section 7.4. In the case of the total fiducial and inclusive cross section, the Monte Carlo statistical uncertainty is derived using Poissonian fluctuation experiments, as also explained in Section 7.4.

CHAPTER 9

RESULTS

9.1 Total fiducial cross section

The results for the total fiducial cross section can be seen in Table 9.1, where the total uncertainty due to both statistical and systematic effects amounts to 2.34%. The total fiducial cross section for the full Run 2 dataset is found to be:

$$\sigma_{fid,t\bar{t}} = 10.67 \pm 0.02 \pm 0.20 \pm 0.14\,\text{pb}$$

where the first uncertainty is the statistical one, the second is the luminosity uncertainty and the last is the systematic uncertainty from all of the other sources. Looking closely at the table and at the different contributions, it is clear that the total uncertainty is dominated by the luminosity uncertainty. It is also by far larger than the statistical uncertainty, making this measurement totally systematic dominated. Another large uncertainty is the one coming from the single top Wt background, where the main contributions are the uncertainties related to its cross section and to the $t\bar{t}/Wt$ interference modelled with the diagram removal and diagram subtraction schemes (see Table 4 in Appendix E). A study performed in ATLAS with the $2015-2016$ data showed that neither the diagram subtraction nor the diagram removal scheme are accurate descriptions of the data, especially in the high invariant mass region, where the data are somewhere in between the two models [115]. These Wt

uncertainties are theoretically limited and until we have a better error estimate on the cross section or a better theoretical and Monte Carlo modelling of the $t\bar{t}/Wt$ interference, this uncertainty is hardly reducible.
The pileup uncertainty is also quite high, probably due to the high pileup conditions of data taking in especially 2017 and 2018. This uncertainty could though be slightly overestimated, since we are looking at a quite pure signal of leptons. To check for this, the isolation of leptons could be measured in-situ in data events, in that way the pileup information is included in the lepton isolation uncertainty and the pileup uncertainty could be removed, so not to include it twice.
The jet and missing energy related uncertainties are very small or even zero, as expected, since no cuts on the jets have been applied. A slightly higher uncertainty is observed for the b-tagging, which comes from the up and down variations of the b-tagging scale factors applied on Monte Carlo events.
Finally the result is affected by the $t\bar{t}$ uncertainties, in particular by the hard scattering uncertainty, pointing to the fact that $t\bar{t}$ Monte Carlo modelling still has room for improvement [19, 105]. As explained in Section 8.2, the hard scattering uncertainty could be evaluated by applying a top p_{T} correction based on NNLO QCD + NLO EW calculations, instead of using the alternative MadGraph5_aMC@NLO generator. In this case the hard scattering uncertainty would drop to 0.24% and the total uncertainty on the total fiducial cross section would drop to 2.31%.

Compared to the results obtained in Run 1 in [13, 14], where the total uncertainty on the total inclusive cross section amounts to 3.9% and 3.6% for the measurement at $\sqrt{s} = 7$ TeV and 8 TeV respectively (the uncertainties on the total fiducial cross section are approximately the same size), the current measurement from Run 2 shows a definite improvement, both due to higher statistics, but also thanks to improved reconstruction algorithms and Monte Carlo modelling. When comparing this result with the latest published result with the data collected in the period $2015-2016$ [16], where the measurement of the total fiducial cross section has a total uncertainty of 2.36%, it can be seen that using the full Run 2 dataset clearly does not improve terribly on the total uncertainty. The statistical improvement due to the bigger size of the dataset impacts the measurement only slightly, because in both this analysis and in [16] the result is completely dominated by systematic uncertainties and in particular by the luminosity uncertainty. Also, even if one of the other biggest systematic uncertainties presented in this analysis are reduced ($t\bar{t}/Wt$ interference, pileup and $t\bar{t}$ modelling), there is no chance of getting a total uncertainty below 2% due to the luminosity uncertainty.

9.2 Total inclusive cross section

The total inclusive cross section for the full Run 2 dataset is found to be:

$$\sigma_{t\bar{t}} = 839.8 \pm 1.3 \pm 16.0 \pm 18.4\,\mathrm{pb}$$

where the first uncertainty is the statistical one, the second is the luminosity uncertainty and the last is the systematic uncertainty from all of the

Table 9.1: Results for the total fiducial cross section, the individual uncertainties on total fiducial cross section and their total.

Fiducial cross section [pb]	10.672
Data statistics %	0.1592
MC statistics %	0.1561
Fragmentation %	0.1370
Hard scattering %	0.4512
Top mass dependence %	0.0000
PDF %	0.0321
ISR %	0.2022
FSR %	0.2645
Electron scale and resolution %	0.1124
Electron efficiency %	0.3569
Muon scale and resolution scale %	0.0482
Muon reconstruction efficiency %	0.2234
Muon trigger, ISO, TTVA efficiency %	0.2682
JVT %	0.0311
JES b-jes response %	0.0514
JES effective NPs %	0.0117
JES EtaInterCalibration %	0.0057
JES flavour %	0.0652
JES pileup %	0.0055
JES PunchThrough %	0.0000
JES HighPt %	0.0000
MET soft term %	0.0000
JER %	0.0000
b-tagging %	0.0791
Wt background %	0.7342
Diboson background %	0.0550
ttV background %	0.0317
Z+jets background %	0.0489
Fakes background %	0.3221
Pileup %	0.6888
Beam energy %	0.2300
Luminosity %	1.9018
Total uncertainty %	2.3358

other sources. The different contributions to the uncertainty can be seen in Table 9.2.
The total uncertainty, which amounts to 2.91%, is higher than the total uncertainty on the total fiducial cross section, due to an increase in the $t\bar{t}$ related uncertainties. All the detector, background and luminosity uncertainties are the same as for the total fiducial cross section.
The reason there is an increase in the $t\bar{t}$ uncertainties is due to the acceptance factor, which is based fully on Monte Carlo and hence can change a lot depending on the type of simulation. In particular the hard scattering uncertainty blows up due to the acceptance factor from MadGraph5_aMC@NLO interfaced with Pythia 8, which is not very well simulated and does not match the available data [19, 105, 116]. As in the case of the total fiducial cross section, the hard scattering uncertainty could be calculated with top p_{T} reweighting to NNLO QCD + NLO EW, instead of using the alternative MadGraph5_aMC@NLO generator. The uncertainty from the top p_{T} reweighting on the total inclusive cross section is 0.64%, and using this as the generator uncertainty would bring the total uncertainty down to 2.32%.
The predicted NNLO value of the total inclusive cross section is for $\sqrt{13}$ TeV and for a top mass of 172.5 GeV $\sigma_{t\bar{t},pred} = 831.76^{+19.77}_{-29.20}(\text{scale})^{+23.18}_{-22.45}(m_t)^{+35.06}_{-35.06}(\text{PDF}+\alpha_S)$ pb [7–11], and the value found in this analysis falls right within one sigma of the predicted value, meaning that the measurement is consistent with the Standard Model framework.
The total uncertainty is lower compared to the one from Run 1 [13, 14], due to an improvement in detector modelling and $t\bar{t}$ simulation, though this uncertainty is well above the one obtained in the measurement with the $2015-2016$ data [16], where the total uncertainty on the total inclusive cross section is 2.4%, and this is caused mainly by the high generator uncertainty (hard scattering) in this analysis. In fact it has become clear, that the MadGraph5_aMC@NLO interfaced with Pythia 8 does not describe data well (other than being simulated with the incorrect branching ratios) [19, 105, 116] and this means a very likely overestimation of the generator uncertainty. While new samples with improved setups and tuning are being developed, this uncertainty could be evaluated with top p_{T} reweighting, and this would bring the total uncertainty to a value slightly lower, as mentioned above, than the one measured in [16], as for the total fiducial cross section.

9.3 Differential cross section

The results for the absolute differential cross section are presented in this section in Table 9.3 - 9.9 and plotted in Fig. 9.1 and Fig. 9.2. The statistical uncertainty increases with increasing p_{T}, combined mass or energy, reaching a maximum of 6%, while it is constant for η and $\Delta\phi$ bins. The luminosity uncertainty is still one of the dominating uncertainties in most bins, as it ranges between $1.9\% - 2.3\%$, but especially in the high p_{T} bins, the Wt uncertainty dominates the total uncertainty. This is mostly due to the $t\bar{t}/Wt$ interference uncertainty, the modelling of which disagrees with the data at high p_{T} values [115] (see tables in Appendix E). The rest of the uncertainties follow the

Table 9.2: Results for the total inclusive cross section, the individual uncertainties on total inclusive cross section and their total.

Inclusive cross section [pb]	839.797
Data statistics %	0.1592
MC statistics %	0.1561
Fragmentation %	0.4145
Hard scattering %	1.6327
Top mass dependence %	0.0000
PDF %	0.4198
ISR %	0.4596
FSR %	0.3234
Electron scale and resolution %	0.1125
Electron efficiency %	0.3569
Muon scale and resolution scale %	0.0482
Muon reconstruction efficiency %	0.2234
Muon trigger, ISO, TTVA efficiency %	0.2682
JVT %	0.0310
JES b-jes response %	0.0514
JES effective NPs %	0.0117
JES EtaInterCalibration %	0.0057
JES flavour %	0.0652
JES pileup %	0.0055
JES PunchThrough %	0.0000
JES HighPt %	0.0000
MET soft term %	0.0000
JER %	0.0000
b-tagging %	0.0791
Wt background %	0.7342
Diboson background %	0.0550
ttV background %	0.0317
Z+jets background %	0.0488
Fakes background %	0.3221
Pileup %	0.6888
Beam energy %	0.2300
Luminosity %	1.9018
Total uncertainty %	2.9071

same trend as for the total fiducial cross section, where the hard scattering and pileup are amongst the highest uncertainties. As for the total fiducial and inclusive cross sections, using top p_{T} reweighting to include corrections for NNLO QCD + NLO EW effects instead of using the alternative MadGraph5_aMC@NLO generator would reduce the hard scattering uncertainty (see tables in Appendix E). The last value in each differential distribution is the cross section calculated with the events from that bin and from the overflow bin. The error contributions divided into categories are shown in Fig. 9.3. A feature that is very visible from Fig. 9.3(b) is a peak in the systematic error around $|\eta| = 1.5$. This is due to large uncertainties in the modelling of the "crack" region between the calorimeter barrel and endcap, see Fig. 5.2(f) and 5.4(f).

The results for the normalised differential cross section are presented in this section in Table 9.10 - 9.16 and plotted in Fig. 9.4 and Fig. 9.5. The statistical uncertainty follows the same trends as for the absolute differential cross section, while on the systematic side, the uncertainty due to the luminosity decreases due to the normalisation and it is no longer one of the dominating uncertainties. Instead the interference between $t\bar{t}/Wt$ becomes one of the most important uncertainties, and it dominates especially the high ends of the p_{T}, combined mass and energy distributions (see Appendix E). The $t\bar{t}$ uncertainties are also amongst the biggest ones, while the lepton and jets uncertainties are very small. As for the absolute differential cross section, an improvement in the hard scattering uncertainty can be achieved by using the top p_{T} reweighted distributions to assess the size of the hard scattering uncertainty (see tables in Appendix E). The last value in each differential distribution is the cross section calculated with the events from that bin and from the overflow bin. The error contributions divided into categories are shown in Fig. 9.6. When comparing the results obtained in this analysis with the ones from the full Run 1 in [17, 18], it is clear that the uncertainties on all bins, both statistical and systematic are very much improved in the same way as the uncertainty on the total fiducial cross section. The uncertainties on the results with the data collected from 2015 − 2016 [16] are instead very close to the ones found in this analysis, again underlying the fact that the measurement is dominated by systematic uncertainties and their calculations have not improved drastically between 2015 − 2016 and the full Run 2. For the normalised differential cross sections though, the large statistics of the full Run 2 sample represent a significant gain over previous measurements, since the systematic uncertainty on the luminosity basically cancels, but the results for the normalised differential distributions cannot be directly compared to the ones in [16], due to the different binning.

A thing to note regarding this analysis though, is that the granularity of the binning of most of the variables is finer, without loosing too much precision on each bin and this is possible thanks to the high statistical power of the Run 2 dataset. Having precise and finer distributions is an advantage for many reasons: these distributions can be used for top pole mass extraction, as will be explained in Chapter 10, and the more bins there are, the higher the number of degrees of freedom will be when comparing the measured differential cross

section with the template distributions with a χ^2. Also the lower uncertainties on the normalised differential distributions will translate to lower systematic uncertainties on the top mass value as well.
These distributions can also be used to study the theoretical/Monte Carlo modelling of top quark processes, by comparing theoretically modelled distributions with different top properties to the measured ones, one example being the $t\bar{t}/Wt$ interference or the top p_{T} spectrum, as done in [20] for example. Certainly the low uncertainty on each bin would help in discerning viable models to non-viable ones when doing a comparison between the data and the alternative modelled distributions. A comparison between the measured distribution and the Monte Carlo predicted ones is carried out for example in Fig. 9.1, 9.2, 9.4 and 9.5, where the measured absolute and differential cross section distributions are plotted together with the particle level predicted differential distributions from three Monte Carlo samples, the nominal Powheg+Pythia 8 sample, the Powheg + Herwig 7 sample and the MadGraph5_aMC@NLO + Pythia 8 sample. It is clear that the Monte Carlo samples do not describe several features of the $t\bar{t}$ system, as the lepton p_{T} and the $\Delta\phi$ distribution. The difference in the lepton p_{T} distributions between the measured cross section and the predicted one is up to $20\% - 30\%$ in the highest bins, as also recently described in [19]. The difference between the measured and the predicted distributions for the $\Delta\phi$ variable follow the same tendencies as [58], where at low $\Delta\phi$ values the predictions undershoot by $\sim 5\%$, while at high $\Delta\phi$ values the predictions overshoot by $\sim 5\%$.

Table 9.3: Differential absolute cross section for p_T (ℓ).

p_T (ℓ) bins [GeV]	25.0-30.0	30.0-40.0	40.0-50.0	50.0-60.0	60.0-75.0	75.0-100.0	100.0-140.0	140.0-180.0	180.0 250.0	250.0 350.0
Cross section [fb/GeV]	468.7729	439.6238	361.9038	281.0505	200.1542	110.3798	42.3049	13.0857	3.2269	0.5156
Data statistics %	0.3900	0.2863	0.3114	0.3422	0.3014	0.3103	0.4107	0.7097	1.0307	2.3652
MC statistics %	0.1228	0.0878	0.0791	0.0837	0.0771	0.0829	0.1045	0.1943	0.3082	0.6999
Fragmentation %	0.9980	0.3481	0.4194	0.0073	0.0314	0.1472	0.7940	1.2142	1.2427	0.9014
Hard scattering %	1.3309	0.6522	0.2043	0.2746	0.4249	0.1373	0.9187	1.0611	2.8096	3.5126
Top mass dependence %	0.0570	0.0396	0.0310	0.0132	0.0362	0.0315	0.0177	0.1534	0.1287	0.1604
PDF %	0.0344	0.0378	0.0419	0.0467	0.0505	0.0559	0.0638	0.0778	0.0921	0.0874
ISR %	0.1870	0.1791	0.1542	0.1387	0.1618	0.2655	0.2248	0.1494	0.0754	0.6469
FSR %	0.2291	0.3573	0.1791	0.2767	0.1073	0.2500	0.1608	0.7469	0.2737	0.4752
Electron scale and resolution %	0.1087	0.1073	0.0153	0.0691	0.0527	0.0711	0.4025	0.8410	1.2802	2.1132
Electron efficiency %	0.6773	0.4157	0.3183	0.3391	0.3425	0.3718	0.4180	0.5231	0.6060	2.4898
Muon scale and resolution scale %	0.0243	0.0156	0.0303	0.0433	0.0594	0.0695	0.1027	0.1142	0.1558	0.3247
Muon reconstruction efficiency %	0.2173	0.2198	0.2205	0.2214	0.2229	0.2252	0.2303	0.2384	0.2493	0.2906
Muon trigger, ISO, TTVA efficiency %	0.3042	0.2818	0.2516	0.3297	0.2457	0.2465	0.2486	0.2542	0.2644	0.3037
JVT %	0.0285	0.0291	0.0278	0.0279	0.0321	0.0327	0.0352	0.0385	0.0495	0.0926
JES b-jes response %	0.0585	0.0468	0.0457	0.0504	0.0473	0.0513	0.0616	0.0487	0.0536	0.0172
JES effective NPs %	0.0226	0.0229	0.0212	0.0284	0.0091	0.0065	0.0215	0.0347	0.0588	0.1058
JES EtaInterCalibration %	0.0262	0.0074	0.0044	0.0175	0.0047	0.0057	0.0064	0.0199	0.0076	0.0482
JES flavour %	0.0506	0.0362	0.0371	0.0351	0.0697	0.0865	0.1190	0.1501	0.2064	0.2755
JES pileup %	0.0661	0.0126	0.0117	0.0225	0.0094	0.0137	0.0344	0.0564	0.0774	0.1329
JES PunchThrough %	0.0000	0.0002	0.0000	0.0000	0.0001	0.0001	0.0001	0.0006	0.0003	0.0001
JES HighPt %	0.0000	0.0000	0.0000	0.0000	0.0000	0.0000	0.0000	0.0000	0.0000	0.0000
MET soft term %	0.0000	0.0000	0.0000	0.0000	0.0000	0.0000	0.0000	0.0000	0.0000	0.0000
JER %	0.0001	0.0000	0.0000	0.0000	0.0000	0.0000	0.0000	0.0000	0.0000	0.0000
b-tagging %	0.0810	0.0805	0.0812	0.0865	0.0828	0.0858	0.0813	0.1027	0.1281	0.2359
Wt background %	0.7051	0.6219	0.5923	0.6044	0.6073	0.8145	1.1682	2.0819	4.0783	12.6392
Diboson background %	0.0473	0.0472	0.0469	0.0447	0.0510	0.0557	0.0723	0.0997	0.1647	0.4076
ttV background %	0.0259	0.0262	0.0271	0.0279	0.0297	0.0336	0.0416	0.0556	0.0803	0.1536
Z+jets background %	0.0639	0.1002	0.0593	0.0147	0.0674	0.0306	0.0219	0.0053	0.0732	0.0722
Fakes background %	0.3789	0.3258	0.3016	0.3132	0.3075	0.3172	0.3260	0.3914	0.4499	0.7359
Pileup %	1.0354	0.9187	0.8783	0.6883	0.5418	0.4769	0.4002	0.4134	0.2396	0.2231
Beam energy %	0.0015	0.0082	0.0021	0.0042	0.0036	0.0085	0.0054	0.0109	0.0121	0.0374
Luminosity %	1.9019	1.8934	1.8882	1.8886	1.8896	1.8992	1.9240	1.9760	2.0582	2.3448
Total uncertainty %	2.9988	2.4612	2.3216	2.2578	2.2146	2.2721	2.7504	3.6721	5.8400	14.0380

Table 9.4: Differential absolute cross section for $|\eta(\ell)|$.

$\|\eta(\ell)\|$ bins	0.0-0.08	0.08-0.17	0.17-0.25	0.25-0.33	0.33-0.42	0.42-0.50	0.50-0.58	0.58-0.67	0.67-0.75	0.75-0.83	0.83-0.92	0.92-1.00	1.00-1.08	1.08-1.17
Cross section [fb/unit $\|\eta\|$]	13010.73	12889.13	12935.14	12901.00	12522.43	12459.39	12129.02	11801.16	11601.87	11181.25	10873.55	10374.68	9937.86	9602.30
Data statistics %	0.3915	0.3381	0.3437	0.3437	0.3348	0.3260	0.3518	0.3395	0.3464	0.3746	0.3615	0.3803	0.3872	0.4027
MC statistics %	0.1469	0.1599	0.1377	0.1423	0.1316	0.1337	0.1270	0.1358	0.1446	0.1425	0.1382	0.1571	0.1679	0.1556
Fragmentation %	0.3613	0.2864	0.0128	0.7077	0.1815	0.1538	0.3174	1.2477	0.1749	0.9827	1.7435	0.3645	1.6660	3.0951
Hard scattering %	0.5622	0.6014	0.4341	0.6293	0.5978	0.0821	0.1220	0.8716	0.5195	1.1267	1.1686	0.1930	1.2543	3.4018
Top mass dependence %	0.0229	0.0308	0.0578	0.0063	0.0300	0.0552	0.0206	0.0552	0.0098	0.0545	0.0290	0.0059	0.0316	0.0377
PDF %	0.0346	0.0296	0.0280	0.0265	0.0272	0.0276	0.0255	0.0225	0.0286	0.0301	0.0262	0.0266	0.0265	0.0255
ISR %	0.1725	0.2235	0.0385	0.3480	0.2686	0.2610	0.2927	0.2250	0.2424	0.0026	0.2205	0.2751	0.2868	0.2992
FSR %	0.5115	0.4219	0.3812	0.5184	0.3249	0.2345	0.5378	0.2456	0.1249	0.5558	0.1343	0.2812	0.1422	0.4599
Electron scale and resolution %	0.0661	0.0815	0.0798	0.0843	0.0794	0.0827	0.0778	0.0923	0.0888	0.0965	0.1010	0.0967	0.1070	0.1061
Electron efficiency %	0.3988	0.3408	0.3270	0.3271	0.3274	0.3275	0.3281	0.3332	0.3385	0.3349	0.3323	0.3327	0.3319	0.3397
Muon scale and resolution scale %	0.0388	0.0345	0.0396	0.0400	0.0379	0.0395	0.0406	0.0394	0.0336	0.0410	0.0514	0.0501	0.0534	0.0655
Muon reconstruction efficiency %	0.5292	0.3362	0.2141	0.2148	0.2122	0.2027	0.2031	0.2029	0.2059	0.2070	0.2060	0.2073	0.2133	0.2123
Muon trigger, ISO, TTVA efficiency %	0.2658	0.2669	0.2668	0.2664	0.2666	0.2666	0.2669	0.2676	0.2671	0.2674	0.2679	0.2674	0.2681	0.2689
JVT %	0.0281	0.0336	0.0321	0.0320	0.0258	0.0289	0.0284	0.0295	0.0287	0.0324	0.0290	0.0285	0.0328	0.0313
JES b-jes response %	0.0468	0.0507	0.0433	0.0518	0.0501	0.0513	0.0555	0.0610	0.0786	0.0510	0.0593	0.0502	0.0668	0.0468
JES effective NPs %	0.0180	0.0136	0.0092	0.0074	0.0067	0.0085	0.0064	0.0136	0.0315	0.0203	0.0177	0.0083	0.0144	0.0074
JES EtaInterCalibration %	0.0204	0.0119	0.0087	0.0176	0.0086	0.0151	0.0138	0.0088	0.0261	0.0324	0.0100	0.0057	0.0409	0.0121
JES flavour %	0.0594	0.0674	0.0666	0.0684	0.0724	0.0774	0.0675	0.0733	0.0658	0.0959	0.0553	0.0621	0.1134	0.0920
JES pileup %	0.0093	0.0045	0.0090	0.0054	0.0114	0.0171	0.0122	0.0086	0.0207	0.0511	0.0086	0.0064	0.0343	0.0154
JES PunchThrough %	0.0000	0.0002	0.0001	0.0002	0.0002	0.0001	0.0002	0.0002	0.0002	0.0002	0.0000	0.0001	0.0000	0.0001
JES HighPt %	0.0000	0.0000	0.0000	0.0000	0.0000	0.0000	0.0000	0.0000	0.0000	0.0000	0.0000	0.0000	0.0000	0.0000
MET soft term %	0.0000	0.0000	0.0000	0.0000	0.0000	0.0000	0.0000	0.0000	0.0000	0.0000	0.0000	0.0000	0.0000	0.0000
JER %	0.0000	0.0000	0.0000	0.0000	0.0001	0.0001	0.0000	0.0001	0.0000	0.0000	0.0000	0.0000	0.0000	0.0000
b-tagging %	0.0882	0.0891	0.1057	0.0824	0.0864	0.0965	0.0884	0.0830	0.0827	0.0928	0.0883	0.0761	0.0732	0.0827
Wt background %	0.5969	0.7955	0.7730	0.7294	0.7104	0.6645	0.7168	0.6683	0.8430	0.7736	0.7837	0.5993	1.0370	0.8125
Diboson background %	0.0454	0.0404	0.0422	0.0454	0.0478	0.0416	0.0489	0.0480	0.0488	0.0507	0.0484	0.0499	0.0571	0.0550
ttV background %	0.0312	0.0314	0.0308	0.0306	0.0308	0.0305	0.0309	0.0312	0.0310	0.0320	0.0316	0.0313	0.0325	0.0320
Z+jets background %	0.0204	0.0484	0.0140	0.0215	0.0186	0.0775	0.0425	0.1627	0.0590	0.0258	0.0208	0.0430	0.0408	0.0703
Fakes background %	0.2528	0.2375	0.2345	0.2482	0.2302	0.2291	0.2658	0.2484	0.2578	0.2524	0.2532	0.2928	0.2718	0.2850
Pileup %	0.7476	0.7086	0.6545	0.6667	0.7112	0.7193	0.7701	0.7288	0.6455	0.6748	0.6319	0.5645	0.6834	0.6540
Beam energy %	0.0100	0.0197	0.0155	0.0039	0.0139	0.0220	0.0188	0.0264	0.0100	0.0155	0.0025	0.0189	0.0094	0.0293
Luminosity %	1.8964	1.9010	1.8971	1.8975	1.8976	1.8961	1.8992	1.9004	1.8997	1.8986	1.8972	1.9005	1.9025	1.8979
Total uncertainty %	2.4545	2.4389	2.3260	2.5133	2.3695	2.2682	2.3803	2.7381	2.3630	2.7746	3.0915	2.2641	3.1846	5.1662

$\|\eta(\ell)\|$ bins	1.17-1.25	1.25-1.33	1.33-1.42	1.42-1.50	1.50-1.58	1.58-1.67	1.67-1.75	1.75-1.83	1.83-1.92	1.92-2.00	2.00-2.08	2.08-2.17	2.17-2.25	2.25-2.33	2.33-2.42	2.45-2.50
Cross section [fb/unit $\|\eta\|$]	9249.35	8746.96	8306.37	7775.90	7296.28	6925.37	6357.71	5797.03	5427.31	4919.86	4662.30	4187.80	3721.92	3169.92	2876.46	2533.02
Data statistics %	0.4180	0.4251	0.4927	0.6024	0.4824	0.4697	0.4836	0.5320	0.5717	0.5872	0.6239	0.6439	0.7036	0.7888	0.8346	1.1204
MC statistics %	0.1568	0.1658	0.1945	0.2615	0.1945	0.1889	0.2230	0.2111	0.2220	0.2504	0.2487	0.2644	0.2719	0.3167	0.3356	0.4000
Fragmentation %	0.3948	1.2715	1.3674	0.4742	4.3655	1.8255	3.5882	0.8915	0.5413	0.1116	0.3121	0.4087	0.2881	1.3125	1.5671	4.2496
Hard scattering %	1.3177	1.3788	1.2157	0.8741	5.4809	2.1614	2.5602	0.4251	1.1064	0.0493	0.2844	1.6983	2.2530	1.3374	0.0367	4.6017
Top mass dependence %	0.0065	0.0347	0.0254	0.0192	0.0356	0.0107	0.0248	0.0231	0.0222	0.0354	0.0192	0.0143	0.0184	0.0330	0.1319	0.0473
PDF %	0.0255	0.0276	0.0321	0.0634	0.0272	0.0287	0.0324	0.0333	0.0385	0.0454	0.0457	0.0503	0.0595	0.0677	0.0810	0.0538
ISR %	0.0132	0.0071	0.1939	0.1329	0.0378	0.6872	0.0096	0.1624	0.0422	0.0706	0.3715	0.1787	0.0426	0.0050	0.3449	0.0985
FSR %	0.1447	0.1450	0.2438	0.0243	0.7165	0.2145	0.1307	0.0687	0.0621	0.2345	0.0729	0.3836	0.1287	0.0162	0.2970	0.1493
Electron scale and resolution %	0.1415	0.1673	0.1375	0.1008	0.2087	0.2073	0.1838	0.1737	0.1321	0.1382	0.1444	0.1333	0.1404	0.1340	0.1971	0.3770
Electron efficiency %	0.3669	0.3671	0.3579	0.3602	0.4589	0.4880	0.4849	0.4900	0.4894	0.4919	0.5909	0.6173	0.6044	0.5941	0.6784	0.7197
Muon scale and resolution scale %	0.0580	0.0476	0.0410	0.0522	0.0654	0.0692	0.0600	0.0490	0.0518	0.0615	0.0613	0.0618	0.0674	0.0931	0.1349	0.1365
Muon reconstruction efficiency %	0.2113	0.2034	0.1750	0.1549	0.1813	0.1934	0.1945	0.1943	0.1934	0.1936	0.1967	0.1956	0.1965	0.1958	0.1956	0.1915
Muon trigger, ISO, TTVA efficiency %	0.2690	0.2693	0.2690	0.2707	0.2709	0.2706	0.2715	0.2720	0.2710	0.2715	0.2710	0.2709	0.2720	0.2732	0.2749	0.2745
JVT %	0.0339	0.0321	0.0307	0.0295	0.0325	0.0345	0.0291	0.0284	0.0367	0.0354	0.0250	0.0242	0.0356	0.0223	0.0337	0.0285
JES b-jes response %	0.0519	0.0403	0.0414	0.0582	0.0377	0.0289	0.0526	0.0631	0.0358	0.0305	0.0579	0.0257	0.0356	0.0309	0.0556	0.0951
JES effective NPs %	0.0092	0.0137	0.0501	0.0331	0.0100	0.0390	0.0220	0.0455	0.0105	0.0092	0.0432	0.0145	0.0112	0.0135	0.0798	0.0883
JES EtaInterCalibration %	0.0079	0.0182	0.0285	0.0071	0.0034	0.0285	0.0116	0.0028	0.0182	0.0212	0.0062	0.0200	0.0041	0.0032	0.0271	0.0523
JES flavour %	0.0862	0.0979	0.0298	0.0524	0.0521	0.0375	0.0455	0.0305	0.0403	0.0595	0.0372	0.0539	0.0511	0.0378	0.0100	0.0058
JES pileup %	0.0163	0.0275	0.0787	0.0101	0.0234	0.0627	0.0155	0.0346	0.0101	0.0115	0.0375	0.0232	0.0183	0.0134	0.0718	0.0743
JES PunchThrough %	0.0001	0.0002	0.0002	0.0002	0.0002	0.0000	0.0005	0.0001	0.0002	0.0002	0.0009	0.0000	0.0007	0.0005	0.0000	0.0009
JES HighPt %	0.0000	0.0000	0.0000	0.0000	0.0000	0.0000	0.0000	0.0000	0.0000	0.0000	0.0000	0.0000	0.0000	0.0000	0.0000	0.0000
MET soft term %	0.0000	0.0000	0.0000	0.0000	0.0000	0.0000	0.0000	0.0000	0.0000	0.0000	0.0000	0.0000	0.0000	0.0000	0.0000	0.0000
JER %	0.0001	0.0000	0.0001	0.0002	0.0000	0.0000	0.0001	0.0000	0.0000	0.0000	0.0000	0.0003	0.0000	0.0001	0.0000	0.0000
b-tagging %	0.0772	0.0799	0.0771	0.0758	0.0662	0.0674	0.0809	0.0669	0.0618	0.0598	0.0688	0.0664	0.0604	0.0635	0.0587	0.0855
Wt background %	0.6533	0.7757	0.6455	0.9631	1.2439	0.7226	0.8040	0.8845	0.7919	0.9022	0.6892	0.9497	0.6790	1.0953	0.9327	0.8565
Diboson background %	0.0571	0.0655	0.0557	0.0597	0.0670	0.0798	0.0635	0.0674	0.0729	0.0777	0.0805	0.0841	0.0853	0.0939	0.0989	0.1088
ttV background %	0.0322	0.0315	0.0321	0.0327	0.0328	0.0315	0.0328	0.0341	0.0317	0.0318	0.0320	0.0316	0.0333	0.0357	0.0348	0.0331
Z+jets background %	0.1371	0.0605	0.0473	0.1706	0.0663	0.1746	0.2775	0.0592	0.0952	0.0411	0.1921	0.0359	0.2668	0.2271	0.1668	0.4364
Fakes background %	0.3240	0.3044	0.3420	0.3219	0.4468	0.5230	0.6179	0.6629	0.7251	0.7515	0.6743	0.5169	0.5859	0.6005	0.5262	0.4848
Pileup %	0.6551	0.6841	0.6743	0.6758	0.7502	0.7368	0.6953	0.7427	0.6571	0.7164	0.7361	0.6709	0.7612	0.6662	0.5633	0.7755
Beam energy %	0.0053	0.0046	0.0388	0.0268	0.0038	0.0229	0.0018	0.0140	0.0329	0.0051	0.0076	0.0251	0.0042	0.0173	0.0503	0.0248
Luminosity %	1.8979	1.8969	1.8963	1.8988	1.9078	1.9090	1.9181	1.9204	1.9186	1.9216	1.9140	1.9033	1.9121	1.9170	1.9153	1.9151
Total uncertainty %	2.6443	2.9694	2.9309	2.6124	7.4980	3.7698	5.0401	2.6841	2.7500	2.5426	2.5404	3.0811	3.3737	3.2373	3.0532	6.8522

Table 9.5: Differential absolute cross section for $E(\ell^+) + E(\ell^-)$.

$E(\ell^+) + E(\ell^-)$ bins [GeV]	50.0-60.0	60.0-70.0	70.0-80.0	80.0-90.0	90.0-110.0	110.0-125.0	125.0-160.0	160.0-200.0	200.0-250.0	250.0-300.0	300.0-370.0	370.0-450.0	450.0-550.0	550.0-700.0	700.0-900.0
Cross section [fb/GeV]	1.4375	9.0958	20.6367	30.9508	44.3327	51.7400	52.3485	43.8647	32.0006	21.2269	12.9273	6.9930	3.4994	1.4392	0.6230
Data statistics %	5.3505	1.9778	1.1975	0.9843	0.5431	0.5932	0.3877	0.3892	0.3954	0.4929	0.5488	0.7125	0.9860	1.1977	1.7894
MC statistics %	6.2128	1.2323	0.4153	0.3189	0.1582	0.1479	0.1021	0.1038	0.1036	0.1302	0.1497	0.1806	0.2469	0.3253	0.4801
Fragmentation %	1.4110	0.9863	0.5351	0.7744	0.3499	0.2391	0.4713	0.2240	0.2867	0.2196	0.6616	0.2520	0.0398	0.4335	0.8419
Hard scattering %	1.8155	3.5941	0.5351	0.7797	0.7324	0.2390	0.8207	0.1558	0.2161	0.8576	0.3534	0.2222	0.2543	1.3862	1.2599
Top mass dependence %	0.2093	0.1949	0.2338	0.0562	0.1123	0.0666	0.0394	0.0048	0.0292	0.0366	0.0168	0.0917	0.0976	0.0280	0.1727
PDF %	0.0361	0.0186	0.0209	0.0225	0.0362	0.0551	0.0725	0.0925	0.1069	0.1211	0.1255	0.1229	0.1145	0.1119	0.1210
ISR %	2.6544	0.1934	0.4197	0.1625	0.2596	0.1508	0.1720	0.2787	0.2353	0.2745	0.4425	0.1481	0.2277	0.1883	0.0017
FSR %	1.5141	0.3597	0.6109	0.7207	0.4693	0.4152	0.1458	0.2215	0.3017	0.1389	0.1902	0.3892	0.1586	0.6034	0.6721
Electron scale and resolution %	0.3135	0.0798	0.0515	0.0428	0.0312	0.0476	0.0613	0.0385	0.0202	0.1556	0.2797	0.4311	0.5913	0.8126	1.5437
Electron efficiency %	0.8306	0.6088	0.5008	0.4479	0.4031	0.3693	0.3401	0.3235	0.3339	0.3539	0.3845	0.4529	0.6240	0.8927	1.3573
Muon scale and resolution scale %	0.6867	0.0547	0.0649	0.0766	0.0153	0.0125	0.0106	0.0358	0.0537	0.0658	0.1016	0.1261	0.1166	0.1952	0.2968
Muon reconstruction efficiency %	0.3473	0.3073	0.2761	0.2690	0.2541	0.2460	0.2343	0.2237	0.2147	0.2087	0.2042	0.2014	0.1989	0.1984	0.2012
Muon trigger, ISO, TTVA efficiency %	0.3075	0.3023	0.2860	0.2860	0.2860	0.2817	0.2750	0.2688	0.2646	0.2621	0.2604	0.2567	0.2525	0.2509	0.2551
JVT %	0.0443	0.0409	0.0290	0.0282	0.0235	0.0276	0.0269	0.0294	0.0288	0.0313	0.0327	0.0349	0.0391	0.0452	0.0251
JES b-jes response %	0.0033	0.2002	0.0912	0.0626	0.0651	0.0532	0.0459	0.0453	0.0414	0.0429	0.0286	0.0748	0.0454	0.0245	0.0307
JES effective NPs %	0.3534	0.1361	0.0824	0.0387	0.0351	0.0252	0.0126	0.0092	0.0186	0.0077	0.0124	0.0079	0.0251	0.0233	0.0755
JES EtaInterCalibration %	0.1067	0.0965	0.1887	0.0236	0.0237	0.0199	0.0091	0.0082	0.0158	0.0080	0.0113	0.0114	0.0213	0.0199	0.0520
JES flavour %	0.4067	0.0244	0.2072	0.0473	0.0210	0.0372	0.0517	0.0588	0.0455	0.0961	0.0740	0.0988	0.1118	0.1221	0.2057
JES pileup %	0.3664	0.1358	0.2428	0.0414	0.0329	0.0140	0.0064	0.0092	0.0172	0.0238	0.0265	0.0216	0.0325	0.0462	0.0892
JES PunchThrough %	0.0000	0.0010	0.0000	0.0000	0.0001	0.0001	0.0001	0.0002	0.0001	0.0000	0.0001	0.0004	0.0011	0.0006	0.0005
JES HighPt %	0.0000	0.0000	0.0000	0.0000	0.0000	0.0000	0.0000	0.0000	0.0000	0.0000	0.0000	0.0000	0.0000	0.0000	0.0000
MET soft term %	0.0000	0.0000	0.0000	0.0000	0.0000	0.0000	0.0000	0.0000	0.0000	0.0000	0.0000	0.0000	0.0000	0.0000	0.0000
JER %	0.0000	0.0000	0.0000	0.0000	0.0001	0.0000	0.0000	0.0000	0.0000	0.0000	0.0001	0.0000	0.0000	0.0000	0.0000
b-tagging %	1.7601	0.3662	0.1168	0.1193	0.1121	0.0983	0.0919	0.0839	0.0794	0.0791	0.0773	0.0716	0.0732	0.0793	0.1005
Wt background %	1.3987	0.9211	0.8019	0.8782	0.6047	0.7318	0.6205	0.5772	0.6334	0.9312	1.2053	1.4476	1.7870	2.2431	3.3775
Diboson background %	0.0461	0.0523	0.0335	0.0305	0.0251	0.0346	0.0351	0.0435	0.0523	0.0625	0.0729	0.0945	0.1165	0.1466	0.2716
ttV background %	0.0214	0.0209	0.0212	0.0209	0.0212	0.0231	0.0245	0.0283	0.0318	0.0346	0.0387	0.0439	0.0482	0.0554	0.0757
Z+jets background %	5.5426	0.7587	0.7619	0.0925	0.0367	0.0659	0.0323	0.1281	0.0751	0.1274	0.0350	0.0928	0.0531	0.0494	0.0095
Fakes background %	0.0649	0.4611	0.2429	0.2560	0.2045	0.1614	0.2223	0.2811	0.3396	0.3672	0.5116	0.5912	0.5554	0.5839	0.7723
Pileup %	1.8777	1.7091	1.2319	1.2010	1.0037	0.8995	0.7896	0.7118	0.6588	0.5182	0.4421	0.4424	0.4260	0.3768	0.3214
Beam energy %	0.1096	0.0237	0.0223	0.0324	0.0103	0.0096	0.0314	0.0028	0.0019	0.0066	0.0024	0.0127	0.0265	0.0201	0.0211
Luminosity %	1.7796	1.9243	1.8767	1.8848	1.8715	1.8739	1.8804	1.8906	1.8991	1.9111	1.9292	1.9437	1.9528	1.9699	2.0437
Total uncertainty %	11.2382	5.3459	3.1130	3.0096	2.5556	2.4235	2.4445	2.2645	2.2942	2.5265	2.6710	2.7971	3.0975	3.8871	5.2037

Table 9.6: Differential absolute cross section for $m(\ell^+\ell^-)$.

$m(\ell^+\ell^-)$ bins [GeV]	0.0-15.0	15.0-20.0	20.0-25.0	25.0-30.0	30.0-35.0	35.0-40.0	40.0-50.0	50.0-60.0	60.0-70.0	70.0-85.0	85.0-100.0	100.0-120.0	120.0-150.0	150.0-175.0	175.0-200.0	200.0-250.0	250.0-300.0	300.0-400.0	400.0-500.0	500.0-650.0	650.0-800.0
Cross section [fb/GeV]	8.2361	19.0791	23.7748	29.5110	33.5749	38.7676	46.1188	56.9246	69.6418	77.9525	77.4567	68.2664	51.4973	34.9697	24.1325	13.8885	6.8427	2.6148	0.7404	0.2153	0.0670
Data statistics %	2.1647	1.7896	1.6258	1.3608	1.2898	1.2280	0.7770	0.7248	0.6543	0.4994	0.4889	0.4493	0.4023	0.5239	0.6295	0.5867	0.8521	0.9474	1.7912	2.7452	5.1331
MC statistics %	0.5542	0.4249	0.3984	0.3463	0.3229	0.2978	0.1975	0.2795	0.2335	0.1511	0.1197	0.1081	0.1050	0.1373	0.1683	0.1532	0.2219	0.2530	0.4954	0.7419	1.4285
Fragmentation %	0.1625	0.3217	0.5809	0.1814	0.8333	0.6033	0.2884	1.2331	1.1467	0.4123	0.1298	0.1852	0.0674	0.2812	0.5158	0.4745	0.2888	0.9258	0.1264	1.8155	0.3771
Hard scattering %	2.3070	1.7911	1.3443	0.2726	1.4060	0.3942	1.8096	0.9429	0.8434	0.3579	0.9731	0.1613	0.4421	0.1978	0.3828	0.0839	1.6217	0.4912	0.7341	3.3446	0.3402
Top mass dependence %	0.3494	0.0042	0.0261	0.1201	0.0546	0.0055	0.0507	0.0536	0.0099	0.0126	0.0394	0.0495	0.1007	0.0150	0.0060	0.0349	0.0025	0.0573	0.1984	0.1690	0.3897
PDF %	0.1156	0.0885	0.0804	0.0855	0.0723	0.0739	0.0714	0.0680	0.0643	0.0629	0.0555	0.0563	0.0571	0.0567	0.0627	0.0569	0.0605	0.0487	0.0488	0.0515	0.1017
ISR %	0.4256	0.4388	0.0230	0.0641	0.4647	0.1294	0.2349	0.1221	0.1102	0.0541	0.1707	0.1243	0.1495	0.2232	0.1355	0.2651	0.6388	0.6588	0.2220	0.1384	1.8017
FSR %	0.0444	1.1469	0.2097	0.2402	0.1749	0.4675	0.0657	0.1528	0.1846	0.3433	0.3439	0.2735	0.1824	0.2525	0.1701	0.2558	0.4198	0.0133	0.4418	0.5582	0.0728
Electron scale and resolution %	0.0699	0.0601	0.0598	0.0664	0.0794	0.0628	0.0599	0.0423	0.0529	0.0266	0.0111	0.0130	0.0218	0.0995	0.1991	0.2568	0.4668	0.6625	1.0106	1.4128	1.9472
Electron efficiency %	0.4968	0.4238	0.4187	0.4167	0.4132	0.4138	0.4139	0.4191	0.4099	0.3852	0.3593	0.3384	0.3275	0.3347	0.3565	0.3994	0.4691	0.5816	0.8009	1.1848	1.8874
Muon scale and resolution scale %	0.0608	0.0749	0.0719	0.0826	0.0751	0.0248	0.0265	0.0225	0.0399	0.0146	0.0311	0.0342	0.0431	0.0591	0.0950	0.0813	0.1349	0.1342	0.1505	0.2248	0.3117
Muon reconstruction efficiency %	0.2277	0.2247	0.2240	0.2277	0.2281	0.2268	0.2287	0.2284	0.2263	0.2249	0.2228	0.2240	0.2239	0.2224	0.2223	0.2212	0.2180	0.2164	0.2138	0.2089	0.2094
Muon trigger, ISO, TTVA efficiency %	0.2949	0.2842	0.2828	0.2823	0.2830	0.2835	0.2842	0.2861	0.2848	0.2814	0.2771	0.2729	0.2669	0.2599	0.2552	0.2502	0.2462	0.2448	0.2453	0.2432	0.2566
JVT %	0.0324	0.0249	0.0176	0.0163	0.0332	0.0263	0.0311	0.0312	0.0326	0.0303	0.0257	0.0273	0.0316	0.0320	0.0304	0.0368	0.0355	0.0321	0.0551	0.0586	0.0839
JES b-jes response %	0.0650	0.0394	0.0290	0.0547	0.0056	0.0019	0.0255	0.0418	0.0823	0.0370	0.0334	0.0437	0.0475	0.0493	0.0567	0.0762	0.0667	0.1049	0.0798	0.1335	0.1644
JES effective NPs %	0.0574	0.0360	0.0232	0.0523	0.0255	0.0136	0.0568	0.0251	0.0465	0.0327	0.0117	0.0076	0.0112	0.0137	0.0108	0.0143	0.0212	0.0075	0.0424	0.0345	0.0475
JES EtaInterCalibration %	0.0289	0.0246	0.0065	0.0385	0.0085	0.0088	0.0848	0.0109	0.0155	0.0295	0.0064	0.0021	0.0069	0.0085	0.0042	0.0049	0.0119	0.0070	0.0254	0.0316	0.0752
JES flavour %	0.0524	0.0245	0.0224	0.0098	0.0304	0.0104	0.1011	0.0329	0.0256	0.0207	0.0447	0.0597	0.0639	0.0757	0.1097	0.1030	0.1401	0.1596	0.2086	0.2306	0.2848
JES pileup %	0.0749	0.0508	0.0167	0.0573	0.0338	0.0148	0.1118	0.0150	0.0369	0.0463	0.0034	0.0130	0.0059	0.0073	0.0214	0.0188	0.0330	0.0175	0.0562	0.0317	0.0738
JES PunchThrough %	0.0000	0.0000	0.0000	0.0000	0.0000	0.0000	0.0002	0.0000	0.0000	0.0002	0.0000	0.0004	0.0002	0.0002	0.0002	0.0004	0.0000	0.0003	0.0000	0.0017	0.0001
JES HighPt %	0.0000	0.0000	0.0000	0.0000	0.0000	0.0000	0.0000	0.0000	0.0000	0.0000	0.0000	0.0000	0.0000	0.0000	0.0000	0.0000	0.0000	0.0000	0.0000	0.0000	0.0000
MET soft term %	0.0000	0.0000	0.0000	0.0000	0.0000	0.0000	0.0000	0.0000	0.0000	0.0000	0.0000	0.0000	0.0000	0.0000	0.0000	0.0000	0.0000	0.0000	0.0000	0.0000	0.0000
JER %	0.0000	0.0000	0.0000	0.0000	0.0000	0.0000	0.0000	0.0000	0.0002	0.0000	0.0000	0.0000	0.0000	0.0001	0.0001	0.0000	0.0000	0.0000	0.0000	0.0000	0.0000
b-tagging %	0.1440	0.1028	0.1001	0.0910	0.0833	0.0903	0.0900	0.1033	0.0847	0.0857	0.0950	0.0859	0.0846	0.0822	0.0876	0.0774	0.0727	0.0696	0.0856	0.0803	0.1255
Wt background %	0.8719	0.7165	0.7238	1.0893	0.5552	0.6906	0.6217	0.6259	0.7554	0.7020	0.6201	0.6729	0.7061	0.7724	0.9954	1.4001	1.5412	2.4730	3.6141	2.9004	7.6963
Diboson background %	0.0482	0.0642	0.0626	0.0572	0.0617	0.0522	0.0549	0.0564	0.0549	0.0496	0.0499	0.0562	0.0511	0.0488	0.0501	0.0592	0.0643	0.0813	0.1144	0.1358	0.1815
ttV background %	0.0208	0.0254	0.0251	0.0218	0.0247	0.0238	0.0242	0.0258	0.0258	0.0263	0.0271	0.0291	0.0310	0.0340	0.0362	0.0408	0.0431	0.0511	0.0646	0.0740	0.1114
Z+jets background %	0.3961	0.1135	0.1208	0.2185	0.4115	0.2343	0.3314	0.3250	0.1960	0.0814	0.0213	0.0033	0.0364	0.0107	0.0135	0.0038	0.0056	0.0128	0.0735	0.0023	0.0074
Fakes background %	0.8972	0.3626	0.3768	0.3767	0.3209	0.4187	0.3367	0.3212	0.3939	0.3882	0.3477	0.2964	0.2847	0.2870	0.2687	0.3309	0.3947	0.5065	0.5875	0.6379	0.9503
Pileup %	1.0688	0.9798	0.8693	0.7461	0.9627	0.9336	1.1414	0.9760	0.9361	0.8851	0.8150	0.7248	0.6410	0.5718	0.4644	0.3655	0.2939	0.3233	0.2766	0.0040	0.3004
Beam energy %	0.0080	0.0504	0.0157	0.0214	0.0078	0.0570	0.0147	0.0427	0.0072	0.0036	0.0175	0.0127	0.0012	0.0144	0.0097	0.0066	0.0339	0.0205	0.0075	0.0205	0.1031
Luminosity %	1.9037	1.8807	1.8839	1.8802	1.8865	1.8974	1.8980	1.9088	1.9106	1.8980	1.8884	1.8887	1.8957	1.9010	1.9056	1.9173	1.9285	1.9466	1.9677	1.9503	2.0485
Total uncertainty %	4.1934	3.7027	3.2117	2.8232	3.1765	2.8034	3.1524	2.9306	2.8598	2.4551	2.5255	2.2937	2.2971	2.3261	2.4733	2.6443	3.3192	3.7041	4.8508	6.2622	10.2100

Table 9.7: Differential absolute cross section for p_{T} (ℓ^{+}) + p_{T} (ℓ^{-}).

p_{T} (ℓ^{+}) + p_{T} (ℓ^{-}) bins [GeV]	50.0-60.0	60.0-70.0	70.0-80.0	80.0-100.0	100.0-125.0	125.0-150.0	150.0-200.0	200.0-250.0	250.0-300.0	300.0-400.0	400.0-600.0
Cross section [fb/GeV]	25.4190	73.1471	104.5368	116.7224	97.5588	63.5721	29.8933	10.3089	3.9637	1.1605	0.1430
Data statistics %	1.2577	0.6761	0.5428	0.3431	0.3404	0.3979	0.4146	0.6564	1.0932	1.4334	2.8288
MC statistics %	0.5705	0.2662	0.1718	0.0977	0.0800	0.1000	0.1070	0.1932	0.2921	0.3850	0.8683
Fragmentation %	2.0867	0.3881	1.0976	0.5318	0.0334	0.2899	0.3702	1.0519	1.5201	1.5707	1.2404
Hard scattering %	1.5056	0.7317	1.0698	0.4903	0.1119	0.4897	0.9757	0.0816	2.1492	3.7171	3.4022
Top mass dependence %	0.1966	0.1385	0.0913	0.1017	0.0940	0.0827	0.0476	0.0568	0.1182	0.2026	0.1231
PDF %	0.0396	0.0425	0.0455	0.0503	0.0630	0.0754	0.0881	0.1064	0.1126	0.1121	0.1054
ISR %	0.3592	0.1570	0.0523	0.2130	0.2129	0.1358	0.2366	0.3875	0.0852	0.3346	0.5727
FSR %	0.9352	0.3178	0.3388	0.1414	0.1975	0.0909	0.2880	0.1967	0.3218	1.1552	0.0515
Electron scale and resolution %	0.0337	0.0589	0.0408	0.0950	0.0760	0.0330	0.2638	0.6173	0.9245	1.2830	1.9828
Electron efficiency %	0.9194	0.5666	0.4417	0.3840	0.3384	0.3302	0.3701	0.4694	0.5656	0.8954	2.0583
Muon scale and resolution scale %	0.1173	0.0648	0.0166	0.0164	0.0371	0.0695	0.0965	0.1206	0.1410	0.1559	0.3689
Muon reconstruction efficiency %	0.2137	0.2153	0.2162	0.2175	0.2205	0.2230	0.2291	0.2373	0.2430	0.2517	0.2813
Muon trigger, ISO, TTVA efficiency %	0.3333	0.2984	0.2809	0.2919	0.2724	0.2584	0.2503	0.2486	0.2500	0.2564	0.2866
JVT %	0.0206	0.0357	0.0278	0.0255	0.0288	0.0291	0.0341	0.0425	0.0410	0.0505	0.0919
JES b-jes response %	0.0728	0.0856	0.0665	0.0487	0.0416	0.0359	0.0417	0.0443	0.0841	0.1127	0.0747
JES effective NPs %	0.0869	0.0575	0.0490	0.0450	0.0120	0.0112	0.0187	0.0507	0.0176	0.0128	0.1173
JES EtaInterCalibration %	0.2051	0.0208	0.0178	0.0213	0.0038	0.0034	0.0037	0.0171	0.0044	0.0110	0.0278
JES flavour %	0.2239	0.0261	0.0118	0.0119	0.0479	0.0736	0.1009	0.1414	0.1692	0.2182	0.3608
JES pileup %	0.2423	0.0519	0.0442	0.0426	0.0033	0.0199	0.0324	0.0743	0.0234	0.0312	0.1357
JES PunchThrough %	0.0004	0.0000	0.0002	0.0002	0.0000	0.0001	0.0001	0.0007	0.0001	0.0004	0.0001
JES HighPt %	0.0000	0.0000	0.0000	0.0000	0.0000	0.0000	0.0000	0.0000	0.0000	0.0000	0.0000
MET soft term %	0.0000	0.0000	0.0000	0.0000	0.0000	0.0000	0.0000	0.0000	0.0000	0.0000	0.0000
JER %	0.0000	0.0000	0.0001	0.0000	0.0000	0.0000	0.0000	0.0000	0.0000	0.0000	0.0000
b-tagging %	0.1487	0.1190	0.1008	0.0845	0.0905	0.0808	0.0860	0.0935	0.0877	0.1137	0.2284
Wt background %	0.6633	0.6876	0.6869	0.5822	0.6295	0.6741	1.0290	2.1374	2.7111	4.3083	11.4244
Diboson background %	0.0431	0.0387	0.0408	0.0383	0.0440	0.0520	0.0662	0.0946	0.1328	0.1724	0.3603
ttV background %	0.0211	0.0225	0.0221	0.0234	0.0259	0.0304	0.0391	0.0528	0.0642	0.0833	0.1426
Z+jets background %	0.4624	0.2297	0.1194	0.0590	0.0362	0.0536	0.0360	0.0274	0.0203	0.0427	0.0384
Fakes background %	0.4670	0.3843	0.3233	0.3231	0.3043	0.3057	0.3145	0.3942	0.4518	0.4298	0.7579
Pileup %	1.4869	1.2527	1.0768	0.9039	0.7227	0.5602	0.3958	0.3103	0.2859	0.2722	0.0119
Beam energy %	0.0279	0.0022	0.0080	0.0076	0.0082	0.0003	0.0062	0.0169	0.0174	0.0645	0.0554
Luminosity %	1.8926	1.8940	1.8786	1.8789	1.8835	1.8936	1.9173	1.9685	2.0064	2.0510	2.2504
Total uncertainty %	4.1765	2.7724	2.9027	2.4143	2.2480	2.2872	2.6023	3.3567	4.6253	6.7627	12.9318

Table 9.8: Differential absolute cross section for p_{T} $(\ell^+\ell^-)$.

p_{T} $(\ell^+\ell^-)$ bins [GeV]	0.0-20.0	20.0-30.0	30.0-45.0	45.0-60.0	60.0-75.0	75.0-100.0	100.0-125.0	125.0-150.0	150.0-200.0	200.0-300.0
Cross section [fb/GeV]	33.1519	69.8572	88.6780	112.3852	122.4377	94.4376	49.1848	20.0082	5.8371	0.8800
Data statistics %	0.6835	0.6510	0.4728	0.4213	0.3946	0.3341	0.4598	0.7100	0.9602	1.7953
MC statistics %	0.2434	0.2133	0.1296	0.1070	0.0990	0.0841	0.1147	0.1841	0.2633	0.5380
Fragmentation %	0.5800	0.3941	0.2617	0.4014	0.1413	0.0908	0.5706	0.8212	0.8187	0.1315
Hard scattering %	0.2319	1.0103	0.4888	0.9200	0.9888	0.0728	0.9012	0.9656	0.9677	1.1914
Top mass dependence %	0.0477	0.0407	0.0227	0.0139	0.0290	0.0036	0.0378	0.0633	0.0468	0.1042
PDF %	0.0267	0.0306	0.0278	0.0296	0.0298	0.0367	0.0544	0.0694	0.0803	0.0775
ISR %	0.1666	0.1260	0.4981	0.2355	0.4737	0.2698	0.3393	0.1970	0.1185	0.0141
FSR %	0.3877	0.6821	0.1088	0.2631	0.3471	0.0823	0.2888	0.0119	0.0872	1.7007
Electron scale and resolution %	0.1448	0.1681	0.1177	0.0653	0.0400	0.0909	0.3225	0.7283	1.1366	1.7032
Electron efficiency %	0.3620	0.3544	0.3572	0.3713	0.3603	0.3414	0.3531	0.4035	0.4923	1.0732
Muon scale and resolution scale %	0.0354	0.0169	0.0257	0.0246	0.0263	0.0567	0.1069	0.1637	0.1802	0.2796
Muon reconstruction efficiency %	0.2191	0.2206	0.2208	0.2201	0.2203	0.2227	0.2257	0.2313	0.2423	0.2793
Muon trigger, ISO, TTVA efficiency %	0.2758	0.2755	0.2704	0.2693	0.2696	0.2687	0.2597	0.2588	0.2657	0.2987
JVT %	0.0354	0.0348	0.0334	0.0333	0.0299	0.0283	0.0239	0.0294	0.0327	0.0848
JES b-jes response %	0.0937	0.1083	0.0900	0.0721	0.0654	0.0358	0.0145	0.0234	0.0564	0.0159
JES effective NPs %	0.0111	0.1092	0.0411	0.0336	0.0240	0.0085	0.0265	0.0709	0.0976	0.1100
JES EtaInterCalibration %	0.0506	0.0661	0.0174	0.0082	0.0152	0.0037	0.0080	0.0243	0.0396	0.0379
JES flavour %	0.1198	0.0260	0.0633	0.0581	0.0666	0.0560	0.0679	0.0871	0.1176	0.1591
JES pileup %	0.0696	0.1069	0.0391	0.0234	0.0151	0.0154	0.0369	0.0877	0.1242	0.1342
JES PunchThrough %	0.0001	0.0003	0.0000	0.0000	0.0000	0.0001	0.0001	0.0003	0.0000	0.0007
JES HighPt %	0.0000	0.0000	0.0000	0.0000	0.0000	0.0000	0.0000	0.0000	0.0000	0.0000
MET soft term %	0.0000	0.0000	0.0000	0.0000	0.0000	0.0000	0.0000	0.0000	0.0000	0.0000
JER %	0.0000	0.0000	0.0000	0.0000	0.0001	0.0000	0.0000	0.0000	0.0000	0.0000
b-tagging %	0.1292	0.1301	0.1119	0.0990	0.0893	0.0849	0.1168	0.1669	0.2293	0.3229
Wt background %	0.7419	0.5818	0.6302	0.6425	0.5867	0.6135	0.8867	1.9483	3.4339	11.8459
Diboson background %	0.0398	0.0427	0.0447	0.0375	0.0353	0.0435	0.0616	0.0937	0.1886	0.5867
ttV background %	0.0265	0.0264	0.0260	0.0250	0.0249	0.0271	0.0340	0.0503	0.0818	0.1774
Z+jets background %	0.1726	0.1861	0.0264	0.0685	0.0620	0.0450	0.0473	0.1656	0.0141	0.1112
Fakes background %	0.3326	0.3171	0.3092	0.3076	0.3114	0.2898	0.3009	0.4125	0.6268	1.0928
Pileup %	0.8557	0.8200	0.7416	0.7892	0.7258	0.6844	0.5024	0.5190	0.4249	0.5374
Beam energy %	0.0191	0.0042	0.0099	0.0024	0.0075	0.0008	0.0038	0.0326	0.0026	0.0066
Luminosity %	1.8910	1.8899	1.8866	1.8848	1.8854	1.8902	1.9036	1.9465	2.0331	2.3170
Total uncertainty %	2.5348	2.6807	2.3891	2.5093	2.5120	2.2320	2.5894	3.3388	4.5785	12.6447

Table 9.9: Differential absolute cross section for $\Delta\phi(\ell^+\ell^-)$.

$\Delta\phi(\ell^+\ell^-)$ bins	0.00-0.10	0.10-0.21	0.21-0.31	0.31-0.42	0.42-0.52	0.52-0.63	0.63-0.73	0.73-0.84	0.84-0.94	0.94-1.05	1.05-1.15	1.15-1.26	1.26-1.36
Cross section [fb/rad]	1121.71	1125.30	1088.25	1139.10	1122.09	1158.53	1176.12	1224.07	1260.98	1259.25	1318.59	1382.21	1441.29
Data statistics %	1.6913	1.6115	1.5714	1.5504	1.5436	1.4472	1.4690	1.4134	1.4680	1.4420	1.4192	1.4002	1.3025
MC statistics %	0.3901	0.3996	0.4017	0.3752	0.3708	0.3642	0.3680	0.3558	0.3567	0.3709	0.3719	0.3405	0.3283
Fragmentation %	1.0067	0.4773	1.3012	0.7964	1.1451	0.9576	0.3863	0.0043	0.5644	0.0964	0.6465	0.6994	0.9659
Hard scattering %	0.6815	1.0152	0.9577	1.3391	2.5493	0.5875	0.4188	0.9332	1.3577	0.8328	1.1443	0.8662	0.8858
Top mass dependence %	0.2007	0.0059	0.0476	0.0261	0.1649	0.1720	0.0569	0.1471	0.1945	0.0117	0.0636	0.0385	0.0042
PDF %	0.0548	0.0528	0.0407	0.0372	0.0469	0.0331	0.0375	0.0475	0.0420	0.0450	0.0420	0.0417	0.0396
ISR %	0.3952	0.0530	0.0613	0.5750	0.2660	0.2759	0.0372	0.2385	0.6290	0.1210	0.1468	0.5850	0.0880
FSR %	0.1986	0.4009	0.1317	0.0627	0.5241	0.0834	0.2200	0.0007	0.5877	0.3919	0.1752	0.2649	0.4424
Electron scale and resolution %	0.1754	0.1683	0.1700	0.1917	0.1711	0.1575	0.1809	0.1490	0.1440	0.1681	0.1469	0.1439	0.1462
Electron efficiency %	0.3842	0.3841	0.3812	0.3788	0.3794	0.3804	0.3766	0.3758	0.3770	0.3727	0.3695	0.3676	0.3666
Muon scale and resolution scale %	0.0873	0.0847	0.0512	0.0813	0.0696	0.0689	0.0840	0.0728	0.0626	0.0630	0.0703	0.0612	0.0568
Muon reconstruction efficiency %	0.2195	0.2184	0.2196	0.2208	0.2195	0.2198	0.2201	0.2208	0.2193	0.2195	0.2220	0.2232	0.2210
Muon trigger, ISO, TTVA efficiency %	0.2758	0.2764	0.2778	0.2773	0.2763	0.2750	0.2758	0.2756	0.2757	0.2755	0.2755	0.2749	0.2737
JVT %	0.0165	0.0208	0.0222	0.0239	0.0289	0.0168	0.0242	0.0268	0.0247	0.0318	0.0267	0.0239	0.0209
JES b-jes response %	0.0368	0.0665	0.0435	0.0055	0.0233	0.0243	0.0144	0.0137	0.0223	0.0199	0.0145	0.0156	0.0113
JES effective NPs %	0.0097	0.0604	0.0436	0.0206	0.0203	0.0107	0.0328	0.0345	0.0425	0.0255	0.0235	0.0306	0.0160
JES EtaInterCalibration %	0.0111	0.0055	0.0148	0.0139	0.0066	0.0241	0.0201	0.0220	0.0213	0.0126	0.0010	0.0080	0.0080
JES flavour %	0.0169	0.0150	0.0292	0.0011	0.0161	0.0244	0.0348	0.0305	0.0275	0.0404	0.0531	0.0121	0.0267
JES pileup %	0.0344	0.0503	0.0450	0.0204	0.0134	0.0137	0.0580	0.0450	0.0590	0.0374	0.0422	0.0233	0.0234
JES PunchThrough %	0.0000	0.0000	0.0000	0.0000	0.0007	0.0000	0.0002	0.0000	0.0006	0.0000	0.0000	0.0000	0.0000
JES HighPt %	0.0000	0.0000	0.0000	0.0000	0.0000	0.0000	0.0000	0.0000	0.0000	0.0000	0.0000	0.0000	0.0000
MET soft term %	0.0000	0.0000	0.0000	0.0000	0.0000	0.0000	0.0000	0.0000	0.0000	0.0000	0.0000	0.0000	0.0000
JER %	0.0009	0.0000	0.0000	0.0000	0.0000	0.0000	0.0000	0.0000	0.0000	0.0000	0.0000	0.0000	0.0000
b-tagging %	0.1319	0.0971	0.1118	0.1109	0.0990	0.1099	0.0965	0.1021	0.0991	0.0946	0.1043	0.0957	0.0989
Wt background %	0.7197	0.5569	0.7811	1.4982	1.0743	0.5894	0.7763	0.8753	0.9150	0.9137	0.7984	0.7913	0.7103
Diboson background %	0.0811	0.0892	0.0842	0.0722	0.0820	0.0658	0.0711	0.0670	0.0766	0.0642	0.0759	0.0600	0.0619
ttV background %	0.0331	0.0339	0.0336	0.0322	0.0317	0.0322	0.0337	0.0318	0.0328	0.0321	0.0308	0.0327	0.0301
Z+jets background %	0.1976	0.1767	0.0237	0.1202	0.1526	0.1499	0.4153	0.1770	0.0964	0.0371	0.1521	0.1795	0.0423
Fakes background %	0.5367	0.3782	0.4450	0.3964	0.3512	0.4444	0.3617	0.3309	0.5382	0.4291	0.4027	0.4511	0.4709
Pileup %	0.7526	0.7635	0.8673	0.8426	0.8365	0.9020	0.9204	0.8446	0.8219	0.7031	0.7732	0.8370	0.7907
Beam energy %	0.0316	0.1083	0.0020	0.0350	0.0590	0.0086	0.0085	0.0303	0.0653	0.0259	0.0332	0.0054	0.0698
Luminosity %	1.8862	1.8805	1.8884	1.8933	1.8838	1.8868	1.8864	1.8843	1.9019	1.8991	1.8985	1.9015	1.9004
Total uncertainty %	3.1683	3.0222	3.2747	3.5147	4.0719	2.9769	2.8832	2.9262	3.3126	2.9201	3.0456	3.0350	2.9994

$\Delta\phi(\ell^+\ell^-)$ bins	1.36-1.47	1.47-1.57	1.57-1.68	1.68-1.78	1.78-1.88	1.88-1.99	1.99-2.09	2.09-2.20	2.20-2.30	2.30-2.41	2.41-2.51	2.51-2.62	2.62-2.72	2.72-2.83	2.83-2.93	2.93-3.04	3.04-3.14
Cross section [fb/rad]	1518.67	1558.40	1634.70	1707.84	1778.35	1815.63	1953.95	2009.68	2123.71	2194.18	2258.18	2303.75	2328.95	2414.87	2441.99	2498.65	2586.68
Data statistics %	1.3442	1.2962	1.2638	1.2344	1.1986	1.1861	1.1350	1.1546	1.0875	1.0391	1.0720	1.0260	1.0418	1.0153	1.0247	1.0015	0.9808
MC statistics %	0.3344	0.3265	0.3191	0.3376	0.3184	0.3630	0.3262	0.3075	0.3125	0.3099	0.2956	0.2924	0.3115	0.2853	0.3127	0.3394	0.2626
Fragmentation %	0.2694	0.4252	0.1509	0.4053	0.6399	0.5295	1.1504	0.2611	0.2990	0.6707	0.0205	0.0599	0.0268	0.5650	0.0341	0.0936	0.2494
Hard scattering %	1.7150	0.9844	1.9093	0.6574	1.7629	0.7220	0.7182	0.9247	1.4716	0.2468	0.0323	1.0686	0.9294	0.0606	0.5106	0.5005	0.0250
Top mass dependence %	0.1379	0.1272	0.1618	0.1318	0.0951	0.1920	0.0223	0.0004	0.0076	0.0387	0.0148	0.0137	0.0321	0.0289	0.0534	0.0073	0.0229
PDF %	0.0430	0.0372	0.0348	0.0440	0.0464	0.0410	0.0385	0.0313	0.0369	0.0344	0.0363	0.0380	0.0341	0.0350	0.0351	0.0352	0.0363
ISR %	0.3928	0.2303	0.3729	0.1628	0.2222	0.7660	0.5666	0.1041	0.1518	0.5170	0.1477	0.1854	0.5383	0.1126	0.4092	0.0975	0.0320
FSR %	0.4062	0.4572	0.6506	0.3965	0.2010	0.1605	0.5947	0.9390	0.4324	0.3686	0.3787	0.4182	0.0054	0.1174	0.3306	0.6951	0.0861
Electron scale and resolution %	0.1233	0.1345	0.1284	0.1235	0.1104	0.1097	0.1023	0.0971	0.0989	0.0931	0.0852	0.0794	0.0696	0.0775	0.0755	0.0795	0.0659
Electron efficiency %	0.3653	0.3607	0.3578	0.3536	0.3515	0.3500	0.3494	0.3494	0.3483	0.3479	0.3525	0.3566	0.3601	0.3646	0.3702	0.3747	0.3768
Muon scale and resolution scale %	0.0596	0.0589	0.0593	0.0574	0.0488	0.0461	0.0441	0.0337	0.0487	0.0453	0.0453	0.0614	0.0322	0.0225	0.0369	0.0297	0.0365
Muon reconstruction efficiency %	0.2235	0.2206	0.2227	0.2229	0.2238	0.2242	0.2256	0.2231	0.2279	0.2251	0.2240	0.2231	0.2259	0.2245	0.2273	0.2252	0.2272
Muon trigger, ISO, TTVA efficiency %	0.2735	0.2727	0.2726	0.2713	0.2710	0.2712	0.2697	0.2683	0.2664	0.2647	0.2638	0.2640	0.2626	0.2612	0.2613	0.2596	0.2587
JVT %	0.0285	0.0246	0.0215	0.0255	0.0279	0.0313	0.0351	0.0244	0.0320	0.0357	0.0376	0.0363	0.0356	0.0313	0.0391	0.0356	0.0361
JES b-jes response %	0.0072	0.0274	0.0127	0.0360	0.0333	0.0584	0.0225	0.0689	0.0753	0.0929	0.0807	0.0918	0.0950	0.1044	0.0868	0.0729	0.1050
JES effective NPs %	0.0196	0.0058	0.0290	0.0454	0.0212	0.0148	0.0296	0.0280	0.0110	0.0449	0.0871	0.0556	0.0286	0.0299	0.0277	0.0430	0.0476
JES EtaInterCalibration %	0.0177	0.0181	0.0101	0.0034	0.0194	0.0153	0.0098	0.0120	0.0083	0.0219	0.1220	0.0366	0.0103	0.0033	0.0150	0.0187	0.0268
JES flavour %	0.0530	0.0290	0.0676	0.0166	0.0571	0.0809	0.0641	0.0652	0.1087	0.0955	0.2145	0.0576	0.1145	0.0987	0.0916	0.0694	0.1063
JES pileup %	0.0365	0.0114	0.0345	0.0327	0.0415	0.0091	0.0376	0.0155	0.0142	0.0358	0.1896	0.0440	0.0288	0.0207	0.0195	0.0325	0.0323
JES PunchThrough %	0.0000	0.0010	0.0000	0.0010	0.0003	0.0003	0.0000	0.0003	0.0000	0.0004	0.0000	0.0000	0.0005	0.0000	0.0007	0.0005	0.0012
JES HighPt %	0.0000	0.0000	0.0000	0.0000	0.0000	0.0000	0.0000	0.0000	0.0000	0.0000	0.0000	0.0000	0.0000	0.0000	0.0000	0.0000	0.0000
MET soft term %	0.0000	0.0000	0.0000	0.0000	0.0000	0.0000	0.0000	0.0000	0.0000	0.0000	0.0000	0.0000	0.0000	0.0000	0.0000	0.0000	0.0000
JER %	0.0000	0.0000	0.0000	0.0000	0.0000	0.0000	0.0000	0.0000	0.0000	0.0000	0.0000	0.0000	0.0000	0.0000	0.0000	0.0000	0.0000
b-tagging %	0.0942	0.0848	0.0905	0.1059	0.0959	0.0868	0.0879	0.0824	0.0889	0.0865	0.1071	0.0971	0.0974	0.1084	0.0907	0.1290	0.0894
Wt background %	0.5482	0.6855	0.9139	0.5992	0.9690	0.8535	0.7121	0.7047	0.7151	0.7748	1.3361	1.0878	0.8155	0.9010	0.8914	0.9410	0.8122
Diboson background %	0.0542	0.0425	0.0478	0.0560	0.0462	0.0540	0.0531	0.0472	0.0454	0.0446	0.0432	0.0499	0.0503	0.0420	0.0469	0.0496	0.0452
ttV background %	0.0301	0.0311	0.0296	0.0314	0.0301	0.0322	0.0315	0.0303	0.0304	0.0309	0.0320	0.0320	0.0314	0.0336	0.0332	0.0316	0.0332
Z+jets background %	0.0289	0.1987	0.1800	0.0109	0.1544	0.1879	0.2019	0.1497	0.0160	0.0541	0.2048	0.0155	0.0077	0.0184	0.2010	0.0494	0.0496
Fakes background %	0.4815	0.3747	0.3157	0.3523	0.2751	0.3476	0.3981	0.3538	0.3972	0.3451	0.4095	0.3744	0.3457	0.3335	0.2618	0.3217	0.3435
Pileup %	0.8146	0.6991	0.7290	0.5876	0.5940	0.5532	0.5588	0.7293	0.6271	0.7290	0.6688	0.5812	0.6548	0.6099	0.5260	0.5586	0.5068
Beam energy %	0.0035	0.0442	0.0005	0.0066	0.0461	0.0380	0.0301	0.0001	0.0105	0.0434	0.0065	0.0493	0.0210	0.0465	0.0176	0.0364	0.0006
Luminosity %	1.9015	1.8962	1.8954	1.8975	1.8984	1.9104	1.9115	1.9074	1.9065	1.9025	1.9109	1.9152	1.9119	1.9090	1.9089	1.9047	1.9013
Total uncertainty %	3.2219	2.8704	3.3673	2.6747	3.2304	2.8489	2.9769	2.8868	2.9547	2.6932	2.8068	2.8488	2.7390	2.5887	2.6094	2.6654	2.4619

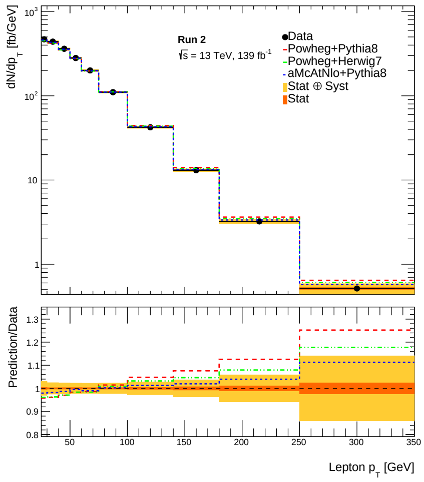

(a)

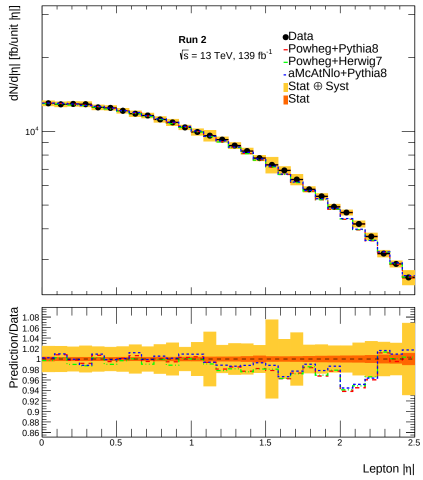

(b)

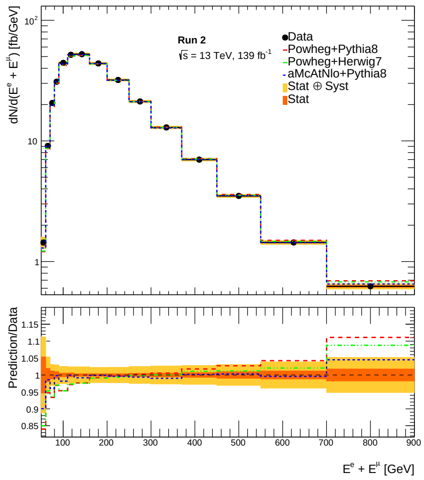

(c)

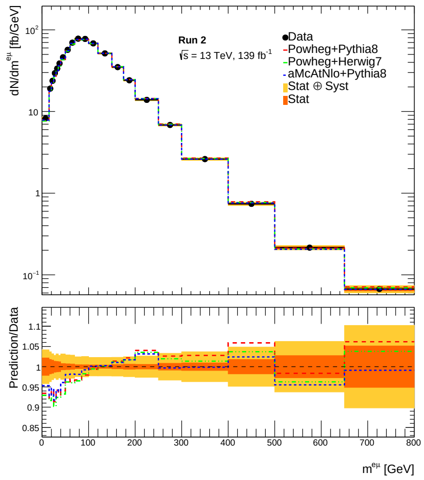

(d)

Figure 9.1: The measured absolute differential cross section is plotted together with the predictions from three different Monte Carlo samples, the nominal Powheg+Pythia 8, the Powheg + Herwig 7 sample and the MadGraph5_aMC@NLO + Pythia 8 sample for the variables $p_{\mathrm{T}}(\ell)$, $\eta(\ell)$, $E(\ell^+) + E(\ell^-)$ and $m(\ell^+\ell^-)$.

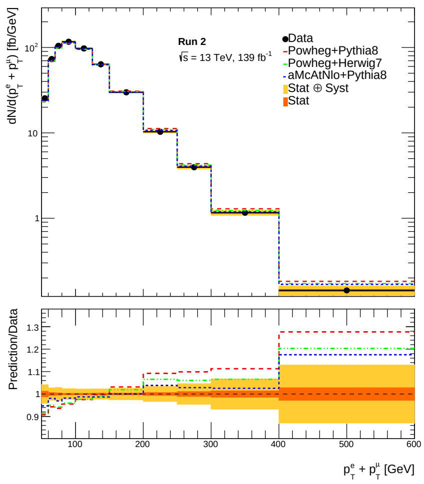

(a)

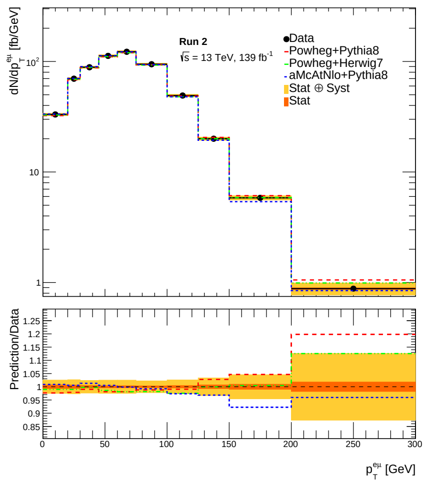

(b)

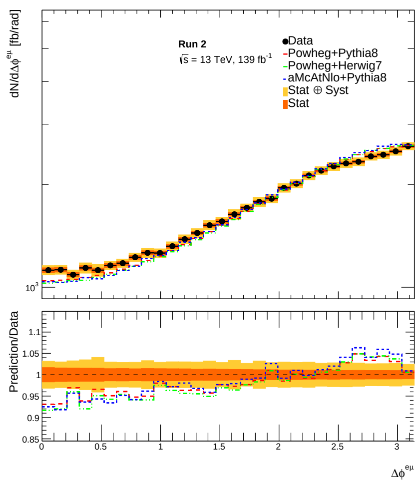

(c)

Figure 9.2: The measured absolute differential cross section is plotted together with the predictions from three different Monte Carlo samples, the nominal Powheg+Pythia 8, the Powheg + Herwig 7 sample and the MadGraph5_aMC@NLO + Pythia 8 sample for the variables $p_{\mathrm{T}}(\ell^+) + p_{\mathrm{T}}(\ell^-)$, $p_{\mathrm{T}}(\ell^+\ell^-)$ and $\Delta\phi(\ell^+\ell^-)$.

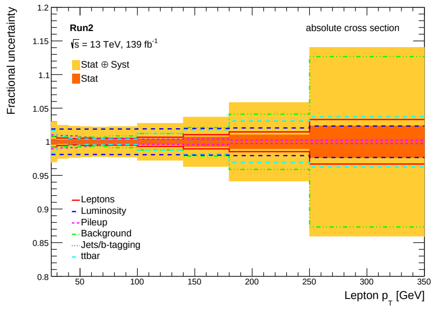

(a)

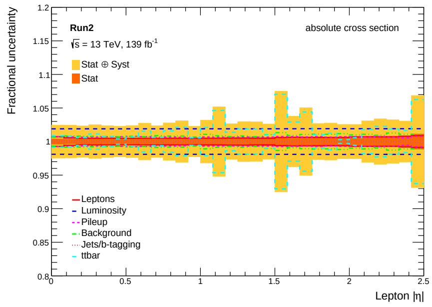

(b)

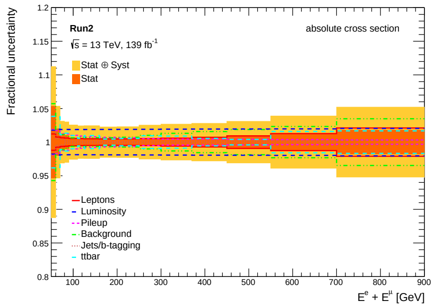

(c)

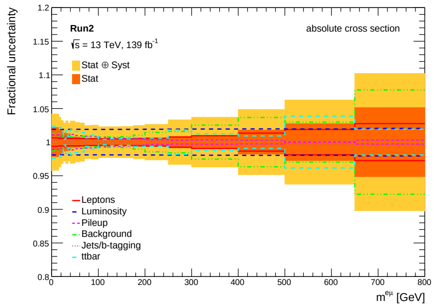

(d)

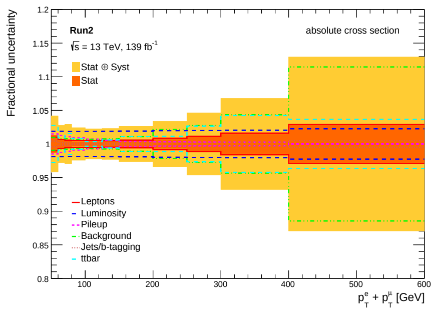

(e)

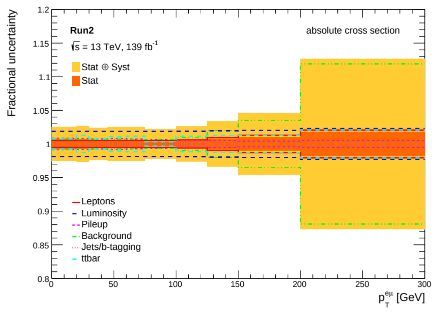

(f)

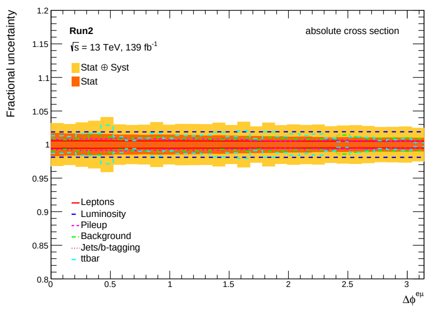

(g)

Figure 9.3: Statistical and total systematic error and contributions from different categories of systematic uncertainties for the absolute differential cross section.

Table 9.10: Normalised differential cross section for p_T (ℓ).

p_T (ℓ) bins [GeV]	25.0-30.0	30.0-40.0	40.0-50.0	50.0-60.0	60.0-75.0	75.0-100.0	100.0-140.0	140.0-180.0	180.0 250.0	250.0 350.0
Normalised cross section [10^{-3}/GeV]	21.8802	20.5197	16.8920	13.1182	9.3423	5.1520	1.9746	0.6108	0.1506	0.0241
Data statistics %	0.3467	0.2353	0.2584	0.2889	0.2639	0.2691	0.3747	0.6991	1.0149	2.3567
MC statistics %	0.1083	0.0684	0.0659	0.0765	0.0720	0.0774	0.0968	0.1894	0.3064	0.7071
Fragmentation %	0.8667	0.2176	0.2888	0.1228	0.0987	0.2770	0.9230	1.3426	1.3711	1.0303
Hard scattering %	1.0372	0.3605	0.0861	0.0160	0.1339	0.1529	1.2058	1.3478	3.0913	3.7922
Top mass dependence %	0.0197	0.0022	0.0064	0.0241	0.0012	0.0058	0.0196	0.1161	0.0914	0.1235
PDF %	0.0142	0.0096	0.0059	0.0023	0.0047	0.0100	0.0183	0.0321	0.0485	0.0581
ISR %	0.0040	0.0032	0.0280	0.0431	0.0202	0.0831	0.0440	0.0311	0.1038	0.4652
FSR %	0.0180	0.1100	0.0679	0.0295	0.1396	0.0029	0.0862	0.4987	0.0265	0.2278
Electron scale and resolution %	0.0647	0.0191	0.1063	0.1631	0.1405	0.0234	0.3089	0.7476	1.1866	2.0194
Electron efficiency %	0.4541	0.1558	0.1101	0.1112	0.1356	0.1580	0.2397	0.3617	0.4570	2.3416
Muon scale and resolution scale %	0.0450	0.0341	0.0144	0.0081	0.0188	0.0268	0.0599	0.0725	0.1189	0.3008
Muon reconstruction efficiency %	0.0055	0.0030	0.0023	0.0014	0.0003	0.0025	0.0077	0.0158	0.0266	0.0680
Muon trigger, ISO, TTVA efficiency %	0.0983	0.0132	0.0187	0.0642	0.0306	0.0319	0.0335	0.0353	0.0430	0.0740
JVT %	0.0021	0.0015	0.0028	0.0028	0.0015	0.0021	0.0046	0.0078	0.0188	0.0620
JES b-jes response %	0.0083	0.0034	0.0045	0.0001	0.0029	0.0010	0.0114	0.0015	0.0034	0.0330
JES effective NPs %	0.0111	0.0107	0.0094	0.0171	0.0084	0.0122	0.0306	0.0436	0.0698	0.1166
JES EtaInterCalibration %	0.0235	0.0050	0.0035	0.0140	0.0024	0.0015	0.0085	0.0224	0.0110	0.0515
JES flavour %	0.0109	0.0244	0.0235	0.0266	0.0094	0.0259	0.0586	0.0896	0.1459	0.2151
JES pileup %	0.0599	0.0118	0.0123	0.0180	0.0128	0.0170	0.0379	0.0604	0.0807	0.1362
JES PunchThrough %	0.0001	0.0002	0.0000	0.0000	0.0001	0.0001	0.0001	0.0006	0.0003	0.0000
JES HighPt %	0.0000	0.0000	0.0000	0.0000	0.0000	0.0000	0.0000	0.0000	0.0000	0.0000
MET soft term %	0.0000	0.0000	0.0000	0.0000	0.0000	0.0000	0.0000	0.0000	0.0000	0.0000
JER %	0.0001	0.0000	0.0000	0.0000	0.0000	0.0000	0.0000	0.0000	0.0000	0.0000
b-tagging %	0.0169	0.0252	0.0115	0.0121	0.0127	0.0177	0.0324	0.0766	0.1042	0.2198
Wt background %	0.2147	0.3029	0.2847	0.2101	0.2192	0.1677	0.6448	1.6182	3.6565	12.2137
Diboson background %	0.0073	0.0068	0.0071	0.0095	0.0034	0.0025	0.0188	0.0471	0.1112	0.3541
ttV background %	0.0049	0.0046	0.0037	0.0029	0.0011	0.0028	0.0108	0.0248	0.0495	0.1228
Z+jets background %	0.0293	0.0491	0.0089	0.0598	0.0220	0.0222	0.0298	0.0521	0.0296	0.1209
Fakes background %	0.0592	0.0112	0.0253	0.0127	0.0185	0.0105	0.0139	0.0797	0.1586	0.4678
Pileup %	0.3124	0.1962	0.1559	0.0341	0.1809	0.2457	0.3224	0.3089	0.4818	0.4986
Beam energy %	0.0048	0.0048	0.0012	0.0009	0.0003	0.0052	0.0086	0.0141	0.0153	0.0342
Luminosity %	0.0016	0.0069	0.0121	0.0117	0.0107	0.0011	0.0237	0.0757	0.1579	0.4444
Total uncertainty %	1.5280	0.6403	0.5465	0.4495	0.4940	0.5508	1.7755	2.8029	5.2847	13.4749

Table 9.11: Normalised differential cross section for $|\eta(\ell)|$.

$\|\eta(\ell)\|$ bins	0.0-0.08	0.08-0.17	0.17-0.25	0.25-0.33	0.33-0.42	0.42-0.50	0.50-0.58	0.58-0.67	0.67-0.75	0.75-0.83	0.83-0.92	0.92-1.00	1.00-1.08
Normalised cross section [10^{-2}/unit $\|\eta\|$]	60.9466	60.3770	60.5925	60.4326	58.6592	58.3639	56.8164	55.2806	54.3470	52.3767	50.9353	48.5985	46.5523
Data statistics %	0.8517	0.7398	0.7400	0.7359	0.7436	0.7193	0.7605	0.7426	0.7572	0.8128	0.8059	0.8401	0.8358
MC statistics %	0.1419	0.1510	0.1311	0.1373	0.1267	0.1290	0.1224	0.1300	0.1387	0.1367	0.1352	0.1524	0.1601
Fragmentation %	0.2212	0.1464	0.1269	0.8464	0.3210	0.2933	0.1772	1.3856	0.0349	0.8416	1.8808	0.5037	1.5240
Hard scattering %	0.1064	0.1454	0.0211	1.0798	0.1419	0.3716	0.5747	1.3209	0.0639	0.6683	1.6166	0.2611	0.7954
Top mass dependence %	0.0046	0.0125	0.0395	0.0120	0.0118	0.0369	0.0024	0.0369	0.0281	0.0727	0.0107	0.0123	0.0133
PDF %	0.0120	0.0103	0.0104	0.0098	0.0088	0.0097	0.0084	0.0090	0.0084	0.0099	0.0086	0.0073	0.0059
ISR %	0.0106	0.0398	0.1440	0.1657	0.0853	0.0784	0.1090	0.0438	0.0592	0.1865	0.0405	0.0919	0.1004
FSR %	0.2547	0.1654	0.1248	0.2614	0.0686	0.0216	0.2809	0.0106	0.3800	0.2992	0.1217	0.0249	0.1137
Electron scale and resolution %	0.0489	0.0327	0.0348	0.0299	0.0358	0.0315	0.0364	0.0218	0.0264	0.0178	0.0137	0.0176	0.0076
Electron efficiency %	0.1286	0.0612	0.0593	0.0602	0.0603	0.0601	0.0599	0.0932	0.1135	0.1083	0.1065	0.1079	0.1108
Muon scale and resolution scale %	0.0164	0.0180	0.0105	0.0111	0.0113	0.0097	0.0170	0.0110	0.0156	0.0112	0.0065	0.0054	0.0091
Muon reconstruction efficiency %	0.3046	0.1125	0.0149	0.0143	0.0154	0.0222	0.0217	0.0220	0.0188	0.0177	0.0186	0.0174	0.0126
Muon trigger, ISO, TTVA efficiency %	0.0127	0.0111	0.0074	0.0071	0.0078	0.0071	0.0060	0.0042	0.0072	0.0062	0.0034	0.0077	0.0068
JVT %	0.0023	0.0032	0.0017	0.0015	0.0046	0.0016	0.0021	0.0009	0.0018	0.0020	0.0015	0.0020	0.0023
JES b-jes response %	0.0042	0.0003	0.0077	0.0008	0.0009	0.0003	0.0045	0.0100	0.0276	0.0000	0.0083	0.0008	0.0157
JES effective NPs %	0.0063	0.0090	0.0120	0.0061	0.0133	0.0117	0.0088	0.0031	0.0209	0.0304	0.0071	0.0072	0.0217
JES EtaInterCalibration %	0.0165	0.0065	0.0047	0.0134	0.0056	0.0107	0.0096	0.0050	0.0225	0.0325	0.0059	0.0099	0.0419
JES flavour %	0.0044	0.0059	0.0039	0.0056	0.0086	0.0136	0.0039	0.0099	0.0024	0.0333	0.0090	0.0023	0.0511
JES pileup %	0.0088	0.0049	0.0115	0.0044	0.0094	0.0203	0.0148	0.0113	0.0208	0.0472	0.0110	0.0089	0.0314
JES PunchThrough %	0.0000	0.0002	0.0001	0.0002	0.0002	0.0001	0.0002	0.0001	0.0002	0.0002	0.0000	0.0001	0.0000
JES HighPt %	0.0000	0.0000	0.0000	0.0000	0.0000	0.0000	0.0000	0.0000	0.0000	0.0000	0.0000	0.0000	0.0000
MET soft term %	0.0000	0.0000	0.0000	0.0000	0.0000	0.0000	0.0000	0.0000	0.0000	0.0000	0.0000	0.0000	0.0000
JER %	0.0000	0.0000	0.0000	0.0000	0.0001	0.0001	0.0000	0.0001	0.0000	0.0000	0.0000	0.0000	0.0000
b-tagging %	0.0167	0.0190	0.0384	0.0079	0.0143	0.0253	0.0126	0.0077	0.0107	0.0199	0.0122	0.0092	0.0397
Wt background %	0.2739	0.1211	0.1372	0.0773	0.0666	0.1535	0.1769	0.2318	0.1872	0.0915	0.2797	0.2478	0.4175
Diboson background %	0.0105	0.0162	0.0140	0.0107	0.0095	0.0149	0.0074	0.0079	0.0077	0.0053	0.0078	0.0064	0.0017
ttV background %	0.0004	0.0003	0.0009	0.0011	0.0009	0.0012	0.0008	0.0005	0.0007	0.0003	0.0001	0.0004	0.0008
Z+jets background %	0.0368	0.0064	0.0451	0.0386	0.0635	0.1279	0.0912	0.1099	0.1083	0.0731	0.0356	0.0122	0.0166
Fakes background %	0.1039	0.1060	0.1093	0.0967	0.1177	0.1148	0.0743	0.0939	0.0841	0.0920	0.0852	0.0452	0.0689
Pileup %	0.0578	0.0192	0.0348	0.0228	0.0213	0.0296	0.0809	0.0394	0.0436	0.0145	0.0582	0.1247	0.0063
Beam energy %	0.0093	0.0189	0.0161	0.0032	0.0145	0.0212	0.0180	0.0269	0.0092	0.0147	0.0019	0.0182	0.0087
Luminosity %	0.0056	0.0010	0.0049	0.0044	0.0043	0.0059	0.0028	0.0016	0.0023	0.0034	0.0048	0.0015	0.0005
Total uncertainty %	1.0366	0.8291	0.8128	1.6004	0.8564	0.9097	1.0509	2.0794	0.9050	1.4159	2.6339	1.0734	1.9754

$\|\eta(\ell)\|$ bins	1.08-1.17	1.17-1.25	1.25-1.33	1.33-1.42	1.42-1.50	1.50-1.58	1.58-1.67	1.67-1.75	1.75-1.83	1.83-1.92	1.92-2.00	2.00-2.08	2.08-2.17	2.17-2.25	2.25-2.33	2.33-2.42	2.45-2.50
Normalised cross section [10^{-2}/unit $\|\eta\|$]	44.9804	43.3271	40.9737	38.9098	36.4249	34.1782	32.4407	29.7816	27.1552	25.4233	23.0463	21.8398	19.6170	17.4347	14.8490	13.4743	11.8655
Data statistics %	0.8754	0.9072	0.9348	1.0610	1.3209	1.0610	1.0335	1.0628	1.1775	1.2621	1.2952	1.3808	1.4250	1.5677	1.7478	1.8557	2.4967
MC statistics %	0.1509	0.1525	0.1636	0.1922	0.2561	0.1922	0.1830	0.2191	0.2101	0.2190	0.2456	0.2459	0.2621	0.2696	0.3168	0.3361	0.3982
Fragmentation %	2.9511	0.2546	1.1301	1.5051	0.6132	4.2198	1.9626	3.7229	0.7506	0.4008	0.2511	0.1719	0.5478	0.1480	1.1709	1.7046	4.1040
Hard scattering %	2.9332	0.8585	0.9193	1.6635	1.3234	5.0028	2.6049	3.0019	0.0301	0.6481	0.5023	0.7364	1.2373	1.7896	0.8780	0.4898	4.1275
Top mass dependence %	0.0194	0.0247	0.0529	0.0436	0.0009	0.0173	0.0076	0.0067	0.0049	0.0405	0.0171	0.0010	0.0040	0.0000	0.0512	0.1136	0.0291
PDF %	0.0064	0.0093	0.0079	0.0298	0.0693	0.0135	0.0155	0.0221	0.0254	0.0342	0.0349	0.0390	0.0441	0.0545	0.0597	0.0735	0.0444
ISR %	0.1105	0.1696	0.1773	0.0141	0.3152	0.2291	0.5057	0.1868	0.0223	0.1420	0.1130	0.1875	0.0039	0.2246	0.1824	0.1628	0.0917
FSR %	0.2033	0.1113	0.1109	0.0127	0.2800	0.4594	0.4697	0.1249	0.1871	0.1941	0.0221	0.1833	0.6387	0.1280	0.2716	0.0407	0.4044
Electron scale and resolution %	0.0082	0.0277	0.0544	0.0248	0.0134	0.0946	0.0933	0.0697	0.0596	0.0181	0.0281	0.0376	0.0193	0.0266	0.0450	0.0856	0.2629
Electron efficiency %	0.1037	0.1090	0.1091	0.0640	0.0206	0.1940	0.2359	0.2302	0.2394	0.2514	0.2541	0.3561	0.3890	0.3731	0.3614	0.3933	0.4409
Muon scale and resolution scale %	0.0187	0.0139	0.0031	0.0091	0.0206	0.0173	0.0212	0.0153	0.0164	0.0131	0.0204	0.0145	0.0199	0.0243	0.0459	0.0895	0.0882
Muon reconstruction efficiency %	0.0136	0.0146	0.0228	0.0534	0.0763	0.0464	0.0316	0.0302	0.0305	0.0314	0.0312	0.0289	0.0299	0.0290	0.0298	0.0300	0.0344
Muon trigger, ISO, TTVA efficiency %	0.0054	0.0061	0.0064	0.0075	0.0111	0.0112	0.0124	0.0136	0.0148	0.0151	0.0152	0.0139	0.0142	0.0153	0.0159	0.0207	0.0248
JVT %	0.0008	0.0034	0.0016	0.0002	0.0010	0.0020	0.0041	0.0014	0.0020	0.0062	0.0049	0.0055	0.0063	0.0051	0.0082	0.0033	0.0019
JES b-jes response %	0.0042	0.0009	0.0107	0.0097	0.0072	0.0134	0.0222	0.0016	0.0121	0.0152	0.0206	0.0069	0.0253	0.0154	0.0202	0.0046	0.0441
JES effective NPs %	0.0113	0.0123	0.0120	0.0386	0.0243	0.0074	0.0279	0.0101	0.0347	0.0117	0.0074	0.0326	0.0242	0.0128	0.0069	0.0689	0.0802
JES EtaInterCalibration %	0.0160	0.0110	0.0210	0.0240	0.0125	0.0085	0.0240	0.0155	0.0052	0.0237	0.0251	0.0047	0.0234	0.0024	0.0050	0.0244	0.0509
JES flavour %	0.0291	0.0224	0.0341	0.0608	0.0135	0.0143	0.0552	0.0190	0.0341	0.0235	0.0049	0.0267	0.0110	0.0162	0.0299	0.0601	0.0583
JES pileup %	0.0163	0.0174	0.0319	0.0744	0.0077	0.0240	0.0582	0.0134	0.0340	0.0097	0.0139	0.0390	0.0274	0.0177	0.0146	0.0699	0.0737
JES PunchThrough %	0.0001	0.0001	0.0002	0.0001	0.0002	0.0002	0.0000	0.0005	0.0001	0.0001	0.0002	0.0009	0.0000	0.0007	0.0005	0.0000	0.0009
JES HighPt %	0.0000	0.0000	0.0000	0.0000	0.0000	0.0000	0.0000	0.0000	0.0000	0.0000	0.0000	0.0000	0.0000	0.0000	0.0000	0.0000	0.0000
MET soft term %	0.0000	0.0000	0.0000	0.0000	0.0000	0.0000	0.0000	0.0000	0.0000	0.0000	0.0000	0.0000	0.0000	0.0000	0.0000	0.0000	0.0000
JER %	0.0000	0.0001	0.0000	0.0001	0.0002	0.0000	0.0000	0.0001	0.0000	0.0000	0.0000	0.0000	0.0003	0.0000	0.0001	0.0000	0.0000
b-tagging %	0.0138	0.0074	0.0117	0.0175	0.0405	0.0274	0.0261	0.0654	0.0176	0.0243	0.0267	0.0205	0.0447	0.0459	0.0352	0.0389	0.0892
Wt background %	0.2051	0.1811	0.1281	0.3072	0.3218	0.7020	0.2751	0.7998	0.3096	0.1665	0.2669	0.1076	0.3277	0.2721	0.6629	0.5258	0.2779
Diboson background %	0.0012	0.0023	0.0112	0.0016	0.0048	0.0113	0.0273	0.0086	0.0131	0.0179	0.0234	0.0246	0.0302	0.0294	0.0380	0.0430	0.0550
ttV background %	0.0003	0.0005	0.0002	0.0005	0.0010	0.0011	0.0002	0.0011	0.0024	0.0000	0.0001	0.0003	0.0001	0.0016	0.0040	0.0031	0.0014
Z+jets background %	0.0164	0.0841	0.1111	0.0071	0.1177	0.0119	0.1215	0.2245	0.0050	0.0429	0.0138	0.1392	0.0188	0.2140	0.1742	0.1135	0.3835
Fakes background %	0.0528	0.0143	0.0330	0.0158	0.0361	0.1132	0.1916	0.2873	0.3318	0.3931	0.4203	0.3443	0.1871	0.2566	0.2732	0.2032	0.1630
Pileup %	0.0358	0.0341	0.0061	0.0159	0.0137	0.0604	0.0481	0.0065	0.0536	0.0323	0.0273	0.0467	0.0174	0.0708	0.0236	0.1270	0.0864
Beam energy %	0.0298	0.0046	0.0039	0.0393	0.0261	0.0031	0.0234	0.0011	0.0133	0.0335	0.0058	0.0069	0.0243	0.0048	0.0179	0.0507	0.0254
Luminosity %	0.0041	0.0041	0.0051	0.0056	0.0032	0.0058	0.0070	0.0161	0.0184	0.0166	0.0196	0.0120	0.0013	0.0102	0.0151	0.0133	0.0131
Total uncertainty %	4.2680	1.3211	1.7657	2.5128	2.0615	6.6949	3.5244	4.9937	1.5188	1.5925	1.5449	1.7014	2.1547	2.4821	2.4690	2.6994	6.4038

Table 9.12: Normalised differential cross section for $E(\ell^+) + E(\ell^-)$.

$E(\ell^+) + E(\ell^-)$ bins [GeV]	50.0-60.0	60.0-70.0	70.0-80.0	80.0-90.0	90.0-110.0	110.0-125.0	125.0-160.0	160.0-200.0	200.0-250.0	250.0-300.0	300.0-370.0	370.0-450.0	450.0-550.0	550.0-700.0	700.0-900.0
Normalised cross section [10^{-3}/GeV]	0.1345	0.8511	1.9310	2.8961	4.1483	4.8414	4.8984	4.1045	2.9944	1.9863	1.2096	0.6544	0.3274	0.1347	0.0583
Data statistics %	5.3448	1.9593	1.1852	0.9588	0.5267	0.5707	0.3502	0.3620	0.3634	0.4598	0.5302	0.6851	0.9683	1.1836	1.7629
MC statistics %	6.2696	1.2356	0.4131	0.3128	0.1546	0.1457	0.0954	0.0956	0.0967	0.1264	0.1464	0.1787	0.2467	0.3248	0.4774
Fragmentation %	1.2885	0.8642	0.6553	0.6527	0.2287	0.1180	0.3499	0.1029	0.1655	0.3402	0.7816	0.3725	0.0811	0.5538	0.9617
Hard scattering %	1.4646	3.2371	0.8779	0.4324	0.3853	0.1065	0.4732	0.1894	0.5600	0.5100	0.6968	0.1232	0.0913	1.0367	1.6002
Top mass dependence %	0.1916	0.2125	0.2159	0.0385	0.0946	0.0489	0.0217	0.0225	0.0115	0.0543	0.0345	0.1093	0.1152	0.0456	0.1550
PDF %	0.1064	0.0740	0.0780	0.0704	0.0591	0.0417	0.0282	0.0199	0.0265	0.0434	0.0519	0.0581	0.0598	0.0729	0.0956
ISR %	2.4250	0.4112	0.2026	0.3773	0.0426	0.0659	0.0443	0.0621	0.0184	0.0584	0.2257	0.3627	0.0101	0.0273	0.2171
FSR %	1.2487	0.0952	0.3460	0.4548	0.2042	0.1504	0.1183	0.0429	0.0372	0.1255	0.0742	0.1241	0.1056	0.8654	0.4062
Electron scale and resolution %	0.3924	0.1237	0.0637	0.1344	0.1219	0.1431	0.1561	0.1334	0.0756	0.0600	0.1840	0.3357	0.4962	0.7173	1.4482
Electron efficiency %	0.6754	0.3731	0.2574	0.2192	0.1928	0.1626	0.1121	0.0692	0.0860	0.1186	0.1493	0.2090	0.4083	0.7000	1.1663
Muon scale and resolution scale %	0.6868	0.0697	0.1072	0.0980	0.0556	0.0463	0.0335	0.0092	0.0156	0.0274	0.0640	0.0836	0.0733	0.1551	0.2650
Muon reconstruction efficiency %	0.1224	0.0830	0.0516	0.0444	0.0292	0.0210	0.0091	0.0019	0.0112	0.0174	0.0220	0.0250	0.0276	0.0283	0.0259
Muon trigger, ISO, TTVA efficiency %	0.1348	0.0924	0.0586	0.0409	0.0258	0.0158	0.0070	0.0046	0.0089	0.0126	0.0156	0.0200	0.0247	0.0288	0.0343
JVT %	0.0146	0.0112	0.0007	0.0015	0.0062	0.0021	0.0028	0.0003	0.0009	0.0016	0.0030	0.0052	0.0094	0.0155	0.0046
JES b-jes response %	0.0457	0.1512	0.0422	0.0136	0.0161	0.0042	0.0031	0.0037	0.0076	0.0061	0.0204	0.0259	0.0036	0.0245	0.0182
JES effective NPs %	0.3449	0.1275	0.0899	0.0306	0.0270	0.0172	0.0026	0.0030	0.0091	0.0133	0.0166	0.0041	0.0297	0.0300	0.0839
JES EtaInterCalibration %	0.1033	0.0930	0.1883	0.0209	0.0209	0.0172	0.0056	0.0042	0.0120	0.0116	0.0140	0.0157	0.0243	0.0243	0.0552
JES flavour %	0.4649	0.0403	0.1533	0.0242	0.0425	0.0263	0.0121	0.0048	0.0239	0.0326	0.0105	0.0361	0.0483	0.0586	0.1427
JES pileup %	0.3672	0.1381	0.2383	0.0424	0.0330	0.0164	0.0044	0.0089	0.0143	0.0233	0.0273	0.0241	0.0344	0.0474	0.0883
JES PunchThrough %	0.0000	0.0010	0.0000	0.0000	0.0001	0.0001	0.0001	0.0002	0.0001	0.0000	0.0001	0.0004	0.0011	0.0006	0.0005
JES HighPt %	0.0000	0.0000	0.0000	0.0000	0.0000	0.0000	0.0000	0.0000	0.0000	0.0000	0.0000	0.0000	0.0000	0.0000	0.0000
MET soft term %	0.0000	0.0000	0.0000	0.0000	0.0000	0.0000	0.0000	0.0000	0.0000	0.0000	0.0000	0.0000	0.0000	0.0000	0.0000
JER %	0.0000	0.0000	0.0000	0.0000	0.0001	0.0000	0.0000	0.0000	0.0000	0.0000	0.0001	0.0000	0.0000	0.0000	0.0000
b-tagging %	1.7353	0.3753	0.0747	0.0750	0.0479	0.0241	0.0159	0.0077	0.0197	0.0166	0.0267	0.0381	0.0477	0.0583	0.0945
Wt background %	1.3826	0.8794	0.8127	0.7450	0.6584	0.5830	0.3815	0.2740	0.2268	0.3485	0.6414	0.9372	1.3060	1.7817	2.9341
Diboson background %	0.0207	0.0080	0.0229	0.0256	0.0334	0.0201	0.0196	0.0112	0.0033	0.0081	0.0184	0.0401	0.0622	0.0922	0.2172
ttV background %	0.0094	0.0100	0.0096	0.0099	0.0097	0.0077	0.0063	0.0025	0.0009	0.0038	0.0078	0.0130	0.0173	0.0245	0.0449
Z+jets background %	5.5817	0.7141	0.8011	0.0529	0.0236	0.1039	0.0128	0.0860	0.0342	0.0862	0.0107	0.0528	0.0163	0.0909	0.0507
Fakes background %	0.3469	0.2502	0.1375	0.1132	0.1256	0.1711	0.1088	0.0537	0.0228	0.0425	0.1890	0.2698	0.2339	0.2613	0.4480
Pileup %	1.1561	0.9944	0.5184	0.4889	0.2913	0.1868	0.0772	0.0006	0.0537	0.1941	0.2704	0.2699	0.2864	0.3358	0.3897
Beam energy %	0.1131	0.0197	0.0185	0.0285	0.0141	0.0134	0.0275	0.0065	0.0018	0.0103	0.0061	0.0164	0.0227	0.0238	0.0247
Luminosity %	0.1209	0.0238	0.0238	0.0157	0.0290	0.0267	0.0201	0.0099	0.0015	0.0106	0.0286	0.0432	0.0523	0.0693	0.1431
Total uncertainty %	10.8778	4.4204	2.1908	1.6988	1.0762	0.9335	0.8361	0.5494	0.7457	0.9039	1.4298	1.4202	1.8217	2.8398	4.4359

Table 9.13: Normalised differential cross section for $m(\ell^+\ell^-)$.

$m(\ell^+\ell^-)$ bins [GeV]	0.0-15.0	15.0-20.0	20.0-25.0	25.0-30.0	30.0-35.0	35.0-40.0	40.0-50.0	50.0-60.0	60.0-70.0	70.0-85.0	85.0-100.0	100.0-120.0	120.0-150.0	150.0-175.0	175.0-200.0	200.0-250.0	250.0-300.0	300.0-400.0	400.0-500.0	500.0-650.0	650.0-800.0
Normalised cross section [10^{-3}/GeV]	0.7692	1.7819	2.2204	2.7562	3.1357	3.6207	4.3072	5.3164	6.5041	7.2803	7.2340	6.3757	4.8096	3.2660	2.2538	1.2971	0.6391	0.2442	0.0691	0.0201	0.0063
Data statistics %	2.1452	1.7702	1.6167	1.3542	1.2788	1.2236	0.7658	0.7061	0.6293	0.4704	0.4582	0.4147	0.3669	0.5010	0.6128	0.5673	0.8305	0.9433	1.7789	2.7302	5.1352
MC statistics %	0.5538	0.4314	0.3997	0.3493	0.3233	0.3001	0.1971	0.2698	0.2243	0.1411	0.1181	0.1047	0.0993	0.1333	0.1675	0.1521	0.2223	0.2522	0.5015	0.7481	1.4422
Fragmentation %	0.0270	0.1319	0.3906	0.0082	0.6425	0.4129	0.0986	1.0416	0.9554	0.2223	0.0596	0.0044	0.2565	0.0914	0.7040	0.6628	0.4774	1.1132	0.0630	2.0012	0.5656
Hard scattering %	2.6676	1.4153	0.9702	0.0976	1.0316	0.0236	1.4337	0.5703	0.4711	0.0125	0.6003	0.2084	0.0713	0.1721	0.7505	0.2856	1.9849	0.8585	1.1006	3.7014	0.0302
Top mass dependence %	0.3281	0.0171	0.0047	0.0987	0.0332	0.0269	0.0719	0.0747	0.0114	0.0086	0.0606	0.0283	0.0794	0.0362	0.0272	0.0137	0.0188	0.0785	0.1772	0.1486	0.4108
PDF %	0.0586	0.0310	0.0273	0.0322	0.0174	0.0187	0.0199	0.0165	0.0124	0.0118	0.0086	0.0043	0.0049	0.0120	0.0160	0.0221	0.0319	0.0373	0.0518	0.0566	0.0952
ISR %	0.2545	0.2673	0.1472	0.2337	0.2934	0.2990	0.0634	0.0485	0.0599	0.2243	0.0005	0.0460	0.0203	0.0532	0.0337	0.0955	0.4681	0.4884	0.0517	0.0277	1.6269
FSR %	0.2070	0.8933	0.0414	0.0119	0.0769	0.2152	0.1857	0.0987	0.0672	0.0916	0.0918	0.0217	0.0691	0.0008	0.0811	0.0038	0.1675	0.2379	0.1899	0.3076	0.3238
Electron scale and resolution %	0.0383	0.0677	0.0384	0.0417	0.0191	0.0500	0.0400	0.0596	0.0461	0.0970	0.0900	0.1020	0.0744	0.0133	0.1029	0.1615	0.3709	0.5670	0.9155	1.3167	1.8522
Electron efficiency %	0.2266	0.1477	0.1378	0.1374	0.1331	0.1327	0.1324	0.1361	0.1272	0.1075	0.0836	0.0573	0.0502	0.0908	0.1384	0.2059	0.2904	0.4083	0.6273	1.0185	1.7176
Muon scale and resolution scale %	0.0660	0.0663	0.0819	0.0682	0.0726	0.0395	0.0342	0.0345	0.0283	0.0300	0.0149	0.0137	0.0078	0.0180	0.0554	0.0388	0.0942	0.0961	0.1107	0.1919	0.2845
Muon reconstruction efficiency %	0.0044	0.0011	0.0010	0.0040	0.0044	0.0030	0.0050	0.0047	0.0025	0.0011	0.0010	0.0003	0.0001	0.0015	0.0016	0.0029	0.0062	0.0078	0.0107	0.0155	0.0155
Muon trigger, ISO, TTVA efficiency %	0.0587	0.0348	0.0329	0.0334	0.0324	0.0325	0.0320	0.0343	0.0306	0.0200	0.0092	0.0066	0.0156	0.0241	0.0295	0.0350	0.0402	0.0443	0.0492	0.0569	0.0661
JVT %	0.0018	0.0057	0.0129	0.0142	0.0026	0.0042	0.0006	0.0007	0.0021	0.0003	0.0048	0.0033	0.0011	0.0015	0.0001	0.0062	0.0049	0.0016	0.0246	0.0281	0.0534
JES b-jes response %	0.0162	0.0094	0.0199	0.0059	0.0544	0.0469	0.0234	0.0071	0.0335	0.0119	0.0155	0.0052	0.0014	0.0005	0.0079	0.0273	0.0179	0.0561	0.0309	0.0846	0.1155
JES effective NPs %	0.0471	0.0260	0.0131	0.0429	0.0331	0.0114	0.0665	0.0152	0.0357	0.0229	0.0030	0.0085	0.0031	0.0063	0.0162	0.0065	0.0302	0.0077	0.0485	0.0295	0.0555
JES EtaInterCalibration %	0.0244	0.0226	0.0010	0.0347	0.0138	0.0039	0.0858	0.0065	0.0110	0.0252	0.0038	0.0058	0.0062	0.0026	0.0070	0.0012	0.0165	0.0051	0.0286	0.0337	0.0788
JES flavour %	0.1111	0.0829	0.0817	0.0689	0.0305	0.0500	0.0516	0.0269	0.0343	0.0497	0.0151	0.0046	0.0053	0.0163	0.0502	0.0433	0.0805	0.0999	0.1489	0.1710	0.2258
JES pileup %	0.0746	0.0467	0.0168	0.0545	0.0365	0.0095	0.1073	0.0185	0.0357	0.0418	0.0069	0.0152	0.0089	0.0108	0.0229	0.0234	0.0354	0.0216	0.0580	0.0367	0.0795
JES PunchThrough %	0.0000	0.0000	0.0000	0.0000	0.0000	0.0000	0.0002	0.0000	0.0000	0.0002	0.0000	0.0004	0.0002	0.0002	0.0002	0.0004	0.0001	0.0003	0.0000	0.0017	0.0001
JES HighPt %	0.0000	0.0000	0.0000	0.0000	0.0000	0.0000	0.0000	0.0000	0.0000	0.0000	0.0000	0.0000	0.0000	0.0000	0.0000	0.0000	0.0000	0.0000	0.0000	0.0000	0.0000
MET soft term %	0.0000	0.0000	0.0000	0.0000	0.0000	0.0000	0.0000	0.0000	0.0000	0.0000	0.0000	0.0000	0.0000	0.0000	0.0000	0.0000	0.0000	0.0000	0.0000	0.0000	0.0000
JER %	0.0000	0.0000	0.0000	0.0000	0.0000	0.0000	0.0000	0.0000	0.0002	0.0000	0.0000	0.0000	0.0000	0.0001	0.0001	0.0000	0.0000	0.0000	0.0000	0.0000	0.0000
b-tagging %	0.0894	0.0520	0.0396	0.0665	0.0539	0.0612	0.0414	0.0601	0.0458	0.0366	0.0227	0.0132	0.0162	0.0172	0.0217	0.0265	0.0329	0.0391	0.0500	0.0629	0.1077
Wt background %	0.9645	0.6695	0.5992	1.1397	0.5578	0.4990	0.5519	0.6165	0.4250	0.3756	0.3278	0.1793	0.0933	0.2493	0.5287	0.9264	1.0723	2.0629	3.2104	2.8333	7.3160
Diboson background %	0.0092	0.0110	0.0097	0.0036	0.0081	0.0046	0.0023	0.0021	0.0014	0.0058	0.0060	0.0054	0.0039	0.0071	0.0060	0.0060	0.0148	0.0291	0.0599	0.0878	0.1314
ttV background %	0.0100	0.0054	0.0057	0.0090	0.0061	0.0070	0.0066	0.0050	0.0051	0.0045	0.0037	0.0017	0.0002	0.0032	0.0053	0.0100	0.0123	0.0203	0.0338	0.0432	0.0805
Z+jets background %	0.3436	0.0620	0.0699	0.1661	0.3587	0.1804	0.2772	0.2698	0.2393	0.0272	0.0743	0.0569	0.0226	0.0448	0.0424	0.0588	0.0498	0.0672	0.0264	0.0574	0.0482
Fakes background %	0.5889	0.1489	0.1200	0.1129	0.1065	0.1151	0.0345	0.0366	0.0552	0.0530	0.0208	0.0513	0.0647	0.0565	0.0753	0.0248	0.0550	0.1694	0.2591	0.3270	0.6512
Pileup %	0.3488	0.2591	0.1487	0.0262	0.2421	0.2127	0.4211	0.2551	0.2155	0.1649	0.0945	0.0042	0.0792	0.1487	0.2559	0.3550	0.4258	0.3972	0.4441	0.7134	1.0180
Beam energy %	0.0035	0.0456	0.0111	0.0168	0.0124	0.0523	0.0193	0.0379	0.0118	0.0009	0.0128	0.0171	0.0033	0.0098	0.0052	0.0111	0.0382	0.0159	0.0030	0.0248	0.1072
Luminosity %	0.0027	0.0203	0.0171	0.0208	0.0145	0.0036	0.0030	0.0078	0.0096	0.0030	0.0126	0.0123	0.0053	0.0000	0.0046	0.0162	0.0275	0.0456	0.0667	0.0492	0.1475
Total uncertainty %	3.7217	2.6077	2.0809	1.8476	1.9632	1.5065	1.8288	1.5968	1.3799	0.7421	0.8598	0.5318	0.5054	0.6409	1.3644	1.3927	2.5956	2.8631	4.0699	6.1119	9.6595

Table 9.14: Normalised differential cross section for p_{T} (ℓ^{+}) + p_{T} (ℓ^{-}).

p_{T} (ℓ^{+}) + p_{T} (ℓ^{-}) bins [GeV]	50.0-60.0	60.0-70.0	70.0-80.0	80.0-100.0	100.0-125.0	125.0-150.0	150.0-200.0	200.0-250.0	250.0-300.0	300.0-400.0	400.0-600.0
Normalised cross section [10^{-3}/GeV]	2.3653	6.8065	9.7273	10.8612	9.0780	5.9155	2.7816	0.9593	0.3688	0.1080	0.0133
Data statistics %	1.2375	0.6413	0.5078	0.3021	0.2997	0.3722	0.3788	0.6422	1.0873	1.4289	2.8218
MC statistics %	0.5671	0.2582	0.1628	0.0899	0.0755	0.0966	0.1043	0.1909	0.2959	0.3854	0.8812
Fragmentation %	1.9719	0.2752	0.9840	0.4188	0.0790	0.4020	0.4822	1.1631	1.6308	1.6814	1.3514
Hard scattering %	1.3815	0.6086	0.9462	0.3674	0.2340	0.3669	1.0968	0.0407	2.2688	3.8348	3.5202
Top mass dependence %	0.1041	0.0455	0.0013	0.0089	0.0012	0.0099	0.0450	0.0365	0.0255	0.1110	0.0316
PDF %	0.0289	0.0250	0.0209	0.0153	0.0040	0.0114	0.0238	0.0427	0.0507	0.0571	0.0724
ISR %	0.1770	0.0229	0.2322	0.0326	0.0332	0.0439	0.0574	0.2088	0.0924	0.5100	0.3953
FSR %	0.7006	0.0845	0.1048	0.0918	0.0359	0.1422	0.0545	0.0369	0.0881	0.9200	0.2842
Electron scale and resolution %	0.0661	0.0291	0.0779	0.1679	0.1499	0.0420	0.1901	0.5436	0.8502	1.2089	1.9090
Electron efficiency %	0.6839	0.2727	0.1690	0.1360	0.0903	0.0952	0.1974	0.3345	0.4450	0.7644	1.9232
Muon scale and resolution scale %	0.1312	0.0931	0.0505	0.0304	0.0122	0.0330	0.0573	0.0885	0.1039	0.1244	0.3502
Muon reconstruction efficiency %	0.0087	0.0070	0.0061	0.0048	0.0017	0.0009	0.0070	0.0152	0.0209	0.0297	0.0592
Muon trigger, ISO, TTVA efficiency %	0.1591	0.0739	0.0370	0.0222	0.0133	0.0266	0.0380	0.0452	0.0503	0.0566	0.0814
JVT %	0.0097	0.0053	0.0025	0.0048	0.0015	0.0012	0.0038	0.0122	0.0107	0.0202	0.0616
JES b-jes response %	0.0226	0.0354	0.0162	0.0015	0.0087	0.0143	0.0086	0.0059	0.0339	0.0625	0.0245
JES effective NPs %	0.0986	0.0457	0.0367	0.0322	0.0026	0.0203	0.0287	0.0616	0.0287	0.0223	0.1286
JES EtaInterCalibration %	0.2044	0.0199	0.0153	0.0177	0.0038	0.0064	0.0052	0.0182	0.0023	0.0143	0.0304
JES flavour %	0.1706	0.0334	0.0469	0.0525	0.0108	0.0154	0.0427	0.0833	0.1110	0.1600	0.3029
JES pileup %	0.2360	0.0482	0.0411	0.0366	0.0083	0.0249	0.0379	0.0797	0.0291	0.0374	0.1392
JES PunchThrough %	0.0004	0.0000	0.0002	0.0002	0.0000	0.0001	0.0001	0.0007	0.0001	0.0004	0.0001
JES HighPt %	0.0000	0.0000	0.0000	0.0000	0.0000	0.0000	0.0000	0.0000	0.0000	0.0000	0.0000
MET soft term %	0.0000	0.0000	0.0000	0.0000	0.0000	0.0000	0.0000	0.0000	0.0000	0.0000	0.0000
JER %	0.0000	0.0000	0.0001	0.0000	0.0000	0.0000	0.0000	0.0000	0.0000	0.0000	0.0000
b-tagging %	0.0998	0.0932	0.0672	0.0141	0.0127	0.0286	0.0413	0.0600	0.0536	0.0834	0.2103
Wt background %	0.5728	0.7227	0.4193	0.4547	0.3308	0.1038	0.5414	1.6782	2.3602	3.9952	11.0901
Diboson background %	0.0112	0.0158	0.0129	0.0147	0.0085	0.0021	0.0142	0.0428	0.0807	0.1202	0.3080
ttV background %	0.0090	0.0076	0.0080	0.0067	0.0042	0.0004	0.0090	0.0227	0.0341	0.0532	0.1126
Z+jets background %	0.5046	0.1785	0.0683	0.0086	0.0170	0.0159	0.0192	0.0764	0.0322	0.0165	0.0875
Fakes background %	0.1792	0.0701	0.0277	0.0183	0.0304	0.0261	0.0291	0.0700	0.1400	0.1727	0.4730
Pileup %	0.7395	0.5054	0.3305	0.1576	0.0239	0.1866	0.3509	0.4357	0.4602	0.4743	0.7312
Beam energy %	0.0320	0.0018	0.0040	0.0036	0.0042	0.0043	0.0022	0.0209	0.0214	0.0606	0.0593
Luminosity %	0.0057	0.0043	0.0197	0.0194	0.0148	0.0047	0.0190	0.0702	0.1081	0.1526	0.3521
Total uncertainty %	3.1636	1.3618	1.5979	0.8402	0.5494	0.7266	1.4500	2.3054	3.9840	6.2618	12.4436

Table 9.15: Normalised differential cross section for p_{T} $(\ell^+\ell^-)$.

p_{T} $(\ell^+\ell^-)$ bins [GeV]	0.0-20.0	20.0-30.0	30.0-45.0	45.0-60.0	60.0-75.0	75.0-100.0	100.0-125.0	125.0-150.0	150.0-200.0	200.0-300.0
Normalised cross section [10^{-3}/GeV]	3.1027	6.5380	8.2995	10.5183	11.4591	8.8385	4.6033	1.8726	0.5463	0.0824
Data statistics %	0.6589	0.6209	0.4336	0.3862	0.3598	0.2975	0.4405	0.6912	0.9408	1.7882
MC statistics %	0.2325	0.2070	0.1197	0.1007	0.0916	0.0783	0.1094	0.1822	0.2592	0.5424
Fragmentation %	0.5052	0.3194	0.1871	0.3267	0.0668	0.0164	0.6446	0.8950	0.8925	0.2058
Hard scattering %	0.4892	0.7498	0.2296	0.6597	0.7284	0.1853	1.1568	1.2210	1.2231	1.4462
Top mass dependence %	0.0219	0.0151	0.0033	0.0119	0.0030	0.0222	0.0120	0.0374	0.0209	0.0783
PDF %	0.0158	0.0065	0.0099	0.0149	0.0131	0.0041	0.0240	0.0405	0.0533	0.0535
ISR %	0.1277	0.4193	0.2034	0.0583	0.1797	0.0247	0.0455	0.0954	0.1721	0.2768
FSR %	0.1358	0.4295	0.1424	0.0113	0.0952	0.1691	0.0369	0.2393	0.1640	1.4449
Electron scale and resolution %	0.2317	0.2509	0.2049	0.1515	0.1184	0.0040	0.2357	0.6414	1.0503	1.6163
Electron efficiency %	0.0857	0.0685	0.0538	0.0535	0.0391	0.0195	0.0831	0.1774	0.2888	0.9041
Muon scale and resolution scale %	0.0571	0.0569	0.0431	0.0307	0.0279	0.0182	0.0651	0.1208	0.1410	0.2529
Muon reconstruction efficiency %	0.0040	0.0024	0.0023	0.0029	0.0027	0.0004	0.0027	0.0084	0.0193	0.0564
Muon trigger, ISO, TTVA efficiency %	0.0091	0.0080	0.0048	0.0105	0.0066	0.0044	0.0152	0.0191	0.0223	0.0502
JVT %	0.0044	0.0038	0.0024	0.0023	0.0011	0.0027	0.0071	0.0016	0.0017	0.0538
JES b-jes response %	0.0402	0.0548	0.0364	0.0186	0.0119	0.0177	0.0391	0.0769	0.1099	0.0694
JES effective NPs %	0.0089	0.0969	0.0290	0.0210	0.0135	0.0143	0.0360	0.0824	0.1094	0.1208
JES EtaInterCalibration %	0.0523	0.0610	0.0135	0.0052	0.0119	0.0045	0.0108	0.0283	0.0438	0.0417
JES flavour %	0.0562	0.0725	0.0033	0.0064	0.0035	0.0087	0.0042	0.0228	0.0543	0.0948
JES pileup %	0.0643	0.1029	0.0356	0.0210	0.0103	0.0197	0.0401	0.0912	0.1275	0.1385
JES PunchThrough %	0.0001	0.0003	0.0001	0.0000	0.0000	0.0001	0.0000	0.0002	0.0000	0.0007
JES HighPt %	0.0000	0.0000	0.0000	0.0000	0.0000	0.0000	0.0000	0.0000	0.0000	0.0000
MET soft term %	0.0000	0.0000	0.0000	0.0000	0.0000	0.0000	0.0000	0.0000	0.0000	0.0000
JER %	0.0000	0.0000	0.0000	0.0000	0.0000	0.0000	0.0000	0.0000	0.0000	0.0000
b-tagging %	0.0969	0.1039	0.0667	0.0462	0.0252	0.0242	0.0967	0.1637	0.2300	0.3134
Wt background %	0.5045	0.4065	0.4846	0.4435	0.3791	0.1980	0.4225	1.4512	3.0185	11.4174
Diboson background %	0.0214	0.0121	0.0105	0.0175	0.0191	0.0097	0.0098	0.0414	0.1363	0.5345
ttV background %	0.0043	0.0044	0.0048	0.0058	0.0059	0.0037	0.0032	0.0195	0.0510	0.1466
Z+jets background %	0.2134	0.1390	0.0560	0.0211	0.0158	0.0084	0.0093	0.1205	0.0417	0.0648
Fakes background %	0.0352	0.0374	0.0261	0.0248	0.0251	0.0378	0.0298	0.1029	0.3195	0.8377
Pileup %	0.1582	0.1222	0.0439	0.0914	0.0281	0.0133	0.1955	0.1784	0.2717	0.1601
Beam energy %	0.0217	0.0069	0.0072	0.0003	0.0047	0.0018	0.0064	0.0298	0.0052	0.0039
Luminosity %	0.0087	0.0098	0.0130	0.0149	0.0143	0.0095	0.0039	0.0468	0.1333	0.4172
Total uncertainty %	1.1963	1.3297	0.8047	0.9706	0.9370	0.4499	1.5042	2.3552	3.7333	11.9590

Table 9.16: Differential normalised cross section for $\Delta\phi(\ell^+\ell^-)$.

$\Delta\phi(\ell^+\ell^-)$ bins	0.00-0.10	0.10-0.21	0.21-0.31	0.31-0.42	0.42-0.52	0.52-0.63	0.63-0.73	0.73-0.84	0.84-0.94	0.94-1.05	1.05-1.15	1.15-1.26	1.26-1.36	1.36-1.47
Normalised cross section [10^{-2}/rad]	21.0254	21.0926	20.3983	21.3515	21.0325	21.7156	22.0452	22.9441	23.6359	23.6035	24.7158	25.9083	27.0156	28.4661
Data statistics %	1.6580	1.5833	1.5461	1.5339	1.5297	1.4302	1.4552	1.3931	1.4602	1.4232	1.4023	1.3856	1.2793	1.3326
MC statistics %	0.3901	0.3990	0.4013	0.3747	0.3727	0.3689	0.3652	0.3555	0.3538	0.3756	0.3683	0.3373	0.3251	0.3375
Fragmentation %	0.6772	0.1496	0.9707	0.4676	0.8151	0.6283	0.0588	0.3305	0.2363	0.2302	0.3182	0.3709	0.6366	0.0577
Hard scattering %	0.1754	0.5074	0.4502	1.8350	2.0339	0.0819	0.9194	0.4259	0.8482	1.3313	0.6359	0.3592	0.3787	1.2038
Top mass dependence %	0.1604	0.0339	0.0076	0.0661	0.2045	0.1320	0.0170	0.1070	0.2340	0.0279	0.0242	0.0015	0.0440	0.0981
PDF %	0.0280	0.0223	0.0176	0.0156	0.0194	0.0193	0.0169	0.0236	0.0185	0.0195	0.0206	0.0229	0.0189	0.0157
ISR %	0.2589	0.0821	0.0735	0.7089	0.4001	0.1405	0.1716	0.1037	0.7628	0.2544	0.2827	0.4493	0.0475	0.5255
FSR %	0.0645	0.1373	0.3934	0.3248	0.2601	0.3449	0.4814	0.2618	0.3244	0.1278	0.4362	0.5264	0.1787	0.6675
Electron scale and resolution %	0.0671	0.0540	0.0563	0.0779	0.0574	0.0435	0.0666	0.0347	0.0308	0.0569	0.0326	0.0325	0.0375	0.0091
Electron efficiency %	0.0931	0.0925	0.0893	0.0869	0.0878	0.0867	0.0844	0.0815	0.0797	0.0754	0.0695	0.0665	0.0605	0.0556
Muon scale and resolution scale %	0.0493	0.0437	0.0117	0.0336	0.0296	0.0266	0.0383	0.0314	0.0268	0.0236	0.0241	0.0158	0.0181	0.0214
Muon reconstruction efficiency %	0.0038	0.0050	0.0038	0.0026	0.0039	0.0036	0.0033	0.0025	0.0042	0.0039	0.0013	0.0007	0.0024	0.0003
Muon trigger, ISO, TTVA efficiency %	0.0188	0.0198	0.0189	0.0181	0.0174	0.0163	0.0164	0.0153	0.0148	0.0136	0.0130	0.0115	0.0097	0.0086
JVT %	0.0131	0.0088	0.0075	0.0058	0.0008	0.0129	0.0055	0.0029	0.0050	0.0021	0.0030	0.0058	0.0088	0.0012
JES b-jes response %	0.0129	0.0169	0.0932	0.0442	0.0263	0.0254	0.0640	0.0634	0.0719	0.0297	0.0351	0.0341	0.0383	0.0424
JES effective NPs %	0.0050	0.0532	0.0503	0.0172	0.0126	0.0081	0.0388	0.0404	0.0482	0.0303	0.0290	0.0233	0.0109	0.0267
JES EtaInterCalibration %	0.0125	0.0023	0.0180	0.0095	0.0064	0.0219	0.0216	0.0234	0.0208	0.0087	0.0051	0.0083	0.0037	0.0195
JES flavour %	0.0480	0.0797	0.0369	0.0641	0.0498	0.0416	0.0319	0.0341	0.0409	0.0247	0.0120	0.0534	0.0382	0.0117
JES pileup %	0.0368	0.0520	0.0418	0.0232	0.0100	0.0117	0.0566	0.0420	0.0571	0.0384	0.0378	0.0276	0.0265	0.0369
JES PunchThrough %	0.0000	0.0000	0.0000	0.0000	0.0007	0.0000	0.0002	0.0000	0.0006	0.0000	0.0000	0.0000	0.0000	0.0000
JES HighPt %	0.0000	0.0000	0.0000	0.0000	0.0000	0.0000	0.0000	0.0000	0.0000	0.0000	0.0000	0.0000	0.0000	0.0000
MET soft term %	0.0000	0.0000	0.0000	0.0000	0.0000	0.0000	0.0000	0.0000	0.0000	0.0000	0.0000	0.0000	0.0000	0.0000
JER %	0.0009	0.0000	0.0000	0.0000	0.0000	0.0000	0.0000	0.0000	0.0000	0.0000	0.0000	0.0000	0.0000	0.0000
b-tagging %	0.0924	0.0716	0.0876	0.0788	0.0665	0.0686	0.0609	0.0595	0.0575	0.0386	0.0727	0.0429	0.0562	0.0367
Wt background %	0.3937	0.7612	0.4744	0.9163	0.8131	0.6878	0.6880	0.5897	0.2981	0.5392	0.1585	0.2439	0.2103	0.4267
Diboson background %	0.0270	0.0351	0.0302	0.0201	0.0278	0.0139	0.0170	0.0128	0.0227	0.0109	0.0234	0.0082	0.0089	0.0018
ttV background %	0.0013	0.0021	0.0018	0.0004	0.0000	0.0004	0.0019	0.0000	0.0010	0.0003	0.0010	0.0009	0.0017	0.0016
Z+jets background %	0.1429	0.1218	0.0371	0.1728	0.2054	0.0949	0.3606	0.1221	0.0402	0.0275	0.0962	0.1240	0.0148	0.0742
Fakes background %	0.1746	0.0575	0.1062	0.0433	0.1254	0.0875	0.0696	0.0835	0.1661	0.0660	0.0380	0.0797	0.0984	0.1088
Pileup %	0.0711	0.0793	0.1815	0.1571	0.1519	0.2184	0.2355	0.1604	0.1382	0.0193	0.0884	0.1525	0.1064	0.1304
Beam energy %	0.0377	0.1016	0.0082	0.0409	0.0524	0.0148	0.0146	0.0364	0.0588	0.0319	0.0393	0.0009	0.0632	0.0028
Luminosity %	0.0154	0.0211	0.0131	0.0082	0.0177	0.0147	0.0151	0.0172	0.0004	0.0024	0.0031	0.0000	0.0011	0.0000
Total uncertainty %	1.9314	1.9027	2.0403	2.7601	2.8837	1.8154	2.0132	1.6935	1.9851	2.0945	1.7147	1.7022	1.5522	2.0735

$\Delta\phi(\ell^+\ell^-)$ bins	1.47-1.57	1.57-1.68	1.68-1.78	1.78-1.88	1.88-1.99	1.99-2.09	2.09-2.20	2.20-2.30	2.30-2.41	2.41-2.51	2.51-2.62	2.62-2.72	2.72-2.83	2.83-2.93	2.93-3.04	3.04-3.14
Normalised cross section [10^{-2}/rad]	29.2108	30.6409	32.0118	33.3336	34.0324	36.6251	37.6696	39.8071	41.1278	42.3275	43.1817	43.6540	45.2645	45.7728	46.8349	48.4849
Data statistics %	1.2633	1.2369	1.2067	1.1869	1.1606	1.1212	1.1398	1.0692	1.0168	1.0403	0.9976	1.0210	0.9862	0.9989	0.9801	0.9518
MC statistics %	0.3281	0.3200	0.3335	0.3169	0.3565	0.3234	0.3019	0.3083	0.3036	0.2909	0.2837	0.3047	0.2789	0.3033	0.3262	0.2579
Fragmentation %	0.0976	0.1758	0.0778	0.3116	0.2015	1.4729	0.0660	0.6243	0.3423	0.3058	0.2665	0.2995	0.2370	0.2922	0.2329	0.0776
Hard scattering %	0.4768	1.3971	0.1514	1.2514	0.2157	1.2173	0.4173	1.9669	0.2571	0.4705	0.5606	0.4221	0.4424	0.0054	1.0006	0.5276
Top mass dependence %	0.0871	0.1223	0.0915	0.0552	0.1518	0.0176	0.0393	0.0474	0.0013	0.0251	0.0539	0.0082	0.0688	0.0133	0.0325	0.0624
PDF %	0.0102	0.0090	0.0137	0.0149	0.0095	0.0092	0.0096	0.0061	0.0068	0.0086	0.0091	0.0144	0.0202	0.0211	0.0304	0.0260
ISR %	0.3645	0.5071	0.0282	0.0869	0.6301	0.4310	0.0303	0.0175	0.3813	0.0132	0.0512	0.4032	0.0215	0.2742	0.0371	0.1024
FSR %	0.1939	0.3864	0.1328	0.4634	0.1021	0.3315	0.6745	0.1688	0.1052	0.1152	0.1554	0.2570	0.1448	0.0672	0.4309	0.1759
Electron scale and resolution %	0.0203	0.0179	0.0092	0.0079	0.0094	0.0210	0.0215	0.0168	0.0267	0.0331	0.0353	0.0460	0.0369	0.0395	0.0398	0.0485
Electron efficiency %	0.0480	0.0409	0.0337	0.0239	0.0169	0.0128	0.0154	0.0265	0.0382	0.0488	0.0625	0.0768	0.0877	0.1012	0.1091	0.1133
Muon scale and resolution scale %	0.0197	0.0241	0.0135	0.0063	0.0275	0.0126	0.0252	0.0242	0.0070	0.0198	0.0358	0.0229	0.0344	0.0124	0.0197	0.0242
Muon reconstruction efficiency %	0.0028	0.0006	0.0004	0.0005	0.0009	0.0023	0.0003	0.0047	0.0018	0.0007	0.0005	0.0026	0.0012	0.0039	0.0018	0.0039
Muon trigger, ISO, TTVA efficiency %	0.0070	0.0057	0.0037	0.0026	0.0030	0.0030	0.0042	0.0065	0.0090	0.0107	0.0114	0.0131	0.0145	0.0157	0.0171	0.0169
JVT %	0.0050	0.0081	0.0042	0.0018	0.0016	0.0054	0.0052	0.0024	0.0061	0.0079	0.0066	0.0060	0.0017	0.0094	0.0060	0.0064
JES b-jes response %	0.0223	0.0369	0.0136	0.0164	0.0088	0.0272	0.0193	0.0257	0.0432	0.0310	0.0422	0.0453	0.0548	0.0371	0.0232	0.0553
JES effective NPs %	0.0047	0.0352	0.0378	0.0216	0.0080	0.0357	0.0239	0.0129	0.0395	0.0940	0.0491	0.0222	0.0224	0.0201	0.0359	0.0415
JES EtaInterCalibration %	0.0188	0.0146	0.0065	0.0174	0.0144	0.0069	0.0069	0.0031	0.0237	0.1194	0.0369	0.0120	0.0063	0.0134	0.0187	0.0278
JES flavour %	0.0358	0.0031	0.0738	0.0126	0.0164	0.0032	0.0081	0.0442	0.0310	0.1534	0.0085	0.0502	0.0341	0.0278	0.0195	0.0417
JES pileup %	0.0095	0.0306	0.0361	0.0442	0.0146	0.0346	0.0161	0.0112	0.0357	0.1827	0.0473	0.0304	0.0243	0.0262	0.0376	0.0349
JES PunchThrough %	0.0009	0.0000	0.0010	0.0003	0.0003	0.0000	0.0003	0.0000	0.0004	0.0000	0.0000	0.0005	0.0000	0.0007	0.0005	0.0012
JES HighPt %	0.0000	0.0000	0.0000	0.0000	0.0000	0.0000	0.0000	0.0000	0.0000	0.0000	0.0000	0.0000	0.0000	0.0000	0.0000	0.0000
MET soft term %	0.0000	0.0000	0.0000	0.0000	0.0000	0.0000	0.0000	0.0000	0.0000	0.0000	0.0000	0.0000	0.0000	0.0000	0.0000	0.0000
JER %	0.0000	0.0000	0.0000	0.0000	0.0000	0.0000	0.0000	0.0000	0.0000	0.0000	0.0000	0.0000	0.0000	0.0000	0.0000	0.0000
b-tagging %	0.0191	0.0378	0.0417	0.0170	0.0559	0.0221	0.0166	0.0443	0.0375	0.0484	0.0447	0.0503	0.0662	0.0834	0.0856	0.0639
Wt background %	0.2412	0.4181	0.3524	0.4820	0.1887	0.2458	0.3515	0.2502	0.9284	0.8130	0.5539	0.2661	0.2720	0.2897	0.4499	0.2310
Diboson background %	0.0156	0.0074	0.0040	0.0094	0.0042	0.0052	0.0078	0.0101	0.0110	0.0128	0.0081	0.0075	0.0172	0.0137	0.0080	0.0120
ttV background %	0.0007	0.0022	0.0004	0.0017	0.0004	0.0003	0.0015	0.0014	0.0009	0.0002	0.0002	0.0004	0.0018	0.0014	0.0002	0.0014
Z+jets background %	0.2515	0.1251	0.0507	0.1000	0.1325	0.1469	0.0938	0.0573	0.0027	0.2585	0.0590	0.0558	0.0707	0.1461	0.1039	0.1031
Fakes background %	0.0149	0.0737	0.0429	0.0999	0.0265	0.0511	0.0334	0.0384	0.0362	0.0597	0.0450	0.0488	0.0520	0.1141	0.0648	0.0560
Pileup %	0.0148	0.0448	0.0974	0.0902	0.1300	0.1255	0.0451	0.0568	0.0449	0.0162	0.1023	0.0292	0.0737	0.1577	0.1255	0.1777
Beam energy %	0.0378	0.0068	0.0004	0.0396	0.0317	0.0239	0.0061	0.0044	0.0493	0.0003	0.0553	0.0147	0.0402	0.0237	0.0423	0.0068
Luminosity %	0.0054	0.0062	0.0040	0.0031	0.0089	0.0100	0.0058	0.0049	0.0010	0.0093	0.0136	0.0104	0.0075	0.0073	0.0031	0.0003
Total uncertainty %	1.4994	2.0597	1.3315	1.9142	1.4383	2.3270	1.4714	2.3675	1.5308	1.5215	1.3540	1.3142	1.1991	1.1925	1.6038	1.1960

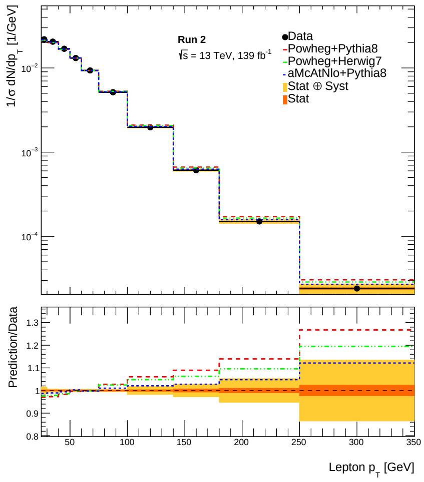

(a)

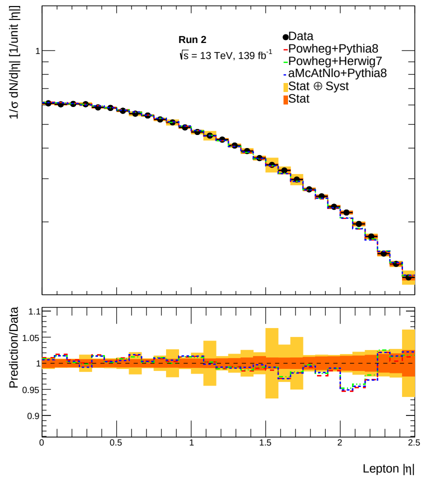

(b)

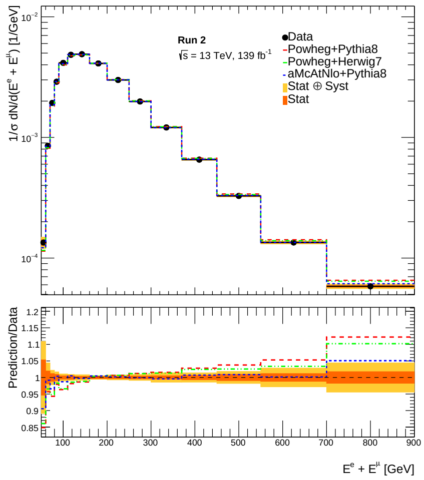

(c)

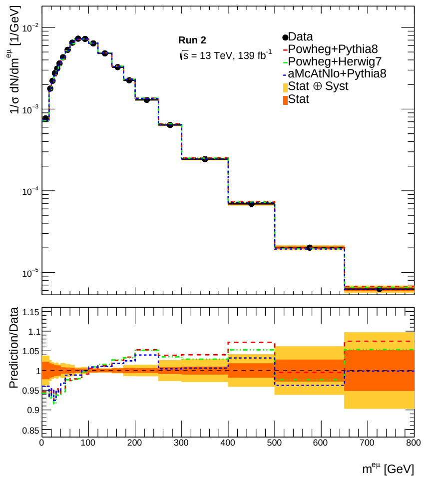

(d)

Figure 9.4: The measured normalised differential cross section is plotted together with the predictions from three different Monte Carlo samples, the nominal Powheg+Pythia 8, the Powheg + Herwig 7 sample and the MadGraph5_aMC@NLO + Pythia 8 sample for the variables $p_{\mathrm{T}}(\ell)$, $\eta(\ell)$, $E(\ell^+) + E(\ell^-)$ and $m(\ell^+\ell^-)$.

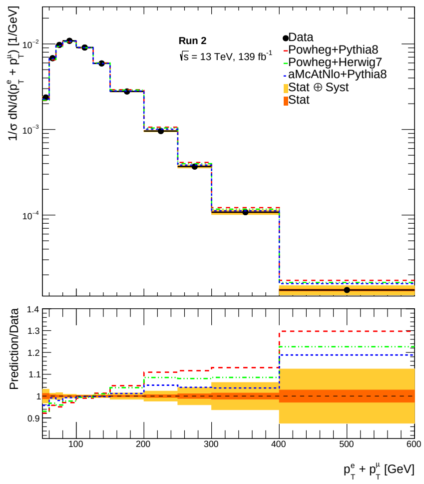

(a)

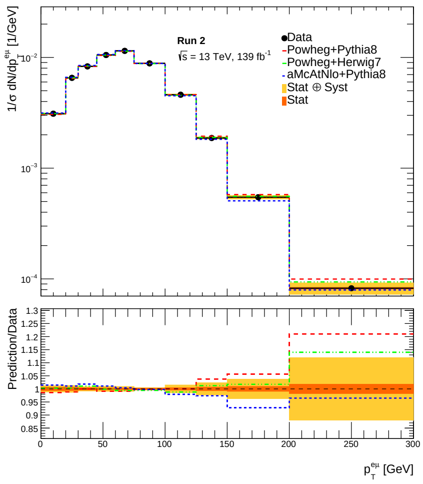

(b)

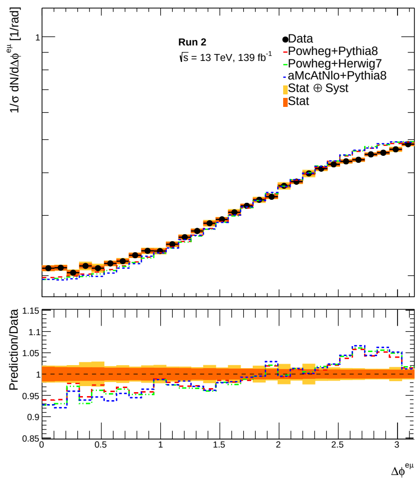

(c)

Figure 9.5: The measured normalised differential cross section is plotted together with the predictions from three different Monte Carlo samples, the nominal Powheg+Pythia 8, the Powheg + Herwig 7 sample and the MadGraph5_aMC@NLO + Pythia 8 sample for the variables $p_{\mathrm{T}}(\ell^+) + p_{\mathrm{T}}(\ell^-)$, $p_{\mathrm{T}}(\ell^+\ell^-)$ and $\Delta\phi(\ell^+\ell^-)$.

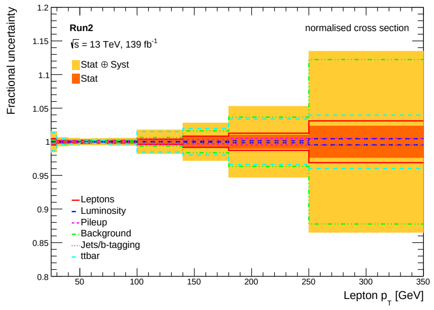

(a)

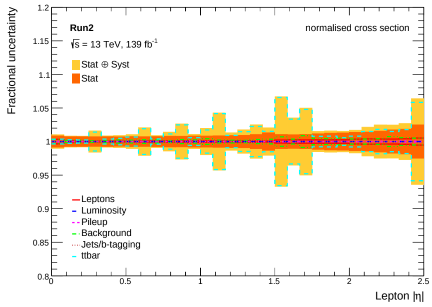

(b)

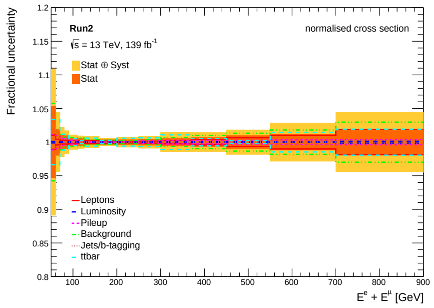

(c)

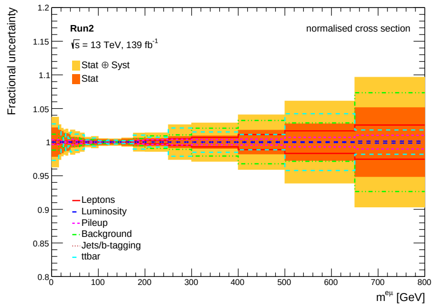

(d)

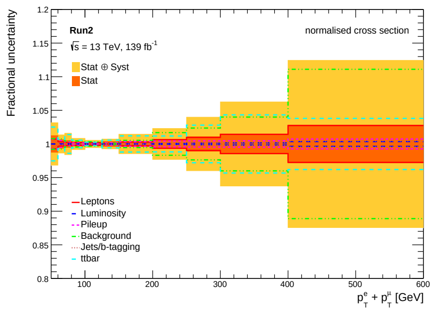

(e)

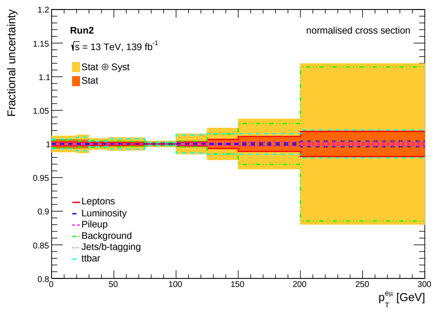

(f)

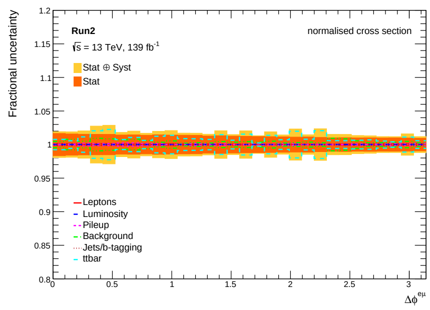

(g)

Figure 9.6: Statistical and total systematic error and contributions from different categories of systematic uncertainties for the normalised differential cross section.

CHAPTER 10

TOWARDS A HIGH PRECISION MEASUREMENT OF THE TOP QUARK MASS

The measured normalised differential distributions at particle level, shown in Chapter 9, for the $t\bar{t}$ production cross section with dileptonic events carry information about the mass of the top quark in their shape, as explained in [24]. Following the ideas presented in [24], five of the seven presented distributions ($p_{\mathrm{T}}(\ell^+\ell^-)$, $p_{\mathrm{T}}(\ell^+)+p_{\mathrm{T}}(\ell^-)$, $p_{\mathrm{T}}(\ell)$, $E(\ell^+)+E(\ell^-)$, $m(\ell^+\ell^-)$) can be exploited to extract the top pole mass thanks to their shape, which is compared to a series of distributions generated from samples with different top masses.
The advantage of this technique is that is does not require the reconstruction of the top quark from its decay products, avoiding in this way the large uncertainties connected to the missing energy of the neutrinos and the uncertainties due to the jets used in the reconstruction. There are of course other drawbacks, as the uncertainties due to the modelling of the p_{T} of the leptonic observables, which currently suffer from the mismodelling of the p_{T} of the top due to missing NNLO correction and EW corrections. These effects can potentially be mitigated in the future thanks to a better understanding of

the top quark and hence a better modelling of the top quark production and decay.
The goal of this chapter is to show how the normalised differential distributions could be used in the future to extract the mass of the top quark by outlining the method with some simplifications. Therefore the measurement shown here is merely an outline of how a top mass precision measurement would be carried out.

10.1 Method

The top pole mass is found thanks to template fits, which means that the measured normalised differential cross section distributions from Chapter 9 are compared to normalised particle level distributions generated with different top mass values. In total five distributions are considered, $p_{\mathrm{T}}(\ell^+\ell^-)$, $p_{\mathrm{T}}(\ell^+)+p_{\mathrm{T}}(\ell^-)$, $p_{\mathrm{T}}(\ell)$, $E(\ell^+)+E(\ell^-)$, $m(\ell^+\ell^-)$, and each distribution is compared to particle level distributions generated with POWHEG + PYTHIA 8 at top masses of 169, 171, 172, 172.25, 175.5, 172.75, 173, 174 and 176 GeV. For each distribution and each top mass point, χ^2 values are computed using the following equation, also used in [17]:

$$\chi^2(m_{\mathrm{top}}) = \boldsymbol{\Delta}^T_{(n-1)}(m_{\mathrm{top}}) \cdot \mathbf{S}^{-1}_{(n-1)} \cdot \boldsymbol{\Delta}_{(n-1)}(m_{\mathrm{top}}) \tag{10.1}$$

where $\boldsymbol{\Delta}(m_{\mathrm{top}})$ is the vector difference between the bins of the measured normalised differential distribution and the particle level prediction at a particular mass point and $\mathbf{S}^{-1}$ is the inverse covariance matrix containing the statistical and systematic uncertainties on the normalised differential distributions as well as off-diagonal correlation terms between bins. Note, however, that the covariance matrix receives no contribution from the modelling of the templates. The correlations arise from different sources: the statistical covariance matrix has mostly negative correlations between bins due to the normalisation of the distributions and they are measured thanks to bootstrapping experiments, as shown in Fig. 7.9(b), while each source of systematic uncertainty is taken as fully correlated between bins of single distributions.
In order to make sure that the covariance matrix $\mathbf{S}^{-1}$ can be inverted (the matrix cannot be singular), one of the bins is eliminated from the covariance matrix and from the vector difference $\boldsymbol{\Delta}(m_{\mathrm{top}})$ and for simplicity, the last bin is eliminated. Equal results are obtained if another bin other than the last is removed.
When all the χ^2 values are calculated, they are divided by the number of degrees of freedom (NDF), which is the number of bins taken into consideration minus one, and the minimum of the χ^2/NDF distribution is found for each distribution by fitting a second degree polynomial to the χ^2/NDF points for each variable, hence giving a value for the most likely top pole mass of the measured distribution. The uncertainty on these values is found by extracting the mass value at $\chi^2_{min} \pm 1$ from the second degree polynomial fit. When all the values are found, they need to be combined in one single value and to this end the BLUE (Best Linear Unbiased Estimator) [117] is used, where all the

correlations between the variables are taken into consideration when finding the average value.

10.2 Templates

The templates are the distributions of the five observables in simulated particle level $e\mu$ events. They are binned in the same way as the data and then normalised to the integrated luminosity of the relevant data period, using the sample k-factor, the filter efficiency and the sum of Monte Carlo weights. Finally, the histograms are normalised to unit area and each bin content is divided by the bin width in order to obtain the normalised differential cross section at the different top mass values. The particle level mass templates distributions are plotted together with the measured normalised differential cross section distribution for variable for $p_{\mathrm{T}}(\ell^+\ell^-)$ in Fig. 10.1 (the plots for the other variables are in Appendix F). Already from Fig. 10.1 it is clear that the mass templates do not model the data properly [19, 20, 95] and this could very well affect the mass measurement to be performed.

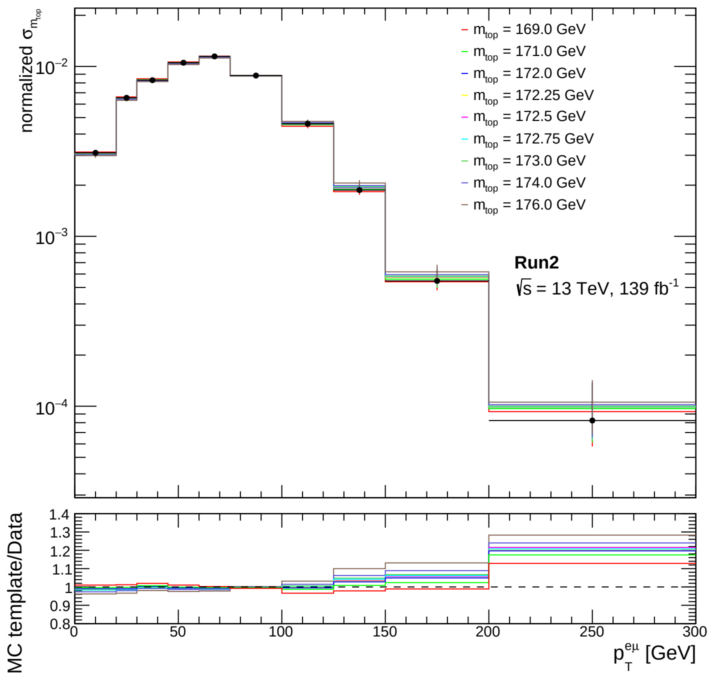

Figure 10.1: Top mass templates distributions at particle level plotted together with the measured normalised differential cross section for variable $p_{\mathrm{T}}(\ell^+\ell^-)$.

The normalised differential cross section values for each bin of each distribution are parametrized, in order to have a smoother distribution of the normalised cross section as a function of the top mass. To do this, for each bin in each distribution, the values of the normalised differential cross section for each top mass point are plotted and fitted to a second degree polynomial. The values used for the templates in χ^2 fits are extracted from the second degree poly-

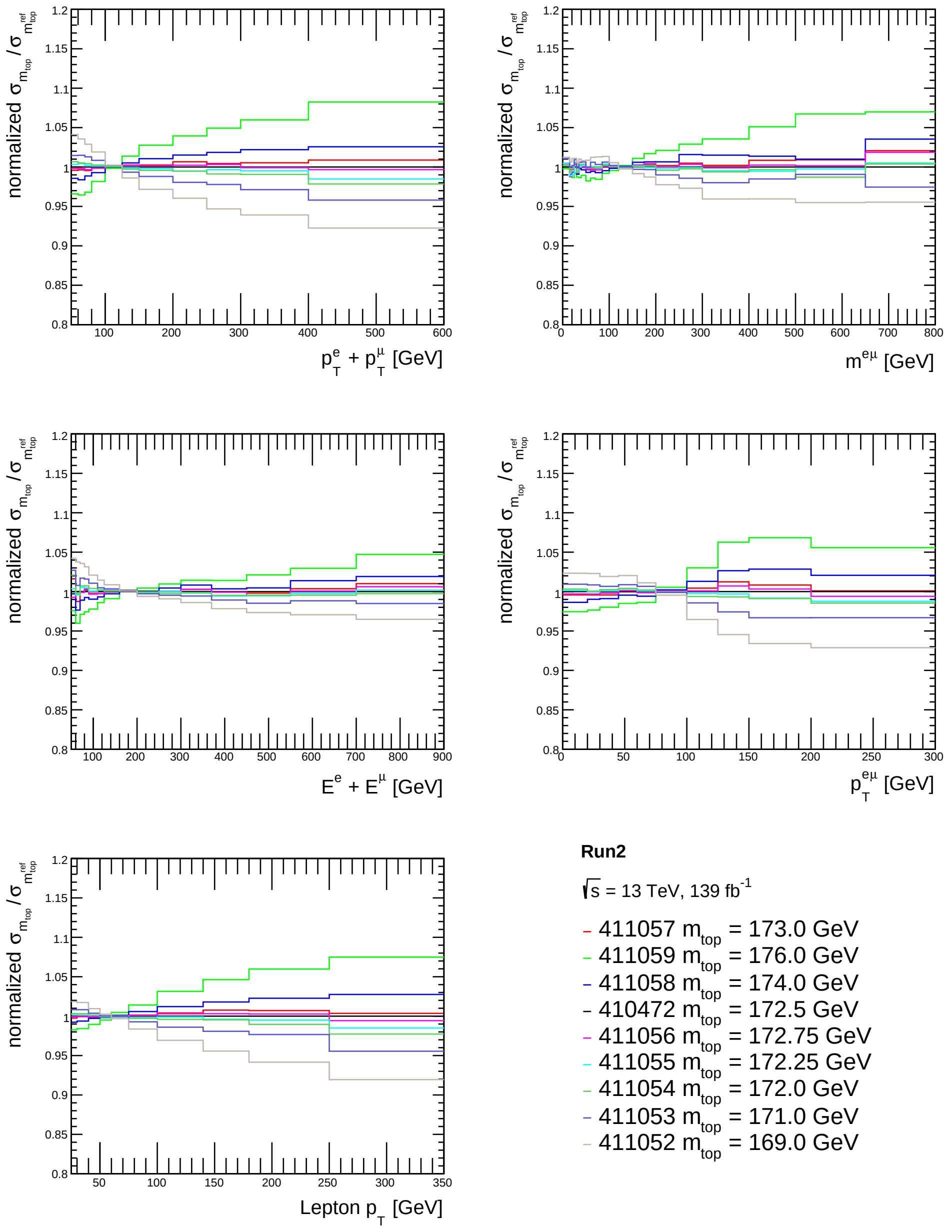

Figure 10.2: Ratio of top mass templates to the nominal top mass template with $m_{\text{top}} = 172.5$ GeV.

nomial fits at the top mass points of the original top mass variation samples. The parametrization for p_{T} $(\ell^+\ell^-)$ is shown for each bin in the distribution in Fig. 10.3, while the parametrization of the templates for the other variables are shown in Appendix G.

10.3 Covariance matrix

The covariance matrix in Eq. 10.1 must contain the information about the uncertainty on the measured normalised differential cross section. The covariance matrix should contain therefore both the statistical and systematic uncertainties, as well as the correlation terms between bins in the off-diagonal elements.

The data statistical covariance matrix is found thanks to bootstrapping experiments, explained in Section 7.4.4, where the diagonal elements are the statistical uncertainty values squared for each bin, while the off-diagonal elements contain the correlations (mostly negative), which arise due to the normalisation and can be seen in Fig. 7.9.

For each systematic uncertainty, a covariance matrix for each distribution is calculated, where the diagonal elements contain the systematic uncertainty squared on the bins of the distributions, while the off diagonal elements contain the correlations between bins of each single distribution and, in this case, all bins within one distribution are taken as fully correlated for every systematic uncertainty. The only systematic uncertainty which has bins that are not fully correlated within one variable is the Monte Carlo statistical uncertainty. When the covariance matrices for all systematic and statistical uncertainties for each variable are calculated, they are summed, so to have at the end five total covariance matrices, one for each variable. The five covariance matrices are presented in Appendix H. The correlation between bins due to statistical and systematic correlations can be found for each bin with the following formula:

$$\rho_{i,j} = \frac{\sigma_{i,j}}{\sigma_i \cdot \sigma_j} \tag{10.2}$$

where $\rho_{i,j}$ is the correlation factor between bins i and j, $\sigma_{i,j}$ is the covariance between bin i and j and σ_i and σ_j are the uncertainties on bin i and bin j respectively (and they are the square root value of the diagonal elements of bin i and j, respectively).

The correlations between bins are positive, even though the statistical correlation due to normalisation is negative, and this is mainly because the statistical uncertainties in most of the bins is lower than the systematic uncertainties, especially the $t\bar{t}$ uncertainties, which are fully correlated (with a correlation factor of 1). In particular the highest bins in the p_{T} distributions are highly correlated, and this is because of the very high uncertainty coming from the $t\bar{t}/Wt$ interference. The correlation matrices can be seen in Fig. 10.4.

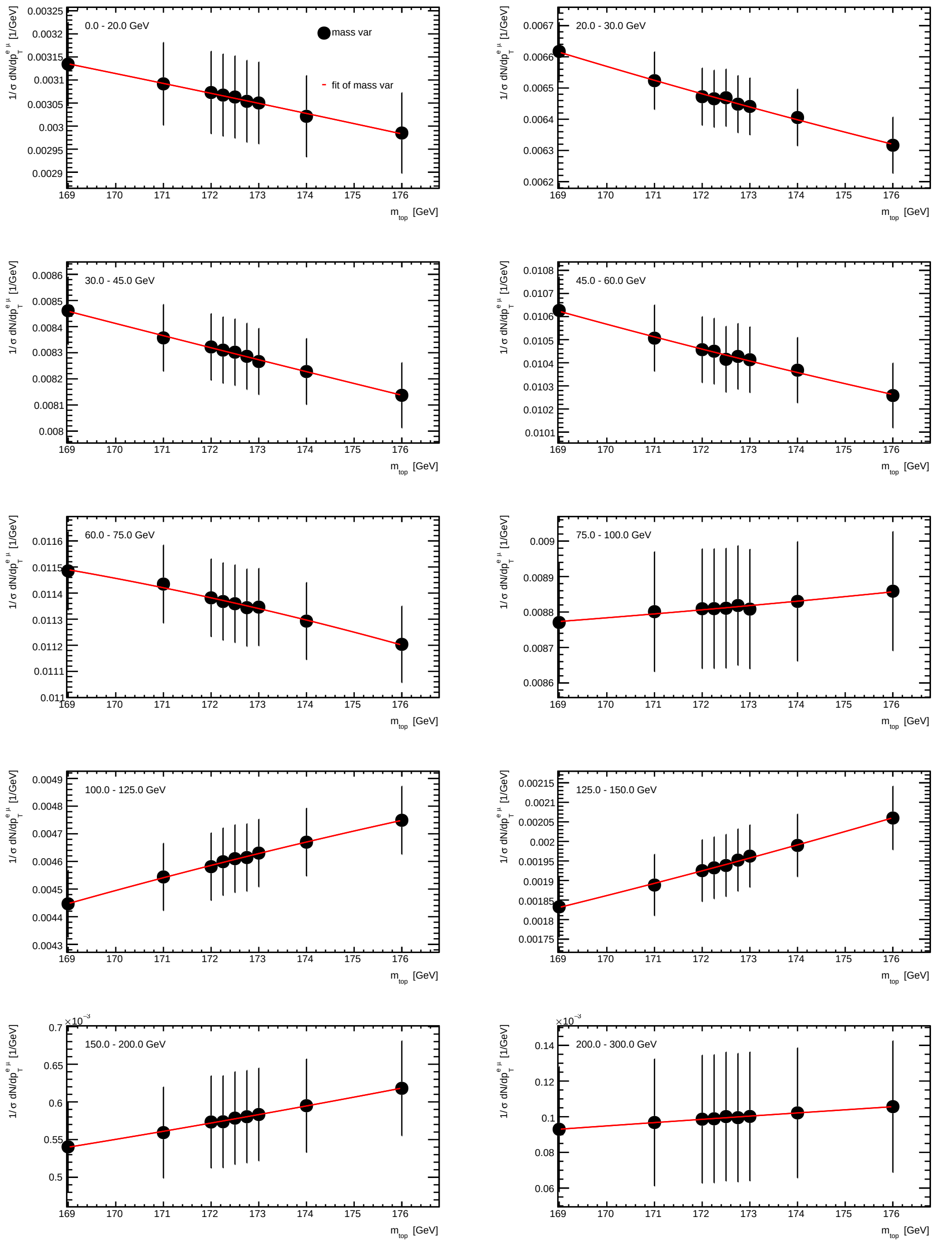

Figure 10.3: Parametrisation of the particle level templates for each bin of $p_{\mathrm{T}}(\ell^+\ell^-)$. The values for each bin are fitted to a second order degree polynomial (in red).

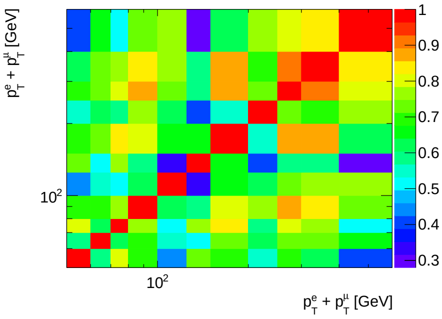

(a)

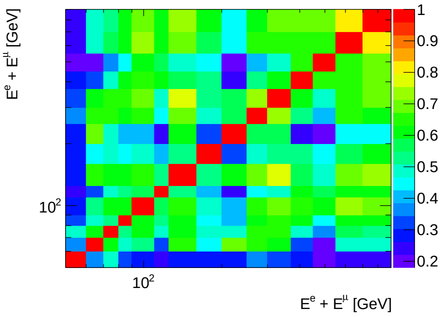

(b)

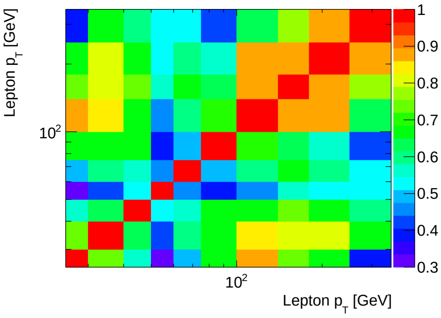

(c)

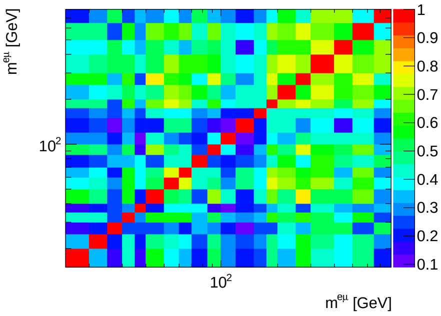

(d)

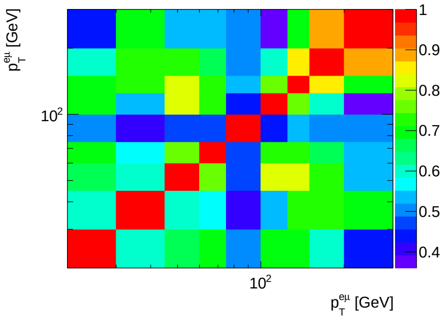

(e)

Figure 10.4: Correlation matrices for statistical and systematic correlations in the covariance matrices for the five variables used for the top mass estimation

10.4 Results

Once the templates and the total covariance matrices are ready, the χ^2/NDF distribution for each variable can be calculated using Eq. 10.1. The results of the χ^2 distributions divided by the number of degrees of freedom can be seen in Fig. 10.5, where the χ^2/NDF are fitted to second order polynomial functions in order to extract the minimum, which is the measured top mass value for each variable. Already from a first look it is quite clear that the most precise and sensitive variable is the $p_{\mathrm{T}}(\ell^+\ell^-)$, because the parabola is the most narrow amongst all the fitted graphs. Another feature that quickly catches the eye is that the χ^2/NDF points calculated with the chosen templates are not placed symmetrically around the minimum of the χ^2/NDF distribution and this is due to shortcomings of the POWHEG + PYTHIA 8 templates where the matrix elements are calculated to NLO, while the parton shower is evaluated only to leading order. Improved templates could come from combining fixed order matrix elements with a parton shower calculated at NLO level, or even at NNLO level, since this would ameliorate the problem with the p_{T} top distributions [20, 118]. Also just reweighing the current templates to include a correction for NNLO QCD + NLO EW effects [20, 106], as done in Section 8.2, could help in solving this challenge. The first example has been already used for the top mass extraction from Run 1 data in [17], where fixed-order calculations from the MCFM generator were used to extract the top mass. No measurements in ATLAS have been published with NNLO calculations yet, since those have only lately started to become available.
The total uncertainty (statistical + systematic) on each mass value is found with the total covariance matrix for that variable, but, to find the statistical uncertainty alone, toy experiments need to be used. For this purpose, the normalised differential cross sections found with data bootstrapping experiments can be used as the measured normalised differential cross section together with the total covariance matrix in Eq. 10.1, so that 1000 values of the top mass are extracted for each variable. The statistical uncertainty on the top mass is then the RMS of these 1000 values from bootstrapping experiments.
The results extracted from Fig. 10.5 can be seen in Table 10.1, where the predicted top mass values for each distribution are shown, as well as their total uncertainty, extracted using the total covariance matrix, their statistical uncertainty, extracted with toy experiments, and the total systematic uncertainty found by taking the difference (in quadrature) between the total and statistical contribution to the error.

The results are not consistent with the current ATLAS combined average of 172.69 ± 0.48 GeV [119] nor with the latest world average of the top pole mass of 173.1 ± 0.9 GeV [120]. In fact they are several standard deviations below the previous results, except for the value extracted from the $p_{\mathrm{T}}(\ell^+\ell^-)$ observable. It is clear that the template modelling of the top p_{T} distribution (predicting a harder spectrum than that observed in data) is the source of the problem, and that reliable results with this method require templates with higher theoretical accuracy, as fixed order calculations including NNLO effects and EW correction, which might ameliorate the mismodelling of the top p_{T}.

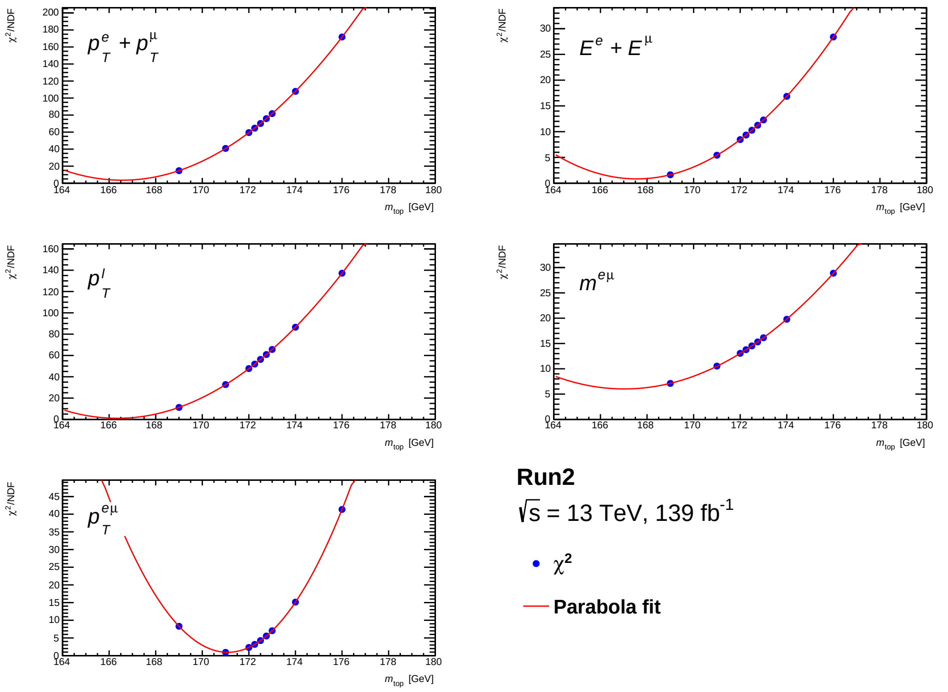

Figure 10.5: χ^2/NDF distribution for the five variables used to find the top mass. Each distribution is fitted to a second degree polynomial to find the minimum of the distribution.

Table 10.1: Top mass values and uncertainties from the five different variables.

Variable	$p_{\mathrm{T}}(\ell)$	$p_{\mathrm{T}}(\ell^+\ell^-)$	$M(\ell^+\ell^-)$	$p_{\mathrm{T}}(\ell^+) + p_{\mathrm{T}}(\ell^-)$	$E(\ell^+) + E(\ell^-)$
Central value	166.35	171.09	167.02	166.56	167.56
Tot uncertainty	0.83	0.77	1.88	0.73	1.61
Stat uncertainty	0.08	0.06	0.11	0.07	0.12
Syst uncertainty	0.82	0.77	1.87	0.72	1.60
Minimum χ^2	1.03	0.9	6.0	3.5	0.8

10.5 BLUE combination

The BLUE combination is developed to combine several measurements of the same quantity, performed with different methods, coming from the same dataset. Since each measurement comes from the same dataset, all the measurements will be more or less correlated with each other and these correlations need to be taken into consideration when finding a combined measurement [117]. In the case of two or more measurements which are fully uncorrelated, the best estimate of the central value and of its uncertainty are the weighted average and the weighted uncertainty [117].
First of all the statistical correlations between the five different top mass measurements need to be measured using correlated sub-samples. To this end, the normalised differential cross section results from the data bootstrapping experiments from Section 7.4.4, together with the total covariance matrix, are used to calculate 1000 different values of the top mass for each variable. From these 1000 values, the correlations between the five variables is found with the standard Pearson correlation equation:

$$\rho = \frac{< \mathbf{m}^i_{\text{top}} \cdot \mathbf{m}^j_{\text{top}} > - < \mathbf{m}^i_{\text{top}} > \cdot < \mathbf{m}^j_{\text{top}} >}{\sigma_{\mathbf{m}^i_{\text{top}}} \cdot \sigma_{\mathbf{m}^j_{\text{top}}}} \tag{10.3}$$

where $\mathbf{m}^i_{\text{top}}$ is the vector of 1000 top mass values extracted with variable i and $\mathbf{m}^j_{\text{top}}$ is the vector of 1000 top mass values extracted with variable j, while $\sigma_{\mathbf{m}^i_{\text{top}}}$ and $\sigma_{\mathbf{m}^j_{\text{top}}}$ are the standard deviations of the top mass vector of variables i and j. The values of the statistical correlation between the five variables can be seen in Fig. 10.6.

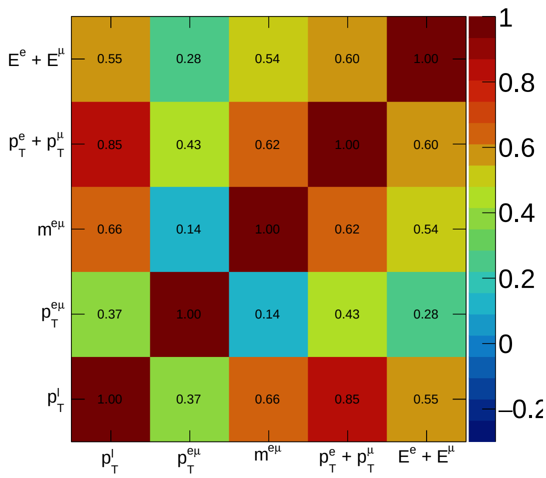

Figure 10.6: Statistical correlation between the five variables used to extract the top mass.

Besides the statistical correlation, the systematic uncertainties also add a contribution to the correlation between the variables, and in this case, where the systematic uncertainties are the dominating uncertainties, they would add a significant contribution. To add the systematic correlations, one would have to estimate the size of each systematic uncertainty on each value of the top mass. Then, since the systematic uncertainties are calculated in the same way for each variable, each source of systematic uncertainty can be taken as 100% correlated between variables. In this quick overview of the top mass estimation, there has not been time to find the size of each systematic uncertainty on each top mass, therefore the BLUE combination will be presented here using only the statistical uncertainty and the statistical correlations.

From the correlation matrix an error matrix can be extracted with the total errors on each measurement in the diagonal elements and the correlation terms in the off-diagonal elements. In this case the error matrix would look like this:

$$E = \begin{bmatrix} \sigma^2_{st,1} & \rho_{2,1}\cdot\sigma_{st,2}\sigma_{st,1} & \rho_{3,1}\cdot\sigma_{st,3}\sigma_{st,1} & \rho_{4,1}\cdot\sigma_{st,4}\sigma_{st,1} & \rho_{5,1}\cdot\sigma_{st,5}\sigma_{st,1} \\ \rho_{1,2}\cdot\sigma_{st,1}\sigma_{st,2} & \sigma^2_{st,2} & \rho_{3,2}\cdot\sigma_{st,3}\sigma_{st,2} & \rho_{4,1}\cdot\sigma_{st,4}\sigma_{st,2} & \rho_{5,2}\cdot\sigma_{st,5}\sigma_{st,2} \\ \rho_{1,3}\cdot\sigma_{st,1}\sigma_{st,3} & \rho_{2,3}\cdot\sigma_{st,2}\sigma_{st,3} & \sigma^2_{st,3} & \rho_{4,3}\cdot\sigma_{st,4}\sigma_{st,3} & \rho_{5,3}\cdot\sigma_{st,5}\sigma_{st,3} \\ \rho_{1,4}\cdot\sigma_{st,1}\sigma_{st,4} & \rho_{2,4}\cdot\sigma_{st,2}\sigma_{st,4} & \rho_{3,4}\cdot\sigma_{st,3}\sigma_{st,4} & \sigma^2_{st,4} & \rho_{5,4}\cdot\sigma_{st,5}\sigma_{st,4} \\ \rho_{1,5}\cdot\sigma_{st,1}\sigma_{st,5} & \rho_{2,5}\cdot\sigma_{st,2}\sigma_{st,5} & \rho_{3,5}\cdot\sigma_{st,3}\sigma_{st,5} & \rho_{4,5}\cdot\sigma_{st,4}\sigma_{st,5} & \sigma^2_{st,5} \end{bmatrix}$$

where $\rho_{i,j}$ is the correlation factor between two variables (with i and j going from 1 to 5) and $\sigma_{st,i}$ is the statistical uncertainty on $m_{\mathrm{top},i}$.

In case we added the systematic uncertainties, the diagonal elements would become:

$$\sigma^2_{st,i} + \sum_x \sigma^2_{x,i} \tag{10.4}$$

and the off-diagonal elements would become:

$$\rho_{i,j}\cdot\sigma_{st,i}\sigma_{st,j} + \sum_x 1\cdot\sigma_{x,i}\sigma_{x,j} \tag{10.5}$$

where $\sigma_{x,i}$ is the systematic uncertainty for one specific systematic source x, and since this has to be done for all the systematic sources, a sum over all the sources is performed.

With the error matrix, weights can be calculated for each variable, so that the combined top mass value is a weighted average according to the errors. The combined estimate becomes then, following [117]:

$$\hat{m_{\mathrm{top}}} = \sum \alpha_i\, m_{\mathrm{top},i} \tag{10.6}$$

where $\hat{m_{\mathrm{top}}}$ is the combined value of the five m_{top} values, α_i is the weight i for the mass estimate from variable i and $m_{\mathrm{top},i}$ is the top mass estimate from variable i. The variance on the combined mass value is then [117]:

$$\sigma^2_{m_{\mathrm{top}}} = \boldsymbol{\alpha}^T\mathbf{E}\boldsymbol{\alpha} \tag{10.7}$$

where $\sigma^2_{m_{\mathrm{top}}}$ is the variance on the top mass combined estimate, α is the vector of weights and $\mathbf{E}$ is the error matrix.

The five weights, whose sum needs to be one, are found so that they minimise the variance of the combined estimate, with:

$$\boldsymbol{\alpha} = \frac{\mathbf{E}^{-1}\mathbf{U}}{\mathbf{U}^T\mathbf{E}^{-1}\mathbf{U}} \tag{10.8}$$

where $\mathbf{U}$ is a vector of ones and $\mathbf{E}^{-1}$ is the inverse error matrix.
Once the weights are found, they can be substituted in Eq. 10.6 and 10.7 to find the combined top mass value and its uncertainty.
As mentioned before this was performed only with the statistical uncertainties and correlations and the resulting $\boldsymbol{\alpha}$ is (for the variables in the following order: $p_{\mathrm{T}}(\ell)$, $p_{\mathrm{T}}(\ell^+\ell^-)$, $m(\ell^+\ell^-)$, $p_{\mathrm{T}}(\ell^+) + p_{\mathrm{T}}(\ell^-)$, $E(\ell^+) + (\ell^-)$):

$$\boldsymbol{\alpha} = \begin{bmatrix} 0.155 \\ 0.607 \\ 0.071 \\ 0.205 \\ -0.038 \end{bmatrix}$$

These weights can be inserted in Eq. 10.6 giving a combined $\hat{m_{\mathrm{top}}} = 169.27$ GeV with a combined statistical uncertainty of $\sigma_{stat} = 0.06$ GeV.
Given the size of the total uncertainty and the correlation between the measurements, the total uncertainty would probably be around $600 - 700$ MeV. Thanks to the high statistics of the full Run 2 dataset and to the improvements in the systematic uncertainty estimations in newer software releases, the experimental precision of the top mass measurement can be very much improved and hopefully, with the new NNLO predictions the templates used for the indirect top mass estimation will improve this measurement even further.

CHAPTER 11

CONCLUSION

In this analysis the $t\bar{t}$ production total fiducial and inclusive cross section and the $t\bar{t}$ production absolute and normalised differential cross sections for seven different variables ($p_{\mathrm{T}}(\ell^+\ell^-)$, $p_{\mathrm{T}}(\ell^+)+p_{\mathrm{T}}(\ell^-)$, $p_{\mathrm{T}}(\ell)$, $E(\ell^+)+E(\ell^-)$, $m(\ell^+\ell^-)$, $|\eta(\ell)|$ and $\Delta\phi(\ell^+\ell^-)$) are measured using the full dataset collected during the Run 2 in the ATLAS experiment at $\sqrt{s} = 13\,\mathrm{TeV}$ with a total integrated luminosity of $139\,\mathrm{fb}^{-1}$. This is done using opposite sign dilepton $e\mu$ events with either one or two associated b-jets and the $t\bar{t}$ production cross section is extracted by fitting with Poissonian statistics the number of data events to the expected number of events modelled with Monte Carlo and data-driven techniques.
The total inclusive cross section was measured to:

$$\sigma_{t\bar{t}} = 839.8 \pm 1.3 \pm 16.0 \pm 18.4\,\mathrm{pb}$$

where the first uncertainty is the statistical one, the second is the luminosity uncertainty and the last is the total systematic uncertainty from all of the other sources other than the luminosity. The combined uncertainties corresponds to a total uncertainty of 2.91%. The total uncertainty on the total fiducial cross section is 2.34% and the difference between the total uncertainty on the total fiducial and inclusive cross section is due to $t\bar{t}$ related uncertainties, in particular the generator uncertainty.
The normalised differential cross section distribution for 5 of the variables ($p_{\mathrm{T}}(\ell^+\ell^-)$, $p_{\mathrm{T}}(\ell^+)+p_{\mathrm{T}}(\ell^-)$, $p_{\mathrm{T}}(\ell)$, $E(\ell^+)+E(\ell^-)$, $m(\ell^+\ell^-)$) are then used to extract the top pole mass by comparing the measured distributions to Monte Carlo templates at different top mass values. For each top mass point and for each variable a χ^2 is calculated with the difference between the measured distribution and the templates at that mass point, weighted by the covariance matrix given by the systematic and statistical uncertainties on each bin and the correlation between bins. The χ^2 distributions for each variable are then fitted to a second degree polynomial, where the minimum of each fit gives the value of the top mass for that variable. The modelling of the Monte Carlo top mass variation templates is found to be not adequate for a top pole mass

extraction, mainly due to a harder p_{T} spectrum, so for a proper top pole mass extraction more advanced templates are needed.

BIBLIOGRAPHY

[1] *2019 Review of Particle Physics - Top Quark*, URL: http://pdg.lbl.gov/2019/listings/rpp2019-list-t-quark.pdf (visited on 04/09/2019).

[2] CDF Collaboration, *Observation of top quark production in $\bar{p}p$ collisions*, Phys. Rev. Lett. **74** (1995) 2626, arXiv: hep-ex/9503002 [hep-ex].

[3] D0 Collaboration, *Observation of the top quark*, Phys. Rev. Lett. **74** (1995) 2632, arXiv: hep-ex/9503003 [hep-ex].

[4] M. Thomson, *Modern particle physics*, Cambridge University Press, 2013, ISBN: 9781107034266.

[5] *2019 Review of Particle Physics - Top Quark*, URL: http://pdg.lbl.gov/2019/reviews/rpp2018-rev-top-quark.pdf (visited on 11/09/2019).

[6] A. Buckley et al., *Global fit of top quark effective theory to data*, Phys. Rev. **D92** (2015) 091501, arXiv: 1506.08845 [hep-ph].

[7] J. Ferrando and D. Wendland, *Reference $t\bar{t}$ production cross sections for use in ATLAS analyses*, tech. rep. ATL-COM-PHYS-2014-112, CERN, 2014, URL: https://cds.cern.ch/record/1662536 (visited on 07/08/2019).

[8] P. Bärnreuther, M. Czakon and A. Mitov, *Percent Level Precision Physics at the Tevatron: First Genuine NNLO QCD Corrections to $q\bar{q} \to t\bar{t} + X$*, Phys. Rev. Lett. **109** (2012) 132001, arXiv: 1204.5201 [hep-ph].

[9] M. Czakon and A. Mitov, *NNLO corrections to top-pair production at hadron colliders: the all-fermionic scattering channels*, JHEP **12** (2012) 054, arXiv: 1207.0236 [hep-ph].

[10] M. Czakon and A. Mitov, *NNLO corrections to top pair production at hadron colliders: the quark-gluon reaction*, JHEP **01** (2013) 080, arXiv: 1210.6832 [hep-ph].

[11] M. Czakon, P. Fiedler and A. Mitov, *Total Top-Quark Pair-Production Cross Section at Hadron Colliders Through* $O(\alpha_S^4)$, Phys. Rev. Lett. **110** (2013) 252004, arXiv: 1303.6254 [hep-ph].

[12] J. Haller et al., *Update of the global electroweak fit and constraints on two-Higgs-doublet models*, Eur. Phys. J. **C78** (2018) 675, arXiv: 1803.01853 [hep-ph].

[13] ATLAS Collaboration, *Measurement of the* $t\bar{t}$ *production cross-section using* $e\mu$ *events with b-tagged jets in pp collisions at* $\sqrt{s} = 7$ *and* 8 *TeV with the ATLAS detector*, Eur. Phys. J. C **74** (2014) 3109, arXiv: 1406.5375 [hep-ex].

[14] R. Hawkings, *Measurement of the* $t\bar{t}$ *production cross-section in pp collisions at* $\sqrt{s}$ =*7-8 TeV using* $e\mu$ *events with b-tagged jets*, tech. rep. ATL-PHYS-INT-2014-025, CERN, 2014, URL: https://cds.cern.ch/record/1952814 (visited on 07/08/2019).

[15] ATLAS Collaboration, *Measurement of the* $t\bar{t}$ *production cross-section using* $e\mu$ *events with b-tagged jets in pp collisions at* $\sqrt{s} = 13$ *TeV with the ATLAS detector*, Phys. Lett. B **761** (2016) 136, arXiv: 1606.02699 [hep-ex].

[16] *Measurement of the* $t\bar{t}$ *production cross-section and lepton differential distributions in* $e\mu$ *dilepton events from pp collisions at* $\sqrt{s} = 13$ *TeV with the ATLAS detector*, tech. rep. ATLAS-CONF-2019-041, CERN, 2019, URL: http://cds.cern.ch/record/2686255 (visited on 02/09/2019).

[17] ATLAS Collaboration, *Measurement of lepton differential distributions and the top quark mass in* $t\bar{t}$ *production in pp collisions at* $\sqrt{s} = 8$ *TeV with the ATLAS detector*, Eur. Phys. J. C **77** (2017) 804, arXiv: 1709.09407 [hep-ex].

[18] R. Hawkings, *Measurement of lepton differential distributions in* $t\bar{t}$ *production in pp collisions at* $\sqrt{s} = 8$ *TeV using* $e\mu$ *events with b-tagged jets*, tech. rep. ATL-COM-PHYS-2015-002, CERN, 2015, URL: https://cds.cern.ch/record/1979932 (visited on 07/08/2019).

[19] *Improvements in* $t\bar{t}$ *modelling using NLO+PS Monte Carlo generators for Run2*, tech. rep. ATL-PHYS-PUB-2018-009, CERN, 2018, URL: https://cds.cern.ch/record/2630327 (visited on 11/09/2019).

[20] M. Czakon, D. Heymes and A. Mitov, *High-precision differential predictions for top-quark pairs at the LHC*, Phys. Rev. Lett. **116** (2016) 082003, arXiv: 1511.00549 [hep-ph].

[21] S. Höche et al., *Next-to-leading order QCD predictions for top-quark pair production with up to two jets merged with a parton shower*, Phys. Lett. **B748** (2015) 74, arXiv: 1402.6293 [hep-ph].

[22] S. Höche, P. Maierhöfer, N. Moretti, S. Pozzorini and F. Siegert, *Next-to-leading order QCD predictions for top-quark pair production with up to three jets*, Eur. Phys. J. **C77** (2017) 145, arXiv: 1607.06934 [hep-ph].

[23] C. Gütschow, J. M. Lindert and M. Schönherr, *Multi-jet merged top-pair production including electroweak corrections*, Eur. Phys. J. **C78** (2018) 317, arXiv: 1803.00950 [hep-ph].

[24] S. Frixione and A. Mitov, *Determination of the top quark mass from leptonic observables*, JHEP **09** (2014) 012, arXiv: 1407.2763 [hep-ph].

[25] A. Pais, *"Subtle is the Lord": The Science and Life of Albert Einstein*, Oxford Press, 1982.

[26] N. Bohr, *On the Constitution of Atoms and Molecules, Part I*, Philosophical Magazine **26** (1913) 1.

[27] J. Chadwick, *Possible Existence of a Neutron*, Nature **129** (1932) 312.

[28] J. D. Cockcroft, E. T. S. Walton and E. Rutherford, *Experiments with high velockty positive ions.-(I) Further developments in the method of obtaining high velocity positive ions*, Proc. R. Soc. Lond. A. **136** (1932).

[29] E. D. Bloom et al., *High-Energy Inelastic e p Scattering at 6-Degrees and 10-Degrees*, Phys. Rev. Lett. **23** (1969) 930.

[30] M. Breidenbach et al., *Observed Behavior of Highly Inelastic electron-Proton Scattering*, Phys. Rev. Lett. **23** (1969) 935.

[31] S. L. Glashow, *Partial Symmetries of Weak Interactions*, Nucl. Phys. **22** (1961) 579.

[32] S. Weinberg, *A Model of Leptons*, Phys. Rev. Lett. **19** (1967) 1264.

[33] MissMJ, *File:Standard Model of Elementary Particles.svg*, available under the Creative Commons CC-BY-3.0 license, URL: https://commons.wikimedia.org/wiki/File:Standard_Model_of_Elementary_Particles.svg (visited on 07/08/2019).

[34] UA1 Collaboration, *Experimental Observation of Isolated Large Transverse Energy Electrons with Associated Missing Energy at* $\sqrt{s} = 540$ *GeV*, Phys. Lett. **122B** (1983) 103.

[35] UA2 Collaboration, *Observation of Single Isolated Electrons of High Transverse Momentum in Events with Missing Transverse Energy at the CERN anti-p p Collider*, Phys. Lett. **122B** (1983) 476.

[36] UA1 Collaboration, *Experimental Observation of Lepton Pairs of Invariant Mass Around 95 GeV/*c^2 *at the CERN SPS Collider*, Phys. Lett. **126B** (1983) 398.

[37] UA2 Collaboration, *Evidence for Z0 $\rightarrow e + e-$ at the CERN anti-p p Collider*, Phys. Lett. **129B** (1983) 130.

[38] ATLAS Collaboration, *Observation of a new particle in the search for the Standard Model Higgs boson with the ATLAS detector at the LHC*, Phys. Lett. **B716** (2012) 1, arXiv: 1207.7214 [hep-ex].

[39] CMS Collaboration, *Observation of a New Boson at a Mass of 125 GeV with the CMS Experiment at the LHC*, Phys. Lett. **B716** (2012) 30, arXiv: 1207.7235 [hep-ex].

[40] S. H. Neddermeyer and C. D. Anderson, *Note on the Nature of Cosmic Ray Particles*, Phys. Rev. **51** (1937) 884.

[41] SLAC-SP-017 Collaboration, *Discovery of a Narrow Resonance in e^+e^- Annihilation*, Phys. Rev. Lett. **33** (1974) 1406.

[42] E598 Collaboration, *Experimental Observation of a Heavy Particle J*, Phys. Rev. Lett. **33** (1974) 1404.

[43] SLAC-SP-017 Collaboration, *Evidence for Anomalous Lepton Production in $e + -e-$ Annihilation*, Phys. Rev. Lett. **35** (1975) 1489.

[44] S. W. Herb et al., *Observation of a Dimuon Resonance at 9.5-GeV in 400-GeV Proton-Nucleus Collisions*, Phys. Rev. Lett. **39** (1977) 252.

[45] *2019 Review of Particle Physics - W boson*, URL: http://pdg.lbl.gov/2019/listings/rpp2019-list-w-boson.pdf (visited on 06/09/2019).

[46] C. D. White, S. Frixione, E. Laenen and F. Maltoni, *Isolating Wt production at the LHC*, JHEP **11** (2009) 074, arXiv: 0908.0631 [hep-ph].

[47] S. Frixione, E. Laenen, P. Motylinski, B. R. Webber and C. D. White, *Single-top hadroproduction in association with a W boson*, JHEP **07** (2008) 029, arXiv: 0805.3067 [hep-ph].

[48] *Top Feynman Diagrams*, URL: https://www-d0.fnal.gov/Run2Physics/top/top_public_web_pages/top_feynman_diagrams.html (visited on 07/08/2019).

[49] *First combination of Tevatron and LHC measurements of the top-quark mass*, (2014), arXiv: 1403.4427 [hep-ex].

[50] L. Cerrito, *Top Quark Mass Summary Plots*, tech. rep. ATL-COM-PHYS-2019-500, CERN, 2019, URL: https://cds.cern.ch/record/2673730 (visited on 07/08/2019).

[51] J. R. Espinosa, *Vacuum Stability and the Higgs Boson*, PoS **LATTICE2013** (2014) 010, arXiv: 1311.1970 [hep-lat].

[52] P. Nason, 'The Top Mass in Hadronic Collisions', *From My Vast Repertoire ...: Guido Altarelli's Legacy*, ed. by A. Levy, S. Forte and G. Ridolfi, 2019 123, arXiv: 1712.02796 [hep-ph].

[53] ATLAS Collaboration, *Observation of Higgs boson production in association with a top quark pair at the LHC with the ATLAS detector*, Phys. Lett. **B784** (2018) 173, arXiv: 1806.00425 [hep-ex].

[54] M. Baak et al., *The global electroweak fit at NNLO and prospects for the LHC and ILC*, Eur. Phys. J. **C74** (2014) 3046, arXiv: 1407.3792 [hep-ph].

[55] ATLAS Collaboration, *A summary of the latest top anti-top cross-section measurements from ATLAS*, tech. rep. ATLAS-PHO-ach-2015-049, 2015, URL: https://cds.cern.ch/record/2054112 (visited on 07/08/2019).

[56] *NNLO+NNLL top-quark-pair cross sections*, URL: https://twiki.cern.ch/twiki/bin/view/LHCPhysics/TtbarNNLO (visited on 07/08/2019).

[57] W. Bernreuther, A. Brandenburg, Z. G. Si and P. Uwer, *Top quark spin correlations at hadron colliders: Predictions at next-to-leading order QCD*, Phys. Rev. Lett. **87** (2001) 242002, arXiv: hep-ph/0107086 [hep-ph].

[58] ATLAS Collaboration, *Measurements of top-quark pair spin correlations in the $e\mu$ channel at $\sqrt{s} = 13$ TeV using pp collisions in the ATLAS detector*, Submitted to: Eur. Phys. J. (2019), arXiv: 1903.07570 [hep-ex].

[59] ATLAS Collaboration, *The ATLAS Experiment at the CERN Large Hadron Collider*, JINST **3** (2008) S08003.

[60] ATLAS Collaboration, *ATLAS pixel detector electronics and sensors*, JINST **3** (2008) P07007.

[61] ATLAS Collaboration, *Operation and performance of the ATLAS semiconductor tracker*, JINST **9** (2014) P08009, arXiv: 1404.7473 [hep-ex].

[62] ATLAS Collaboration, *Performance of the ATLAS Transition Radiation Tracker in Run 1 of the LHC: tracker properties*, JINST **12** (2017) P05002, arXiv: 1702.06473 [hep-ex].

[63] ATLAS Collaboration, *Performance of the ATLAS Track Reconstruction Algorithms in Dense Environments in LHC Run 2*, Eur. Phys. J. **C77** (2017) 673, arXiv: 1704.07983 [hep-ex].

[64] *Performance of the ATLAS Inner Detector Track and Vertex Reconstruction in the High Pile-Up LHC Environment*, tech. rep. ATLAS-CONF-2012-042, CERN, 2012, URL: https://cds.cern.ch/record/1435196 (visited on 07/08/2019).

[65] ATLAS Collaboration, *Readiness of the ATLAS Liquid Argon Calorimeter for LHC Collisions*, Eur. Phys. J. **C70** (2010) 723, arXiv: 0912.2642 [physics.ins-det].

[66] ATLAS Collaboration, *Readiness of the ATLAS Tile Calorimeter for LHC collisions*, Eur. Phys. J. **C70** (2010) 1193, arXiv: 1007.5423 [physics.ins-det].

[67] ATLAS Collaboration, *The ATLAS Data Acquisition and High Level Trigger system*, JINST **11** (2016) P06008.

[68] *Luminosity determination in pp collisions at* $\sqrt{s} = 13$ *TeV using the ATLAS detector at the LHC*, tech. rep. ATLAS-CONF-2019-021, CERN, 2019, URL: https://cds.cern.ch/record/2677054 (visited on 14/09/2019).

[69] ATLAS Data Quality Group, *GoodRunListsForAnalysisRun2*, URL: https://twiki.cern.ch/twiki/bin/view/AtlasProtected/GoodRunListsForAnalysisRun2 (visited on 07/08/2019).

[70] ATLAS Collaboration, *The ATLAS Simulation Infrastructure*, Eur. Phys. J. C **70** (2010) 823, arXiv: 1005.4568 [physics.ins-det].

[71] P. Nason, *A New method for combining NLO QCD with shower Monte Carlo algorithms*, JHEP **11** (2004) 040, arXiv: hep-ph/0409146 [hep-ph].

[72] S. Frixione, P. Nason and C. Oleari, *Matching NLO QCD computations with Parton Shower simulations: the POWHEG method*, JHEP **11** (2007) 070, arXiv: 0709.2092 [hep-ph].

[73] S. Alioli, P. Nason, C. Oleari and E. Re, *A general framework for implementing NLO calculations in shower Monte Carlo programs: the POWHEG BOX*, JHEP **06** (2010) 043, arXiv: 1002.2581 [hep-ph].

[74] R. D. Ball et al., *Parton distributions for the LHC Run II*, JHEP **04** (2015) 040, arXiv: 1410.8849 [hep-ph].

[75] T. Sjostrand, S. Mrenna and P. Z. Skands, *A Brief Introduction to PYTHIA 8.1*, Comput. Phys. Commun. **178** (2008) 852, arXiv: 0710.3820 [hep-ph].

[76] T. Sjostrand, S. Mrenna and P. Z. Skands, *PYTHIA 6.4 Physics and Manual*, JHEP **05** (2006) 026, arXiv: hep-ph/0603175 [hep-ph].

[77] ATLAS Collaboration, *ATLAS Pythia 8 tunes to* 7 *TeV data*, ATL-PHYS-PUB-2014-021, 2014, URL: https://cds.cern.ch/record/1966419 (visited on 07/08/2019).

[78] R. D. Ball et al., *Parton distributions with LHC data*, Nucl. Phys. **B867** (2013) 244, arXiv: 1207.1303 [hep-ph].

[79] S. Agostinelli et al., *GEANT4: A Simulation toolkit*, Nucl. Instrum. Meth. **A506** (2003) 250.

[80] J. Bellm et al., *Herwig 7.0/Herwig++ 3.0 release note*, Eur. Phys. J. **C76** (2016) no. 4 196, arXiv: 1512.01178 [hep-ph].

[81] S. Gieseke, C. Rohr and A. Siodmok, *Colour reconnections in Herwig++*, Eur. Phys. J. **C72** (2012) 2225, arXiv: 1206.0041 [hep-ph].

[82] W. Lukas, 'Fast Simulation for ATLAS: Atlfast-II and ISF', 2012, URL: http://cdsweb.cern.ch/record/1458503/files/ATL-SOFT-PROC-2012-065.pdf (visited on 07/08/2019).

[83] J. Alwall et al., *The automated computation of tree-level and next-to-leading order differential cross sections, and their matching to parton shower simulations*, JHEP **07** (2014) 079, arXiv: 1405.0301 [hep-ph].

[84] E. Re, *Single-top Wt-channel production matched with parton showers using the POWHEG method*, Eur. Phys. J. **C71** (2011) 1547, arXiv: 1009.2450 [hep-ph].

[85] F. Cascioli et al., *Precise Higgs-background predictions: merging NLO QCD and squared quark-loop corrections to four-lepton + 0,1 jet production*, JHEP **01** (2014) 046, arXiv: 1309.0500 [hep-ph].

[86] ATLAS Collaboration, *Electron reconstruction and identification in the ATLAS experiment using the 2015 and 2016 LHC proton-proton collision data at* $\sqrt{s}$ *= 13 TeV*, Submitted to: Eur. Phys. J. (2019), arXiv: 1902.04655 [physics.ins-det].

[87] ATLAS Collaboration, *Muon reconstruction performance of the ATLAS detector in proton–proton collision data at* $\sqrt{s}$ *=13 TeV*, Eur. Phys. J. **C76** (2016) 292, arXiv: 1603.05598 [hep-ex].

[88] M. Cacciari, G. P. Salam and G. Soyez, *The anti-*k_t *jet clustering algorithm*, JHEP **04** (2008) 063, arXiv: 0802.1189 [hep-ph].

[89] ATLAS Collaboration, *Monte Carlo Calibration and Combination of In-situ Measurements of Jet Energy Scale, Jet Energy Resolution and Jet Mass in ATLAS*, ATLAS-CONF-2015-037, 2015, URL: https://cds.cern.ch/record/2044941 (visited on 07/08/2019).

[90] ATLAS Collaboration, *Jet Calibration and Systematic Uncertainties for Jets Reconstructed in the ATLAS Detector at* $\sqrt{s} = 13$ *TeV*, ATL-PHYS-PUB-2015-015, 2015, URL: https://cds.cern.ch/record/2037613 (visited on 07/08/2019).

[91] ATLAS Collaboration, *Performance of pile-up mitigation techniques for jets in pp collisions at* $\sqrt{s} = 8$ *TeV using the ATLAS detector*, Eur. Phys. J. C **76** (2016) 581, arXiv: 1510.03823 [hep-ex].

[92] G. Aad et al., *ATLAS b-jet identification performance and efficiency measurement with $t\bar{t}$ events in pp collisions at $\sqrt{s} = 13$ TeV*, (2019), arXiv: 1907.05120 [hep-ex].

[93] ATLAS Collaboration, *Measurements of b-jet tagging efficiency with the ATLAS detector using $t\bar{t}$ events at $\sqrt{s} = 13$ TeV*, JHEP **08** (2018) 089, arXiv: 1805.01845 [hep-ex].

[94] LHC Top Working Group, *ParticleLevelTopDefinitions*, URL: https://twiki.cern.ch/twiki/bin/view/LHCPhysics/ParticleLevelTopDefinitions (visited on 07/08/2019).

[95] ATLAS Collaboration, *Further studies on simulation of top-quark production for the ATLAS experiment at $\sqrt{s} = 13$ TeV*, ATL-PHYS-PUB-2016-016, 2016, URL: https://cds.cern.ch/record/2205262 (visited on 14/09/2019).

[96] A. V. Lipatov, G. I. Lykasov, M. A. Malyshev, A. A. Prokhorov and S. M. Turchikhin, *Hard production of a Z boson plus heavy flavor jets at LHC and the intrinsic charm content of a proton*, Phys. Rev. **D97** (2018) 114019, arXiv: 1802.05085 [hep-ph].

[97] ATLAS Collaboration, *Measurement of the top quark branching ratios into channels with leptons and quarks with the ATLAS detector*, Phys. Rev. D **92** (2015) 072005, arXiv: 1506.05074 [hep-ex].

[98] R. Brun and F. Rademakers, *ROOT: An object oriented data analysis framework*, Nucl. Instrum. Meth. **A389** (1997) 81.

[99] *2012 Review of Particle Physics - W boson*, URL: http://pdg.lbl.gov/2012/listings/rpp2012-list-w-boson.pdf (visited on 06/09/2019).

[100] S. Camarda, J. Cuth and M. Schott, *Determination of the muonic branching ratio of the W boson and its total width via cross-section measurements at the Tevatron and LHC*, Eur. Phys. J. **C76** (2016) 613, arXiv: 1607.05084 [hep-ex].

[101] R. Barlow, *Application of the Bootstrap resampling technique to Particle Physics experiments*, MAN/HEP/99/4 (2000), URL: http://www.hep.manchester.ac.uk/preprints/manhep99-4.ps (visited on 07/08/2019).

[102] R. Barlow, *SLUO Lectures on Statistical and Numerical Methods in HEP. Lecture 6: Resampling and the Bootstrap*, URL: https://www-group.slac.stanford.edu/sluo/Lectures/stat_lecture_files/sluolec6.pdf (visited on 06/09/2019).

[103] ATLAS Collaboration, *Electron identification measurements in ATLAS using $\sqrt{s} = 13$ TeV data with 50 ns bunch spacing*, ATL-PHYS-PUB-2015-041, 2015, URL: https://cds.cern.ch/record/2048202 (visited on 14/09/2019).

[104] ATLAS Collaboration,
Jet energy scale measurements and their systematic uncertainties in proton–proton collisions at $\sqrt{s} = 13$ *TeV with the ATLAS detector*, Phys. Rev. D **96** (2017) 072002, arXiv: 1703.09665 [hep-ex].

[105] ATLAS Collaboration,
Studies on top-quark Monte Carlo modelling for Top2016, ATL-PHYS-PUB-2016-020, 2016, URL: https://cds.cern.ch/record/2216168 (visited on 14/09/2019).

[106] M. Czakon et al.,
Top-pair production at the LHC through NNLO QCD and NLO EW, JHEP **10** (2017) 186, arXiv: 1705.04105 [hep-ph].

[107] J. Butterworth et al., *PDF4LHC recommendations for LHC Run II*, J. Phys. **G43** (2016) 023001, arXiv: 1510.03865 [hep-ph].

[108] N. Kidonakis, *Two-loop soft anomalous dimensions for single top quark associated production with a W- or H-*, Phys. Rev. **D82** (2010) 054018, arXiv: 1005.4451 [hep-ph].

[109] ATLAS Collaboration, *Single Boson and Diboson Production Cross Sections in pp collisions at* $\sqrt{s} = 7$ *TeV*, (2010), URL: https://cds.cern.ch/record/1287902 (visited on 07/08/2019).

[110] R. Hawkings, *Measurement of the* $t\bar{t}$ *production cross-section and lepton differential distributions in pp collisions at* $\sqrt{s} = 13$ *TeV with 2015-16 ATLAS data*, tech. rep. ATL-COM-PHYS-2018-1163, CERN, 2018, URL: https://cds.cern.ch/record/2634819 (visited on 07/08/2019).

[111] O. Bessidskaia Bylund et al., *Measurement of the* $t\bar{t}Z$ *and* $t\bar{t}W$ *production cross sections in multilepton final states using* 36 fb^{-1} *of pp collisions at 13 TeV at the LHC*, (2016), URL: https://cds.cern.ch/record/2235582 (visited on 07/08/2019).

[112] G. Avoni et al., *The new LUCID-2 detector for luminosity measurement and monitoring in ATLAS*, JINST **13** (2018) P07017.

[113] E. Todesco and J. Wenninger,
Large Hadron Collider momentum calibration and accuracy, Phys. Rev. Accel. Beams **20** (2017) 081003.

[114] A. Buckley et al.,
LHAPDF6: parton density access in the LHC precision era, Eur. Phys. J. **C75** (2015) 132, arXiv: 1412.7420 [hep-ph].

[115] ATLAS Collaboration, *Probing the quantum interference between singly and doubly resonant top-quark production in pp collisions at* $\sqrt{s} = 13$ *TeV with the ATLAS detector*, Phys. Rev. Lett. **121** (2018) 152002, arXiv: 1806.04667 [hep-ex].

[116] *Progress in* $t\bar{t}$ *modelling and tuning*,
URL: https://indico.cern.ch/event/795477/contributions/3378784/attachments/1848561/3033832/MCandTuning_AndreaKnue_22052019.pdf (visited on 30/08/2019).

[117] L. Lyons, D. Gibaut and P. Clifford,
How to Combine Correlated Estimates of a Single Physical Quantity,
Nucl. Instrum. Meth. **A270** (1988) 110.

[118] CMS Collaboration,
Measurements of $\mathrm{t\bar{t}}$ *differential cross sections in proton-proton collisions at* $\sqrt{s} =$ *13 TeV using events containing two leptons*,
JHEP **02** (2019) 149, arXiv: 1811.06625 [hep-ex].

[119] ATLAS Collaboration,
Measurement of the top quark mass in the $t\bar{t} \rightarrow$ *lepton+jets channel from* $\sqrt{s} = 8$ *TeV ATLAS data and combination with previous results*,
Eur. Phys. J. **C79** (2019) 290, arXiv: 1810.01772 [hep-ex].

[120] *2019 Review of Particle Physics - Quarks*,
URL: http://pdg.lbl.gov/2019/tables/rpp2019-sum-quarks.pdf
(visited on 07/08/2019).

LIST OF FIGURES

LIST OF TABLES

APPENDIX

A Detailed list of samples and metadata

Table 1: List of DSID for the TOPQ1 Monte Carlo samples and their cross section σ, k-factor and filter efficiency.

DSID	σ [nb]	k-factor	filter efficiency
410472	0.72977	1.1398	0.10546
410470	7.2977	1.1398	0.54384
410482	0.72974	1.1398	0.10546
410465	0.71204	1.1681	0.10718
410252	0.076277	1.1484	1
410558	0.73015	1.1391	0.10544
411052	0.08464	1.1407	1
411053	0.080106	1.1404	1
411054	0.077947	1.1402	1
411055	0.077418	1.1401	1
411056	0.076373	1.1401	1
411057	0.075857	1.14	1
411058	0.073831	1.1399	1
411059	0.069969	1.1395	1
410648	0.003997	0.9451	1
410649	0.003994	0.9458	1
410646	0.037936	0.945	1
410647	0.037905	0.9457	1
410656	0.0038902	0.9704	1
410657	0.0039665	0.9493	1
410658	0.036996	1.1935	1
410659	0.022175	1.1849	1
411038	0.0039993	0.9446	1
411039	0.003996	0.9453	1
412003	0.007903	0.9559	1
411107	0.04005	0.9457	1
411108	0.040018	0.9457	1
411109	0.038823	0.9455	1
411110	0.038793	0.9455	1
411111	0.038229	0.9454	1
411112	0.038198	0.9454	1
411113	0.038082	0.9454	1
411114	0.038051	0.9454	1
411115	0.037789	0.9453	1
411116	0.03776	0.9453	1
411117	0.037646	0.9453	1
411118	0.037615	0.9453	1
411119	0.037072	0.9452	1
411120	0.037043	0.9452	1
411121	0.03596	0.9450	1
411122			

DSID	σ [nb]	k-factor	filter efficiency
410155	0.00054822	1.096	1
410156	0.00015503	1.11	1
410157	0.00052821	1.11	1
410218	3.6864e-05	1.12	1
410219	3.6865e-05	1.12	1
410220	3.6555e-05	1.12	1
345940	5.1156e-05	1.1	1
364250	0.001252	1	1
364253	0.0045765	1	1
364254	0.012501	1	1
364255	0.0032344	1	1
364283	1.0545e-05	1	1
364284	4.7168e-05	1	1
364285	0.00011629	1	1
364287	4.0847e-05	1	1
364288	0.0014484	1	1
364289	0.0029708	1	1
364290	0.00017238	1	1
345705	9.9577e-06	1	1
345706	1.0163e-05	1	1
345723	7.1055e-06	1	1
363355	0.015560	1	0.27686
363356	0.015563	1	0.14135
363357	0.0067951	1	1
363358	0.0034328	1	1
363359	0.024707	1	1
363360	0.024726	1	1
363389	0.011419	1	1
363394	0.0012561	1	1

Table 2: List of DSID for the TOPQ1 Monte Carlo samples and their cross section σ, k-factor and filter efficiency.

DSID	σ [nb]	k-factor	filter efficiency
364156	19.149	0.9702	0.8245
364157	19.142	0.9702	0.13091
364158	19.138	0.9702	0.044641
364159	0.94552	0.9702	0.6743
364160	0.94544	0.9702	0.24335
364161	0.94414	0.9702	0.084708
364162	0.3397	0.9702	0.60292
364163	0.33988	0.9702	0.29253
364164	0.33964	0.9702	0.110298
364165	0.072079	0.9702	0.54768
364166	0.0721	0.9702	0.32016
364167	0.072058	0.9702	0.12542
364168	0.015006	0.9702	1
364169	0.0012348	0.9702	1
364170	19.153	0.9702	0.82467
364171	19.145	0.9702	0.13086
364172	19.138	0.9702	0.04482
364173	0.94498	0.9702	0.67483
364174	0.94574	0.9702	0.24413
364175	0.94579	0.9702	0.10341
364176	0.33967	0.9702	0.59875
364177	0.33987	0.9702	0.28876
364178	0.33964	0.9702	0.10898
364179	0.072074	0.9702	0.5483
364180	0.072105	0.9702	0.31969
364181	0.072091	0.9702	0.13706
364182	0.015047	0.9702	1
364183	0.0012344	0.9702	1
364184	19.155	0.9702	0.82462
364185	19.149	0.9702	0.13152
364186	19.148	0.9702	0.045111
364187	0.94502	0.9702	0.67562
364188	0.94623	0.9702	0.24247
364189	0.94571	0.9702	0.10391
364190	0.33978	0.9702	0.59872
364191	0.33966	0.9702	0.28477
364192	0.33935	0.9702	0.10599
364193	0.072091	0.9702	0.54837
364194	0.071994	0.9702	0.31881
364195	0.071945	0.9702	0.13597
364196	0.015052	0.9702	1
364197	0.0012341	0.9702	1

DSID	σ [nb]	k-factor	filter efficiency
364100	1.9824	0.9751	0.82175
364101	1.9821	0.9751	0.11358
364102	1.9815	0.9751	0.065797
364103	0.10913	0.9751	0.68948
364104	0.10881	0.9751	0.19704
364105	0.10898	0.9751	0.11768
364106	0.039873	0.9751	0.60281
364107	0.03986	0.9751	0.23529
364108	0.039891	0.9751	0.15623
364109	0.0085256	0.9751	0.56023
364110	0.0085259	0.9751	0.26641
364111	0.0085274	0.9751	0.17659
364112	0.0017871	0.9751	1
364113	0.0001476	0.9751	1
364114	1.9816	0.9751	0.82133
364115	1.9815	0.9751	0.11386
364116	1.9821	0.9751	0.065754
364117	0.11065	0.9751	0.69423
364118	0.1105	0.9751	0.18855
364119	0.11046	0.9751	0.11827
364120	0.040679	0.9751	0.61619
364121	0.040671	0.9751	0.23293
364122	0.040674	0.9751	0.15333
364123	0.0086701	0.9751	0.56739
364124	0.0086689	0.9751	0.26608
364125	0.0086806	0.9751	0.17629
364126	0.0018092	0.9751	1
364127	0.00014875	0.9751	1
364128	1.9817	0.9751	0.83449
364129	1.9817	0.9751	0.10956
364130	1.9821	0.9751	0.065757
364131	0.11061	0.9751	0.69266
364132	0.11056	0.9751	0.19023
364133	0.11066	0.9751	0.110886
364134	0.040771	0.9751	0.61809
364135	0.040716	0.9751	0.23429
364136	0.040741	0.9751	0.15589
364137	0.0086639	0.9751	0.5634
364138	0.008676	0.9751	0.26433
364139	0.0086795	0.9751	0.17627
364140	0.0018075	0.9751	1
364141	0.00014826	0.9751	1
364198	2.4143	0.9751	0.96536
364199	2.4144	0.9751	0.0344249
364200	0.0503299	0.9751	0.89308
364201	0.050291	0.9751	0.11212
364202	0.0032396	0.9751	0.853639
364203	0.0032814	0.9751	0.1602
364204	2.4153	0.9751	0.965199
364205	2.4155	0.9751	0.0346949
364206	0.050354	0.9751	0.89325
364207	0.050483	0.9751	0.1087
364208	0.0032539	0.9751	0.85487
364209	0.0032524	0.9751	0.15349
364210	2.4159	0.9751	0.96534
364211	2.4144	0.9751	0.034669
364212	0.050373	0.9751	0.893129
364213	0.050470	0.9751	0.10985
364214	0.003285	0.9751	0.85551
364215	0.0032803	0.9751	0.15623
361106	1.8942	1.0260	1
361107	1.8909	1.0261	1
361108	1.9011	1.0261	1

B b-tagging efficiency

The b-tagging efficiency is fitted in the double tagging equation together with the cross section and the values extracted are shown here in Fig. 1 for the b-tagging efficiency from the total event count, see Eq. 7.5 and in Fig. 2 for the b-tagging efficiency for the differential distributions, see Eq. 7.15. The errorbars in the plots reflect the uncertainty on the b-tagging efficiency from the fit. No statistical or systematic analysis is performed on the extracted values.

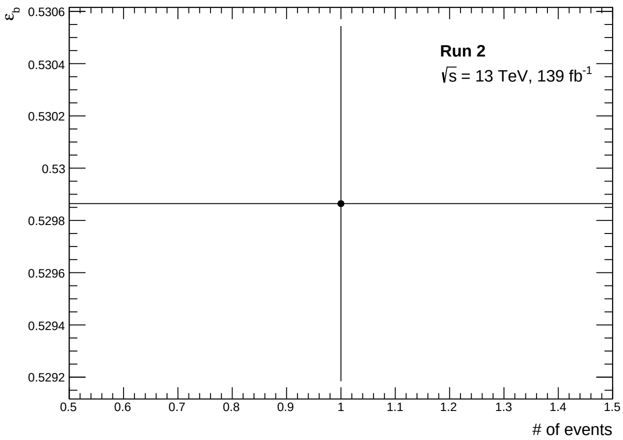

Figure 1: b-tagging efficiency for the total event count from the fit of Eq. 7.5 with the nominal reconstruction efficiency and b-tagging correlation coefficient from dilepton POWHEG + PYTHIA 8 sample and the nominal background. The errorbars reflect the error on the b-tagging efficiency from the fit.

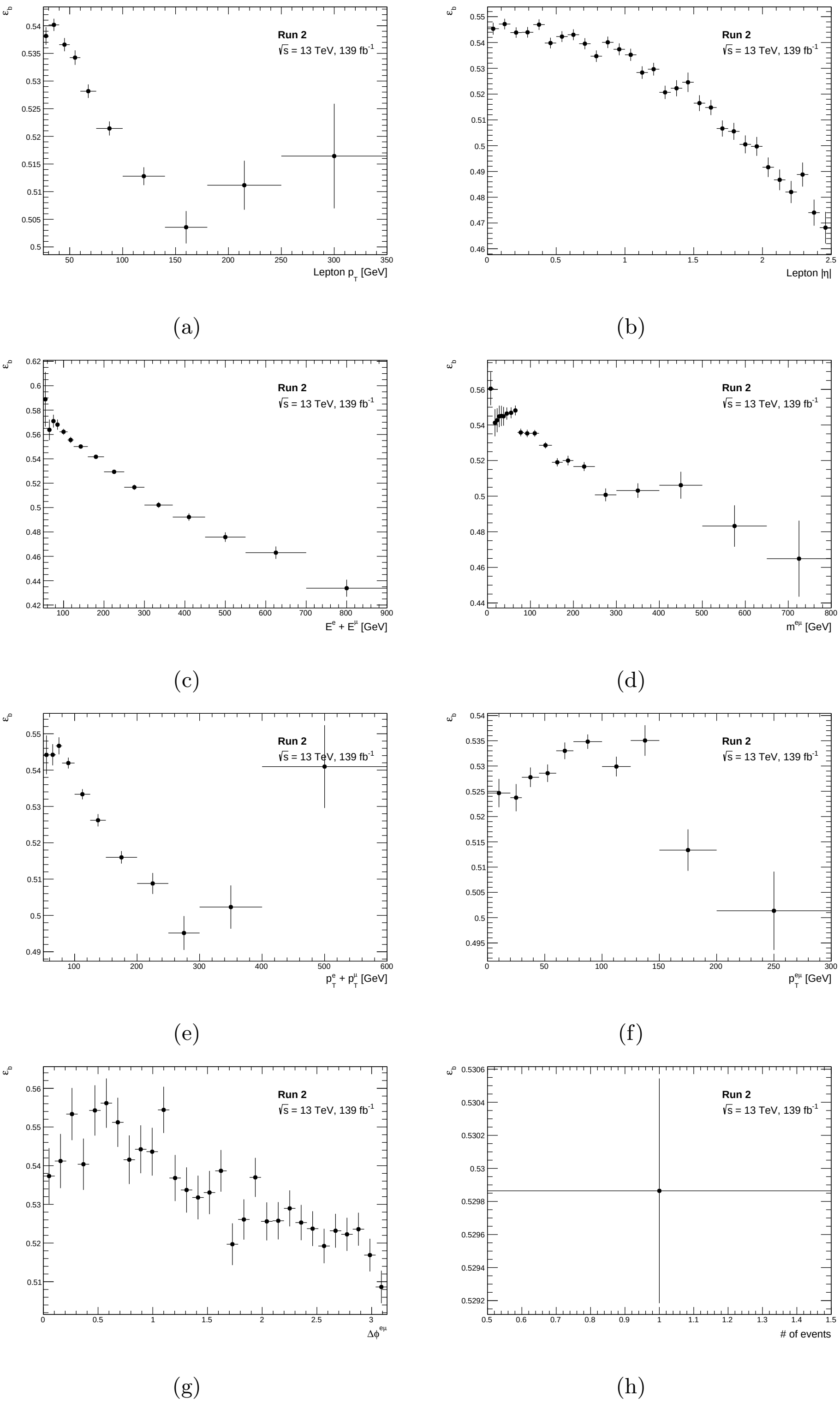

Figure 2: b-tagging efficiency for each bin of each distributions from the fit of Eq. 7.15 with the nominal reconstruction efficiency and b-tagging correlation coefficieny from dilepton POWHEG + PYTHIA 8 sample and the nominal background. The errorbars reflect the error on the b-tagging efficiency from the fit.

C Validation tests for normalised differential cross section distributions

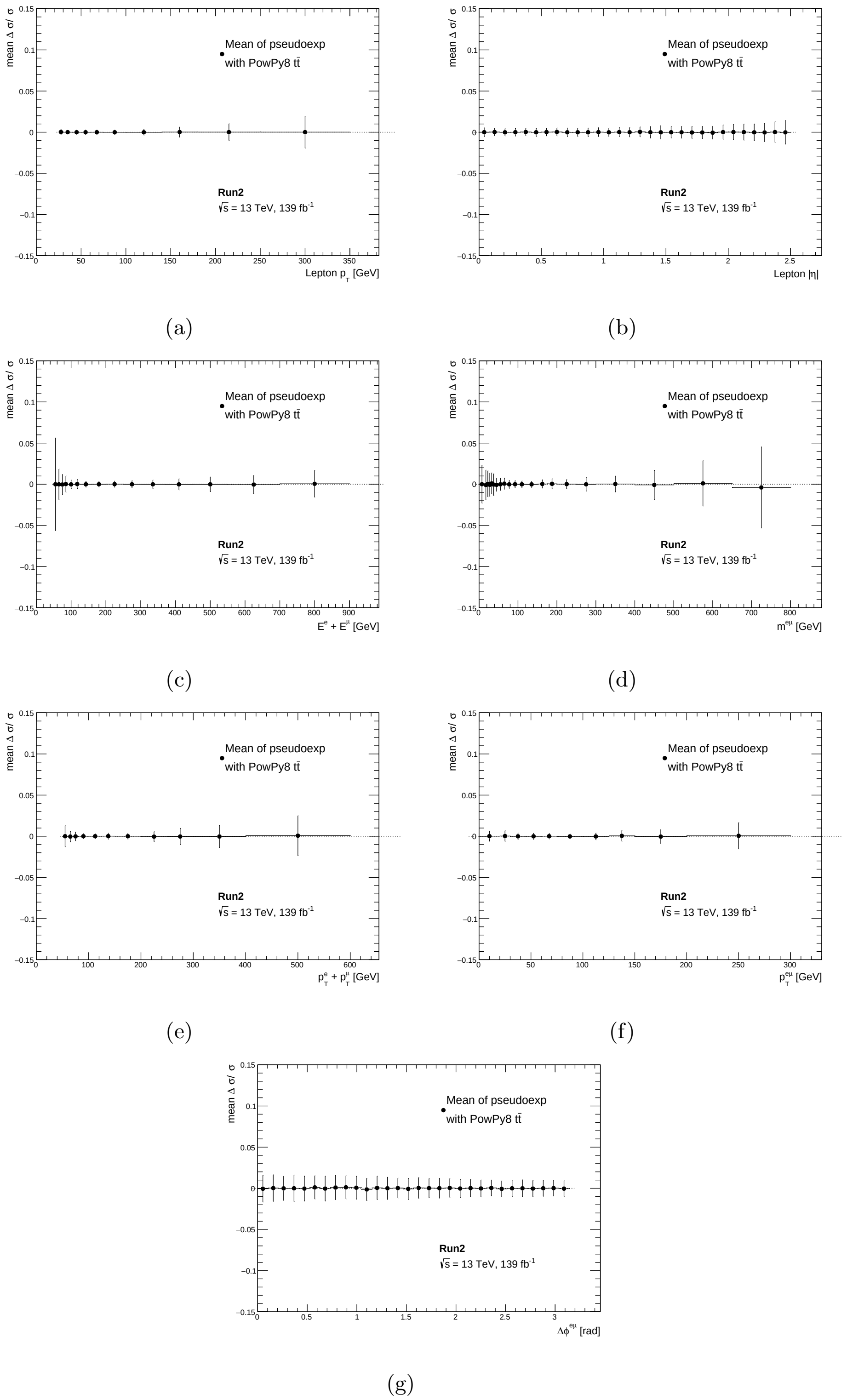

Figure 3: Mean and standard deviations extracted from the gaussian functions fitted to the 1000 internal bias tests pseudo-experiments results for each bin in each normalised distribution. The mean is in all cases consistent with zero within the standard deviation, demonstrating that the double tagging technique has no internal bias.

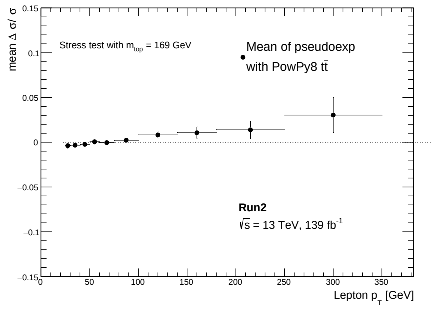

(a)

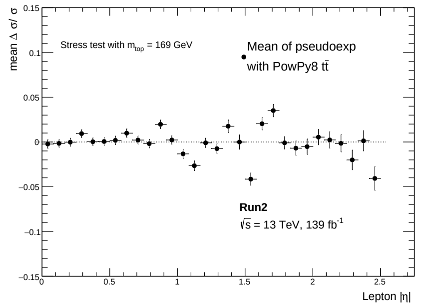

(b)

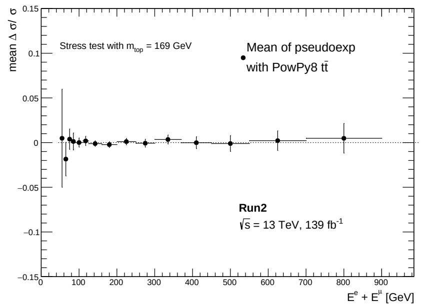

(c)

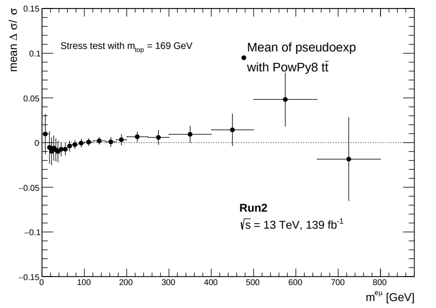

(d)

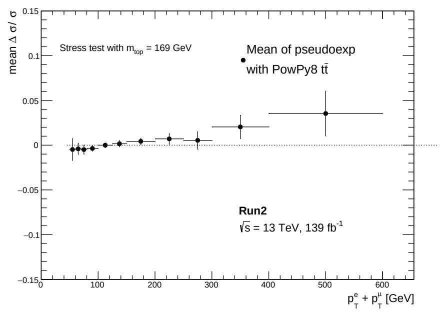

(e)

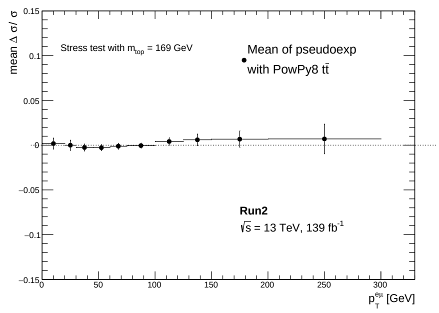

(f)

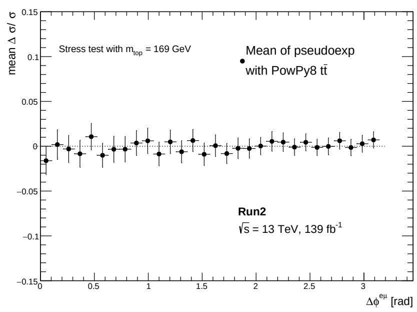

(g)

Figure 4: Mean and standard deviations extracted from the gaussian functions fitted to the 1000 pseudo-experiments results for each bin in each normalised distribution using the $t\bar{t}$ POWHEG + PYTHIA 8 sample with $m_{\text{top}} = 169$ GeV as signal sample

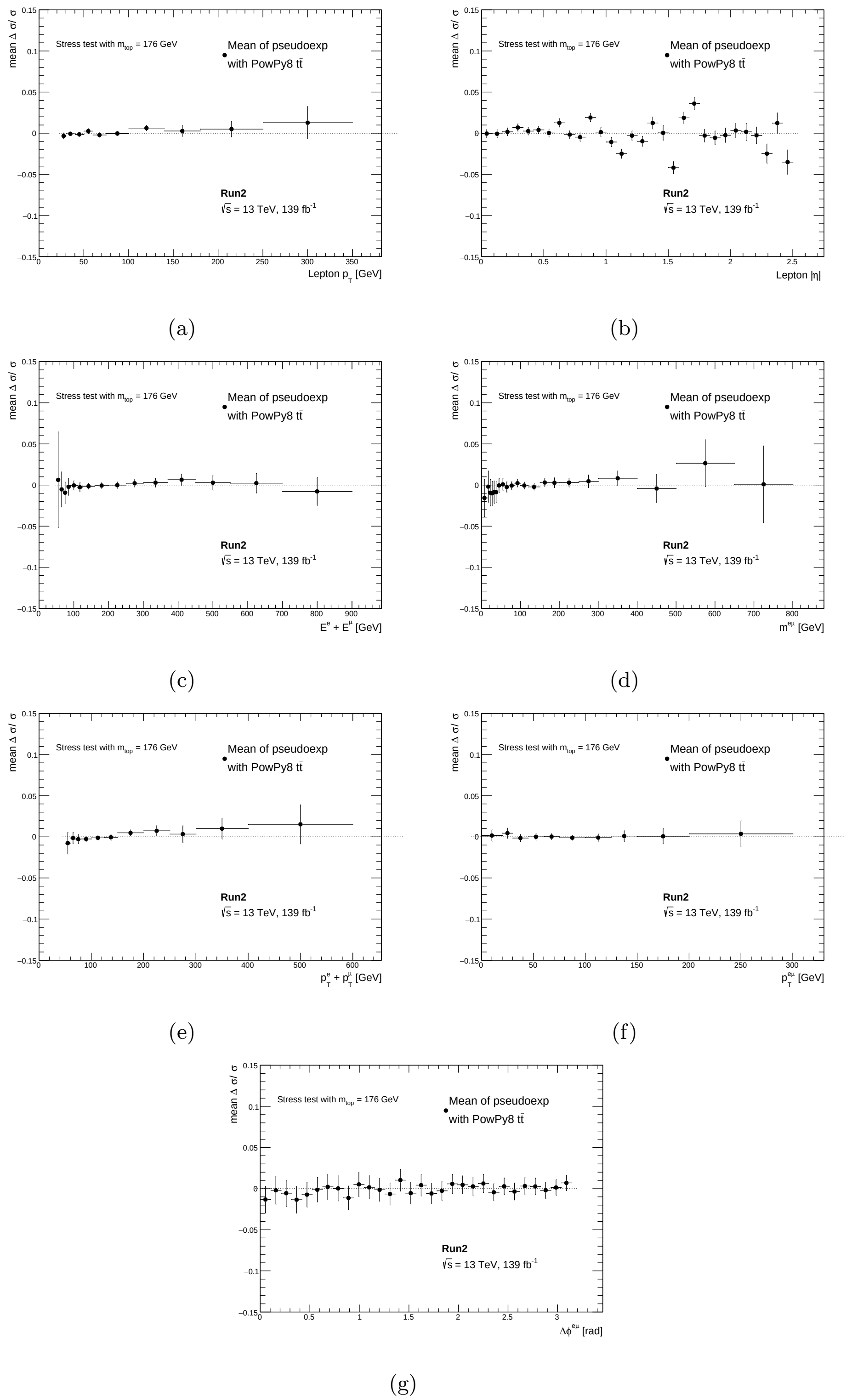

Figure 5: Mean and standard deviations extracted from the gaussian functions fitted to the 1000 pseudo-experiments results for each bin in each normalised distribution using the $t\bar{t}$ Powheg + Pythia 8 sample with $m_{\text{top}} = 176$ GeV as signal sample

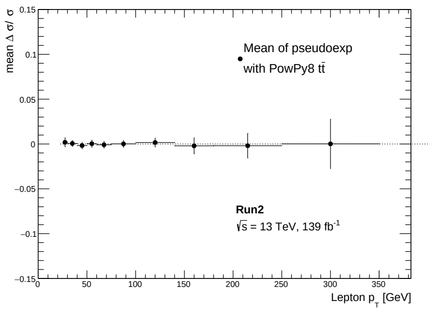

(a)

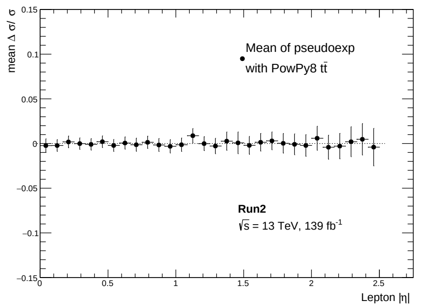

(b)

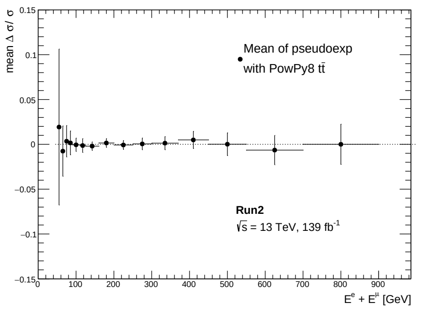

(c)

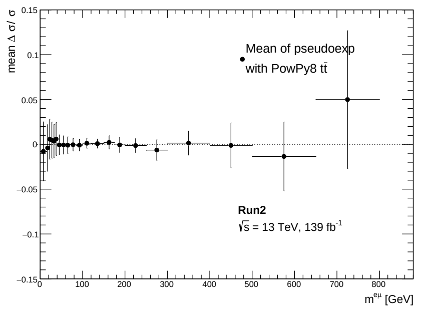

(d)

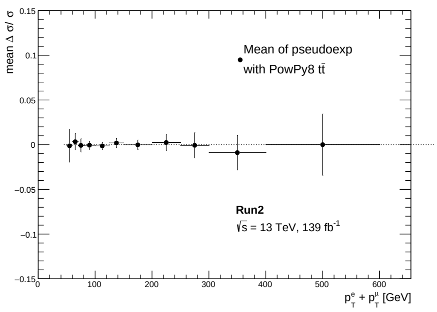

(e)

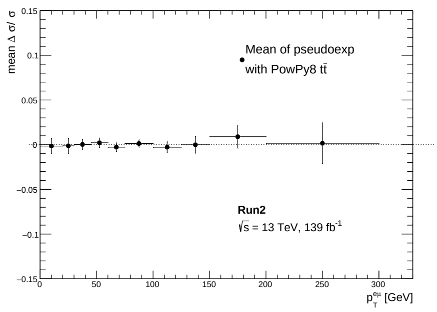

(f)

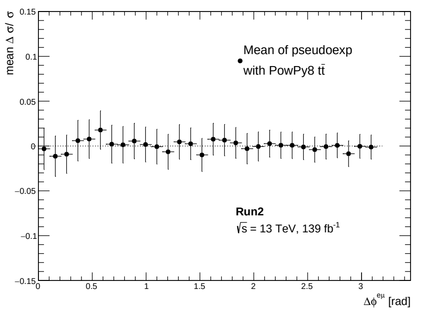

(g)

Figure 6: Mean and standard deviations extracted from the gaussian functions fitted to the 1000 pseudo-experiments results for each bin in each normalised distribution performed on a subpart of the total $t\bar{t}$ sample for closure tests. The mean is in all cases consistent with zero within the standard deviation, demonstrating that the double tagging technique works.

D Components of all detector uncertainties

Table 3: All contributions to detector uncertainties

Uncertainty type	Type	Contributions
Electron scale and resolution	Up/Down	EG_RESOLUTION_ALL, EG_SCALE_ALL, EG_SCALE_AF2
Electron efficiency	Up/Down	weight_leptonSF_EL_SF_Trigger, weight_leptonSF_EL_SF_Reco, weight_leptonSF_EL_SF_ID, weight_leptonSF_EL_SF_Isol
Muon scale and resolution scale	Up/Down	MUON_ID, MUON_MS, MUON_SAGITTA_RESBIAS, MUON_SAGITTA_RHO, MUON_SCALE
Muon reconstruction efficiency	Up/Down	weight_leptonSF_MU_SF_ID_STAT, weight_leptonSF_MU_SF_ID_SYST, weight_leptonSF_MU_SF_ID_STAT_LOWPT, weight_leptonSF_MU_SF_ID_SYST_LOWPT
Muon trigger, ISO, TTVA efficiency	Up/Down	weight_leptonSF_MU_SF_Trigger_STAT, weight_leptonSF_MU_SF_Trigger_SYST, weight_leptonSF_MU_SF_Isol_STAT, weight_leptonSF_MU_SF_Isol_SYST, weight_leptonSF_MU_SF_TTVA_STAT, weight_leptonSF_MU_SF_TTVA_SYST
JVT	Up/Down	weight_jvt, weight_jvt
JES b-jes response	Up/Down	JET_CategoryReduction_JET_BJES_Response
JES effective NPs	Up/Down	JET_CategoryReduction_JET_EffectiveNP_Detector1, JET_CategoryReduction_JET_EffectiveNP_Detector2, JET_CategoryReduction_JET_EffectiveNP_Mixed1, JET_CategoryReduction_JET_EffectiveNP_Mixed2, JET_CategoryReduction_JET_EffectiveNP_Mixed3, JET_CategoryReduction_JET_EffectiveNP_Modelling1, JET_CategoryReduction_JET_EffectiveNP_Modelling2, JET_CategoryReduction_JET_EffectiveNP_Modelling3, JET_CategoryReduction_JET_EffectiveNP_Modelling4, JET_CategoryReduction_JET_EffectiveNP_Statistical1, JET_CategoryReduction_JET_EffectiveNP_Statistical2, JET_CategoryReduction_JET_EffectiveNP_Statistical3, JET_CategoryReduction_JET_EffectiveNP_Statistical4, JET_CategoryReduction_JET_EffectiveNP_Statistical5, JET_CategoryReduction_JET_EffectiveNP_Statistical6
JES EtaInterCalibration	Up/Down	JET_CategoryReduction_JET_EtaIntercalibration_Modelling, JET_CategoryReduction_JET_EtaIntercalibration_NonClosure_highE, JET_CategoryReduction_JET_EtaIntercalibration_NonClosure_negEta, JET_CategoryReduction_JET_EtaIntercalibration_NonClosure_posEta, JET_CategoryReduction_JET_EtaIntercalibration_TotalStat
JES flavour	Up/Down	JET_CategoryReduction_JET_Flavor_Composition, JET_CategoryReduction_JET_Flavor_Response
JES pileup	Up/Down	JET_CategoryReduction_JET_Pileup_OffsetMu, JET_CategoryReduction_JET_Pileup_OffsetNPV, JET_CategoryReduction_JET_Pileup_PtTerm, JET_CategoryReduction_JET_Pileup_RhoTopology
JES PunchThrough	Up/Down	JET_CategoryReduction_JET_PunchThrough_MC16
JES HighPt	Up/Down	JET_CategoryReduction_JET_SingleParticle_HighPt
MET soft term	Up/Down	MET_SoftTrk_ResoPara, MET_SoftTrk_ResoPerp, MET_SoftTrk
JER	Up/Down	JET_CategoryReduction_JET_JER_DataVsMC, JET_CategoryReduction_JET_JER_EffectiveNP_1, JET_CategoryReduction_JET_JER_EffectiveNP_2, JET_CategoryReduction_JET_JER_EffectiveNP_3, JET_CategoryReduction_JET_JER_EffectiveNP_4, JET_CategoryReduction_JET_JER_EffectiveNP_5, JET_CategoryReduction_JET_JER_EffectiveNP_6, JET_CategoryReduction_JET_JER_EffectiveNP_7restTerm
b-tagging	Up/Down	weight_bTagSF_MV2c10_70_eigenvars_B[0], weight_bTagSF_MV2c10_70_eigenvars_B[1], weight_bTagSF_MV2c10_70_eigenvars_B[2], weight_bTagSF_MV2c10_70_eigenvars_B[3], weight_bTagSF_MV2c10_70_eigenvars_B[4], weight_bTagSF_MV2c10_70_eigenvars_B[5], weight_bTagSF_MV2c10_70_eigenvars_B[6], weight_bTagSF_MV2c10_70_eigenvars_B[7], weight_bTagSF_MV2c10_70_eigenvars_B[8], weight_bTagSF_MV2c10_70_eigenvars_C[0], weight_bTagSF_MV2c10_70_eigenvars_C[1], weight_bTagSF_MV2c10_70_eigenvars_C[2], weight_bTagSF_MV2c10_70_eigenvars_C[3], weight_bTagSF_MV2c10_70_eigenvars_Light[0], weight_bTagSF_MV2c10_70_eigenvars_Light[1], weight_bTagSF_MV2c10_70_eigenvars_Light[2], weight_bTagSF_MV2c10_70_eigenvars_Light[3], weight_bTagSF_MV2c10_70_eigenvars_Light[4], weight_bTagSF_MV2c10_70_extrapolation, weight_bTagSF_MV2c10_70_extrapolation_from_charm
Pileup	Up/Down	weight_pileup

E Detailed tables of systematic uncertainties

In this section the detailed tables of all the uncertainties for the total and differential cross section are presented. The total uncertainty is not computed, as the alternative generator uncertainty with top p_{T} reweighting is added to the tables as well

Table 4: Detailed results of the systematic uncertainties for the total fiducial cross section.

Fiducial cross section [pb]	10.672
Data statistics %	0.1592
MC statistics %	0.1561
Fragmentation %	0.1370
Hard scattering %	0.4512
top pT %	0.2418
Top mass dependence %	0.0000
PDF %	0.0321
ISR %	0.2022
FSR %	0.2645
Electron scale %	0.1122
Electron resolution %	0.0075
Electron trigger efficiency %	0.0502
Electron reconstruction efficiency %	0.1520
Electron ISO efficiency %	0.1010
Electron ID efficiency %	0.3026
Muon scale %	0.0481
Muon resolution %	0.0030
Muon reconstruction efficiency %	0.2234
Muon trigger efficiency %	0.0504
Muon ISO efficiency %	0.2625
Muon TTVA efficiency %	0.0220
JVT %	0.0311
JES b-jes response %	0.0514
JES effective NPs %	0.0117
JES EtaInterCalibration %	0.0057
JES flavour %	0.0652
JES pileup %	0.0055
JES PunchThrough %	0.0000
JES HighPt %	0.0000
MET soft term %	0.0000
JER %	0.0000
b-tagging %	0.0791
Wt cross section %	0.5143
Wt/$t\bar{t}$ interference %	0.3774
Wt hard scattering %	0.2293
Wt fragmentation %	0.2514
Wt ISR %	0.0108
Wt FSR %	0.1272
Diboson cross section %	0.0215
Diboson scale %	0.0502
ttV background %	0.0317
Z modelling %	0.0457
Z factor %	0.0172
Fakes background %	0.3221
Pileup %	0.6888
Beam energy %	0.2300
Luminosity %	1.9018

Table 5: Detailed results of the systematic uncertainties for the total inclusive cross section.

Inclusive cross section [pb]	839.797
Data statistics %	0.1592
MC statistics %	0.1561
Fragmentation %	0.4145
Hard scattering %	1.6327
top pT %	0.6379
Top mass dependence %	0.0000
PDF %	0.4198
ISR %	0.4596
FSR %	0.3234
Electron scale %	0.1122
Electron resolution %	0.0075
Electron trigger efficiency %	0.0502
Electron reconstruction efficiency %	0.1520
Electron ISO efficiency %	0.1010
Electron ID efficiency %	0.3026
Muon scale %	0.0481
Muon resolution %	0.0030
Muon reconstruction efficiency %	0.2234
Muon trigger efficiency %	0.0504
Muon ISO efficiency %	0.2625
Muon TTVA efficiency %	0.0220
JVT %	0.0310
JES b-jes response %	0.0514
JES effective NPs %	0.0117
JES EtaInterCalibration %	0.0057
JES flavour %	0.0652
JES pileup %	0.0055
JES PunchThrough %	0.0000
JES HighPt %	0.0000
MET soft term %	0.0000
JER %	0.0000
b-tagging %	0.0791
Wt cross section %	0.5143
Wt/$t\bar{t}$ interference %	0.3774
Wt hard scattering %	0.2293
Wt fragmentation %	0.2514
Wt ISR %	0.0107
Wt FSR %	0.1272
Diboson cross section %	0.0215
Diboson scale %	0.0502
ttV background %	0.0317
Z modelling %	0.0457
Z factor %	0.0172
Fakes background %	0.3221
Pileup %	0.6888
Beam energy %	0.2300
Luminosity %	1.9018

Table 6: Differential absolute cross section for p_T (ℓ) with detailed systematic uncertainties.

p_T (ℓ) bins [GeV]	25.0-30.0	30.0-40.0	40.0-50.0	50.0-60.0	60.0-75.0	75.0-100.0	100.0-140.0	140.0-180.0	180.0 250.0	250.0 350.0
Cross section [fb/GeV]	468.7729	439.6238	361.9038	281.0505	200.1542	110.3798	42.3049	13.0857	3.2269	0.5156
Data statistics %	0.3900	0.2863	0.3114	0.3422	0.3014	0.3103	0.4107	0.7097	1.0307	2.3652
MC statistics %	0.1228	0.0878	0.0791	0.0837	0.0771	0.0829	0.1045	0.1943	0.3082	0.6999
Fragmentation %	0.9980	0.3481	0.4194	0.0073	0.0314	0.1472	0.7940	1.2142	1.2427	0.9014
Hard scattering %	1.3309	0.6522	0.2043	0.2746	0.4249	0.1373	0.9187	1.0611	2.8096	3.5126
top pT %	0.0702	0.0563	0.0659	0.0764	0.0949	0.0985	0.0946	0.0675	0.0891	0.1977
Top mass dependence %	0.0570	0.0396	0.0310	0.0132	0.0362	0.0315	0.0177	0.1534	0.1287	0.1604
PDF %	0.0344	0.0378	0.0419	0.0467	0.0505	0.0559	0.0638	0.0778	0.0921	0.0874
ISR %	0.1870	0.1791	0.1542	0.1387	0.1618	0.2655	0.2248	0.1494	0.0754	0.6469
FSR %	0.2291	0.3573	0.1791	0.2767	0.1073	0.2500	0.1608	0.7469	0.2737	0.4752
Electron scale %	0.0814	0.1072	0.0109	0.0682	0.0458	0.0703	0.4025	0.8408	1.2802	2.1122
Electron resolution %	0.0720	0.0050	0.0107	0.0111	0.0262	0.0102	0.0045	0.0178	0.0097	0.0661
Electron trigger efficiency %	0.0965	0.0518	0.0408	0.0416	0.0407	0.0481	0.0505	0.0507	0.0515	0.0566
Electron reconstruction efficiency %	0.2312	0.1363	0.1170	0.1273	0.1418	0.1660	0.1771	0.1822	0.1906	0.2157
Electron ISO efficiency %	0.1155	0.0910	0.0807	0.0832	0.0882	0.1097	0.1206	0.1790	0.2003	0.3337
Electron ID efficiency %	0.6186	0.3785	0.2818	0.3002	0.2962	0.3104	0.3554	0.4537	0.5367	2.4572
Muon scale %	0.0034	0.0105	0.0296	0.0425	0.0584	0.0686	0.1027	0.1129	0.1444	0.2147
Muon resolution %	0.0240	0.0115	0.0065	0.0080	0.0108	0.0112	0.0023	0.0171	0.0587	0.2436
Muon reconstruction efficiency %	0.2173	0.2198	0.2205	0.2214	0.2229	0.2252	0.2303	0.2384	0.2493	0.2906
Muon trigger efficiency %	0.1523	0.0613	0.0490	0.0435	0.0324	0.0299	0.0268	0.0238	0.0215	0.0208
Muon ISO efficiency %	0.2616	0.2744	0.2460	0.3261	0.2426	0.2437	0.2462	0.2520	0.2624	0.3018
Muon TTVA efficiency %	0.0305	0.0192	0.0204	0.0217	0.0218	0.0219	0.0222	0.0228	0.0238	0.0270
JVT %	0.0285	0.0291	0.0278	0.0279	0.0321	0.0327	0.0352	0.0385	0.0495	0.0926
JES b-jes response %	0.0585	0.0468	0.0457	0.0504	0.0473	0.0513	0.0616	0.0487	0.0536	0.0172
JES effective NPs %	0.0226	0.0229	0.0212	0.0284	0.0091	0.0065	0.0215	0.0347	0.0588	0.1058
JES EtaInterCalibration %	0.0262	0.0074	0.0044	0.0175	0.0047	0.0057	0.0064	0.0199	0.0076	0.0482
JES flavour %	0.0506	0.0362	0.0371	0.0351	0.0697	0.0865	0.1190	0.1501	0.2064	0.2755
JES pileup %	0.0661	0.0126	0.0117	0.0225	0.0094	0.0137	0.0344	0.0564	0.0774	0.1329
JES PunchThrough %	0.0000	0.0002	0.0000	0.0000	0.0001	0.0001	0.0001	0.0006	0.0003	0.0001
JES HighPt %	0.0000	0.0000	0.0000	0.0000	0.0000	0.0000	0.0000	0.0000	0.0000	0.0000
MET soft term %	0.0000	0.0000	0.0000	0.0000	0.0000	0.0000	0.0000	0.0000	0.0000	0.0000
JER %	0.0001	0.0000	0.0000	0.0000	0.0000	0.0000	0.0000	0.0000	0.0000	0.0000
b-tagging %	0.0810	0.0805	0.0812	0.0865	0.0828	0.0858	0.0813	0.1027	0.1281	0.2359
Wt cross section %	0.4750	0.4742	0.4800	0.4878	0.4913	0.5193	0.5878	0.7231	0.9471	1.7088
Wt/$t\bar{t}$ interference %	0.1695	0.0355	0.0686	0.1300	0.1419	0.4641	0.9453	1.8920	3.8905	12.2558
Wt hard scattering %	0.3033	0.2875	0.1526	0.1668	0.2279	0.3087	0.1811	0.0486	0.2039	0.3232
Wt fragmentation %	0.3653	0.2571	0.2937	0.2590	0.1502	0.2350	0.2005	0.3924	0.0020	0.4636
Wt ISR %	0.0561	0.0539	0.0530	0.0416	0.0172	0.0272	0.1380	0.2728	0.6606	2.5031
Wt FSR %	0.1193	0.0949	0.0574	0.1175	0.1802	0.1644	0.1831	0.0316	0.3481	0.1975
Diboson cross section %	0.0194	0.0193	0.0194	0.0188	0.0192	0.0213	0.0259	0.0367	0.0576	0.1441
Diboson scale %	0.0965	0.0518	0.0408	0.0416	0.0407	0.0481	0.0505	0.0507	0.0515	0.0566
ttV background %	0.0259	0.0262	0.0271	0.0279	0.0297	0.0336	0.0416	0.0556	0.0803	0.1536
Z modelling %	0.0426	0.0944	0.0565	0.0115	0.0669	0.0303	0.0214	0.0026	0.0731	0.0722
Z factor %	0.0476	0.0338	0.0182	0.0092	0.0083	0.0048	0.0044	0.0046	0.0037	0.0018
Fakes background %	0.3789	0.3258	0.3016	0.3132	0.3075	0.3172	0.3260	0.3914	0.4499	0.7359
Pileup %	1.0354	0.9187	0.8783	0.6883	0.5418	0.4769	0.4002	0.4134	0.2396	0.2231
Beam energy %	0.0015	0.0082	0.0021	0.0042	0.0036	0.0085	0.0054	0.0109	0.0121	0.0374
Luminosity %	1.9019	1.8934	1.8882	1.8886	1.8896	1.8992	1.9240	1.9760	2.0582	2.3448

Table 7: Differential absolute cross section for $|\eta(\ell)|$ with detailed systematic uncertainties.

$\lvert\eta(\ell)\rvert$ bins	0.0-0.08	0.08-0.17	0.17-0.25	0.25-0.33	0.33-0.42	0.42-0.50	0.50-0.58	0.58-0.67	0.67-0.75	0.75-0.83	0.83-0.92	0.92-1.00
Cross section [fb/unit $\lvert\eta\rvert$]	13010.73	12889.13	12935.14	12901.00	12522.43	12459.39	12129.02	11801.16	11601.87	11181.25	10873.55	10374.68
Data statistics %	0.3915	0.3381	0.3437	0.3437	0.3348	0.3260	0.3518	0.3395	0.3464	0.3746	0.3615	0.3803
MC statistics %	0.1469	0.1599	0.1377	0.1423	0.1316	0.1337	0.1270	0.1358	0.1446	0.1425	0.1382	0.1571
Fragmentation %	0.3613	0.2864	0.0128	0.7077	0.1815	0.1538	0.3174	1.2477	0.1749	0.9827	1.7435	0.3645
Hard scattering %	0.5622	0.6014	0.4341	0.6293	0.5978	0.0821	0.1220	0.8716	0.5195	1.1267	1.1686	0.1930
top pT %	0.2730	0.2755	0.2492	0.2530	0.2501	0.2462	0.2473	0.2295	0.2505	0.2605	0.2363	0.2528
Top mass dependence %	0.0229	0.0308	0.0578	0.0063	0.0300	0.0552	0.0206	0.0552	0.0098	0.0545	0.0290	0.0059
PDF %	0.0346	0.0296	0.0280	0.0265	0.0272	0.0276	0.0255	0.0225	0.0286	0.0301	0.0262	0.0266
ISR %	0.1725	0.2235	0.0385	0.3480	0.2686	0.2610	0.2927	0.2250	0.2424	0.0026	0.2205	0.2751
FSR %	0.5115	0.4219	0.3812	0.5184	0.3249	0.2345	0.5378	0.2456	0.1249	0.5558	0.1343	0.2812
Electron scale %	0.0651	0.0814	0.0798	0.0842	0.0784	0.0826	0.0776	0.0920	0.0888	0.0961	0.1004	0.0966
Electron resolution %	0.0114	0.0037	0.0007	0.0044	0.0125	0.0038	0.0053	0.0072	0.0003	0.0082	0.0105	0.0044
Electron trigger efficiency %	0.0730	0.0545	0.0391	0.0394	0.0430	0.0411	0.0369	0.0486	0.0646	0.0557	0.0476	0.0622
Electron reconstruction efficiency %	0.1784	0.1446	0.1351	0.1347	0.1345	0.1346	0.1358	0.1528	0.1574	0.1525	0.1462	0.1459
Electron ISO efficiency %	0.1295	0.0948	0.0850	0.0846	0.0845	0.0845	0.0853	0.1007	0.1055	0.1011	0.0948	0.0943
Electron ID efficiency %	0.3243	0.2886	0.2828	0.2831	0.2830	0.2834	0.2839	0.2742	0.2730	0.2749	0.2789	0.2769
Muon scale %	0.0365	0.0337	0.0390	0.0395	0.0378	0.0393	0.0376	0.0390	0.0333	0.0399	0.0508	0.0496
Muon resolution %	0.0134	0.0078	0.0068	0.0061	0.0030	0.0041	0.0155	0.0052	0.0051	0.0094	0.0080	0.0069
Muon reconstruction efficiency %	0.5292	0.3362	0.2141	0.2148	0.2122	0.2027	0.2031	0.2029	0.2059	0.2070	0.2060	0.2073
Muon trigger efficiency %	0.0394	0.0415	0.0437	0.0439	0.0432	0.0439	0.0451	0.0468	0.0453	0.0457	0.0488	0.0447
Muon ISO efficiency %	0.2616	0.2622	0.2621	0.2618	0.2621	0.2621	0.2622	0.2626	0.2623	0.2626	0.2625	0.2628
Muon TTVA efficiency %	0.0257	0.0268	0.0240	0.0221	0.0220	0.0217	0.0217	0.0216	0.0215	0.0215	0.0214	0.0214
JVT %	0.0281	0.0336	0.0321	0.0320	0.0258	0.0289	0.0284	0.0295	0.0287	0.0324	0.0290	0.0285
JES b-jes response %	0.0468	0.0507	0.0433	0.0518	0.0501	0.0513	0.0555	0.0610	0.0786	0.0510	0.0593	0.0502
JES effective NPs %	0.0180	0.0136	0.0092	0.0074	0.0067	0.0085	0.0064	0.0136	0.0315	0.0203	0.0177	0.0083
JES EtaInterCalibration %	0.0204	0.0119	0.0087	0.0176	0.0086	0.0151	0.0138	0.0088	0.0261	0.0324	0.0100	0.0057
JES flavour %	0.0594	0.0674	0.0666	0.0684	0.0724	0.0774	0.0675	0.0733	0.0658	0.0959	0.0553	0.0621
JES pileup %	0.0093	0.0045	0.0090	0.0054	0.0114	0.0171	0.0122	0.0086	0.0207	0.0511	0.0086	0.0064
JES PunchThrough %	0.0000	0.0002	0.0001	0.0002	0.0002	0.0001	0.0002	0.0002	0.0002	0.0002	0.0000	0.0001
JES HighPt %	0.0000	0.0000	0.0000	0.0000	0.0000	0.0000	0.0000	0.0000	0.0000	0.0000	0.0000	0.0000
MET soft term %	0.0000	0.0000	0.0000	0.0000	0.0000	0.0000	0.0000	0.0000	0.0000	0.0000	0.0000	0.0000
JER %	0.0000	0.0000	0.0000	0.0000	0.0001	0.0001	0.0000	0.0001	0.0000	0.0000	0.0000	0.0000
b-tagging %	0.0882	0.0891	0.1057	0.0824	0.0864	0.0965	0.0884	0.0830	0.0827	0.0928	0.0883	0.0761
Wt cross section %	0.5244	0.5361	0.5305	0.5237	0.5294	0.5272	0.5253	0.5280	0.5270	0.5264	0.5216	0.5186
Wt/$t\bar{t}$ interference %	0.2026	0.4013	0.3902	0.3666	0.3170	0.2753	0.4100	0.3850	0.4965	0.4066	0.5617	0.1922
Wt hard scattering %	0.0478	0.2575	0.1496	0.2098	0.2115	0.1276	0.0707	0.0835	0.2779	0.2138	0.0885	0.1051
Wt fragmentation %	0.1533	0.3391	0.3547	0.2134	0.2554	0.2203	0.2130	0.0915	0.3299	0.3213	0.1204	0.1497
Wt ISR %	0.0214	0.0023	0.0030	0.0108	0.0038	0.0057	0.0206	0.0230	0.0156	0.0053	0.0261	0.0327
Wt FSR %	0.1183	0.0551	0.1246	0.1836	0.1177	0.1518	0.1378	0.0606	0.0156	0.0843	0.0598	0.1367
Diboson cross section %	0.0180	0.0175	0.0178	0.0178	0.0194	0.0182	0.0192	0.0187	0.0200	0.0201	0.0200	0.0207
Diboson scale %	0.0730	0.0545	0.0391	0.0394	0.0430	0.0411	0.0369	0.0486	0.0646	0.0557	0.0476	0.0622
ttV background %	0.0312	0.0314	0.0308	0.0306	0.0308	0.0305	0.0309	0.0312	0.0310	0.0320	0.0316	0.0313
Z modelling %	0.0149	0.0451	0.0067	0.0129	0.0120	0.0764	0.0397	0.1614	0.0568	0.0215	0.0161	0.0393
Z factor %	0.0139	0.0175	0.0123	0.0172	0.0143	0.0129	0.0152	0.0198	0.0160	0.0141	0.0131	0.0174
Fakes background %	0.2528	0.2375	0.2345	0.2482	0.2302	0.2291	0.2658	0.2484	0.2578	0.2524	0.2532	0.2928
Pileup %	0.7476	0.7086	0.6545	0.6667	0.7112	0.7193	0.7701	0.7288	0.6455	0.6748	0.6319	0.5645
Beam energy %	0.0100	0.0197	0.0155	0.0039	0.0139	0.0220	0.0188	0.0264	0.0100	0.0155	0.0025	0.0189
Luminosity %	1.8964	1.9010	1.8971	1.8975	1.8976	1.8961	1.8992	1.9004	1.8997	1.8986	1.8972	1.9005

$\lvert\eta(\ell)\rvert$ bins	1.00-1.08	1.08-1.17	1.17-1.25	1.25-1.33	1.33-1.42	1.42-1.50	1.50-1.58	1.58-1.67	1.67-1.75	1.75-1.83	1.83-1.92	1.92-2.00	2.00-2.08	2.08-2.17	2.17-2.25	2.25-2.33	2.33-2.42	2.45-2.50
Cross section [fb/unit $\lvert\eta\rvert$]	9937.86	9602.30	9249.35	8746.96	8306.37	7775.90	7296.28	6925.37	6357.71	5797.03	5427.31	4919.86	4662.30	4187.80	3721.92	3169.92	2876.46	2533.02
Data statistics %	0.3872	0.4027	0.4180	0.4251	0.4927	0.6024	0.4824	0.4697	0.4836	0.5320	0.5717	0.5872	0.6239	0.6439	0.7036	0.7888	0.8346	1.1204
MC statistics %	0.1679	0.1556	0.1568	0.1658	0.1945	0.2615	0.1945	0.1889	0.2230	0.2111	0.2220	0.2504	0.2487	0.2644	0.2719	0.3167	0.3356	0.4000
Fragmentation %	1.6660	3.0951	0.3948	1.2715	1.3674	0.4742	4.3655	1.8255	3.5882	0.8915	0.5413	0.1116	0.3121	0.4087	0.2881	1.3125	1.5671	4.2496
Hard scattering %	1.2543	3.4018	1.3177	1.3788	1.2157	0.8741	5.4809	2.1614	2.5602	0.4251	1.1064	0.0493	0.2844	1.6983	2.2530	1.3374	0.0367	4.6017
top pT %	0.2490	0.2384	0.2260	0.2342	0.2410	0.1987	0.2134	0.2199	0.2011	0.1798	0.1983	0.1865	0.1809	0.1782	0.1519	0.1579	0.1328	0.1918
Top mass dependence %	0.0316	0.0377	0.0065	0.0347	0.0254	0.0192	0.0356	0.0107	0.0248	0.0231	0.0222	0.0354	0.0192	0.0143	0.0184	0.0330	0.1319	0.0473
PDF %	0.0265	0.0255	0.0255	0.0276	0.0321	0.0634	0.0272	0.0287	0.0324	0.0333	0.0385	0.0454	0.0457	0.0503	0.0595	0.0677	0.0810	0.0538
ISR %	0.2868	0.2992	0.0132	0.0071	0.1939	0.1329	0.0378	0.6872	0.0096	0.1624	0.0422	0.0706	0.3715	0.1787	0.0426	0.0050	0.3449	0.0985
FSR %	0.1422	0.4599	0.1447	0.1450	0.2438	0.0243	0.7165	0.2145	0.1307	0.0687	0.0621	0.2345	0.0729	0.3836	0.1287	0.0162	0.2970	0.1493
Electron scale %	0.1066	0.1059	0.1414	0.1672	0.1363	0.1006	0.2085	0.2072	0.1836	0.1733	0.1316	0.1358	0.1436	0.1331	0.1397	0.1236	0.1928	0.3766
Electron resolution %	0.0099	0.0059	0.0046	0.0028	0.0183	0.0067	0.0092	0.0058	0.0093	0.0127	0.0113	0.0254	0.0151	0.0061	0.0140	0.0518	0.0409	0.0173
Electron trigger efficiency %	0.0564	0.0458	0.0415	0.0405	0.0390	0.0323	0.0471	0.0485	0.0461	0.0503	0.0592	0.0619	0.0540	0.0530	0.0532	0.0526	0.0878	0.1396
Electron reconstruction efficiency %	0.1457	0.1494	0.1593	0.1597	0.1567	0.1533	0.1685	0.1713	0.1710	0.1723	0.1753	0.1753	0.1618	0.1603	0.1605	0.1603	0.1759	0.1799
Electron ISO efficiency %	0.0946	0.0977	0.1087	0.1090	0.1055	0.1013	0.1085	0.1093	0.1089	0.1133	0.1261	0.1259	0.1147	0.1134	0.1131	0.1124	0.1503	0.1662
Electron ID efficiency %	0.2771	0.2853	0.3093	0.3095	0.3014	0.3081	0.4101	0.4411	0.4380	0.4416	0.4351	0.4377	0.5540	0.5828	0.5692	0.5584	0.6317	0.6622
Muon scale %	0.0526	0.0642	0.0565	0.0475	0.0406	0.0489	0.0653	0.0685	0.0590	0.0467	0.0507	0.0593	0.0611	0.0602	0.0650	0.0921	0.1308	0.1355
Muon resolution %	0.0093	0.0128	0.0131	0.0036	0.0060	0.0183	0.0027	0.0094	0.0111	0.0148	0.0106	0.0162	0.0050	0.0137	0.0176	0.0136	0.0329	0.0168
Muon reconstruction efficiency %	0.2133	0.2123	0.2113	0.2034	0.1750	0.1549	0.1813	0.1934	0.1945	0.1943	0.1934	0.1936	0.1967	0.1956	0.1965	0.1958	0.1956	0.1915
Muon trigger efficiency %	0.0459	0.0551	0.0566	0.0564	0.0566	0.0595	0.0611	0.0626	0.0636	0.0650	0.0654	0.0655	0.0639	0.0642	0.0653	0.0658	0.0712	0.0631
Muon ISO efficiency %	0.2633	0.2623	0.2622	0.2625	0.2622	0.2633	0.2631	0.2625	0.2631	0.2633	0.2621	0.2626	0.2625	0.2624	0.2632	0.2642	0.2645	0.2662
Muon TTVA efficiency %	0.0211	0.0210	0.0209	0.0209	0.0204	0.0195	0.0205	0.0210	0.0211	0.0213	0.0217	0.0217	0.0210	0.0210	0.0211	0.0226	0.0226	0.0230
JVT %	0.0328	0.0313	0.0339	0.0321	0.0307	0.0295	0.0325	0.0345	0.0291	0.0284	0.0367	0.0354	0.0250	0.0242	0.0356	0.0223	0.0337	0.0285
JES b-jes response %	0.0668	0.0468	0.0519	0.0403	0.0414	0.0582	0.0377	0.0289	0.0526	0.0631	0.0358	0.0305	0.0579	0.0257	0.0356	0.0309	0.0556	0.0951
JES effective NPs %	0.0144	0.0074	0.0092	0.0137	0.0501	0.0331	0.0100	0.0390	0.0220	0.0455	0.0105	0.0092	0.0432	0.0145	0.0112	0.0135	0.0798	0.0883
JES EtaInterCalibration %	0.0409	0.0121	0.0079	0.0182	0.0285	0.0071	0.0034	0.0285	0.0116	0.0028	0.0182	0.0212	0.0062	0.0200	0.0041	0.0032	0.0271	0.0523
JES flavour %	0.1134	0.0920	0.0862	0.0979	0.0298	0.0524	0.0521	0.0375	0.0455	0.0305	0.0403	0.0595	0.0372	0.0539	0.0511	0.0378	0.0100	0.0058
JES pileup %	0.0343	0.0154	0.0163	0.0275	0.0787	0.0101	0.0234	0.0627	0.0155	0.0346	0.0101	0.0115	0.0375	0.0232	0.0183	0.0134	0.0718	0.0743
JES PunchThrough %	0.0000	0.0001	0.0001	0.0002	0.0002	0.0002	0.0002	0.0000	0.0005	0.0001	0.0002	0.0002	0.0009	0.0000	0.0007	0.0005	0.0000	0.0009
JES HighPt %	0.0000	0.0000	0.0000	0.0000	0.0000	0.0000	0.0000	0.0000	0.0000	0.0000	0.0000	0.0000	0.0000	0.0000	0.0000	0.0000	0.0000	0.0000
MET soft term %	0.0000	0.0000	0.0000	0.0000	0.0000	0.0000	0.0000	0.0000	0.0000	0.0000	0.0000	0.0000	0.0000	0.0000	0.0000	0.0000	0.0000	0.0000
JER %	0.0000	0.0000	0.0001	0.0000	0.0001	0.0002	0.0000	0.0000	0.0001	0.0000	0.0000	0.0000	0.0000	0.0003	0.0000	0.0001	0.0000	0.0000
b-tagging %	0.0732	0.0827	0.0772	0.0799	0.0771	0.0758	0.0662	0.0674	0.0809	0.0669	0.0618	0.0598	0.0688	0.0664	0.0604	0.0635	0.0587	0.0855
Wt cross section %	0.5256	0.5117	0.5008	0.5107	0.4977	0.5027	0.5012	0.4853	0.4854	0.4954	0.4828	0.4813	0.4632	0.4706	0.4686	0.4792	0.4815	0.4766
Wt/$t\bar{t}$ interference %	0.4683	0.3251	0.2642	0.3477	0.3525	0.5415	0.4131	0.3751	0.3794	0.3614	0.5051	0.4403	0.3055	0.4940	0.3986	0.3750	0.2899	0.3321
Wt hard scattering %	0.5377	0.2577	0.1609	0.3335	0.2075	0.4798	0.7750	0.2994	0.4809	0.5304	0.2856	0.4281	0.2878	0.4669	0.0172	0.8655	0.7229	0.3915
Wt fragmentation %	0.5264	0.4402	0.1756	0.2604	0.0212	0.3781	0.6978	0.0079	0.1039	0.3413	0.2361	0.4043	0.2384	0.3792	0.1510	0.0986	0.0760	0.4757
Wt ISR %	0.0184	0.0520	0.0234	0.0140	0.0348	0.0062	0.0187	0.0254	0.0118	0.0014	0.0012	0.0440	0.0095	0.0331	0.0388	0.0456	0.0497	0.0018
Wt FSR %	0.1154	0.1726	0.2212	0.2022	0.0076	0.0925	0.1940	0.2356	0.1572	0.0920	0.0413	0.1997	0.1654	0.2710	0.2409	0.2618	0.1524	0.1290
Diboson cross section %	0.0218	0.0211	0.0211	0.0218	0.0219	0.0215	0.0249	0.0255	0.0257	0.0274	0.0277	0.0295	0.0307	0.0312	0.0336	0.0348	0.0386	0.0401
Diboson scale %	0.0564	0.0458	0.0415	0.0405	0.0390	0.0323	0.0471	0.0485	0.0461	0.0503	0.0592	0.0619	0.0540	0.0530	0.0532	0.0526	0.0878	0.1396
ttV background %	0.0325	0.0320	0.0322	0.0315	0.0321	0.0327	0.0328	0.0315	0.0328	0.0341	0.0317	0.0318	0.0320	0.0316	0.0333	0.0357	0.0348	0.0331
Z modelling %	0.0352	0.0679	0.1356	0.0594	0.0449	0.1692	0.0629	0.1729	0.2758	0.0565	0.0943	0.0378	0.1907	0.0331	0.2655	0.2256	0.1648	0.4344
Z factor %	0.0206	0.0179	0.0197	0.0111	0.0148	0.0223	0.0211	0.0243	0.0310	0.0177	0.0132	0.0162	0.0226	0.0141	0.0256	0.0262	0.0260	0.0424
Fakes background %	0.2718	0.2850	0.3240	0.3044	0.3420	0.3219	0.4468	0.5230	0.6179	0.6629	0.7251	0.7515	0.6743	0.5169	0.5859	0.6005	0.5262	0.4848
Pileup %	0.6834	0.6540	0.6551	0.6841	0.6743	0.6758	0.7502	0.7368	0.6953	0.7427	0.6571	0.7164	0.7361	0.6709	0.7612	0.6662	0.5633	0.7755
Beam energy %	0.0094	0.0293	0.0053	0.0046	0.0388	0.0268	0.0038	0.0229	0.0018	0.0140	0.0329	0.0051	0.0076	0.0251	0.0042	0.0173	0.0503	0.0248
Luminosity %	1.9025	1.8979	1.8979	1.8969	1.8963	1.8988	1.9078	1.9090	1.9181	1.9204	1.9186	1.9216	1.9140	1.9033	1.9121	1.9170	1.9153	1.9151

Table 8: Differential absolute cross section for $E(\ell^+) + E(\ell^-)$ with detailed systematic uncertainties.

$E(\ell^+) + E(\ell^-)$ bins [GeV]	50.0-60.0	60.0-70.0	70.0-80.0	80.0-90.0	90.0-110.0	110.0-125.0	125.0-160.0	160.0-200.0	200.0-250.0	250.0-300.0	300.0-370.0	370.0-450.0	450.0-550.0	550.0-700.0	700.0-900.0
Cross section [fb/GeV]	1.4375	9.0958	20.6367	30.9508	44.3327	51.7400	52.3485	43.8647	32.0006	21.2269	12.9273	6.9930	3.4994	1.4392	0.6230
Data statistics %	5.3505	1.9778	1.1975	0.9843	0.5431	0.5932	0.3877	0.3892	0.3954	0.4929	0.5488	0.7125	0.9860	1.1977	1.7894
MC statistics %	6.2128	1.2323	0.4153	0.3189	0.1582	0.1479	0.1021	0.1038	0.1036	0.1302	0.1497	0.1806	0.2469	0.3253	0.4801
Fragmentation %	1.4110	0.9863	0.5351	0.7744	0.3499	0.2391	0.4713	0.2240	0.2867	0.2196	0.6616	0.2520	0.0398	0.4335	0.8419
Hard scattering %	1.8155	3.5941	0.5351	0.7797	0.7324	0.2390	0.8207	0.1558	0.2161	0.8576	0.3534	0.2222	0.2543	1.3862	1.2599
top pT %	0.0100	0.0779	0.0767	0.0557	0.0472	0.0140	0.0479	0.1334	0.2065	0.2585	0.2722	0.2809	0.2691	0.2438	0.2097
Top mass dependence %	0.2093	0.1949	0.2338	0.0562	0.1123	0.0666	0.0394	0.0048	0.0292	0.0366	0.0168	0.0917	0.0976	0.0280	0.1727
PDF %	0.0361	0.0186	0.0209	0.0225	0.0362	0.0551	0.0725	0.0925	0.1069	0.1211	0.1255	0.1229	0.1145	0.1119	0.1210
ISR %	2.6544	0.1934	0.4197	0.1625	0.2596	0.1508	0.1720	0.2787	0.2353	0.2745	0.4425	0.1481	0.2277	0.1883	0.0017
FSR %	1.5141	0.3597	0.6109	0.7207	0.4693	0.4152	0.1458	0.2215	0.3017	0.1389	0.1902	0.3892	0.1586	0.6034	0.6721
Electron scale %	0.2255	0.0052	0.0378	0.0385	0.0262	0.0468	0.0607	0.0380	0.0201	0.1548	0.2792	0.4310	0.5910	0.8125	1.5436
Electron resolution %	0.2178	0.0796	0.0350	0.0187	0.0170	0.0086	0.0087	0.0063	0.0016	0.0164	0.0166	0.0026	0.0167	0.0096	0.0165
Electron trigger efficiency %	0.2159	0.1202	0.0868	0.0715	0.0574	0.0502	0.0462	0.0441	0.0437	0.0446	0.0476	0.0533	0.0613	0.0717	0.0838
Electron reconstruction efficiency %	0.2603	0.2253	0.1788	0.1546	0.1358	0.1298	0.1325	0.1402	0.1484	0.1572	0.1671	0.1796	0.1935	0.2091	0.2315
Electron ISO efficiency %	0.1098	0.1000	0.0859	0.0800	0.0752	0.0749	0.0795	0.0870	0.0965	0.1072	0.1199	0.1364	0.1566	0.1911	0.2678
Electron ID efficiency %	0.7506	0.5436	0.4516	0.4065	0.3676	0.3337	0.2995	0.2748	0.2797	0.2950	0.3214	0.3892	0.5689	0.8435	1.3077
Muon scale %	0.0448	0.0027	0.0623	0.0254	0.0122	0.0022	0.0100	0.0357	0.0509	0.0609	0.0955	0.1257	0.1154	0.1893	0.2443
Muon resolution %	0.6853	0.0546	0.0182	0.0722	0.0091	0.0123	0.0034	0.0023	0.0171	0.0248	0.0346	0.0095	0.0168	0.0480	0.1685
Muon reconstruction efficiency %	0.3473	0.3073	0.2761	0.2690	0.2541	0.2460	0.2343	0.2237	0.2147	0.2087	0.2042	0.2014	0.1989	0.1984	0.2012
Muon trigger efficiency %	0.1841	0.1441	0.1107	0.0926	0.0748	0.0633	0.0546	0.0481	0.0440	0.0410	0.0386	0.0360	0.0340	0.0318	0.0303
Muon ISO efficiency %	0.2435	0.2641	0.2625	0.2695	0.2751	0.2735	0.2686	0.2636	0.2600	0.2581	0.2566	0.2533	0.2493	0.2480	0.2523
Muon TTVA efficiency %	0.0366	0.0298	0.0254	0.0242	0.0233	0.0228	0.0224	0.0219	0.0214	0.0211	0.0211	0.0211	0.0212	0.0214	0.0221
JVT %	0.0443	0.0409	0.0290	0.0282	0.0235	0.0276	0.0269	0.0294	0.0288	0.0313	0.0327	0.0349	0.0391	0.0452	0.0251
JES b-jes response %	0.0033	0.2002	0.0912	0.0626	0.0651	0.0532	0.0459	0.0453	0.0414	0.0429	0.0286	0.0748	0.0454	0.0245	0.0307
JES effective NPs %	0.3534	0.1361	0.0824	0.0387	0.0351	0.0252	0.0126	0.0092	0.0186	0.0077	0.0124	0.0079	0.0251	0.0233	0.0755
JES EtaInterCalibration %	0.1067	0.0965	0.1887	0.0236	0.0237	0.0199	0.0091	0.0082	0.0158	0.0080	0.0113	0.0114	0.0213	0.0199	0.0520
JES flavour %	0.4067	0.0244	0.2072	0.0473	0.0210	0.0372	0.0517	0.0588	0.0455	0.0961	0.0740	0.0988	0.1118	0.1221	0.2057
JES pileup %	0.3664	0.1358	0.2428	0.0414	0.0329	0.0140	0.0064	0.0092	0.0172	0.0238	0.0265	0.0216	0.0325	0.0462	0.0892
JES PunchThrough %	0.0000	0.0010	0.0000	0.0000	0.0001	0.0001	0.0001	0.0002	0.0001	0.0000	0.0001	0.0004	0.0011	0.0006	0.0005
JES HighPt %	0.0000	0.0000	0.0000	0.0000	0.0000	0.0000	0.0000	0.0000	0.0000	0.0000	0.0000	0.0000	0.0000	0.0000	0.0000
MET soft term %	0.0000	0.0000	0.0000	0.0000	0.0000	0.0000	0.0000	0.0000	0.0000	0.0000	0.0000	0.0000	0.0000	0.0000	0.0000
JER %	0.0000	0.0000	0.0000	0.0000	0.0001	0.0000	0.0000	0.0000	0.0000	0.0000	0.0001	0.0000	0.0000	0.0000	0.0000
b-tagging %	1.7601	0.3662	0.1168	0.1193	0.1121	0.0983	0.0919	0.0839	0.0794	0.0791	0.0773	0.0716	0.0732	0.0793	0.1005
Wt cross section %	0.3324	0.4041	0.4120	0.4431	0.4438	0.4707	0.4827	0.4988	0.5135	0.5394	0.5588	0.5814	0.6065	0.6378	0.7666
Wt/$t\bar{t}$ interference %	0.5778	0.3099	0.4249	0.3308	0.2938	0.2186	0.0214	0.0866	0.2680	0.6529	0.8962	1.2231	1.5826	2.0537	3.1581
Wt hard scattering %	0.2218	0.7606	0.3064	0.4898	0.1246	0.2475	0.1225	0.1194	0.2324	0.2503	0.2641	0.4163	0.3403	0.3854	0.6411
Wt fragmentation %	1.0702	0.0186	0.4198	0.4630	0.2315	0.4198	0.3221	0.2422	0.0283	0.2021	0.3459	0.2020	0.3683	0.1818	0.0057
Wt ISR %	0.1716	0.0668	0.1307	0.0755	0.1071	0.1234	0.0949	0.0411	0.0019	0.0658	0.1324	0.1804	0.2607	0.3357	0.4687
Wt FSR %	0.5367	0.0758	0.0748	0.0742	0.0413	0.1163	0.1544	0.0484	0.1039	0.2050	0.3612	0.1218	0.0419	0.3356	0.4644
Diboson cross section %	0.0124	0.0212	0.0169	0.0155	0.0142	0.0140	0.0148	0.0172	0.0195	0.0234	0.0273	0.0344	0.0403	0.0528	0.0996
Diboson scale %	0.2159	0.1202	0.0868	0.0715	0.0574	0.0502	0.0462	0.0441	0.0437	0.0446	0.0476	0.0533	0.0613	0.0717	0.0838
ttV background %	0.0214	0.0209	0.0212	0.0209	0.0212	0.0231	0.0245	0.0283	0.0318	0.0346	0.0387	0.0439	0.0482	0.0554	0.0757
Z modelling %	5.5418	0.7328	0.7587	0.0661	0.0208	0.0629	0.0286	0.1271	0.0744	0.1269	0.0334	0.0925	0.0527	0.0491	0.0080
Z factor %	0.0957	0.1964	0.0699	0.0647	0.0303	0.0195	0.0150	0.0158	0.0104	0.0110	0.0106	0.0065	0.0068	0.0058	0.0051
Fakes background %	0.0649	0.4611	0.2429	0.2560	0.2045	0.1614	0.2223	0.2811	0.3396	0.3672	0.5116	0.5912	0.5554	0.5839	0.7723
Pileup %	1.8777	1.7091	1.2319	1.2010	1.0037	0.8995	0.7896	0.7118	0.6588	0.5182	0.4421	0.4424	0.4260	0.3768	0.3214
Beam energy %	0.1096	0.0237	0.0223	0.0324	0.0103	0.0096	0.0314	0.0028	0.0019	0.0066	0.0024	0.0127	0.0265	0.0201	0.0211
Luminosity %	1.7796	1.9243	1.8767	1.8848	1.8715	1.8739	1.8804	1.8906	1.8991	1.9111	1.9292	1.9437	1.9528	1.9699	2.0437

Table 9: Differential absolute cross section for $m(\ell^+\ell^-)$ with detailed systematic uncertainties.

$m(\ell^+\ell^-)$ bins [GeV]	0.0-15.0	15.0-20.0	20.0-25.0	25.0-30.0	30.0-35.0	35.0-40.0	40.0-50.0	50.0-60.0	60.0-70.0	70.0-85.0	85.0-100.0	100.0-120.0	120.0-150.0	150.0-175.0	175.0-200.0	200.0-250.0	250.0-300.0	300.0-400.0	400.0-500.0	500.0-650.0	650.0-800.0
Cross section [fb/GeV]	8.2361	19.0791	23.7748	29.5110	33.5749	38.7676	46.1188	56.9246	69.6418	77.9525	77.4567	68.2664	51.4973	34.9697	24.1325	13.8885	6.8427	2.6148	0.7404	0.2153	0.0670
Data statistics %	2.1647	1.7896	1.6258	1.3608	1.2898	1.2280	0.7770	0.7248	0.6543	0.4994	0.4889	0.4493	0.4023	0.5239	0.6295	0.5867	0.8521	0.9474	1.7912	2.7452	5.1331
MC statistics %	0.5542	0.4249	0.3984	0.3463	0.3229	0.2978	0.1975	0.2795	0.2335	0.1511	0.1197	0.1081	0.1050	0.1373	0.1683	0.1532	0.2219	0.2530	0.4954	0.7419	1.4285
Fragmentation %	0.1625	0.3217	0.5809	0.1814	0.8333	0.6033	0.2884	1.2331	1.1467	0.4123	0.1298	0.1852	0.0674	0.2812	0.5158	0.4745	0.2888	0.9258	0.1264	1.8155	0.3771
Hard scattering %	2.3070	1.7911	1.3443	0.2726	1.4060	0.3942	1.8096	0.9429	0.8434	0.3579	0.9731	0.1613	0.4421	0.1978	0.3828	0.0839	1.6217	0.4912	0.7341	3.3446	0.3402
top pT %	0.1606	0.0666	0.0433	0.0103	0.0175	0.0137	0.0137	0.0399	0.0420	0.0337	0.0165	0.0046	0.0429	0.0832	0.1195	0.1863	0.2370	0.2950	0.3255	0.4210	0.5563
Top mass dependence %	0.3494	0.0042	0.0261	0.1201	0.0546	0.0055	0.0507	0.0536	0.0099	0.0126	0.0394	0.0495	0.1007	0.0150	0.0060	0.0349	0.0025	0.0573	0.1984	0.1690	0.3897
PDF %	0.1156	0.0885	0.0804	0.0855	0.0723	0.0739	0.0714	0.0680	0.0643	0.0629	0.0555	0.0563	0.0571	0.0567	0.0627	0.0569	0.0605	0.0487	0.0488	0.0515	0.1017
ISR %	0.4256	0.4388	0.0230	0.0641	0.4647	0.1294	0.2349	0.1221	0.1102	0.0541	0.1707	0.1243	0.1495	0.2232	0.1355	0.2651	0.6388	0.6588	0.2220	0.1384	1.8017
FSR %	0.0444	1.1469	0.2097	0.2402	0.1749	0.4675	0.0657	0.1528	0.1846	0.3433	0.3439	0.2735	0.1824	0.2525	0.1701	0.2558	0.4198	0.0133	0.4418	0.5582	0.0728
Electron scale %	0.0677	0.0393	0.0579	0.0597	0.0779	0.0579	0.0594	0.0373	0.0504	0.0005	0.0058	0.0062	0.0218	0.0994	0.1983	0.2568	0.4666	0.6624	1.0091	1.3976	1.9446
Electron resolution %	0.0176	0.0455	0.0146	0.0291	0.0152	0.0244	0.0083	0.0201	0.0162	0.0266	0.0094	0.0114	0.0001	0.0045	0.0177	0.0037	0.0123	0.0139	0.0537	0.2067	0.0996
Electron trigger efficiency %	0.0672	0.0617	0.0606	0.0606	0.0609	0.0613	0.0614	0.0634	0.0588	0.0534	0.0491	0.0462	0.0443	0.0443	0.0454	0.0472	0.0493	0.0521	0.0550	0.0567	0.0626
Electron reconstruction efficiency %	0.1681	0.1562	0.1570	0.1562	0.1566	0.1567	0.1561	0.1587	0.1538	0.1449	0.1398	0.1389	0.1426	0.1501	0.1580	0.1671	0.1766	0.1868	0.1981	0.2052	0.2243
Electron ISO efficiency %	0.0916	0.0890	0.0894	0.0895	0.0898	0.0900	0.0898	0.0909	0.0896	0.0868	0.0860	0.0879	0.0933	0.1016	0.1105	0.1236	0.1425	0.1690	0.2068	0.2458	0.3364
Electron ID efficiency %	0.4535	0.3788	0.3728	0.3709	0.3667	0.3672	0.3676	0.3717	0.3645	0.3420	0.3159	0.2921	0.2761	0.2778	0.2963	0.3378	0.4076	0.5216	0.7459	1.1394	1.8425
Muon scale %	0.0105	0.0336	0.0055	0.0509	0.0206	0.0109	0.0149	0.0138	0.0290	0.0145	0.0299	0.0330	0.0422	0.0585	0.0904	0.0800	0.1271	0.1252	0.1437	0.1856	0.2232
Muon resolution %	0.0599	0.0670	0.0717	0.0650	0.0722	0.0222	0.0219	0.0178	0.0274	0.0019	0.0085	0.0090	0.0086	0.0087	0.0290	0.0147	0.0454	0.0482	0.0446	0.1269	0.2175
Muon reconstruction efficiency %	0.2277	0.2247	0.2240	0.2277	0.2281	0.2268	0.2287	0.2284	0.2263	0.2249	0.2228	0.2240	0.2239	0.2224	0.2223	0.2212	0.2180	0.2164	0.2138	0.2089	0.2094
Muon trigger efficiency %	0.1118	0.0881	0.0863	0.0869	0.0857	0.0857	0.0851	0.0872	0.0833	0.0723	0.0603	0.0492	0.0384	0.0306	0.0265	0.0228	0.0199	0.0177	0.0166	0.0152	0.0156
Muon ISO efficiency %	0.2719	0.2692	0.2684	0.2677	0.2687	0.2692	0.2702	0.2715	0.2714	0.2710	0.2695	0.2676	0.2633	0.2571	0.2529	0.2482	0.2445	0.2432	0.2438	0.2418	0.2551
Muon TTVA efficiency %	0.0229	0.0231	0.0230	0.0230	0.0231	0.0231	0.0231	0.0234	0.0229	0.0223	0.0218	0.0216	0.0216	0.0216	0.0216	0.0217	0.0217	0.0216	0.0217	0.0213	0.0220
JVT %	0.0324	0.0249	0.0176	0.0163	0.0332	0.0263	0.0311	0.0312	0.0326	0.0303	0.0257	0.0273	0.0316	0.0320	0.0304	0.0368	0.0355	0.0321	0.0551	0.0586	0.0839
JES b-jes response %	0.0650	0.0394	0.0290	0.0547	0.0056	0.0019	0.0255	0.0418	0.0823	0.0370	0.0334	0.0437	0.0475	0.0493	0.0567	0.0762	0.0667	0.1049	0.0798	0.1335	0.1644
JES effective NPs %	0.0574	0.0360	0.0232	0.0523	0.0255	0.0136	0.0568	0.0251	0.0465	0.0327	0.0117	0.0076	0.0112	0.0137	0.0108	0.0143	0.0212	0.0075	0.0424	0.0345	0.0475
JES EtaInterCalibration %	0.0289	0.0246	0.0065	0.0385	0.0085	0.0088	0.0848	0.0109	0.0155	0.0295	0.0064	0.0021	0.0069	0.0085	0.0042	0.0049	0.0119	0.0070	0.0254	0.0316	0.0752
JES flavour %	0.0524	0.0245	0.0224	0.0098	0.0304	0.0104	0.1011	0.0329	0.0256	0.0207	0.0447	0.0597	0.0639	0.0757	0.1097	0.1030	0.1401	0.1596	0.2086	0.2306	0.2848
JES pileup %	0.0749	0.0508	0.0167	0.0573	0.0338	0.0148	0.1118	0.0150	0.0369	0.0463	0.0034	0.0130	0.0059	0.0073	0.0214	0.0188	0.0330	0.0175	0.0562	0.0317	0.0738
JES PunchThrough %	0.0000	0.0000	0.0000	0.0000	0.0000	0.0000	0.0002	0.0000	0.0000	0.0002	0.0000	0.0004	0.0002	0.0002	0.0002	0.0004	0.0000	0.0003	0.0000	0.0017	0.0001
JES HighPt %	0.0000	0.0000	0.0000	0.0000	0.0000	0.0000	0.0000	0.0000	0.0000	0.0000	0.0000	0.0000	0.0000	0.0000	0.0000	0.0000	0.0000	0.0000	0.0000	0.0000	0.0000
MET soft term %	0.0000	0.0000	0.0000	0.0000	0.0000	0.0000	0.0000	0.0000	0.0000	0.0000	0.0000	0.0000	0.0000	0.0000	0.0000	0.0000	0.0000	0.0000	0.0000	0.0000	0.0000
JER %	0.0000	0.0000	0.0000	0.0000	0.0000	0.0000	0.0000	0.0000	0.0002	0.0000	0.0000	0.0000	0.0000	0.0001	0.0001	0.0000	0.0000	0.0000	0.0000	0.0000	0.0000
b-tagging %	0.1440	0.1028	0.1001	0.0910	0.0833	0.0903	0.0900	0.1033	0.0847	0.0857	0.0950	0.0859	0.0846	0.0822	0.0876	0.0774	0.0727	0.0696	0.0856	0.0803	0.1255
Wt cross section %	0.4349	0.4738	0.4762	0.4578	0.4712	0.4728	0.4678	0.4690	0.4705	0.4747	0.4875	0.4993	0.5212	0.5352	0.5561	0.5743	0.5923	0.6169	0.6595	0.5895	0.7940
Wt/$t\bar{t}$ interference %	0.5079	0.2229	0.2590	0.8053	0.1419	0.1371	0.2183	0.2915	0.0305	0.0188	0.0038	0.1647	0.3441	0.4888	0.7876	1.0943	1.3415	2.3361	3.4688	2.2270	7.4469
Wt hard scattering %	0.2139	0.3405	0.1599	0.4490	0.1981	0.1244	0.1135	0.2073	0.3609	0.2310	0.2825	0.2020	0.1434	0.1356	0.2172	0.5004	0.2831	0.2968	0.0742	1.3545	1.2325
Wt fragmentation %	0.4521	0.2272	0.4179	0.2780	0.0564	0.4269	0.3217	0.1837	0.4519	0.4328	0.2384	0.3520	0.2566	0.1314	0.0802	0.0021	0.2546	0.1868	0.5058	0.9352	0.3116
Wt ISR %	0.1756	0.0476	0.0912	0.0815	0.0938	0.1059	0.0503	0.0913	0.0879	0.0500	0.0830	0.0426	0.0092	0.0346	0.0839	0.1305	0.2743	0.3816	0.4914	0.6003	1.1892
Wt FSR %	0.1792	0.2633	0.1472	0.2069	0.1218	0.1599	0.0331	0.0426	0.0791	0.1548	0.0580	0.0992	0.1482	0.1854	0.0240	0.4069	0.0696	0.0962	0.3018	0.1887	0.3400
Diboson cross section %	0.0203	0.0214	0.0245	0.0210	0.0215	0.0225	0.0201	0.0214	0.0210	0.0202	0.0199	0.0194	0.0204	0.0204	0.0212	0.0227	0.0261	0.0317	0.0410	0.0530	0.0990
Diboson scale %	0.0672	0.0617	0.0606	0.0606	0.0609	0.0613	0.0614	0.0634	0.0588	0.0534	0.0491	0.0462	0.0443	0.0443	0.0454	0.0472	0.0493	0.0521	0.0550	0.0567	0.0626
ttV background %	0.0208	0.0254	0.0251	0.0218	0.0247	0.0238	0.0242	0.0258	0.0258	0.0263	0.0271	0.0291	0.0310	0.0340	0.0362	0.0408	0.0431	0.0511	0.0646	0.0740	0.1114
Z modelling %	0.3956	0.1132	0.1206	0.2180	0.4106	0.2315	0.3267	0.3125	0.1806	0.0731	0.0209	0.0025	0.0363	0.0106	0.0135	0.0038	0.0056	0.0128	0.0734	0.0023	0.0074
Z factor %	0.0198	0.0093	0.0060	0.0149	0.0271	0.0361	0.0558	0.0892	0.0762	0.0359	0.0038	0.0021	0.0024	0.0016	0.0007	0.0002	0.0003	0.0005	0.0037	0.0001	0.0004
Fakes background %	0.8972	0.3626	0.3768	0.3767	0.3209	0.4187	0.3367	0.3212	0.3939	0.3882	0.3477	0.2964	0.2847	0.2870	0.2687	0.3309	0.3947	0.5065	0.5875	0.6379	0.9503
Pileup %	1.0688	0.9798	0.8693	0.7461	0.9627	0.9336	1.1414	0.9760	0.9361	0.8851	0.8150	0.7248	0.6410	0.5718	0.4644	0.3655	0.2939	0.3233	0.2766	0.0040	0.3004
Beam energy %	0.0080	0.0504	0.0157	0.0214	0.0078	0.0570	0.0147	0.0427	0.0072	0.0036	0.0175	0.0127	0.0012	0.0144	0.0097	0.0066	0.0339	0.0205	0.0075	0.0205	0.1031
Luminosity %	1.9037	1.8807	1.8839	1.8802	1.8865	1.8974	1.8980	1.9088	1.9106	1.8980	1.8884	1.8887	1.8957	1.9010	1.9056	1.9173	1.9285	1.9466	1.9677	1.9503	2.0485

Table 10: Differential absolute cross section for p_{T} (ℓ^{+}) + p_{T} (ℓ^{-}) with detailed systematic uncertainties.

p_{T} (ℓ^{+}) + p_{T} (ℓ^{-}) bins [GeV]	50.0-60.0	60.0-70.0	70.0-80.0	80.0-100.0	100.0-125.0	125.0-150.0	150.0-200.0	200.0-250.0	250.0-300.0	300.0-400.0	400.0-600.0
Cross section [fb/GeV]	25.4190	73.1471	104.5368	116.7224	97.5588	63.5721	29.8933	10.3089	3.9637	1.1605	0.1430
Data statistics %	1.2577	0.6761	0.5428	0.3431	0.3404	0.3979	0.4146	0.6564	1.0932	1.4334	2.8288
MC statistics %	0.5705	0.2662	0.1718	0.0977	0.0800	0.1000	0.1070	0.1932	0.2921	0.3850	0.8683
Fragmentation %	2.0867	0.3881	1.0976	0.5318	0.0334	0.2899	0.3702	1.0519	1.5201	1.5707	1.2404
Hard scattering %	1.5056	0.7317	1.0698	0.4903	0.1119	0.4897	0.9757	0.0816	2.1492	3.7171	3.4022
top pT %	0.0704	0.0658	0.0623	0.0508	0.0497	0.0588	0.0513	0.0440	0.0137	0.0392	0.1653
Top mass dependence %	0.1966	0.1385	0.0913	0.1017	0.0940	0.0827	0.0476	0.0568	0.1182	0.2026	0.1231
PDF %	0.0396	0.0425	0.0455	0.0503	0.0630	0.0754	0.0881	0.1064	0.1126	0.1121	0.1054
ISR %	0.3592	0.1570	0.0523	0.2130	0.2129	0.1358	0.2366	0.3875	0.0852	0.3346	0.5727
FSR %	0.9352	0.3178	0.3388	0.1414	0.1975	0.0909	0.2880	0.1967	0.3218	1.1552	0.0515
Electron scale %	0.0193	0.0517	0.0027	0.0937	0.0759	0.0330	0.2638	0.6172	0.9240	1.2829	1.9824
Electron resolution %	0.0276	0.0282	0.0407	0.0155	0.0041	0.0002	0.0019	0.0108	0.0296	0.0163	0.0424
Electron trigger efficiency %	0.1712	0.0789	0.0567	0.0474	0.0437	0.0449	0.0466	0.0487	0.0495	0.0509	0.0535
Electron reconstruction efficiency %	0.2787	0.1843	0.1419	0.1290	0.1340	0.1502	0.1660	0.1816	0.1901	0.1974	0.2142
Electron ISO efficiency %	0.1258	0.1004	0.0853	0.0796	0.0832	0.0957	0.1108	0.1500	0.1803	0.2214	0.3478
Electron ID efficiency %	0.8500	0.5204	0.4055	0.3496	0.2962	0.2744	0.3082	0.4031	0.4989	0.8433	2.0167
Muon scale %	0.0385	0.0411	0.0082	0.0111	0.0338	0.0688	0.0952	0.1112	0.1354	0.1393	0.2231
Muon resolution %	0.1108	0.0501	0.0144	0.0120	0.0154	0.0099	0.0157	0.0466	0.0395	0.0700	0.2938
Muon reconstruction efficiency %	0.2137	0.2153	0.2162	0.2175	0.2205	0.2230	0.2291	0.2373	0.2430	0.2517	0.2813
Muon trigger efficiency %	0.2152	0.1311	0.0943	0.0677	0.0451	0.0322	0.0231	0.0169	0.0137	0.0122	0.0113
Muon ISO efficiency %	0.2524	0.2670	0.2638	0.2831	0.2678	0.2555	0.2483	0.2469	0.2486	0.2551	0.2852
Muon TTVA efficiency %	0.0325	0.0240	0.0216	0.0214	0.0214	0.0216	0.0219	0.0226	0.0230	0.0236	0.0259
JVT %	0.0206	0.0357	0.0278	0.0255	0.0288	0.0291	0.0341	0.0425	0.0410	0.0505	0.0919
JES b-jes response %	0.0728	0.0856	0.0665	0.0487	0.0416	0.0359	0.0417	0.0443	0.0841	0.1127	0.0747
JES effective NPs %	0.0869	0.0575	0.0490	0.0450	0.0120	0.0112	0.0187	0.0507	0.0176	0.0128	0.1173
JES EtaInterCalibration %	0.2051	0.0208	0.0178	0.0213	0.0038	0.0034	0.0037	0.0171	0.0044	0.0110	0.0278
JES flavour %	0.2239	0.0261	0.0118	0.0119	0.0479	0.0736	0.1009	0.1414	0.1692	0.2182	0.3608
JES pileup %	0.2423	0.0519	0.0442	0.0426	0.0033	0.0199	0.0324	0.0743	0.0234	0.0312	0.1357
JES PunchThrough %	0.0004	0.0000	0.0002	0.0002	0.0000	0.0001	0.0001	0.0007	0.0001	0.0004	0.0001
JES HighPt %	0.0000	0.0000	0.0000	0.0000	0.0000	0.0000	0.0000	0.0000	0.0000	0.0000	0.0000
MET soft term %	0.0000	0.0000	0.0000	0.0000	0.0000	0.0000	0.0000	0.0000	0.0000	0.0000	0.0000
JER %	0.0000	0.0000	0.0001	0.0000	0.0000	0.0000	0.0000	0.0000	0.0000	0.0000	0.0000
b-tagging %	0.1487	0.1190	0.1008	0.0845	0.0905	0.0808	0.0860	0.0935	0.0877	0.1137	0.2284
Wt cross section %	0.3871	0.4098	0.4246	0.4482	0.4772	0.5068	0.5723	0.7056	0.7996	0.9325	1.4241
Wt/$t\bar{t}$ interference %	0.2516	0.4193	0.0973	0.1679	0.0533	0.2823	0.7806	1.8884	2.5360	4.0976	11.0556
Wt hard scattering %	0.3778	0.1690	0.3710	0.1744	0.2393	0.2834	0.1789	0.4414	0.0896	0.4605	0.0442
Wt fragmentation %	0.2751	0.2954	0.3545	0.2421	0.2805	0.1814	0.1785	0.4489	0.0744	0.0436	0.0195
Wt ISR %	0.0909	0.1033	0.0892	0.1111	0.0668	0.0015	0.0774	0.2692	0.4644	0.8107	2.5018
Wt FSR %	0.0108	0.0501	0.1037	0.0922	0.1589	0.0680	0.2283	0.1891	0.2238	0.1752	0.0294
Diboson cross section %	0.0195	0.0190	0.0182	0.0171	0.0171	0.0196	0.0237	0.0337	0.0457	0.0622	0.1358
Diboson scale %	0.1712	0.0789	0.0567	0.0474	0.0437	0.0449	0.0466	0.0487	0.0495	0.0509	0.0535
ttV background %	0.0211	0.0225	0.0221	0.0234	0.0259	0.0304	0.0391	0.0528	0.0642	0.0833	0.1426
Z modelling %	0.4514	0.2118	0.1119	0.0556	0.0354	0.0533	0.0357	0.0273	0.0201	0.0424	0.0383
Z factor %	0.1005	0.0889	0.0416	0.0197	0.0077	0.0056	0.0047	0.0021	0.0025	0.0043	0.0006
Fakes background %	0.4670	0.3843	0.3233	0.3231	0.3043	0.3057	0.3145	0.3942	0.4518	0.4298	0.7579
Pileup %	1.4869	1.2527	1.0768	0.9039	0.7227	0.5602	0.3958	0.3103	0.2859	0.2722	0.0119
Beam energy %	0.0279	0.0022	0.0080	0.0076	0.0082	0.0003	0.0062	0.0169	0.0174	0.0645	0.0554
Luminosity %	1.8926	1.8940	1.8786	1.8789	1.8835	1.8936	1.9173	1.9685	2.0064	2.0510	2.2504

Table 11: Differential absolute cross section for p_{T} $(\ell^+\ell^-)$ with detailed systematic uncertainties.

p_{T} $(\ell^+\ell^-)$ bins [GeV]	0.0-20.0	20.0-30.0	30.0-45.0	45.0-60.0	60.0-75.0	75.0-100.0	100.0-125.0	125.0-150.0	150.0-200.0	200.0-300.0
Cross section [fb/GeV]	33.1519	69.8572	88.6780	112.3852	122.4377	94.4376	49.1848	20.0082	5.8371	0.8800
Data statistics %	0.6835	0.6510	0.4728	0.4213	0.3946	0.3341	0.4598	0.7100	0.9602	1.7953
MC statistics %	0.2434	0.2133	0.1296	0.1070	0.0990	0.0841	0.1147	0.1841	0.2633	0.5380
Fragmentation %	0.5800	0.3941	0.2617	0.4014	0.1413	0.0908	0.5706	0.8212	0.8187	0.1315
Hard scattering %	0.2319	1.0103	0.4888	0.9200	0.9888	0.0728	0.9012	0.9656	0.9677	1.1914
top pT %	0.2072	0.2009	0.2142	0.2674	0.2692	0.2108	0.1172	0.0533	0.0228	0.0985
Top mass dependence %	0.0477	0.0407	0.0227	0.0139	0.0290	0.0036	0.0378	0.0633	0.0468	0.1042
PDF %	0.0267	0.0306	0.0278	0.0296	0.0298	0.0367	0.0544	0.0694	0.0803	0.0775
ISR %	0.1666	0.1260	0.4981	0.2355	0.4737	0.2698	0.3393	0.1970	0.1185	0.0141
FSR %	0.3877	0.6821	0.1088	0.2631	0.3471	0.0823	0.2888	0.0119	0.0872	1.7007
Electron scale %	0.1419	0.1603	0.1177	0.0647	0.0301	0.0903	0.3225	0.7283	1.1350	1.7032
Electron resolution %	0.0287	0.0507	0.0030	0.0089	0.0263	0.0099	0.0012	0.0018	0.0597	0.0047
Electron trigger efficiency %	0.0520	0.0498	0.0507	0.0545	0.0501	0.0472	0.0480	0.0505	0.0526	0.0568
Electron reconstruction efficiency %	0.1401	0.1427	0.1473	0.1540	0.1488	0.1472	0.1572	0.1698	0.1807	0.2064
Electron ISO efficiency %	0.0885	0.0895	0.0918	0.0951	0.0941	0.0957	0.1076	0.1279	0.1570	0.2411
Electron ID efficiency %	0.3176	0.3078	0.3081	0.3195	0.3103	0.2890	0.2934	0.3392	0.4270	1.0236
Muon scale %	0.0009	0.0124	0.0067	0.0172	0.0207	0.0539	0.1044	0.1624	0.1695	0.2025
Muon resolution %	0.0354	0.0115	0.0248	0.0175	0.0162	0.0177	0.0231	0.0202	0.0610	0.1928
Muon reconstruction efficiency %	0.2191	0.2206	0.2208	0.2201	0.2203	0.2227	0.2257	0.2313	0.2423	0.2793
Muon trigger efficiency %	0.0569	0.0551	0.0555	0.0615	0.0577	0.0470	0.0377	0.0344	0.0327	0.0305
Muon ISO efficiency %	0.2690	0.2690	0.2637	0.2612	0.2625	0.2637	0.2560	0.2555	0.2626	0.2959
Muon TTVA efficiency %	0.0214	0.0218	0.0219	0.0222	0.0218	0.0217	0.0219	0.0224	0.0234	0.0265
JVT %	0.0354	0.0348	0.0334	0.0333	0.0299	0.0283	0.0239	0.0294	0.0327	0.0848
JES b-jes response %	0.0937	0.1083	0.0900	0.0721	0.0654	0.0358	0.0145	0.0234	0.0564	0.0159
JES effective NPs %	0.0111	0.1092	0.0411	0.0336	0.0240	0.0085	0.0265	0.0709	0.0976	0.1100
JES EtaInterCalibration %	0.0506	0.0661	0.0174	0.0082	0.0152	0.0037	0.0080	0.0243	0.0396	0.0379
JES flavour %	0.1198	0.0260	0.0633	0.0581	0.0666	0.0560	0.0679	0.0871	0.1176	0.1591
JES pileup %	0.0696	0.1069	0.0391	0.0234	0.0151	0.0154	0.0369	0.0877	0.1242	0.1342
JES PunchThrough %	0.0001	0.0003	0.0000	0.0000	0.0000	0.0001	0.0001	0.0003	0.0000	0.0007
JES HighPt %	0.0000	0.0000	0.0000	0.0000	0.0000	0.0000	0.0000	0.0000	0.0000	0.0000
MET soft term %	0.0000	0.0000	0.0000	0.0000	0.0000	0.0000	0.0000	0.0000	0.0000	0.0000
JER %	0.0000	0.0000	0.0000	0.0000	0.0001	0.0000	0.0000	0.0000	0.0000	0.0000
b-tagging %	0.1292	0.1301	0.1119	0.0990	0.0893	0.0849	0.1168	0.1669	0.2293	0.3229
Wt cross section %	0.4565	0.4627	0.4663	0.4685	0.4754	0.4985	0.5340	0.6315	0.8261	1.5334
Wt/$t\bar{t}$ interference %	0.1137	0.0621	0.1407	0.0972	0.0528	0.1537	0.6389	1.7252	3.2530	11.2006
Wt hard scattering %	0.4825	0.1715	0.3006	0.3229	0.2306	0.1663	0.0337	0.3359	0.0072	1.5198
Wt fragmentation %	0.2644	0.2866	0.1482	0.2700	0.2119	0.1940	0.2315	0.5058	0.4474	0.9740
Wt ISR %	0.0623	0.0877	0.0694	0.0779	0.0768	0.0429	0.0164	0.1976	0.5719	3.0094
Wt FSR %	0.1500	0.0348	0.2069	0.0254	0.1070	0.1928	0.1948	0.1136	0.0041	0.4533
Diboson cross section %	0.0206	0.0195	0.0192	0.0173	0.0161	0.0168	0.0211	0.0306	0.0579	0.1764
Diboson scale %	0.0520	0.0498	0.0507	0.0545	0.0501	0.0472	0.0480	0.0505	0.0526	0.0568
ttV background %	0.0265	0.0264	0.0260	0.0250	0.0249	0.0271	0.0340	0.0503	0.0818	0.1774
Z modelling %	0.1674	0.1826	0.0109	0.0658	0.0603	0.0440	0.0465	0.1652	0.0032	0.1096
Z factor %	0.0422	0.0358	0.0240	0.0191	0.0147	0.0092	0.0085	0.0117	0.0137	0.0187
Fakes background %	0.3326	0.3171	0.3092	0.3076	0.3114	0.2898	0.3009	0.4125	0.6268	1.0928
Pileup %	0.8557	0.8200	0.7416	0.7892	0.7258	0.6844	0.5024	0.5190	0.4249	0.5374
Beam energy %	0.0191	0.0042	0.0099	0.0024	0.0075	0.0008	0.0038	0.0326	0.0026	0.0066
Luminosity %	1.8910	1.8899	1.8866	1.8848	1.8854	1.8902	1.9036	1.9465	2.0331	2.3170

Table 12: Differential absolute cross section for $\Delta\phi(\ell^+\ell^-)$ with detailed systematic uncertainties.

$\Delta\phi(\ell^+\ell^-)$ bins	0.00-0.10	0.10-0.21	0.21-0.31	0.31-0.42	0.42-0.52	0.52-0.63	0.63-0.73	0.73-0.84	0.84-0.94	0.94-1.05	1.05-1.15	1.15-1.26	1.26-1.36	1.36-1.47	1.47-1.57	1.57-1.68	1.68-1.78	1.78-1.88	1.88-1.99	1.99-2.09	2.09-2.20	2.20-2.30	2.30-2.41	2.41-2.51	2.51-2.62	2.62-2.72	2.72-2.83	2.83-2.93	2.93-3.04	3.04-3.14
Cross section [fb/rad]	1121.71	1125.30	1088.25	1139.10	1122.09	1158.53	1176.12	1224.07	1260.98	1259.25	1318.59	1382.21	1441.29	1518.67	1558.40	1634.70	1707.84	1778.35	1815.63	1953.95	2009.68	2123.71	2194.18	2258.18	2303.75	2328.95	2414.87	2441.99	2498.65	2586.68
Data statistics %	1.6913	1.6115	1.5714	1.5504	1.5436	1.4472	1.4690	1.4134	1.4680	1.4420	1.4192	1.4002	1.3025	1.3442	1.2962	1.2638	1.2344	1.1986	1.1861	1.1350	1.1546	1.0875	1.0391	1.0720	1.0260	1.0418	1.0153	1.0247	1.0015	0.9808
MC statistics %	0.3901	0.3996	0.4017	0.3752	0.3708	0.3642	0.3680	0.3558	0.3567	0.3709	0.3719	0.3405	0.3283	0.3344	0.3265	0.3191	0.3376	0.3184	0.3630	0.3262	0.3075	0.3125	0.3099	0.2956	0.2924	0.3115	0.2853	0.3127	0.3394	0.2626
Fragmentation %	1.0067	0.4773	1.3012	0.7964	1.1451	0.9576	0.3863	0.0043	0.5644	0.0964	0.6465	0.6994	0.9659	0.2694	0.4252	0.1509	0.4053	0.6399	0.5295	1.1504	0.2611	0.2990	0.6707	0.0205	0.0599	0.0268	0.5650	0.0341	0.0936	0.2494
Hard scattering %	0.6815	1.0152	0.9577	1.3391	2.5493	0.5875	0.4188	0.9332	1.3577	0.8328	1.1443	0.8662	0.8858	1.7150	0.9844	1.9093	0.6574	1.7629	0.7220	0.7182	0.9247	1.4716	0.2468	0.0323	1.0686	0.9294	0.0606	0.5106	0.5005	0.0250
top pT %	0.0530	0.0365	0.0516	0.0580	0.0741	0.0443	0.0516	0.0597	0.0392	0.0686	0.0753	0.0791	0.0849	0.1060	0.1114	0.1077	0.1260	0.1455	0.1476	0.1550	0.1806	0.1916	0.2089	0.2196	0.2426	0.2542	0.2778	0.2902	0.3212	0.3043
Top mass dependence %	0.2007	0.0059	0.0476	0.0261	0.1649	0.1720	0.0569	0.1471	0.1945	0.0117	0.0636	0.0385	0.0042	0.1379	0.1272	0.1618	0.1318	0.0951	0.1920	0.0223	0.0004	0.0076	0.0387	0.0148	0.0137	0.0321	0.0289	0.0534	0.0073	0.0229
PDF %	0.0548	0.0528	0.0407	0.0372	0.0469	0.0331	0.0375	0.0475	0.0420	0.0450	0.0420	0.0417	0.0396	0.0430	0.0372	0.0348	0.0440	0.0464	0.0410	0.0385	0.0313	0.0369	0.0344	0.0363	0.0380	0.0341	0.0350	0.0351	0.0352	0.0363
ISR %	0.3952	0.0530	0.0613	0.5750	0.2660	0.2759	0.0372	0.2385	0.6290	0.1210	0.1468	0.5850	0.0880	0.3928	0.2303	0.3729	0.1628	0.2222	0.7660	0.5666	0.1041	0.1518	0.5170	0.1477	0.1854	0.5383	0.1126	0.4092	0.0975	0.0320
FSR %	0.1986	0.4009	0.1317	0.0627	0.5241	0.0834	0.2200	0.0007	0.5877	0.3919	0.1752	0.2649	0.4424	0.4062	0.4572	0.6506	0.3965	0.2010	0.1605	0.5947	0.9390	0.4324	0.3686	0.3787	0.4182	0.0054	0.1174	0.3306	0.6951	0.0861
Electron scale %	0.1691	0.1681	0.1685	0.1899	0.1696	0.1564	0.1800	0.1488	0.1427	0.1677	0.1467	0.1416	0.1457	0.1231	0.1340	0.1284	0.1232	0.1104	0.1097	0.0996	0.0970	0.0989	0.0907	0.0849	0.0794	0.0695	0.0774	0.0755	0.0766	0.0658
Electron resolution %	0.0465	0.0091	0.0228	0.0264	0.0228	0.0180	0.0177	0.0073	0.0197	0.0111	0.0078	0.0253	0.0123	0.0068	0.0124	0.0027	0.0094	0.0011	0.0003	0.0232	0.0050	0.0010	0.0211	0.0074	0.0016	0.0035	0.0050	0.0002	0.0214	0.0030
Electron trigger efficiency %	0.0542	0.0545	0.0542	0.0543	0.0549	0.0540	0.0533	0.0539	0.0533	0.0529	0.0527	0.0523	0.0517	0.0515	0.0511	0.0508	0.0507	0.0500	0.0492	0.0494	0.0492	0.0482	0.0482	0.0487	0.0479	0.0478	0.0477	0.0481	0.0479	0.0477
Electron reconstruction efficiency %	0.1496	0.1505	0.1498	0.1502	0.1497	0.1487	0.1491	0.1496	0.1492	0.1486	0.1494	0.1483	0.1482	0.1484	0.1484	0.1491	0.1487	0.1490	0.1500	0.1509	0.1511	0.1516	0.1522	0.1536	0.1550	0.1562	0.1565	0.1572	0.1569	0.1571
Electron ISO efficiency %	0.0913	0.0924	0.0922	0.0923	0.0925	0.0920	0.0920	0.0923	0.0923	0.0925	0.0932	0.0928	0.0931	0.0935	0.0942	0.0951	0.0954	0.0964	0.0975	0.0987	0.1000	0.1009	0.1027	0.1049	0.1073	0.1094	0.1113	0.1133	0.1139	0.1144
Electron ID efficiency %	0.3376	0.3367	0.3338	0.3309	0.3316	0.3335	0.3292	0.3278	0.3294	0.3248	0.3205	0.3190	0.3179	0.3163	0.3108	0.3068	0.3021	0.2993	0.2967	0.2952	0.2947	0.2930	0.2915	0.2954	0.2988	0.3016	0.3062	0.3118	0.3171	0.3192
Muon scale %	0.0790	0.0792	0.0505	0.0811	0.0631	0.0670	0.0817	0.0693	0.0575	0.0582	0.0689	0.0605	0.0525	0.0569	0.0552	0.0548	0.0563	0.0484	0.0371	0.0433	0.0287	0.0429	0.0444	0.0417	0.0473	0.0300	0.0174	0.0368	0.0288	0.0320
Muon resolution %	0.0371	0.0300	0.0087	0.0055	0.0294	0.0159	0.0196	0.0221	0.0247	0.0240	0.0139	0.0091	0.0216	0.0178	0.0204	0.0227	0.0110	0.0058	0.0275	0.0084	0.0175	0.0231	0.0091	0.0177	0.0392	0.0119	0.0142	0.0025	0.0074	0.0176
Muon reconstruction efficiency %	0.2195	0.2184	0.2196	0.2208	0.2195	0.2198	0.2201	0.2208	0.2193	0.2195	0.2220	0.2232	0.2210	0.2235	0.2206	0.2227	0.2229	0.2238	0.2242	0.2256	0.2231	0.2279	0.2251	0.2240	0.2231	0.2259	0.2245	0.2273	0.2252	0.2272
Muon trigger efficiency %	0.0697	0.0707	0.0693	0.0687	0.0681	0.0673	0.0672	0.0660	0.0654	0.0641	0.0634	0.0619	0.0602	0.0591	0.0574	0.0559	0.0540	0.0517	0.0505	0.0489	0.0472	0.0449	0.0426	0.0411	0.0403	0.0390	0.0380	0.0368	0.0360	0.0367
Muon ISO efficiency %	0.2659	0.2663	0.2681	0.2677	0.2669	0.2657	0.2665	0.2666	0.2669	0.2670	0.2672	0.2669	0.2661	0.2661	0.2657	0.2659	0.2650	0.2651	0.2655	0.2643	0.2632	0.2617	0.2603	0.2596	0.2600	0.2587	0.2574	0.2578	0.2561	0.2552
Muon TTVA efficiency %	0.0220	0.0220	0.0221	0.0223	0.0223	0.0222	0.0221	0.0222	0.0221	0.0222	0.0222	0.0221	0.0220	0.0220	0.0220	0.0220	0.0220	0.0220	0.0220	0.0220	0.0219	0.0219	0.0219	0.0219	0.0219	0.0219	0.0219	0.0220	0.0219	0.0218
JVT %	0.0165	0.0208	0.0222	0.0239	0.0289	0.0168	0.0242	0.0268	0.0247	0.0318	0.0267	0.0239	0.0209	0.0285	0.0246	0.0215	0.0255	0.0279	0.0313	0.0351	0.0244	0.0320	0.0357	0.0376	0.0363	0.0356	0.0313	0.0391	0.0356	0.0361
JES b-jes response %	0.0368	0.0665	0.0435	0.0055	0.0233	0.0243	0.0144	0.0137	0.0223	0.0199	0.0145	0.0156	0.0113	0.0072	0.0274	0.0127	0.0360	0.0333	0.0584	0.0225	0.0689	0.0753	0.0929	0.0807	0.0918	0.0950	0.1044	0.0868	0.0729	0.1050
JES effective NPs %	0.0097	0.0604	0.0436	0.0206	0.0203	0.0107	0.0328	0.0345	0.0425	0.0255	0.0235	0.0306	0.0160	0.0196	0.0058	0.0290	0.0454	0.0212	0.0148	0.0296	0.0280	0.0110	0.0449	0.0871	0.0556	0.0286	0.0299	0.0277	0.0430	0.0476
JES EtaInterCalibration %	0.0111	0.0055	0.0148	0.0139	0.0066	0.0241	0.0201	0.0220	0.0213	0.0126	0.0010	0.0080	0.0080	0.0177	0.0181	0.0101	0.0034	0.0194	0.0153	0.0098	0.0120	0.0083	0.0219	0.1220	0.0366	0.0103	0.0033	0.0150	0.0187	0.0268
JES flavour %	0.0169	0.0150	0.0292	0.0011	0.0161	0.0244	0.0348	0.0305	0.0275	0.0404	0.0531	0.0121	0.0267	0.0530	0.0290	0.0676	0.0166	0.0571	0.0809	0.0641	0.0652	0.1087	0.0955	0.2145	0.0576	0.1145	0.0987	0.0916	0.0694	0.1063
JES pileup %	0.0344	0.0503	0.0450	0.0204	0.0134	0.0137	0.0580	0.0450	0.0590	0.0374	0.0422	0.0233	0.0234	0.0365	0.0114	0.0345	0.0327	0.0415	0.0091	0.0376	0.0155	0.0142	0.0358	0.1896	0.0440	0.0288	0.0207	0.0195	0.0325	0.0323
JES PunchThrough %	0.0000	0.0000	0.0000	0.0000	0.0007	0.0000	0.0002	0.0000	0.0006	0.0000	0.0000	0.0000	0.0000	0.0000	0.0010	0.0000	0.0010	0.0003	0.0003	0.0000	0.0003	0.0000	0.0004	0.0000	0.0000	0.0005	0.0000	0.0007	0.0005	0.0012
JES HighPt %	0.0000	0.0000	0.0000	0.0000	0.0000	0.0000	0.0000	0.0000	0.0000	0.0000	0.0000	0.0000	0.0000	0.0000	0.0000	0.0000	0.0000	0.0000	0.0000	0.0000	0.0000	0.0000	0.0000	0.0000	0.0000	0.0000	0.0000	0.0000	0.0000	0.0000
MET soft term %	0.0000	0.0000	0.0000	0.0000	0.0000	0.0000	0.0000	0.0000	0.0000	0.0000	0.0000	0.0000	0.0000	0.0000	0.0000	0.0000	0.0000	0.0000	0.0000	0.0000	0.0000	0.0000	0.0000	0.0000	0.0000	0.0000	0.0000	0.0000	0.0000	0.0000
JER %	0.0009	0.0000	0.0000	0.0000	0.0000	0.0000	0.0000	0.0000	0.0000	0.0000	0.0000	0.0000	0.0000	0.0000	0.0000	0.0000	0.0000	0.0000	0.0000	0.0000	0.0000	0.0000	0.0000	0.0000	0.0000	0.0000	0.0000	0.0000	0.0000	0.0000
b-tagging %	0.1319	0.0971	0.1118	0.1109	0.0990	0.1099	0.0965	0.1021	0.0991	0.0946	0.1043	0.0957	0.0989	0.0942	0.0848	0.0905	0.1059	0.0959	0.0868	0.0879	0.0824	0.0889	0.0865	0.1071	0.0971	0.0974	0.1084	0.0907	0.1290	0.0894
Wt cross section %	0.4417	0.4478	0.4666	0.4888	0.4754	0.4565	0.4650	0.4723	0.4791	0.4929	0.4890	0.4885	0.4927	0.4922	0.4999	0.5099	0.5155	0.5270	0.5357	0.5286	0.5239	0.5253	0.5218	0.5419	0.5560	0.5544	0.5476	0.5467	0.5419	0.5204
Wt/$t\bar{t}$ interference %	0.1064	0.1884	0.0311	0.8775	0.1332	0.0997	0.3885	0.0181	0.4843	0.4927	0.4618	0.4569	0.3536	0.2023	0.3649	0.5956	0.1945	0.7534	0.4953	0.3295	0.2033	0.1241	0.0769	0.4861	0.5494	0.4787	0.4556	0.5083	0.2679	0.4447
Wt hard scattering %	0.4710	0.2059	0.2509	0.8113	0.3297	0.2282	0.4067	0.6928	0.3047	0.0558	0.1912	0.3522	0.0598	0.0822	0.1502	0.2983	0.1306	0.0216	0.2432	0.0035	0.0627	0.2827	0.5477	0.9956	0.7245	0.0785	0.4300	0.1926	0.6673	0.3456
Wt fragmentation %	0.1351	0.0712	0.4685	0.7269	0.7529	0.0600	0.2239	0.2080	0.5079	0.5553	0.3574	0.1065	0.3472	0.0875	0.2339	0.3002	0.0314	0.2773	0.3609	0.3354	0.3604	0.3194	0.0174	0.3928	0.2135	0.2125	0.2220	0.2665	0.2100	0.1293
Wt ISR %	0.0525	0.1197	0.0458	0.0242	0.0568	0.0951	0.0801	0.0406	0.0803	0.0049	0.0385	0.0142	0.0866	0.0124	0.0238	0.0333	0.0056	0.0261	0.0156	0.0176	0.0010	0.0520	0.0703	0.0077	0.0430	0.0325	0.0134	0.0164	0.0172	0.0056
Wt FSR %	0.2622	0.1109	0.3270	0.2202	0.4814	0.2535	0.1163	0.1335	0.1260	0.1941	0.1388	0.2081	0.0714	0.0528	0.0947	0.2006	0.1932	0.1248	0.0813	0.0790	0.2167	0.1881	0.1296	0.3309	0.0079	0.2761	0.2647	0.3593	0.1741	0.2343
Diboson cross section %	0.0262	0.0281	0.0267	0.0234	0.0268	0.0234	0.0237	0.0230	0.0246	0.0210	0.0217	0.0218	0.0231	0.0212	0.0202	0.0194	0.0217	0.0195	0.0193	0.0224	0.0183	0.0191	0.0178	0.0192	0.0189	0.0224	0.0209	0.0223	0.0205	0.0206
Diboson scale %	0.0542	0.0545	0.0542	0.0543	0.0549	0.0540	0.0533	0.0539	0.0533	0.0529	0.0527	0.0523	0.0517	0.0515	0.0511	0.0508	0.0507	0.0500	0.0492	0.0494	0.0492	0.0482	0.0482	0.0487	0.0479	0.0478	0.0477	0.0481	0.0479	0.0477
ttV background %	0.0331	0.0339	0.0336	0.0322	0.0317	0.0322	0.0337	0.0318	0.0328	0.0321	0.0308	0.0327	0.0301	0.0301	0.0311	0.0296	0.0314	0.0301	0.0322	0.0315	0.0303	0.0304	0.0309	0.0320	0.0320	0.0314	0.0336	0.0332	0.0316	0.0332
Z modelling %	0.1968	0.1757	0.0167	0.1191	0.1517	0.1487	0.4145	0.1759	0.0934	0.0275	0.1492	0.1774	0.0390	0.0203	0.1979	0.1789	0.0035	0.1538	0.1860	0.2007	0.1467	0.0035	0.0512	0.2047	0.0052	0.0012	0.0164	0.1999	0.0493	0.0489
Z factor %	0.0178	0.0186	0.0168	0.0167	0.0163	0.0193	0.0256	0.0192	0.0238	0.0249	0.0294	0.0275	0.0163	0.0205	0.0187	0.0198	0.0103	0.0140	0.0267	0.0219	0.0297	0.0156	0.0175	0.0079	0.0146	0.0076	0.0083	0.0213	0.0037	0.0081
Fakes background %	0.5367	0.3782	0.4450	0.3964	0.3512	0.4444	0.3617	0.3309	0.5382	0.4291	0.4027	0.4511	0.4709	0.4815	0.3747	0.3157	0.3523	0.2751	0.3476	0.3981	0.3538	0.3972	0.3451	0.4095	0.3744	0.3457	0.3335	0.2618	0.3217	0.3435
Pileup %	0.7526	0.7635	0.8673	0.8426	0.8365	0.9020	0.9204	0.8446	0.8219	0.7031	0.7732	0.8370	0.7907	0.8146	0.6991	0.7290	0.5876	0.5940	0.5532	0.5588	0.7293	0.6271	0.7290	0.6688	0.5812	0.6548	0.6099	0.5260	0.5586	0.5068
Beam energy %	0.0316	0.1083	0.0020	0.0350	0.0590	0.0086	0.0085	0.0303	0.0653	0.0259	0.0332	0.0054	0.0698	0.0035	0.0442	0.0005	0.0066	0.0461	0.0380	0.0301	0.0001	0.0105	0.0434	0.0065	0.0493	0.0210	0.0465	0.0176	0.0364	0.0006
Luminosity %	1.8862	1.8805	1.8884	1.8933	1.8838	1.8868	1.8864	1.8843	1.9019	1.8991	1.8985	1.9015	1.9004	1.9015	1.8962	1.8954	1.8975	1.8984	1.9104	1.9115	1.9074	1.9065	1.9025	1.9109	1.9152	1.9119	1.9090	1.9089	1.9047	1.9013

Table 13: Normalised differential cross section for p_{T} (ℓ) with detailed systematic uncertainties.

p_{T} (ℓ) bins [GeV]	25.0-30.0	30.0-40.0	40.0-50.0	50.0-60.0	60.0-75.0	75.0-100.0	100.0-140.0	140.0-180.0	180.0 250.0	250.0 350.0
Normalised cross section [10^{-3}/GeV]	21.8802	20.5197	16.8920	13.1182	9.3423	5.1520	1.9746	0.6108	0.1506	0.0241
Data statistics %	0.3467	0.2353	0.2584	0.2889	0.2639	0.2691	0.3747	0.6991	1.0149	2.3567
MC statistics %	0.1083	0.0684	0.0659	0.0765	0.0720	0.0774	0.0968	0.1894	0.3064	0.7071
Fragmentation %	0.8667	0.2176	0.2888	0.1228	0.0987	0.2770	0.9230	1.3426	1.3711	1.0303
Hard scattering %	1.0372	0.3605	0.0861	0.0160	0.1339	0.1529	1.2058	1.3478	3.0913	3.7922
top pT %	0.0067	0.0206	0.0110	0.0005	0.0180	0.0216	0.0177	0.0094	0.0121	0.1207
Top mass dependence %	0.0197	0.0022	0.0064	0.0241	0.0012	0.0058	0.0196	0.1161	0.0914	0.1235
PDF %	0.0142	0.0096	0.0059	0.0023	0.0047	0.0100	0.0183	0.0321	0.0485	0.0581
ISR %	0.0040	0.0032	0.0280	0.0431	0.0202	0.0831	0.0440	0.0311	0.1038	0.4652
FSR %	0.0180	0.1100	0.0679	0.0295	0.1396	0.0029	0.0862	0.4987	0.0265	0.2278
Electron scale %	0.0123	0.0135	0.1046	0.1619	0.1394	0.0233	0.3088	0.7471	1.1865	2.0186
Electron resolution %	0.0635	0.0135	0.0193	0.0196	0.0176	0.0016	0.0041	0.0264	0.0183	0.0576
Electron trigger efficiency %	0.0451	0.0005	0.0105	0.0097	0.0107	0.0032	0.0008	0.0007	0.0002	0.0053
Electron reconstruction efficiency %	0.0792	0.0156	0.0349	0.0246	0.0101	0.0140	0.0252	0.0303	0.0387	0.0638
Electron ISO efficiency %	0.0164	0.0082	0.0185	0.0159	0.0110	0.0106	0.0214	0.0798	0.1012	0.2346
Electron ID efficiency %	0.4445	0.1548	0.1022	0.1069	0.1343	0.1570	0.2375	0.3515	0.4440	2.3290
Muon scale %	0.0396	0.0325	0.0135	0.0005	0.0154	0.0255	0.0597	0.0699	0.1013	0.1716
Muon resolution %	0.0215	0.0104	0.0053	0.0081	0.0108	0.0082	0.0049	0.0195	0.0622	0.2470
Muon reconstruction efficiency %	0.0055	0.0030	0.0023	0.0014	0.0003	0.0025	0.0077	0.0158	0.0266	0.0680
Muon trigger efficiency %	0.0977	0.0067	0.0056	0.0112	0.0222	0.0247	0.0277	0.0308	0.0331	0.0338
Muon ISO efficiency %	0.0064	0.0111	0.0178	0.0632	0.0211	0.0203	0.0188	0.0173	0.0274	0.0656
Muon TTVA efficiency %	0.0084	0.0029	0.0016	0.0005	0.0005	0.0004	0.0004	0.0008	0.0018	0.0050
JVT %	0.0021	0.0015	0.0028	0.0028	0.0015	0.0021	0.0046	0.0078	0.0188	0.0620
JES b-jes response %	0.0083	0.0034	0.0045	0.0001	0.0029	0.0010	0.0114	0.0015	0.0034	0.0330
JES effective NPs %	0.0111	0.0107	0.0094	0.0171	0.0084	0.0122	0.0306	0.0436	0.0698	0.1166
JES EtaInterCalibration %	0.0235	0.0050	0.0035	0.0140	0.0024	0.0015	0.0085	0.0224	0.0110	0.0515
JES flavour %	0.0109	0.0244	0.0235	0.0266	0.0094	0.0259	0.0586	0.0896	0.1459	0.2151
JES pileup %	0.0599	0.0118	0.0123	0.0180	0.0128	0.0170	0.0379	0.0604	0.0807	0.1362
JES PunchThrough %	0.0001	0.0002	0.0000	0.0000	0.0001	0.0001	0.0001	0.0006	0.0003	0.0000
JES HighPt %	0.0000	0.0000	0.0000	0.0000	0.0000	0.0000	0.0000	0.0000	0.0000	0.0000
MET soft term %	0.0000	0.0000	0.0000	0.0000	0.0000	0.0000	0.0000	0.0000	0.0000	0.0000
JER %	0.0001	0.0000	0.0000	0.0000	0.0000	0.0000	0.0000	0.0000	0.0000	0.0000
b-tagging %	0.0169	0.0252	0.0115	0.0121	0.0127	0.0177	0.0324	0.0766	0.1042	0.2198
Wt cross section %	0.0332	0.0341	0.0283	0.0205	0.0169	0.0111	0.0795	0.2149	0.4389	1.2006
Wt/$t\bar{t}$ interference %	0.1555	0.2891	0.2561	0.1949	0.1830	0.1381	0.6177	1.5614	3.5534	11.8915
Wt hard scattering %	0.0732	0.0574	0.0772	0.0630	0.0020	0.0786	0.0488	0.1809	0.0260	0.0930
Wt fragmentation %	0.1108	0.0029	0.0394	0.0048	0.1037	0.0191	0.0536	0.1378	0.2515	0.2088
Wt ISR %	0.0561	0.0539	0.0530	0.0417	0.0172	0.0272	0.1379	0.2728	0.6606	2.5033
Wt FSR %	0.0041	0.0286	0.0660	0.0060	0.0568	0.0409	0.0597	0.0918	0.2244	0.0744
Diboson cross section %	0.0018	0.0019	0.0017	0.0024	0.0019	0.0001	0.0048	0.0155	0.0364	0.1230
Diboson scale %	0.0451	0.0005	0.0105	0.0097	0.0107	0.0032	0.0008	0.0007	0.0002	0.0053
ttV background %	0.0049	0.0046	0.0037	0.0029	0.0011	0.0028	0.0108	0.0248	0.0495	0.1228
Z modelling %	0.0049	0.0468	0.0089	0.0590	0.0193	0.0173	0.0261	0.0502	0.0255	0.1197
Z factor %	0.0289	0.0151	0.0005	0.0095	0.0104	0.0139	0.0143	0.0141	0.0151	0.0169
Fakes background %	0.0592	0.0112	0.0253	0.0127	0.0185	0.0105	0.0139	0.0797	0.1586	0.4678
Pileup %	0.3124	0.1962	0.1559	0.0341	0.1809	0.2457	0.3224	0.3089	0.4818	0.4986
Beam energy %	0.0048	0.0048	0.0012	0.0009	0.0003	0.0052	0.0086	0.0141	0.0153	0.0342
Luminosity %	0.0016	0.0069	0.0121	0.0117	0.0107	0.0011	0.0237	0.0757	0.1579	0.4444

Table 14: Normalised differential cross section for $|\eta(\ell)|$ with detailed systematic uncertainties.

$\lvert\eta(\ell)\rvert$ bins	0.0-0.08	0.08-0.17	0.17-0.25	0.25-0.33	0.33-0.42	0.42-0.50	0.50-0.58	0.58-0.67	0.67-0.75	0.75-0.83	0.83-0.92	0.92-1.00	1.00-1.08	1.08-1.17
Normalised cross section $[10^{-2}/\text{unit } \lvert\eta\rvert]$	60.9466	60.3770	60.5925	60.4326	58.6592	58.3639	56.8164	55.2806	54.3470	52.3767	50.9353	48.5985	46.5523	44.9804
Data statistics %	0.8517	0.7398	0.7400	0.7359	0.7436	0.7193	0.7605	0.7426	0.7572	0.8128	0.8059	0.8401	0.8358	0.8754
MC statistics %	0.1419	0.1510	0.1311	0.1373	0.1267	0.1290	0.1224	0.1300	0.1387	0.1367	0.1352	0.1524	0.1601	0.1509
Fragmentation %	0.2212	0.1464	0.1269	0.8464	0.3210	0.2933	0.1772	1.3856	0.0349	0.8416	1.8808	0.5037	1.5240	2.9511
Hard scattering %	0.1064	0.1454	0.0211	1.0798	0.1419	0.3716	0.5747	1.3209	0.0639	0.6683	1.6166	0.2611	0.7954	2.9332
top pT %	0.0392	0.0417	0.0154	0.0192	0.0163	0.0125	0.0136	0.0042	0.0167	0.0267	0.0025	0.0190	0.0153	0.0047
Top mass dependence %	0.0046	0.0125	0.0395	0.0120	0.0118	0.0369	0.0024	0.0369	0.0281	0.0727	0.0107	0.0123	0.0133	0.0194
PDF %	0.0120	0.0103	0.0104	0.0098	0.0088	0.0097	0.0084	0.0090	0.0084	0.0099	0.0086	0.0073	0.0059	0.0064
ISR %	0.0106	0.0398	0.1440	0.1657	0.0853	0.0784	0.1090	0.0438	0.0592	0.1865	0.0405	0.0919	0.1004	0.1105
FSR %	0.2547	0.1654	0.1248	0.2614	0.0686	0.0216	0.2809	0.0106	0.3800	0.2992	0.1217	0.0249	0.1137	0.2033
Electron scale %	0.0487	0.0325	0.0341	0.0297	0.0355	0.0313	0.0363	0.0218	0.0251	0.0178	0.0134	0.0172	0.0073	0.0080
Electron resolution %	0.0036	0.0041	0.0071	0.0034	0.0047	0.0040	0.0025	0.0006	0.0081	0.0004	0.0027	0.0034	0.0021	0.0019
Electron trigger efficiency %	0.0226	0.0041	0.0113	0.0111	0.0075	0.0094	0.0136	0.0018	0.0141	0.0052	0.0028	0.0117	0.0060	0.0046
Electron reconstruction efficiency %	0.0255	0.0083	0.0178	0.0182	0.0184	0.0183	0.0171	0.0001	0.0045	0.0004	0.0067	0.0070	0.0072	0.0035
Electron ISO efficiency %	0.0275	0.0072	0.0170	0.0175	0.0176	0.0176	0.0168	0.0013	0.0034	0.0009	0.0072	0.0077	0.0074	0.0043
Electron ID efficiency %	0.1209	0.0601	0.0527	0.0535	0.0541	0.0537	0.0532	0.0931	0.1125	0.1082	0.1060	0.1067	0.1101	0.1034
Muon scale %	0.0121	0.0149	0.0096	0.0091	0.0108	0.0093	0.0110	0.0096	0.0153	0.0087	0.0022	0.0010	0.0040	0.0156
Muon resolution %	0.0110	0.0100	0.0043	0.0064	0.0034	0.0029	0.0129	0.0055	0.0026	0.0070	0.0062	0.0053	0.0082	0.0103
Muon reconstruction efficiency %	0.3046	0.1125	0.0149	0.0143	0.0154	0.0222	0.0217	0.0220	0.0188	0.0177	0.0186	0.0174	0.0126	0.0136
Muon trigger efficiency %	0.0120	0.0097	0.0071	0.0069	0.0077	0.0070	0.0058	0.0041	0.0072	0.0062	0.0033	0.0076	0.0066	0.0053
Muon ISO efficiency %	0.0010	0.0005	0.0005	0.0008	0.0005	0.0005	0.0004	0.0003	0.0003	0.0002	0.0001	0.0003	0.0008	0.0002
Muon TTVA efficiency %	0.0041	0.0053	0.0020	0.0012	0.0012	0.0012	0.0012	0.0006	0.0005	0.0005	0.0008	0.0008	0.0011	0.0011
JVT %	0.0023	0.0032	0.0017	0.0015	0.0046	0.0016	0.0021	0.0009	0.0018	0.0020	0.0015	0.0020	0.0023	0.0008
JES b-jes response %	0.0042	0.0003	0.0077	0.0008	0.0009	0.0003	0.0045	0.0100	0.0276	0.0000	0.0083	0.0008	0.0157	0.0042
JES effective NPs %	0.0063	0.0090	0.0120	0.0061	0.0133	0.0117	0.0088	0.0031	0.0209	0.0304	0.0071	0.0072	0.0217	0.0113
JES EtaInterCalibration %	0.0165	0.0065	0.0047	0.0134	0.0056	0.0107	0.0096	0.0050	0.0225	0.0325	0.0059	0.0099	0.0419	0.0160
JES flavour %	0.0044	0.0059	0.0039	0.0056	0.0086	0.0136	0.0039	0.0099	0.0024	0.0333	0.0090	0.0023	0.0511	0.0291
JES pileup %	0.0088	0.0049	0.0115	0.0044	0.0094	0.0203	0.0148	0.0113	0.0208	0.0472	0.0110	0.0089	0.0314	0.0163
JES PunchThrough %	0.0000	0.0002	0.0001	0.0002	0.0002	0.0001	0.0002	0.0001	0.0002	0.0002	0.0000	0.0001	0.0000	0.0001
JES HighPt %	0.0000	0.0000	0.0000	0.0000	0.0000	0.0000	0.0000	0.0000	0.0000	0.0000	0.0000	0.0000	0.0000	0.0000
MET soft term %	0.0000	0.0000	0.0000	0.0000	0.0000	0.0000	0.0000	0.0000	0.0000	0.0000	0.0000	0.0000	0.0000	0.0000
JER %	0.0000	0.0000	0.0000	0.0000	0.0001	0.0001	0.0000	0.0001	0.0000	0.0000	0.0000	0.0000	0.0000	0.0000
b-tagging %	0.0167	0.0190	0.0384	0.0079	0.0143	0.0253	0.0126	0.0077	0.0107	0.0199	0.0122	0.0092	0.0397	0.0138
Wt cross section %	0.0114	0.0230	0.0175	0.0106	0.0164	0.0142	0.0122	0.0150	0.0139	0.0134	0.0085	0.0056	0.0126	0.0013
Wt/$t\bar{t}$ interference %	0.1722	0.0258	0.0147	0.0087	0.0582	0.0998	0.0344	0.0095	0.1206	0.0310	0.1856	0.1825	0.0925	0.0501
Wt hard scattering %	0.1882	0.0209	0.0867	0.0266	0.0249	0.1086	0.1654	0.1526	0.0413	0.0226	0.1477	0.1311	0.3005	0.0211
Wt fragmentation %	0.0981	0.0873	0.1029	0.0381	0.0038	0.0312	0.0385	0.1597	0.0781	0.0695	0.1309	0.1016	0.2741	0.1881
Wt ISR %	0.0103	0.0135	0.0142	0.0219	0.0073	0.0054	0.0317	0.0119	0.0045	0.0058	0.0150	0.0216	0.0073	0.0409
Wt FSR %	0.0091	0.0722	0.0028	0.0561	0.0097	0.0245	0.0104	0.0667	0.1117	0.0430	0.0675	0.0093	0.0119	0.0452
Diboson cross section %	0.0038	0.0043	0.0040	0.0040	0.0024	0.0036	0.0026	0.0031	0.0018	0.0017	0.0018	0.0011	0.0000	0.0006
Diboson scale %	0.0226	0.0041	0.0113	0.0111	0.0075	0.0094	0.0136	0.0018	0.0141	0.0052	0.0028	0.0117	0.0060	0.0046
ttV background %	0.0004	0.0003	0.0009	0.0011	0.0009	0.0012	0.0008	0.0005	0.0007	0.0003	0.0001	0.0004	0.0008	0.0003
Z modelling %	0.0366	0.0064	0.0448	0.0386	0.0634	0.1278	0.0912	0.1099	0.1083	0.0730	0.0354	0.0122	0.0163	0.0164
Z factor %	0.0035	0.0001	0.0051	0.0002	0.0031	0.0045	0.0023	0.0024	0.0014	0.0033	0.0044	0.0000	0.0031	0.0005
Fakes background %	0.1039	0.1060	0.1093	0.0967	0.1177	0.1148	0.0743	0.0939	0.0841	0.0920	0.0852	0.0452	0.0689	0.0528
Pileup %	0.0578	0.0192	0.0348	0.0228	0.0213	0.0296	0.0809	0.0394	0.0436	0.0145	0.0582	0.1247	0.0063	0.0358
Beam energy %	0.0093	0.0189	0.0161	0.0032	0.0145	0.0212	0.0180	0.0269	0.0092	0.0147	0.0019	0.0182	0.0087	0.0298
Luminosity %	0.0056	0.0010	0.0049	0.0044	0.0043	0.0059	0.0028	0.0016	0.0023	0.0034	0.0048	0.0015	0.0005	0.0041

$\lvert\eta(\ell)\rvert$ bins	1.17-1.25	1.25-1.33	1.33-1.42	1.42-1.50	1.50-1.58	1.58-1.67	1.67-1.75	1.75-1.83	1.83-1.92	1.92-2.00	2.00-2.08	2.08-2.17	2.17-2.25	2.25-2.33	2.33-2.42	2.45-2.50
Normalised cross section $[10^{-2}/\text{unit } \lvert\eta\rvert]$	43.3271	40.9737	38.9098	36.4249	34.1782	32.4407	29.7816	27.1552	25.4233	23.0463	21.8398	19.6170	17.4347	14.8490	13.4743	11.8655
Data statistics %	0.9072	0.9348	1.0610	1.3209	1.0610	1.0335	1.0628	1.1775	1.2621	1.2952	1.3808	1.4250	1.5677	1.7478	1.8557	2.4967
MC statistics %	0.1525	0.1636	0.1922	0.2561	0.1922	0.1830	0.2191	0.2101	0.2190	0.2456	0.2459	0.2621	0.2696	0.3168	0.3361	0.3982
Fragmentation %	0.2546	1.1301	1.5051	0.6132	4.2198	1.9626	3.7229	0.7506	0.4008	0.2511	0.1719	0.5478	0.1480	1.1709	1.7046	4.1040
Hard scattering %	0.8585	0.9193	1.6635	1.3234	5.0028	2.6049	3.0019	0.0301	0.6481	0.5023	0.7364	1.2373	1.7896	0.8780	0.4898	4.1275
top pT %	0.0077	0.0005	0.0073	0.0350	0.0202	0.0138	0.0326	0.0538	0.0353	0.0471	0.0527	0.0554	0.0817	0.0757	0.1007	0.0419
Top mass dependence %	0.0247	0.0529	0.0436	0.0009	0.0173	0.0076	0.0067	0.0049	0.0405	0.0171	0.0010	0.0040	0.0000	0.0512	0.1136	0.0291
PDF %	0.0093	0.0079	0.0298	0.0693	0.0135	0.0155	0.0221	0.0254	0.0342	0.0349	0.0390	0.0441	0.0545	0.0597	0.0735	0.0444
ISR %	0.1696	0.1773	0.0141	0.3152	0.2291	0.5057	0.1868	0.0223	0.1420	0.1130	0.1875	0.0039	0.2246	0.1824	0.1628	0.0917
FSR %	0.1113	0.1109	0.0127	0.2800	0.4594	0.4697	0.1249	0.1871	0.1941	0.0221	0.1833	0.6387	0.1280	0.2716	0.0407	0.4044
Electron scale %	0.0275	0.0534	0.0225	0.0133	0.0946	0.0933	0.0697	0.0594	0.0177	0.0219	0.0297	0.0193	0.0258	0.0098	0.0789	0.2627
Electron resolution %	0.0032	0.0106	0.0104	0.0011	0.0014	0.0021	0.0015	0.0049	0.0035	0.0176	0.0229	0.0018	0.0062	0.0440	0.0331	0.0094
Electron trigger efficiency %	0.0090	0.0100	0.0114	0.0181	0.0033	0.0020	0.0044	0.0001	0.0088	0.0115	0.0036	0.0026	0.0027	0.0022	0.0373	0.0891
Electron reconstruction efficiency %	0.0064	0.0068	0.0038	0.0004	0.0156	0.0184	0.0181	0.0194	0.0224	0.0224	0.0089	0.0074	0.0076	0.0074	0.0230	0.0270
Electron ISO efficiency %	0.0066	0.0069	0.0035	0.0007	0.0064	0.0073	0.0069	0.0113	0.0241	0.0239	0.0127	0.0114	0.0110	0.0103	0.0482	0.0642
Electron ID efficiency %	0.1083	0.1082	0.0628	0.0097	0.1932	0.2351	0.2294	0.2383	0.2491	0.2517	0.3557	0.3887	0.3729	0.3612	0.3879	0.4262
Muon scale %	0.0079	0.0011	0.0080	0.0003	0.0167	0.0199	0.0104	0.0019	0.0021	0.0108	0.0125	0.0116	0.0165	0.0435	0.0822	0.0869
Muon resolution %	0.0115	0.0029	0.0042	0.0206	0.0045	0.0073	0.0113	0.0163	0.0129	0.0173	0.0074	0.0161	0.0179	0.0146	0.0354	0.0148
Muon reconstruction efficiency %	0.0146	0.0228	0.0534	0.0763	0.0464	0.0316	0.0302	0.0305	0.0314	0.0312	0.0289	0.0299	0.0290	0.0298	0.0300	0.0344
Muon trigger efficiency %	0.0060	0.0063	0.0073	0.0108	0.0111	0.0124	0.0135	0.0148	0.0151	0.0152	0.0138	0.0141	0.0153	0.0158	0.0205	0.0244
Muon ISO efficiency %	0.0003	0.0001	0.0004	0.0009	0.0007	0.0004	0.0008	0.0009	0.0007	0.0007	0.0008	0.0008	0.0011	0.0019	0.0023	0.0039
Muon TTVA efficiency %	0.0010	0.0011	0.0016	0.0025	0.0015	0.0010	0.0009	0.0007	0.0003	0.0003	0.0010	0.0011	0.0010	0.0014	0.0015	0.0019
JVT %	0.0034	0.0016	0.0002	0.0010	0.0020	0.0041	0.0014	0.0020	0.0062	0.0049	0.0055	0.0063	0.0051	0.0082	0.0033	0.0019
JES b-jes response %	0.0009	0.0107	0.0097	0.0072	0.0134	0.0222	0.0016	0.0121	0.0152	0.0206	0.0069	0.0253	0.0154	0.0202	0.0046	0.0441
JES effective NPs %	0.0123	0.0120	0.0386	0.0243	0.0074	0.0279	0.0101	0.0347	0.0117	0.0074	0.0326	0.0242	0.0128	0.0069	0.0689	0.0802
JES EtaInterCalibration %	0.0110	0.0210	0.0240	0.0125	0.0085	0.0240	0.0155	0.0052	0.0237	0.0251	0.0047	0.0234	0.0024	0.0050	0.0244	0.0509
JES flavour %	0.0224	0.0341	0.0608	0.0135	0.0143	0.0552	0.0190	0.0341	0.0235	0.0049	0.0267	0.0110	0.0162	0.0299	0.0601	0.0583
JES pileup %	0.0174	0.0319	0.0744	0.0077	0.0240	0.0582	0.0134	0.0340	0.0097	0.0139	0.0390	0.0274	0.0177	0.0146	0.0699	0.0737
JES PunchThrough %	0.0001	0.0002	0.0001	0.0002	0.0002	0.0000	0.0005	0.0001	0.0001	0.0002	0.0009	0.0000	0.0007	0.0005	0.0000	0.0009
JES HighPt %	0.0000	0.0000	0.0000	0.0000	0.0000	0.0000	0.0000	0.0000	0.0000	0.0000	0.0000	0.0000	0.0000	0.0000	0.0000	0.0000
MET soft term %	0.0000	0.0000	0.0000	0.0000	0.0000	0.0000	0.0000	0.0000	0.0000	0.0000	0.0000	0.0000	0.0000	0.0000	0.0000	0.0000
JER %	0.0001	0.0000	0.0001	0.0002	0.0000	0.0000	0.0001	0.0000	0.0000	0.0000	0.0000	0.0003	0.0000	0.0001	0.0000	0.0000
b-tagging %	0.0074	0.0117	0.0175	0.0405	0.0274	0.0261	0.0654	0.0176	0.0243	0.0267	0.0205	0.0447	0.0459	0.0352	0.0389	0.0892
Wt cross section %	0.0123	0.0024	0.0154	0.0104	0.0119	0.0277	0.0277	0.0177	0.0303	0.0318	0.0499	0.0425	0.0445	0.0339	0.0316	0.0365
Wt/$t\bar{t}$ interference %	0.1108	0.0277	0.0228	0.1654	0.0375	0.0003	0.0039	0.0140	0.1291	0.0646	0.0697	0.1182	0.0231	0.0004	0.0852	0.0431
Wt hard scattering %	0.0754	0.0967	0.0289	0.2427	0.5372	0.0627	0.7157	0.2932	0.0490	0.1912	0.0512	0.2299	0.2188	0.6275	0.4852	0.1546
Wt fragmentation %	0.0758	0.0088	0.2721	0.1262	0.4451	0.2431	0.3546	0.0895	0.0154	0.1523	0.0132	0.1273	0.1004	0.1526	0.1751	0.2235
Wt ISR %	0.0122	0.0251	0.0237	0.0049	0.0076	0.0143	0.0007	0.0097	0.0099	0.0329	0.0017	0.0442	0.0277	0.0567	0.0386	0.0129
Wt FSR %	0.0937	0.0748	0.1349	0.0350	0.0665	0.1081	0.0298	0.0352	0.0860	0.0722	0.0380	0.1435	0.1134	0.1343	0.0250	0.0016
Diboson cross section %	0.0007	0.0000	0.0001	0.0003	0.0031	0.0037	0.0039	0.0056	0.0059	0.0077	0.0089	0.0094	0.0118	0.0130	0.0168	0.0183
Diboson scale %	0.0090	0.0100	0.0114	0.0181	0.0033	0.0020	0.0044	0.0001	0.0088	0.0115	0.0036	0.0026	0.0027	0.0022	0.0373	0.0891
ttV background %	0.0005	0.0002	0.0005	0.0010	0.0011	0.0002	0.0011	0.0024	0.0000	0.0001	0.0003	0.0001	0.0016	0.0040	0.0031	0.0014
Z modelling %	0.0841	0.1109	0.0066	0.1176	0.0113	0.1213	0.2241	0.0050	0.0427	0.0137	0.1391	0.0185	0.2139	0.1740	0.1132	0.3826
Z factor %	0.0023	0.0063	0.0026	0.0048	0.0037	0.0069	0.0135	0.0003	0.0042	0.0012	0.0052	0.0033	0.0081	0.0088	0.0086	0.0250
Fakes background %	0.0143	0.0330	0.0158	0.0361	0.1132	0.1916	0.2873	0.3318	0.3931	0.4203	0.3443	0.1871	0.2566	0.2732	0.2032	0.1630
Pileup %	0.0341	0.0061	0.0159	0.0137	0.0604	0.0481	0.0065	0.0536	0.0323	0.0273	0.0467	0.0174	0.0708	0.0236	0.1270	0.0864
Beam energy %	0.0046	0.0039	0.0393	0.0261	0.0031	0.0234	0.0011	0.0133	0.0335	0.0058	0.0069	0.0243	0.0048	0.0179	0.0507	0.0254
Luminosity %	0.0041	0.0051	0.0056	0.0032	0.0058	0.0070	0.0161	0.0184	0.0166	0.0196	0.0120	0.0013	0.0102	0.0151	0.0133	0.0131

Table 15: Normalised differential cross section for $E(\ell^{+}) + E(\ell^{-})$ with detailed systematic uncertainties.

$E(\ell^{+}) + E(\ell^{-})$ bins [GeV]	50.0-60.0	60.0-70.0	70.0-80.0	80.0-90.0	90.0-110.0	110.0-125.0	125.0-160.0	160.0-200.0	200.0-250.0	250.0-300.0	300.0-370.0	370.0-450.0	450.0-550.0	550.0-700.0	700.0-900.0
Normalised cross section [10^{-3}/GeV]	0.1345	0.8511	1.9310	2.8961	4.1483	4.8414	4.8984	4.1045	2.9944	1.9863	1.2096	0.6544	0.3274	0.1347	0.0583
Data statistics %	5.3448	1.9593	1.1852	0.9588	0.5267	0.5707	0.3502	0.3620	0.3634	0.4598	0.5302	0.6851	0.9683	1.1836	1.7629
MC statistics %	6.2696	1.2356	0.4131	0.3128	0.1546	0.1457	0.0954	0.0956	0.0967	0.1264	0.1464	0.1787	0.2467	0.3248	0.4774
Fragmentation %	1.2885	0.8642	0.6553	0.6527	0.2287	0.1180	0.3499	0.1029	0.1655	0.3402	0.7816	0.3725	0.0811	0.5538	0.9617
Hard scattering %	1.4646	3.2371	0.8779	0.4324	0.3853	0.1065	0.4732	0.1894	0.5600	0.5100	0.6968	0.1232	0.0913	1.0367	1.6002
top pT %	0.1418	0.2096	0.2083	0.1874	0.1789	0.1457	0.0839	0.0015	0.0745	0.1265	0.1401	0.1488	0.1370	0.1117	0.0777
Top mass dependence %	0.1916	0.2125	0.2159	0.0385	0.0946	0.0489	0.0217	0.0225	0.0115	0.0543	0.0345	0.1093	0.1152	0.0456	0.1550
PDF %	0.1064	0.0740	0.0780	0.0704	0.0591	0.0417	0.0282	0.0199	0.0265	0.0434	0.0519	0.0581	0.0598	0.0729	0.0956
ISR %	2.4250	0.4112	0.2026	0.3773	0.0426	0.0659	0.0443	0.0621	0.0184	0.0584	0.2257	0.3627	0.0101	0.0273	0.2171
FSR %	1.2487	0.0952	0.3460	0.4548	0.2042	0.1504	0.1183	0.0429	0.0372	0.1255	0.0742	0.1241	0.1056	0.8654	0.4062
Electron scale %	0.3211	0.1006	0.0576	0.1340	0.1216	0.1422	0.1561	0.1334	0.0753	0.0594	0.1838	0.3357	0.4956	0.7171	1.4482
Electron resolution %	0.2255	0.0719	0.0273	0.0109	0.0092	0.0164	0.0009	0.0015	0.0062	0.0086	0.0088	0.0051	0.0245	0.0174	0.0087
Electron trigger efficiency %	0.1650	0.0693	0.0359	0.0207	0.0066	0.0007	0.0047	0.0068	0.0071	0.0062	0.0032	0.0024	0.0104	0.0209	0.0329
Electron reconstruction efficiency %	0.1091	0.0740	0.0276	0.0034	0.0155	0.0215	0.0188	0.0111	0.0028	0.0059	0.0159	0.0283	0.0422	0.0579	0.0802
Electron ISO efficiency %	0.0107	0.0009	0.0131	0.0191	0.0239	0.0241	0.0196	0.0121	0.0026	0.0082	0.0208	0.0373	0.0575	0.0921	0.1688
Electron ID efficiency %	0.6457	0.3590	0.2531	0.2173	0.1906	0.1594	0.1087	0.0669	0.0856	0.1180	0.1469	0.2036	0.4019	0.6912	1.1508
Muon scale %	0.0880	0.0459	0.1054	0.0686	0.0554	0.0454	0.0331	0.0074	0.0077	0.0177	0.0523	0.0826	0.0722	0.1461	0.2011
Muon resolution %	0.6812	0.0524	0.0191	0.0699	0.0052	0.0093	0.0051	0.0054	0.0135	0.0209	0.0368	0.0130	0.0127	0.0520	0.1725
Muon reconstruction efficiency %	0.1224	0.0830	0.0516	0.0444	0.0292	0.0210	0.0091	0.0019	0.0112	0.0174	0.0220	0.0250	0.0276	0.0283	0.0259
Muon trigger efficiency %	0.1321	0.0918	0.0585	0.0404	0.0226	0.0111	0.0028	0.0042	0.0083	0.0114	0.0139	0.0165	0.0184	0.0205	0.0220
Muon ISO efficiency %	0.0224	0.0064	0.0020	0.0065	0.0124	0.0111	0.0064	0.0020	0.0031	0.0051	0.0071	0.0113	0.0164	0.0202	0.0263
Muon TTVA efficiency %	0.0146	0.0077	0.0033	0.0022	0.0013	0.0009	0.0005	0.0003	0.0007	0.0010	0.0011	0.0012	0.0012	0.0011	0.0009
JVT %	0.0146	0.0112	0.0007	0.0015	0.0062	0.0021	0.0028	0.0003	0.0009	0.0016	0.0030	0.0052	0.0094	0.0155	0.0046
JES b-jes response %	0.0457	0.1512	0.0422	0.0136	0.0161	0.0042	0.0031	0.0037	0.0076	0.0061	0.0204	0.0259	0.0036	0.0245	0.0182
JES effective NPs %	0.3449	0.1275	0.0899	0.0306	0.0270	0.0172	0.0026	0.0030	0.0091	0.0133	0.0166	0.0041	0.0297	0.0300	0.0839
JES EtaInterCalibration %	0.1033	0.0930	0.1883	0.0209	0.0209	0.0172	0.0056	0.0042	0.0120	0.0116	0.0140	0.0157	0.0243	0.0243	0.0552
JES flavour %	0.4649	0.0403	0.1533	0.0242	0.0425	0.0263	0.0121	0.0048	0.0239	0.0326	0.0105	0.0361	0.0483	0.0586	0.1427
JES pileup %	0.3672	0.1381	0.2383	0.0424	0.0330	0.0164	0.0044	0.0089	0.0143	0.0233	0.0273	0.0241	0.0344	0.0474	0.0883
JES PunchThrough %	0.0000	0.0010	0.0000	0.0000	0.0001	0.0001	0.0001	0.0002	0.0001	0.0000	0.0001	0.0004	0.0011	0.0006	0.0005
JES HighPt %	0.0000	0.0000	0.0000	0.0000	0.0000	0.0000	0.0000	0.0000	0.0000	0.0000	0.0000	0.0000	0.0000	0.0000	0.0000
MET soft term %	0.0000	0.0000	0.0000	0.0000	0.0000	0.0000	0.0000	0.0000	0.0000	0.0000	0.0000	0.0000	0.0000	0.0000	0.0000
JER %	0.0000	0.0000	0.0000	0.0000	0.0001	0.0000	0.0000	0.0000	0.0000	0.0000	0.0001	0.0000	0.0000	0.0000	0.0000
b-tagging %	1.7353	0.3753	0.0747	0.0750	0.0479	0.0241	0.0159	0.0077	0.0197	0.0166	0.0267	0.0381	0.0477	0.0583	0.0945
Wt cross section %	0.1779	0.1061	0.0982	0.0671	0.0664	0.0395	0.0275	0.0114	0.0033	0.0292	0.0486	0.0712	0.0963	0.1276	0.2564
Wt/$t\bar{t}$ interference %	0.8990	0.6320	0.7466	0.6528	0.6159	0.5409	0.3444	0.2368	0.0559	0.3277	0.5702	0.8961	1.2544	1.7240	2.8248
Wt hard scattering %	0.4462	0.5340	0.0808	0.2638	0.1006	0.0220	0.1027	0.1058	0.0070	0.0248	0.0386	0.1904	0.1147	0.1596	0.4148
Wt fragmentation %	0.8207	0.2654	0.1720	0.2150	0.0159	0.1720	0.0745	0.0053	0.2186	0.0452	0.0982	0.0453	0.1206	0.0654	0.2412
Wt ISR %	0.1730	0.0681	0.1320	0.0768	0.1084	0.1247	0.0962	0.0424	0.0032	0.0645	0.1311	0.1791	0.2595	0.3344	0.4674
Wt FSR %	0.4113	0.0493	0.1998	0.0508	0.1664	0.0089	0.0291	0.0767	0.0213	0.0798	0.2357	0.0035	0.1668	0.2102	0.3387
Diboson cross section %	0.0091	0.0003	0.0045	0.0059	0.0073	0.0074	0.0066	0.0042	0.0019	0.0019	0.0059	0.0129	0.0189	0.0314	0.0782
Diboson scale %	0.1650	0.0693	0.0359	0.0207	0.0066	0.0007	0.0047	0.0068	0.0071	0.0062	0.0032	0.0024	0.0104	0.0209	0.0329
ttV background %	0.0094	0.0100	0.0096	0.0099	0.0097	0.0077	0.0063	0.0025	0.0009	0.0038	0.0078	0.0130	0.0173	0.0245	0.0449
Z modelling %	5.5805	0.6915	0.7994	0.0251	0.0202	0.1039	0.0124	0.0860	0.0333	0.0859	0.0076	0.0515	0.0116	0.0901	0.0490
Z factor %	0.1139	0.1783	0.0517	0.0465	0.0121	0.0014	0.0032	0.0023	0.0077	0.0072	0.0076	0.0116	0.0114	0.0124	0.0130
Fakes background %	0.3469	0.2502	0.1375	0.1132	0.1256	0.1711	0.1088	0.0537	0.0228	0.0425	0.1890	0.2698	0.2339	0.2613	0.4480
Pileup %	1.1561	0.9944	0.5184	0.4889	0.2913	0.1868	0.0772	0.0006	0.0537	0.1941	0.2704	0.2699	0.2864	0.3358	0.3897
Beam energy %	0.1131	0.0197	0.0185	0.0285	0.0141	0.0134	0.0275	0.0065	0.0018	0.0103	0.0061	0.0164	0.0227	0.0238	0.0247
Luminosity %	0.1209	0.0238	0.0238	0.0157	0.0290	0.0267	0.0201	0.0099	0.0015	0.0106	0.0286	0.0432	0.0523	0.0693	0.1431

Table 16: Normalised differential cross section for $m(\ell^+\ell^-)$ with detailed systematic uncertainties.

$m(\ell^+\ell^-)$ bins [GeV]	0.0-15.0	15.0-20.0	20.0-25.0	25.0-30.0	30.0-35.0	35.0-40.0	40.0-50.0	50.0-60.0	60.0-70.0	70.0-85.0	85.0-100.0	100.0-120.0	120.0-150.0	150.0-175.0	175.0-200.0	200.0-250.0	250.0-300.0	300.0-400.0	400.0-500.0	500.0-650.0	650.0-800.0
Normalised cross section [10^{-3}/GeV]	0.7692	1.7819	2.2204	2.7562	3.1357	3.6207	4.3072	5.3164	6.5041	7.2803	7.2340	6.3757	4.8096	3.2660	2.2538	1.2971	0.6391	0.2442	0.0691	0.0201	0.0063
Data statistics %	2.1452	1.7702	1.6167	1.3542	1.2788	1.2236	0.7658	0.7061	0.6293	0.4704	0.4582	0.4147	0.3669	0.5010	0.6128	0.5673	0.8305	0.9433	1.7789	2.7302	5.1352
MC statistics %	0.5538	0.4314	0.3997	0.3493	0.3233	0.3001	0.1971	0.2698	0.2243	0.1411	0.1181	0.1047	0.0993	0.1333	0.1675	0.1521	0.2223	0.2522	0.5015	0.7481	1.4422
Fragmentation %	0.0270	0.1319	0.3906	0.0082	0.6425	0.4129	0.0986	1.0416	0.9554	0.2223	0.0596	0.0044	0.2565	0.0914	0.7040	0.6628	0.4774	1.1132	0.0630	2.0012	0.5656
Hard scattering %	2.6676	1.4153	0.9702	0.0976	1.0316	0.0236	1.4337	0.5703	0.4711	0.0125	0.6003	0.2084	0.0713	0.1721	0.7505	0.2856	1.9849	0.8585	1.1006	3.7014	0.0302
top pT %	0.1972	0.1033	0.0799	0.0470	0.0541	0.0504	0.0503	0.0765	0.0787	0.0704	0.0532	0.0321	0.0062	0.0465	0.0828	0.1495	0.2002	0.2582	0.2887	0.3842	0.5194
Top mass dependence %	0.3281	0.0171	0.0047	0.0987	0.0332	0.0269	0.0719	0.0747	0.0114	0.0086	0.0606	0.0283	0.0794	0.0362	0.0272	0.0137	0.0188	0.0785	0.1772	0.1486	0.4108
PDF %	0.0586	0.0310	0.0273	0.0322	0.0174	0.0187	0.0199	0.0165	0.0124	0.0118	0.0086	0.0043	0.0049	0.0120	0.0160	0.0221	0.0319	0.0373	0.0518	0.0566	0.0952
ISR %	0.2545	0.2673	0.1472	0.2337	0.2934	0.2990	0.0634	0.0485	0.0599	0.2243	0.0005	0.0460	0.0203	0.0532	0.0337	0.0955	0.4681	0.4884	0.0517	0.0277	1.6269
FSR %	0.2070	0.8933	0.0414	0.0119	0.0769	0.2152	0.1857	0.0987	0.0672	0.0916	0.0918	0.0217	0.0691	0.0008	0.0811	0.0038	0.1675	0.2379	0.1899	0.3076	0.3238
Electron scale %	0.0281	0.0565	0.0378	0.0361	0.0179	0.0378	0.0364	0.0585	0.0454	0.0952	0.0900	0.1020	0.0740	0.0036	0.1025	0.1610	0.3709	0.5666	0.9134	1.3017	1.8490
Electron resolution %	0.0259	0.0372	0.0063	0.0208	0.0069	0.0327	0.0166	0.0117	0.0079	0.0182	0.0011	0.0031	0.0082	0.0128	0.0094	0.0121	0.0040	0.0222	0.0620	0.1983	0.1080
Electron trigger efficiency %	0.0163	0.0109	0.0097	0.0097	0.0100	0.0104	0.0105	0.0125	0.0079	0.0025	0.0018	0.0046	0.0066	0.0066	0.0054	0.0037	0.0016	0.0012	0.0042	0.0059	0.0117
Electron reconstruction efficiency %	0.0167	0.0049	0.0056	0.0049	0.0052	0.0053	0.0047	0.0074	0.0025	0.0065	0.0116	0.0125	0.0088	0.0012	0.0067	0.0157	0.0252	0.0354	0.0467	0.0538	0.0729
Electron ISO efficiency %	0.0072	0.0098	0.0095	0.0093	0.0091	0.0089	0.0090	0.0079	0.0092	0.0120	0.0128	0.0109	0.0056	0.0027	0.0117	0.0248	0.0437	0.0701	0.1080	0.1469	0.2375
Electron ID efficiency %	0.2252	0.1469	0.1370	0.1366	0.1323	0.1319	0.1316	0.1351	0.1266	0.1066	0.0818	0.0547	0.0487	0.0905	0.1376	0.2038	0.2859	0.4007	0.6162	1.0064	1.6995
Muon scale %	0.0336	0.0105	0.0385	0.0069	0.0234	0.0331	0.0291	0.0302	0.0150	0.0296	0.0141	0.0110	0.0018	0.0145	0.0464	0.0360	0.0830	0.0812	0.0996	0.1416	0.1792
Muon resolution %	0.0568	0.0655	0.0723	0.0678	0.0688	0.0215	0.0180	0.0167	0.0240	0.0050	0.0048	0.0081	0.0076	0.0108	0.0302	0.0146	0.0445	0.0513	0.0482	0.1296	0.2209
Muon reconstruction efficiency %	0.0044	0.0011	0.0010	0.0040	0.0044	0.0030	0.0050	0.0047	0.0025	0.0011	0.0010	0.0003	0.0001	0.0015	0.0016	0.0029	0.0062	0.0078	0.0107	0.0155	0.0155
Muon trigger efficiency %	0.0580	0.0343	0.0325	0.0331	0.0319	0.0319	0.0313	0.0334	0.0295	0.0185	0.0065	0.0046	0.0155	0.0232	0.0273	0.0310	0.0340	0.0361	0.0372	0.0386	0.0382
Muon ISO efficiency %	0.0086	0.0057	0.0049	0.0042	0.0052	0.0057	0.0067	0.0079	0.0078	0.0078	0.0065	0.0047	0.0017	0.0065	0.0111	0.0163	0.0215	0.0258	0.0321	0.0418	0.0540
Muon TTVA efficiency %	0.0009	0.0011	0.0010	0.0010	0.0011	0.0011	0.0011	0.0014	0.0009	0.0004	0.0003	0.0005	0.0005	0.0006	0.0006	0.0006	0.0007	0.0008	0.0009	0.0012	0.0010
JVT %	0.0018	0.0057	0.0129	0.0142	0.0026	0.0042	0.0006	0.0007	0.0021	0.0003	0.0048	0.0033	0.0011	0.0015	0.0001	0.0062	0.0049	0.0016	0.0246	0.0281	0.0534
JES b-jes response %	0.0162	0.0094	0.0199	0.0059	0.0544	0.0469	0.0234	0.0071	0.0335	0.0119	0.0155	0.0052	0.0014	0.0005	0.0079	0.0273	0.0179	0.0561	0.0309	0.0846	0.1155
JES effective NPs %	0.0471	0.0260	0.0131	0.0429	0.0331	0.0114	0.0665	0.0152	0.0357	0.0229	0.0030	0.0085	0.0031	0.0063	0.0162	0.0065	0.0302	0.0077	0.0485	0.0295	0.0555
JES EtaInterCalibration %	0.0244	0.0226	0.0010	0.0347	0.0138	0.0039	0.0858	0.0065	0.0110	0.0252	0.0038	0.0058	0.0062	0.0026	0.0070	0.0012	0.0165	0.0051	0.0286	0.0337	0.0788
JES flavour %	0.1111	0.0829	0.0817	0.0689	0.0305	0.0500	0.0516	0.0269	0.0343	0.0497	0.0151	0.0046	0.0053	0.0163	0.0502	0.0433	0.0805	0.0999	0.1489	0.1710	0.2258
JES pileup %	0.0746	0.0467	0.0168	0.0545	0.0365	0.0095	0.1073	0.0185	0.0357	0.0418	0.0069	0.0152	0.0089	0.0108	0.0229	0.0234	0.0354	0.0216	0.0580	0.0367	0.0795
JES PunchThrough %	0.0000	0.0000	0.0000	0.0000	0.0000	0.0000	0.0002	0.0000	0.0000	0.0002	0.0000	0.0004	0.0002	0.0002	0.0002	0.0004	0.0001	0.0003	0.0000	0.0017	0.0001
JES HighPt %	0.0000	0.0000	0.0000	0.0000	0.0000	0.0000	0.0000	0.0000	0.0000	0.0000	0.0000	0.0000	0.0000	0.0000	0.0000	0.0000	0.0000	0.0000	0.0000	0.0000	0.0000
MET soft term %	0.0000	0.0000	0.0000	0.0000	0.0000	0.0000	0.0000	0.0000	0.0000	0.0000	0.0000	0.0000	0.0000	0.0000	0.0000	0.0000	0.0000	0.0000	0.0000	0.0000	0.0000
JER %	0.0000	0.0000	0.0000	0.0000	0.0000	0.0000	0.0000	0.0000	0.0002	0.0000	0.0000	0.0000	0.0000	0.0001	0.0001	0.0000	0.0000	0.0000	0.0000	0.0000	0.0000
b-tagging %	0.0894	0.0520	0.0396	0.0665	0.0539	0.0612	0.0414	0.0601	0.0458	0.0366	0.0227	0.0132	0.0162	0.0172	0.0217	0.0265	0.0329	0.0391	0.0500	0.0629	0.1077
Wt cross section %	0.0745	0.0357	0.0333	0.0516	0.0382	0.0366	0.0416	0.0405	0.0390	0.0347	0.0219	0.0102	0.0118	0.0258	0.0467	0.0649	0.0829	0.1075	0.1501	0.0801	0.2846
Wt/$t\bar{t}$ interference %	0.8138	0.5297	0.5657	1.1104	0.4490	0.4442	0.5251	0.5981	0.3379	0.3263	0.3037	0.1433	0.0355	0.1797	0.4777	0.7834	1.0298	2.0214	3.1506	1.9127	7.1165
Wt hard scattering %	0.4382	0.1150	0.0652	0.2233	0.0271	0.1006	0.1115	0.0179	0.1353	0.0057	0.0571	0.0232	0.0816	0.0894	0.0080	0.2746	0.0577	0.0714	0.1507	1.5762	1.0050
Wt fragmentation %	0.1928	0.0315	0.1587	0.0191	0.3144	0.1677	0.0627	0.0749	0.1926	0.1736	0.0204	0.0929	0.0022	0.1271	0.1781	0.2602	0.0042	0.0718	0.2464	1.1909	0.5689
Wt ISR %	0.1741	0.0461	0.0897	0.0800	0.0923	0.1044	0.0488	0.0898	0.0864	0.0484	0.0815	0.0411	0.0077	0.0361	0.0854	0.1320	0.2758	0.3832	0.4929	0.6019	1.1908
Wt FSR %	0.0546	0.3873	0.0227	0.0824	0.0026	0.0354	0.0912	0.0817	0.0453	0.0304	0.0663	0.0251	0.0238	0.0610	0.1004	0.2823	0.0548	0.0281	0.1772	0.3126	0.2165
Diboson cross section %	0.0011	0.0000	0.0032	0.0004	0.0001	0.0012	0.0012	0.0001	0.0003	0.0011	0.0015	0.0020	0.0010	0.0010	0.0001	0.0014	0.0047	0.0104	0.0196	0.0316	0.0776
Diboson scale %	0.0163	0.0109	0.0097	0.0097	0.0100	0.0104	0.0105	0.0125	0.0079	0.0025	0.0018	0.0046	0.0066	0.0066	0.0054	0.0037	0.0016	0.0012	0.0042	0.0059	0.0117
ttV background %	0.0100	0.0054	0.0057	0.0090	0.0061	0.0070	0.0066	0.0050	0.0051	0.0045	0.0037	0.0017	0.0002	0.0032	0.0053	0.0100	0.0123	0.0203	0.0338	0.0432	0.0805
Z modelling %	0.3436	0.0613	0.0687	0.1661	0.3586	0.1795	0.2747	0.2605	0.2324	0.0212	0.0728	0.0544	0.0155	0.0413	0.0383	0.0556	0.0462	0.0646	0.0215	0.0541	0.0445
Z factor %	0.0009	0.0096	0.0129	0.0040	0.0082	0.0172	0.0369	0.0703	0.0573	0.0170	0.0151	0.0168	0.0165	0.0173	0.0182	0.0191	0.0186	0.0184	0.0152	0.0190	0.0185
Fakes background %	0.5889	0.1489	0.1200	0.1129	0.1065	0.1151	0.0345	0.0366	0.0552	0.0530	0.0208	0.0513	0.0647	0.0565	0.0753	0.0248	0.0550	0.1694	0.2591	0.3270	0.6512
Pileup %	0.3488	0.2591	0.1487	0.0262	0.2421	0.2127	0.4211	0.2551	0.2155	0.1649	0.0945	0.0042	0.0792	0.1487	0.2559	0.3550	0.4258	0.3972	0.4441	0.7134	1.0180
Beam energy %	0.0035	0.0456	0.0111	0.0168	0.0124	0.0523	0.0193	0.0379	0.0118	0.0009	0.0128	0.0171	0.0033	0.0098	0.0052	0.0111	0.0382	0.0159	0.0030	0.0248	0.1072
Luminosity %	0.0027	0.0203	0.0171	0.0208	0.0145	0.0036	0.0030	0.0078	0.0096	0.0030	0.0126	0.0123	0.0053	0.0000	0.0046	0.0162	0.0275	0.0456	0.0667	0.0492	0.1475

Table 17: Normalised differential cross section for p_{T} (ℓ^{+}) + p_{T} (ℓ^{-}) with detailed systematic uncertainties.

p_{T} (ℓ^{+}) + p_{T} (ℓ^{-}) bins [GeV]	50.0-60.0	60.0-70.0	70.0-80.0	80.0-100.0	100.0-125.0	125.0-150.0	150.0-200.0	200.0-250.0	250.0-300.0	300.0-400.0	400.0-600.0
Normalised cross section [10^{-3}/GeV]	2.3653	6.8065	9.7273	10.8612	9.0780	5.9155	2.7816	0.9593	0.3688	0.1080	0.0133
Data statistics %	1.2375	0.6413	0.5078	0.3021	0.2997	0.3722	0.3788	0.6422	1.0873	1.4289	2.8218
MC statistics %	0.5671	0.2582	0.1628	0.0899	0.0755	0.0966	0.1043	0.1909	0.2959	0.3854	0.8812
Fragmentation %	1.9719	0.2752	0.9840	0.4188	0.0790	0.4020	0.4822	1.1631	1.6308	1.6814	1.3514
Hard scattering %	1.3815	0.6086	0.9462	0.3674	0.2340	0.3669	1.0968	0.0407	2.2688	3.8348	3.5202
top pT %	0.0186	0.0140	0.0104	0.0010	0.0021	0.0069	0.0006	0.0078	0.0382	0.0911	0.2173
Top mass dependence %	0.1041	0.0455	0.0013	0.0089	0.0012	0.0099	0.0450	0.0365	0.0255	0.1110	0.0316
PDF %	0.0289	0.0250	0.0209	0.0153	0.0040	0.0114	0.0238	0.0427	0.0507	0.0571	0.0724
ISR %	0.1770	0.0229	0.2322	0.0326	0.0332	0.0439	0.0574	0.2088	0.0924	0.5100	0.3953
FSR %	0.7006	0.0845	0.1048	0.0918	0.0359	0.1422	0.0545	0.0369	0.0881	0.9200	0.2842
Electron scale %	0.0547	0.0223	0.0713	0.1677	0.1499	0.0410	0.1898	0.5433	0.8499	1.2089	1.9083
Electron resolution %	0.0370	0.0188	0.0313	0.0061	0.0053	0.0092	0.0113	0.0202	0.0202	0.0070	0.0518
Electron trigger efficiency %	0.1190	0.0266	0.0045	0.0048	0.0085	0.0074	0.0056	0.0035	0.0028	0.0013	0.0013
Electron reconstruction efficiency %	0.1271	0.0327	0.0097	0.0226	0.0176	0.0014	0.0144	0.0300	0.0385	0.0458	0.0626
Electron ISO efficiency %	0.0281	0.0027	0.0124	0.0181	0.0145	0.0020	0.0132	0.0523	0.0826	0.1237	0.2501
Electron ID efficiency %	0.6608	0.2694	0.1682	0.1328	0.0869	0.0949	0.1963	0.3290	0.4356	0.7529	1.9058
Muon scale %	0.0774	0.0800	0.0471	0.0278	0.0051	0.0299	0.0563	0.0723	0.0964	0.1004	0.1842
Muon resolution %	0.1059	0.0477	0.0182	0.0124	0.0111	0.0140	0.0107	0.0510	0.0386	0.0735	0.2978
Muon reconstruction efficiency %	0.0087	0.0070	0.0061	0.0048	0.0017	0.0009	0.0070	0.0152	0.0209	0.0297	0.0592
Muon trigger efficiency %	0.1580	0.0738	0.0370	0.0104	0.0122	0.0251	0.0342	0.0405	0.0437	0.0452	0.0461
Muon ISO efficiency %	0.0158	0.0036	0.0015	0.0196	0.0052	0.0088	0.0164	0.0200	0.0249	0.0339	0.0670
Muon TTVA efficiency %	0.0105	0.0022	0.0009	0.0007	0.0007	0.0006	0.0006	0.0008	0.0011	0.0017	0.0038
JVT %	0.0097	0.0053	0.0025	0.0048	0.0015	0.0012	0.0038	0.0122	0.0107	0.0202	0.0616
JES b-jes response %	0.0226	0.0354	0.0162	0.0015	0.0087	0.0143	0.0086	0.0059	0.0339	0.0625	0.0245
JES effective NPs %	0.0986	0.0457	0.0367	0.0322	0.0026	0.0203	0.0287	0.0616	0.0287	0.0223	0.1286
JES EtaInterCalibration %	0.2044	0.0199	0.0153	0.0177	0.0038	0.0064	0.0052	0.0182	0.0023	0.0143	0.0304
JES flavour %	0.1706	0.0334	0.0469	0.0525	0.0108	0.0154	0.0427	0.0833	0.1110	0.1600	0.3029
JES pileup %	0.2360	0.0482	0.0411	0.0366	0.0083	0.0249	0.0379	0.0797	0.0291	0.0374	0.1392
JES PunchThrough %	0.0004	0.0000	0.0002	0.0002	0.0000	0.0001	0.0001	0.0007	0.0001	0.0004	0.0001
JES HighPt %	0.0000	0.0000	0.0000	0.0000	0.0000	0.0000	0.0000	0.0000	0.0000	0.0000	0.0000
MET soft term %	0.0000	0.0000	0.0000	0.0000	0.0000	0.0000	0.0000	0.0000	0.0000	0.0000	0.0000
JER %	0.0000	0.0000	0.0001	0.0000	0.0000	0.0000	0.0000	0.0000	0.0000	0.0000	0.0000
b-tagging %	0.0998	0.0932	0.0672	0.0141	0.0127	0.0286	0.0413	0.0600	0.0536	0.0834	0.2103
Wt cross section %	0.1139	0.0912	0.0764	0.0528	0.0238	0.0058	0.0713	0.2046	0.2986	0.4315	0.9231
Wt/$t\bar{t}$ interference %	0.5190	0.6863	0.3651	0.4355	0.3212	0.0134	0.5104	1.6152	2.2611	3.8185	10.7579
Wt hard scattering %	0.1473	0.0610	0.1405	0.0557	0.0091	0.0531	0.0511	0.2107	0.3190	0.6891	0.1855
Wt fragmentation %	0.0226	0.0429	0.1018	0.0103	0.0280	0.0709	0.0737	0.1960	0.1776	0.2084	0.2324
Wt ISR %	0.0811	0.0936	0.0795	0.1014	0.0571	0.0082	0.0871	0.2789	0.4741	0.8205	2.5116
Wt FSR %	0.1302	0.1694	0.0157	0.0273	0.0394	0.0514	0.1087	0.0695	0.1043	0.0554	0.0894
Diboson cross section %	0.0013	0.0018	0.0026	0.0037	0.0037	0.0013	0.0029	0.0129	0.0249	0.0414	0.1150
Diboson scale %	0.1190	0.0266	0.0045	0.0048	0.0085	0.0074	0.0056	0.0035	0.0028	0.0013	0.0013
ttV background %	0.0090	0.0076	0.0080	0.0067	0.0042	0.0004	0.0090	0.0227	0.0341	0.0532	0.1126
Z modelling %	0.4981	0.1647	0.0649	0.0086	0.0116	0.0063	0.0113	0.0743	0.0269	0.0045	0.0853
Z factor %	0.0804	0.0687	0.0214	0.0005	0.0125	0.0146	0.0155	0.0181	0.0177	0.0159	0.0196
Fakes background %	0.1792	0.0701	0.0277	0.0183	0.0304	0.0261	0.0291	0.0700	0.1400	0.1727	0.4730
Pileup %	0.7395	0.5054	0.3305	0.1576	0.0239	0.1866	0.3509	0.4357	0.4602	0.4743	0.7312
Beam energy %	0.0320	0.0018	0.0040	0.0036	0.0042	0.0043	0.0022	0.0209	0.0214	0.0606	0.0593
Luminosity %	0.0057	0.0043	0.0197	0.0194	0.0148	0.0047	0.0190	0.0702	0.1081	0.1526	0.3521

Table 18: Normalised differential cross section for p_{T} $(\ell^{+}\ell^{-})$ with detailed systematic uncertainties.

p_{T} $(\ell^{+}\ell^{-})$ bins [GeV]	0.0-20.0	20.0-30.0	30.0-45.0	45.0-60.0	60.0-75.0	75.0-100.0	100.0-125.0	125.0-150.0	150.0-200.0	200.0-300.0
Normalised cross section [10^{-3}/GeV]	3.1027	6.5380	8.2995	10.5183	11.4591	8.8385	4.6033	1.8726	0.5463	0.0824
Data statistics %	0.6589	0.6209	0.4336	0.3862	0.3598	0.2975	0.4405	0.6912	0.9408	1.7882
MC statistics %	0.2325	0.2070	0.1197	0.1007	0.0916	0.0783	0.1094	0.1822	0.2592	0.5424
Fragmentation %	0.5052	0.3194	0.1871	0.3267	0.0668	0.0164	0.6446	0.8950	0.8925	0.2058
Hard scattering %	0.4892	0.7498	0.2296	0.6597	0.7284	0.1853	1.1568	1.2210	1.2231	1.4462
top pT %	0.0021	0.0043	0.0091	0.0622	0.0639	0.0057	0.0878	0.1515	0.1819	0.1065
Top mass dependence %	0.0219	0.0151	0.0033	0.0119	0.0030	0.0222	0.0120	0.0374	0.0209	0.0783
PDF %	0.0158	0.0065	0.0099	0.0149	0.0131	0.0041	0.0240	0.0405	0.0533	0.0535
ISR %	0.1277	0.4193	0.2034	0.0583	0.1797	0.0247	0.0455	0.0954	0.1721	0.2768
FSR %	0.1358	0.4295	0.1424	0.0113	0.0952	0.1691	0.0369	0.2393	0.1640	1.4449
Electron scale %	0.2288	0.2472	0.2046	0.1515	0.1170	0.0035	0.2356	0.6414	1.0481	1.6163
Electron resolution %	0.0366	0.0427	0.0109	0.0010	0.0184	0.0020	0.0067	0.0062	0.0676	0.0032
Electron trigger efficiency %	0.0017	0.0004	0.0005	0.0043	0.0001	0.0031	0.0022	0.0003	0.0024	0.0066
Electron reconstruction efficiency %	0.0114	0.0087	0.0042	0.0026	0.0027	0.0042	0.0058	0.0184	0.0292	0.0549
Electron ISO efficiency %	0.0112	0.0102	0.0080	0.0047	0.0056	0.0041	0.0079	0.0282	0.0573	0.1413
Electron ID efficiency %	0.0842	0.0672	0.0530	0.0531	0.0386	0.0184	0.0825	0.1742	0.2815	0.8913
Muon scale %	0.0450	0.0564	0.0374	0.0268	0.0234	0.0098	0.0603	0.1184	0.1254	0.1584
Muon resolution %	0.0352	0.0075	0.0216	0.0150	0.0151	0.0154	0.0245	0.0242	0.0643	0.1971
Muon reconstruction efficiency %	0.0040	0.0024	0.0023	0.0029	0.0027	0.0004	0.0027	0.0084	0.0193	0.0564
Muon trigger efficiency %	0.0058	0.0040	0.0044	0.0103	0.0066	0.0041	0.0135	0.0167	0.0184	0.0206
Muon ISO efficiency %	0.0070	0.0069	0.0020	0.0016	0.0010	0.0014	0.0070	0.0093	0.0124	0.0455
Muon TTVA efficiency %	0.0006	0.0002	0.0001	0.0003	0.0002	0.0002	0.0002	0.0005	0.0015	0.0045
JVT %	0.0044	0.0038	0.0024	0.0023	0.0011	0.0027	0.0071	0.0016	0.0017	0.0538
JES b-jes response %	0.0402	0.0548	0.0364	0.0186	0.0119	0.0177	0.0391	0.0769	0.1099	0.0694
JES effective NPs %	0.0089	0.0969	0.0290	0.0210	0.0135	0.0143	0.0360	0.0824	0.1094	0.1208
JES EtaInterCalibration %	0.0523	0.0610	0.0135	0.0052	0.0119	0.0045	0.0108	0.0283	0.0438	0.0417
JES flavour %	0.0562	0.0725	0.0033	0.0064	0.0035	0.0087	0.0042	0.0228	0.0543	0.0948
JES pileup %	0.0643	0.1029	0.0356	0.0210	0.0103	0.0197	0.0401	0.0912	0.1275	0.1385
JES PunchThrough %	0.0001	0.0003	0.0001	0.0000	0.0000	0.0001	0.0000	0.0002	0.0000	0.0007
JES HighPt %	0.0000	0.0000	0.0000	0.0000	0.0000	0.0000	0.0000	0.0000	0.0000	0.0000
MET soft term %	0.0000	0.0000	0.0000	0.0000	0.0000	0.0000	0.0000	0.0000	0.0000	0.0000
JER %	0.0000	0.0000	0.0000	0.0000	0.0000	0.0000	0.0000	0.0000	0.0000	0.0000
b-tagging %	0.0969	0.1039	0.0667	0.0462	0.0252	0.0242	0.0967	0.1637	0.2300	0.3134
Wt cross section %	0.0521	0.0459	0.0423	0.0402	0.0332	0.0101	0.0254	0.1228	0.3175	1.0248
Wt/$t\bar{t}$ interference %	0.4287	0.3773	0.4555	0.4122	0.3680	0.1621	0.3216	1.4045	2.9275	10.8499
Wt hard scattering %	0.2519	0.0584	0.0704	0.0926	0.0006	0.0636	0.2632	0.1056	0.2367	1.2867
Wt fragmentation %	0.0183	0.0405	0.0976	0.0239	0.0341	0.0519	0.0145	0.2592	0.2008	0.7262
Wt ISR %	0.0607	0.0860	0.0677	0.0763	0.0752	0.0412	0.0180	0.1993	0.5736	3.0112
Wt FSR %	0.0235	0.0916	0.0803	0.1009	0.0194	0.0663	0.0682	0.0129	0.1223	0.5790
Diboson cross section %	0.0004	0.0016	0.0019	0.0037	0.0049	0.0043	0.0001	0.0096	0.0368	0.1553
Diboson scale %	0.0017	0.0004	0.0005	0.0043	0.0001	0.0031	0.0022	0.0003	0.0024	0.0066
ttV background %	0.0043	0.0044	0.0048	0.0058	0.0059	0.0037	0.0032	0.0195	0.0510	0.1466
Z modelling %	0.2120	0.1378	0.0556	0.0211	0.0155	0.0007	0.0018	0.1204	0.0415	0.0648
Z factor %	0.0246	0.0183	0.0064	0.0015	0.0029	0.0083	0.0091	0.0059	0.0038	0.0012
Fakes background %	0.0352	0.0374	0.0261	0.0248	0.0251	0.0378	0.0298	0.1029	0.3195	0.8377
Pileup %	0.1582	0.1222	0.0439	0.0914	0.0281	0.0133	0.1955	0.1784	0.2717	0.1601
Beam energy %	0.0217	0.0069	0.0072	0.0003	0.0047	0.0018	0.0064	0.0298	0.0052	0.0039
Luminosity %	0.0087	0.0098	0.0130	0.0149	0.0143	0.0095	0.0039	0.0468	0.1333	0.4172

Table 19: Differential normalised cross section for $\Delta\phi(\ell^+\ell^-)$ with detailed systematic uncertainties.

$\Delta\phi(\ell^+\ell^-)$ bins	0.00-0.10	0.10-0.21	0.21-0.31	0.31-0.42	0.42-0.52	0.52-0.63	0.63-0.73	0.73-0.84	0.84-0.94	0.94-1.05	1.05-1.15	1.15-1.26	1.26-1.36	1.36-1.47	1.47-1.57	1.57-1.68	1.68-1.78	1.78-1.88	1.88-1.99	1.99-2.09	2.09-2.20	2.20-2.30	2.30-2.41	2.41-2.51	2.51-2.62	2.62-2.72	2.72-2.83	2.83-2.93	2.93-3.04	3.04-3.14
Normalised cross section [10^{-2}/rad]	21.0254	21.0926	20.3983	21.3515	21.0325	21.7156	22.0452	22.9441	23.6359	23.6035	24.7158	25.9083	27.0156	28.4661	29.2108	30.6409	32.0118	33.3336	34.0324	36.6251	37.6696	39.8071	41.1278	42.3275	43.1817	43.6540	45.2645	45.7728	46.8349	48.4849
Data statistics %	1.6580	1.5833	1.5461	1.5339	1.5297	1.4302	1.4552	1.3931	1.4602	1.4232	1.4023	1.3856	1.2793	1.3326	1.2633	1.2369	1.2067	1.1869	1.1606	1.1212	1.1398	1.0692	1.0168	1.0403	0.9976	1.0210	0.9862	0.9989	0.9801	0.9518
MC statistics %	0.3901	0.3990	0.4013	0.3747	0.3727	0.3689	0.3652	0.3555	0.3538	0.3756	0.3683	0.3373	0.3251	0.3375	0.3281	0.3200	0.3335	0.3169	0.3565	0.3234	0.3019	0.3083	0.3036	0.2909	0.2837	0.3047	0.2789	0.3033	0.3262	0.2579
Fragmentation %	0.6772	0.1496	0.9707	0.4676	0.8151	0.6283	0.0588	0.3305	0.2363	0.2302	0.3182	0.3709	0.6366	0.0577	0.0976	0.1758	0.0778	0.3116	0.2015	1.4729	0.0660	0.6243	0.3423	0.3058	0.2665	0.2995	0.2370	0.2922	0.2329	0.0776
Hard scattering %	0.1754	0.5074	0.4502	1.8350	2.0339	0.0819	0.9194	0.4259	0.8482	1.3313	0.6359	0.3592	0.3787	1.2038	0.4768	1.3971	0.1514	1.2514	0.2157	1.2173	0.4173	1.9669	0.2571	0.4705	0.5606	0.4221	0.4424	0.0054	1.0006	0.5276
top pT %	0.1108	0.1273	0.1122	0.1059	0.0898	0.1195	0.1123	0.1042	0.1246	0.0953	0.0886	0.0848	0.0790	0.0579	0.0525	0.0563	0.0380	0.0185	0.0164	0.0091	0.0165	0.0275	0.0448	0.0555	0.0784	0.0900	0.1136	0.1259	0.1569	0.1400
Top mass dependence %	0.1604	0.0339	0.0076	0.0661	0.2045	0.1320	0.0170	0.1070	0.2340	0.0279	0.0242	0.0015	0.0440	0.0981	0.0871	0.1223	0.0915	0.0552	0.1518	0.0176	0.0393	0.0474	0.0013	0.0251	0.0539	0.0082	0.0688	0.0133	0.0325	0.0624
PDF %	0.0280	0.0223	0.0176	0.0156	0.0194	0.0193	0.0169	0.0236	0.0185	0.0195	0.0206	0.0229	0.0189	0.0157	0.0102	0.0090	0.0137	0.0149	0.0095	0.0092	0.0096	0.0061	0.0068	0.0086	0.0091	0.0144	0.0202	0.0211	0.0304	0.0260
ISR %	0.2589	0.0821	0.0735	0.7089	0.4001	0.1405	0.1716	0.1037	0.7628	0.2544	0.2827	0.4493	0.0475	0.5255	0.3645	0.5071	0.0282	0.0869	0.6301	0.4310	0.0303	0.0175	0.3813	0.0132	0.0512	0.4032	0.0215	0.2742	0.0371	0.1024
FSR %	0.0645	0.1373	0.3934	0.3248	0.2601	0.3449	0.4814	0.2618	0.3244	0.1278	0.4362	0.5264	0.1787	0.6675	0.1939	0.3864	0.1328	0.4634	0.1021	0.3315	0.6745	0.1688	0.1052	0.1152	0.1554	0.2570	0.1448	0.0672	0.4309	0.1759
Electron scale %	0.0550	0.0540	0.0544	0.0757	0.0555	0.0424	0.0659	0.0347	0.0286	0.0536	0.0326	0.0275	0.0316	0.0090	0.0199	0.0143	0.0091	0.0037	0.0044	0.0145	0.0171	0.0152	0.0234	0.0293	0.0347	0.0446	0.0368	0.0386	0.0375	0.0483
Electron resolution %	0.0385	0.0011	0.0147	0.0184	0.0147	0.0099	0.0096	0.0008	0.0116	0.0191	0.0003	0.0173	0.0203	0.0013	0.0044	0.0108	0.0014	0.0070	0.0083	0.0152	0.0130	0.0070	0.0130	0.0154	0.0064	0.0115	0.0030	0.0083	0.0133	0.0051
Electron trigger efficiency %	0.0039	0.0042	0.0039	0.0040	0.0046	0.0037	0.0030	0.0036	0.0030	0.0026	0.0024	0.0020	0.0014	0.0012	0.0008	0.0005	0.0004	0.0003	0.0011	0.0009	0.0011	0.0021	0.0021	0.0016	0.0024	0.0025	0.0026	0.0022	0.0024	0.0026
Electron reconstruction efficiency %	0.0022	0.0013	0.0020	0.0017	0.0022	0.0032	0.0028	0.0022	0.0026	0.0032	0.0024	0.0035	0.0036	0.0034	0.0034	0.0027	0.0031	0.0029	0.0018	0.0010	0.0008	0.0002	0.0004	0.0018	0.0032	0.0043	0.0047	0.0054	0.0051	0.0053
Electron ISO efficiency %	0.0091	0.0080	0.0082	0.0081	0.0080	0.0084	0.0085	0.0081	0.0081	0.0079	0.0072	0.0076	0.0073	0.0069	0.0062	0.0053	0.0050	0.0040	0.0030	0.0017	0.0004	0.0005	0.0023	0.0045	0.0069	0.0090	0.0109	0.0129	0.0135	0.0140
Electron ID efficiency %	0.0925	0.0920	0.0888	0.0864	0.0873	0.0861	0.0839	0.0810	0.0792	0.0749	0.0690	0.0660	0.0599	0.0551	0.0474	0.0404	0.0332	0.0234	0.0165	0.0126	0.0154	0.0264	0.0381	0.0486	0.0620	0.0761	0.0869	0.1002	0.1081	0.1123
Muon scale %	0.0309	0.0311	0.0023	0.0330	0.0149	0.0189	0.0335	0.0212	0.0094	0.0101	0.0208	0.0124	0.0043	0.0088	0.0071	0.0067	0.0082	0.0003	0.0111	0.0048	0.0194	0.0052	0.0037	0.0064	0.0009	0.0182	0.0307	0.0114	0.0193	0.0161
Muon resolution %	0.0384	0.0307	0.0115	0.0062	0.0256	0.0188	0.0186	0.0232	0.0251	0.0214	0.0122	0.0099	0.0176	0.0196	0.0184	0.0232	0.0108	0.0063	0.0252	0.0117	0.0160	0.0237	0.0059	0.0188	0.0358	0.0139	0.0155	0.0049	0.0036	0.0180
Muon reconstruction efficiency %	0.0038	0.0050	0.0038	0.0026	0.0039	0.0036	0.0033	0.0025	0.0042	0.0039	0.0013	0.0007	0.0024	0.0003	0.0028	0.0006	0.0004	0.0005	0.0009	0.0023	0.0003	0.0047	0.0018	0.0007	0.0005	0.0026	0.0012	0.0039	0.0018	0.0039
Muon trigger efficiency %	0.0184	0.0194	0.0180	0.0174	0.0168	0.0160	0.0159	0.0147	0.0141	0.0128	0.0121	0.0106	0.0089	0.0078	0.0061	0.0046	0.0027	0.0004	0.0008	0.0025	0.0041	0.0064	0.0087	0.0102	0.0110	0.0123	0.0133	0.0145	0.0153	0.0146
Muon ISO efficiency %	0.0036	0.0040	0.0056	0.0051	0.0044	0.0033	0.0041	0.0042	0.0044	0.0045	0.0047	0.0045	0.0037	0.0037	0.0033	0.0034	0.0025	0.0026	0.0029	0.0017	0.0005	0.0011	0.0025	0.0033	0.0032	0.0046	0.0060	0.0059	0.0075	0.0085
Muon TTVA efficiency %	0.0002	0.0003	0.0003	0.0004	0.0004	0.0003	0.0003	0.0003	0.0003	0.0003	0.0003	0.0002	0.0002	0.0001	0.0001	0.0001	0.0000	0.0000	0.0000	0.0000	0.0001	0.0002	0.0002	0.0002	0.0002	0.0002	0.0002	0.0002	0.0003	0.0003
JVT %	0.0131	0.0088	0.0075	0.0058	0.0008	0.0129	0.0055	0.0029	0.0050	0.0021	0.0030	0.0058	0.0088	0.0012	0.0050	0.0081	0.0042	0.0018	0.0016	0.0054	0.0052	0.0024	0.0061	0.0079	0.0066	0.0060	0.0017	0.0094	0.0060	0.0064
JES b-jes response %	0.0129	0.0169	0.0932	0.0442	0.0263	0.0254	0.0640	0.0634	0.0719	0.0297	0.0351	0.0341	0.0383	0.0424	0.0223	0.0369	0.0136	0.0164	0.0088	0.0272	0.0193	0.0257	0.0432	0.0310	0.0422	0.0453	0.0548	0.0371	0.0232	0.0553
JES effective NPs %	0.0050	0.0532	0.0503	0.0172	0.0126	0.0081	0.0388	0.0404	0.0482	0.0303	0.0290	0.0233	0.0109	0.0267	0.0047	0.0352	0.0378	0.0216	0.0080	0.0357	0.0239	0.0129	0.0395	0.0940	0.0491	0.0222	0.0224	0.0201	0.0359	0.0415
JES EtaInterCalibration %	0.0125	0.0023	0.0180	0.0095	0.0064	0.0219	0.0216	0.0234	0.0208	0.0087	0.0051	0.0083	0.0037	0.0195	0.0188	0.0146	0.0065	0.0174	0.0144	0.0069	0.0069	0.0031	0.0237	0.1194	0.0369	0.0120	0.0063	0.0134	0.0187	0.0278
JES flavour %	0.0480	0.0797	0.0369	0.0641	0.0498	0.0416	0.0319	0.0341	0.0409	0.0247	0.0120	0.0534	0.0382	0.0117	0.0358	0.0031	0.0738	0.0126	0.0164	0.0032	0.0081	0.0442	0.0310	0.1534	0.0085	0.0502	0.0341	0.0278	0.0195	0.0417
JES pileup %	0.0368	0.0520	0.0418	0.0232	0.0100	0.0117	0.0566	0.0420	0.0571	0.0384	0.0378	0.0276	0.0265	0.0369	0.0095	0.0306	0.0361	0.0442	0.0146	0.0346	0.0161	0.0112	0.0357	0.1827	0.0473	0.0304	0.0243	0.0262	0.0376	0.0349
JES PunchThrough %	0.0000	0.0000	0.0000	0.0000	0.0007	0.0000	0.0002	0.0000	0.0006	0.0000	0.0000	0.0000	0.0000	0.0000	0.0009	0.0000	0.0010	0.0003	0.0003	0.0000	0.0003	0.0000	0.0004	0.0000	0.0000	0.0005	0.0000	0.0007	0.0005	0.0012
JES HighPt %	0.0000	0.0000	0.0000	0.0000	0.0000	0.0000	0.0000	0.0000	0.0000	0.0000	0.0000	0.0000	0.0000	0.0000	0.0000	0.0000	0.0000	0.0000	0.0000	0.0000	0.0000	0.0000	0.0000	0.0000	0.0000	0.0000	0.0000	0.0000	0.0000	0.0000
MET soft term %	0.0000	0.0000	0.0000	0.0000	0.0000	0.0000	0.0000	0.0000	0.0000	0.0000	0.0000	0.0000	0.0000	0.0000	0.0000	0.0000	0.0000	0.0000	0.0000	0.0000	0.0000	0.0000	0.0000	0.0000	0.0000	0.0000	0.0000	0.0000	0.0000	0.0000
JER %	0.0009	0.0000	0.0000	0.0000	0.0000	0.0000	0.0000	0.0000	0.0000	0.0000	0.0000	0.0000	0.0000	0.0000	0.0000	0.0000	0.0000	0.0000	0.0000	0.0000	0.0000	0.0000	0.0000	0.0000	0.0000	0.0000	0.0000	0.0000	0.0000	0.0000
b-tagging %	0.0924	0.0716	0.0876	0.0788	0.0665	0.0686	0.0609	0.0595	0.0575	0.0386	0.0727	0.0429	0.0562	0.0367	0.0191	0.0378	0.0417	0.0170	0.0559	0.0221	0.0166	0.0443	0.0375	0.0484	0.0447	0.0503	0.0662	0.0834	0.0856	0.0639
Wt cross section %	0.0718	0.0656	0.0468	0.0246	0.0380	0.0569	0.0484	0.0411	0.0343	0.0205	0.0244	0.0249	0.0207	0.0212	0.0135	0.0035	0.0021	0.0136	0.0222	0.0152	0.0105	0.0118	0.0084	0.0285	0.0426	0.0410	0.0342	0.0332	0.0285	0.0070
Wt/$t\bar{t}$ interference %	0.2369	0.5307	0.3740	0.5316	0.2102	0.4423	0.0443	0.3609	0.1397	0.1481	0.1173	0.1124	0.0095	0.1413	0.0208	0.2506	0.1490	0.4079	0.1507	0.0145	0.1403	0.2192	0.4195	0.1415	0.2046	0.1341	0.1111	0.1636	0.0760	0.1003
Wt hard scattering %	0.2392	0.4361	0.0196	0.5787	0.0982	0.4584	0.6365	0.4605	0.0733	0.2864	0.0400	0.1206	0.1711	0.3127	0.0808	0.0669	0.1004	0.2523	0.0119	0.2272	0.2933	0.0513	0.7771	0.7626	0.4921	0.1524	0.1983	0.0385	0.4351	0.1141
Wt fragmentation %	0.1292	0.1929	0.2033	0.4611	0.4869	0.2041	0.0407	0.0565	0.2426	0.2898	0.0925	0.1578	0.0823	0.1767	0.0307	0.0354	0.2953	0.0126	0.0960	0.0706	0.0955	0.0546	0.2813	0.1278	0.0510	0.0520	0.0425	0.0019	0.0545	0.1350
Wt ISR %	0.0348	0.1020	0.0281	0.0064	0.0391	0.0773	0.0624	0.0229	0.0626	0.0227	0.0208	0.0035	0.0688	0.0302	0.0415	0.0155	0.0122	0.0439	0.0334	0.0353	0.0187	0.0698	0.0525	0.0100	0.0253	0.0502	0.0044	0.0014	0.0350	0.0122
Wt FSR %	0.1364	0.2360	0.2014	0.0947	0.6060	0.1278	0.2416	0.0081	0.0006	0.3192	0.0135	0.0824	0.0541	0.1780	0.2199	0.3256	0.0676	0.0008	0.0441	0.0465	0.0912	0.0625	0.0041	0.2052	0.1332	0.1506	0.1391	0.2335	0.0485	0.1088
Diboson cross section %	0.0048	0.0067	0.0053	0.0020	0.0054	0.0020	0.0023	0.0016	0.0032	0.0004	0.0003	0.0004	0.0017	0.0002	0.0012	0.0020	0.0003	0.0019	0.0021	0.0010	0.0031	0.0023	0.0036	0.0022	0.0025	0.0010	0.0005	0.0009	0.0009	0.0008
Diboson scale %	0.0039	0.0042	0.0039	0.0040	0.0046	0.0037	0.0030	0.0036	0.0030	0.0026	0.0024	0.0020	0.0014	0.0012	0.0008	0.0005	0.0004	0.0003	0.0011	0.0009	0.0011	0.0021	0.0021	0.0016	0.0024	0.0025	0.0026	0.0022	0.0024	0.0026
ttV background %	0.0013	0.0021	0.0018	0.0004	0.0000	0.0004	0.0019	0.0000	0.0010	0.0003	0.0010	0.0009	0.0017	0.0016	0.0007	0.0022	0.0004	0.0017	0.0004	0.0003	0.0015	0.0014	0.0009	0.0002	0.0002	0.0004	0.0018	0.0014	0.0002	0.0014
Z modelling %	0.1429	0.1218	0.0371	0.1728	0.2054	0.0948	0.3605	0.1221	0.0396	0.0263	0.0954	0.1235	0.0148	0.0741	0.2515	0.1251	0.0503	0.0999	0.1322	0.1468	0.0929	0.0572	0.0026	0.2583	0.0590	0.0550	0.0702	0.1460	0.1030	0.1027
Z factor %	0.0009	0.0017	0.0001	0.0002	0.0006	0.0024	0.0087	0.0023	0.0068	0.0080	0.0124	0.0106	0.0006	0.0036	0.0018	0.0028	0.0067	0.0030	0.0097	0.0049	0.0128	0.0013	0.0006	0.0090	0.0023	0.0094	0.0087	0.0043	0.0133	0.0088
Fakes background %	0.1746	0.0575	0.1062	0.0433	0.1254	0.0875	0.0696	0.0835	0.1661	0.0660	0.0380	0.0797	0.0984	0.1088	0.0149	0.0737	0.0429	0.0999	0.0265	0.0511	0.0334	0.0384	0.0362	0.0597	0.0450	0.0488	0.0520	0.1141	0.0648	0.0560
Pileup %	0.0711	0.0793	0.1815	0.1571	0.1519	0.2184	0.2355	0.1604	0.1382	0.0193	0.0884	0.1525	0.1064	0.1304	0.0148	0.0448	0.0974	0.0902	0.1300	0.1255	0.0451	0.0568	0.0449	0.0162	0.1023	0.0292	0.0737	0.1577	0.1255	0.1777
Beam energy %	0.0377	0.1016	0.0082	0.0409	0.0524	0.0148	0.0146	0.0364	0.0588	0.0319	0.0393	0.0009	0.0632	0.0028	0.0378	0.0068	0.0004	0.0396	0.0317	0.0239	0.0061	0.0044	0.0493	0.0003	0.0553	0.0147	0.0402	0.0237	0.0423	0.0068
Luminosity %	0.0154	0.0211	0.0131	0.0082	0.0177	0.0147	0.0151	0.0172	0.0004	0.0024	0.0031	0.0000	0.0011	0.0000	0.0054	0.0062	0.0040	0.0031	0.0089	0.0100	0.0058	0.0049	0.0010	0.0093	0.0136	0.0104	0.0075	0.0073	0.0031	0.0003

F Particle level templates

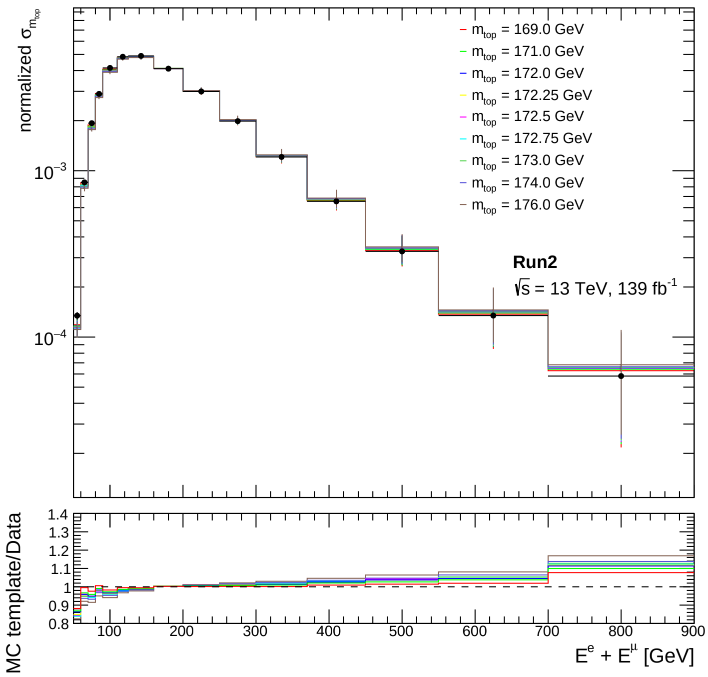

Figure 7: Top mass templates distributions at particle level plotted together with the measured normalised differential cross section for variable $E(\ell^+) + E(\ell^-)$.

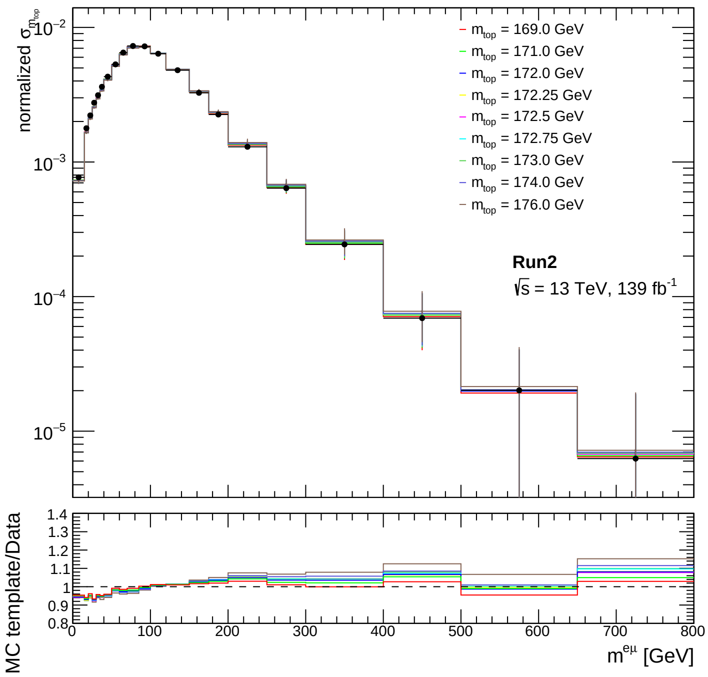

Figure 8: Top mass templates distributions at particle level plotted together with the measured normalised differential cross section for variable $m(\ell^+\ell^-)$.

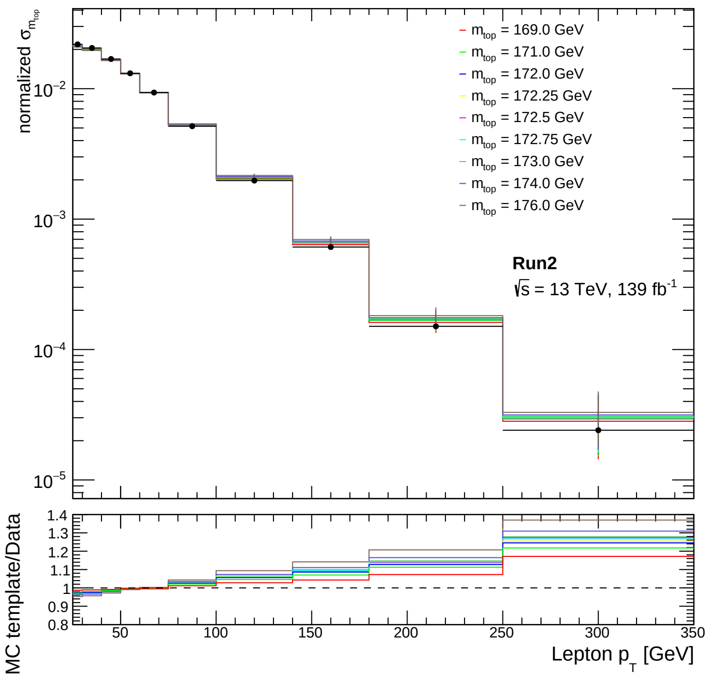

Figure 9: Top mass templates distributions at particle level plotted together with the measured normalised differential cross section for variable $p_{\mathrm{T}}(\ell)$.

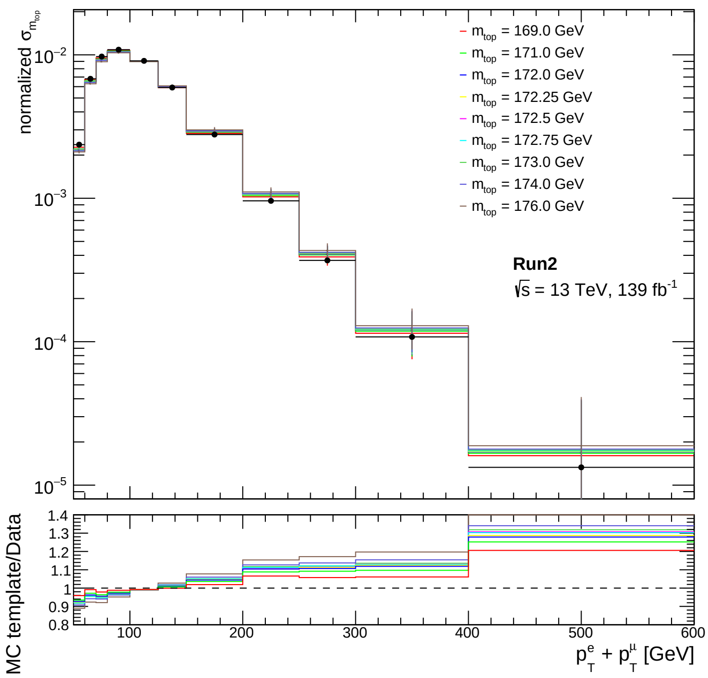

Figure 10: Top mass templates distributions at particle level plotted together with the measured normalised differential cross section for variable $p_{\mathrm{T}}(\ell^{+}) + p_{\mathrm{T}}(\ell^{-})$.

G Parametrization of particle level templates

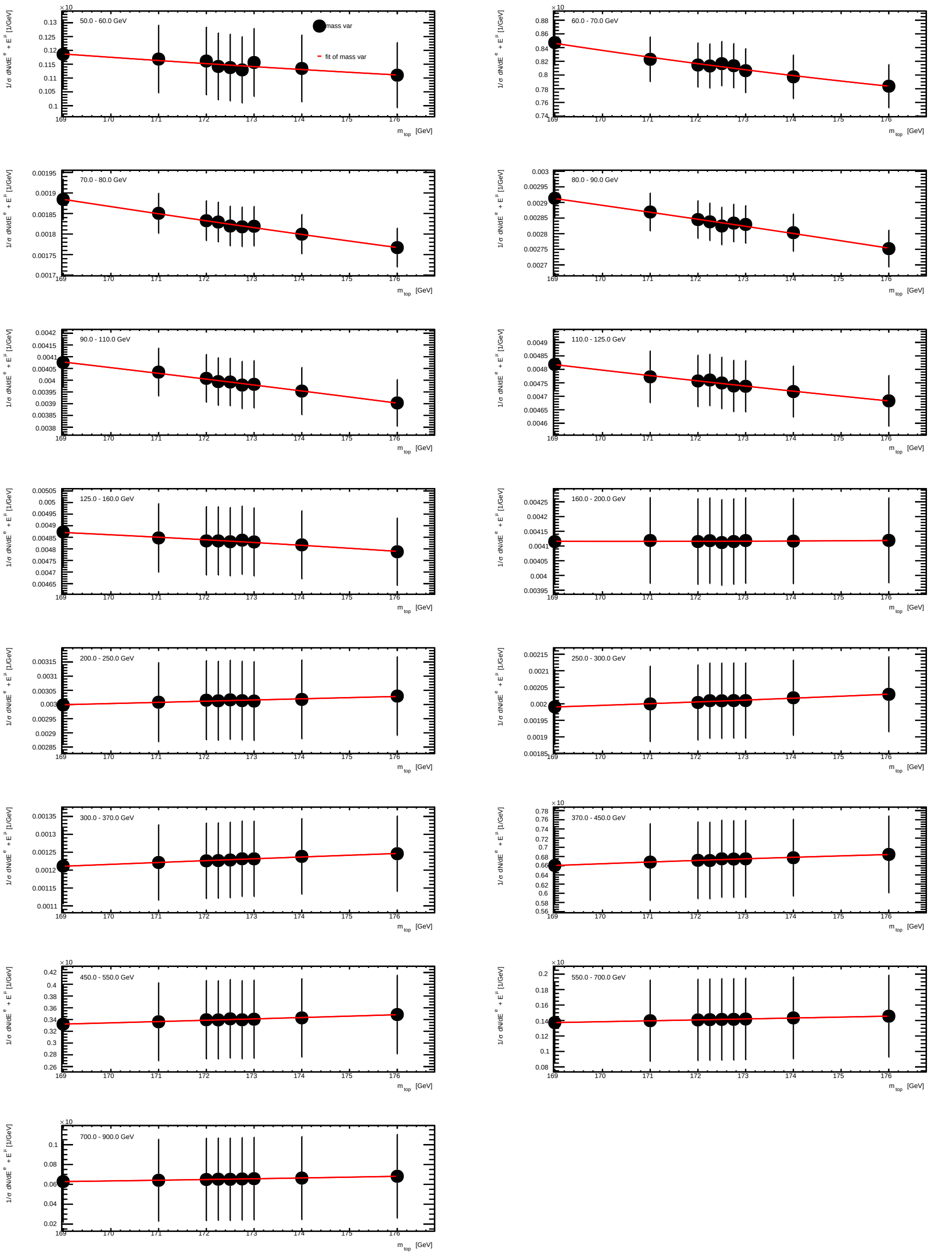

Figure 11: Parametrisation of the particle level templates for each bin of $E(\ell^+) + E(\ell^-)$. The values for each bin are fitted to a second order degree polynomial (in red).

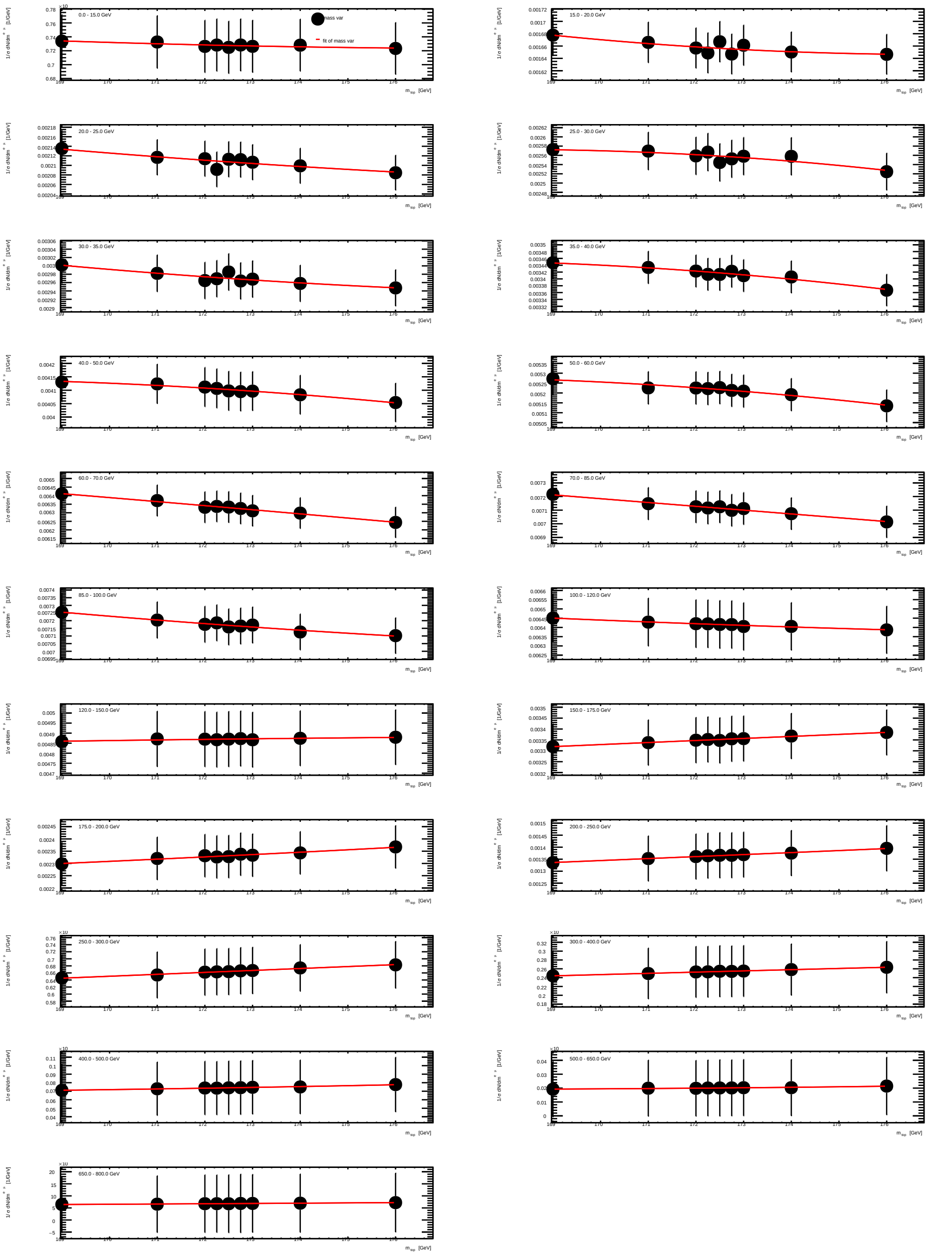

Figure 12: Parametrisation of the particle level templates for each bin of $m(\ell^+\ell^-)$. The values for each bin are fitted to a second order degree polynomial (in red).

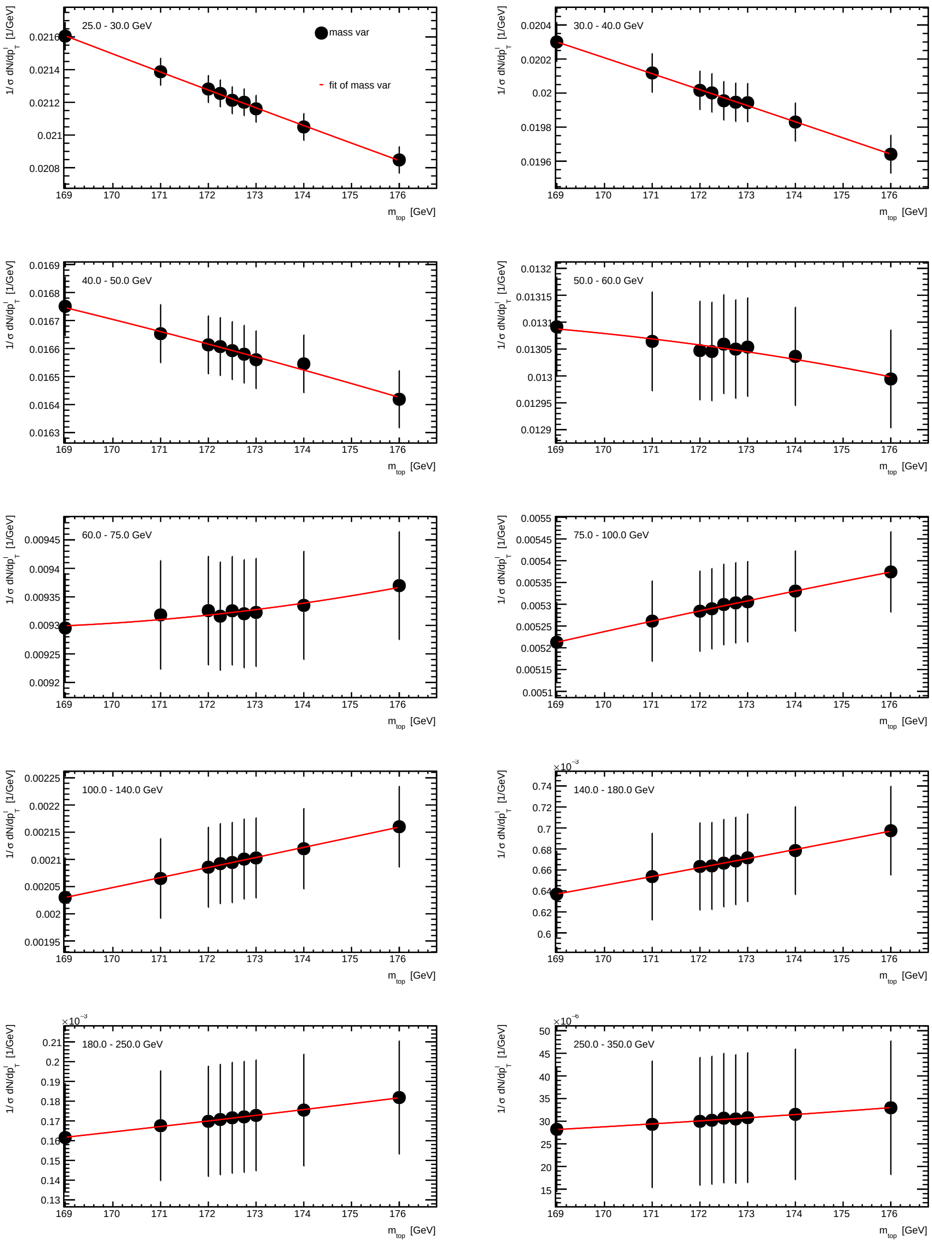

Figure 13: Parametrisation of the particle level templates for each bin of p_{T} (ℓ). The values for each bin are fitted to a second order degree polynomial (in red).

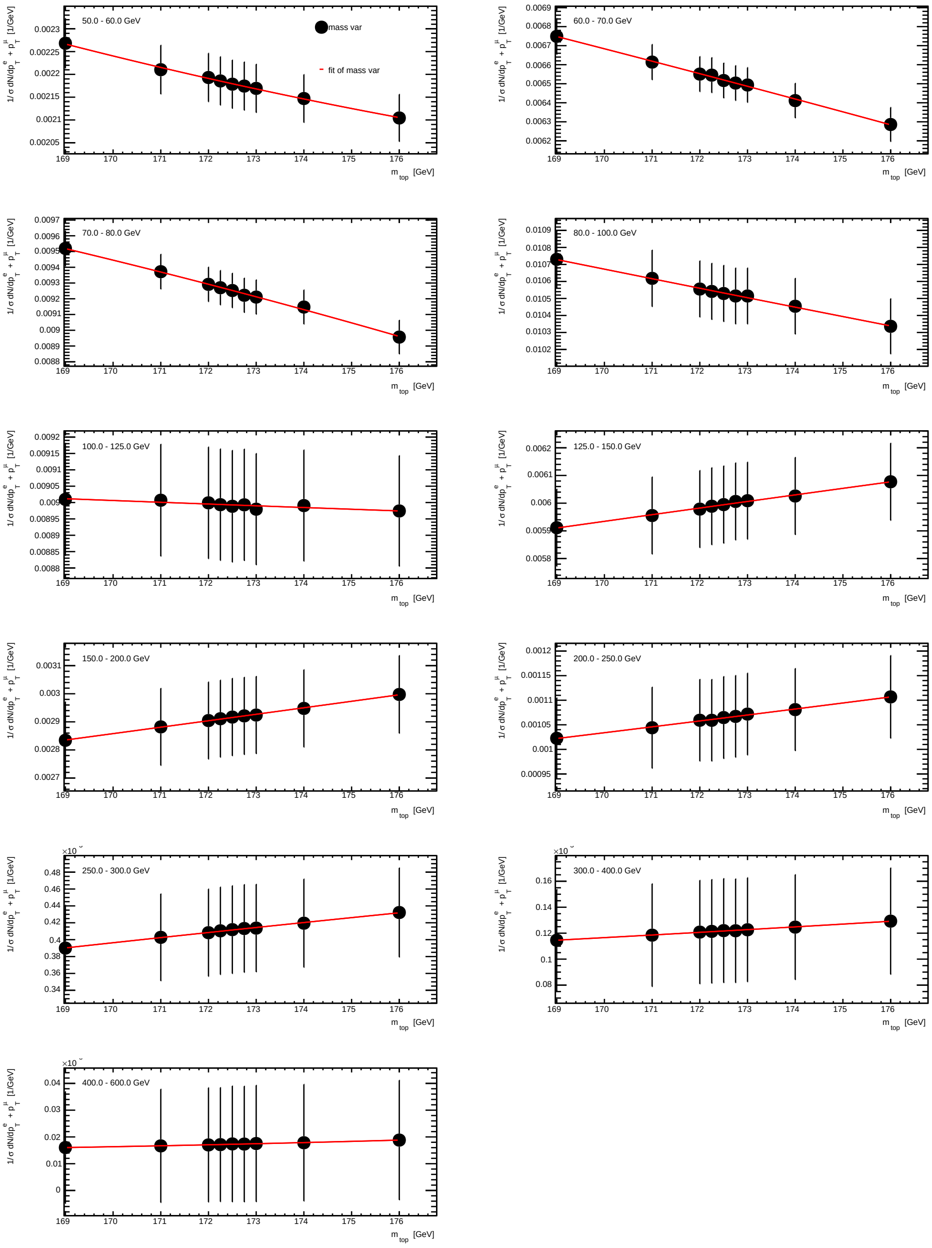

Figure 14: Parametrisation of the particle level templates for each bin of p_{T} (ℓ^{+}) + p_{T} (ℓ^{-}). The values for each bin are fitted to a second order degree polynomial (in red).

H Covariance matrices

Table 20: Covariance matrix for $p_T(\ell^+\ell^-)$. Each entry in the covariance matrix has units [1/GeV^2].

$p_T(\ell^+\ell^-)$ bins [GeV]	0–20	20–30	30–45	45–60	60–75	75–100	100–125	125–150	150–200	200–300
0 − 20	1.3252e−9	1.9065e−9	1.3792e−9	2.4245e−9	2.1271e−9	5.6069e−10	1.7050e−9	1.1417e−9	4.7580e−10	1.7310e−10
20 − 30	1.9065e−9	7.3739e−9	3.4008e−9	5.7949e−9	6.4423e−9	1.7284e−9	4.0129e−9	2.6233e−9	1.0335e−9	3.7700e−10
30 − 45	1.3792e−9	3.4008e−9	4.3619e−9	3.9296e−9	3.9901e−9	1.0545e−9	2.4088e−9	2.1173e−9	9.9747e−10	4.4026e−10
45 − 60	2.4245e−9	5.7949e−9	3.9296e−9	1.0309e−8	8.1139e−9	1.8306e−9	5.7127e−9	3.6348e−9	1.5119e−9	5.4949e−10
60 − 75	2.1271e−9	6.4423e−9	3.9901e−9	8.1139e−9	1.1418e−8	2.0261e−9	5.4536e−9	3.4708e−9	1.4299e−9	5.4550e−10
75 − 100	5.6069e−10	1.7284e−9	1.0545e−9	1.8306e−9	2.0261e−9	1.5292e−9	1.2001e−9	8.8731e−10	3.9503e−10	1.9187e−10
100 − 125	1.7050e−9	4.0129e−9	2.4088e−9	5.7127e−9	5.4536e−9	1.2001e−9	4.7686e−9	2.3397e−9	8.5727e−10	2.4140e−10
125 − 150	1.1417e−9	2.6233e−9	2.1173e−9	3.6348e−9	3.4708e−9	8.8731e−10	2.3397e−9	1.9328e−9	7.7328e−10	3.0816e−10
150 − 200	4.7580e−10	1.0335e−9	9.9747e−10	1.5119e−9	1.4299e−9	3.9503e−10	8.5727e−10	7.7328e−10	4.1375e−10	1.7530e−10
200 − 300	1.7310e−10	3.7700e−10	4.4026e−10	5.4949e−10	5.4550e−10	1.9187e−10	2.4140e−10	3.0816e−10	1.7530e−10	9.6756e−11

Table 21: Covariance matrix for $p_{\mathrm{T}}(\ell^{+}) + p_{\mathrm{T}}(\ell^{-})$. Each entry in the covariance matrix has units [1/GeV^2].

$p_{\mathrm{T}}(\ell^{+}) + p_{\mathrm{T}}(\ell^{-})$ bins [GeV]	50–60	60–70	70–80	80–100	100–125	125–150	150–200	200–250	250–300	300–400	400–600
50 − 60	5.4132e−9	4.0313e−9	9.1093e−9	4.6675e−9	1.5939e−9	2.2696e−9	2.0987e−9	8.8477e−10	7.3004e−10	3.1467e−10	4.8048e−11
60 − 70	4.0313e−9	8.2729e−9	8.9241e−9	5.5928e−9	2.5250e−9	1.9362e−9	2.6989e−9	1.2235e−9	9.6024e−10	4.5037e−10	1.0029e−10
70 − 80	9.1093e−9	8.9241e−9	2.3908e−8	1.0684e−8	4.0211e−9	4.9378e−9	5.1281e−9	2.0133e−9	1.7999e−9	7.8251e−10	1.2640e−10
80 − 100	4.6675e−9	5.5928e−9	1.0684e−8	8.2316e−9	2.8448e−9	2.3111e−9	2.8877e−9	1.5300e−9	1.1484e−9	5.1780e−10	1.0954e−10
100 − 125	1.5939e−9	2.5250e−9	4.0211e−9	2.8448e−9	2.4406e−9	6.6517e−10	1.2749e−9	6.6946e−10	5.3890e−10	2.5366e−10	6.0876e−11
125 − 150	2.2696e−9	1.9362e−9	4.9378e−9	2.3111e−9	6.6517e−10	1.8146e−9	1.1543e−9	3.8026e−10	3.7673e−10	1.6332e−10	1.9470e−11
150 − 200	2.0987e−9	2.6989e−9	5.1281e−9	2.8877e−9	1.2749e−9	1.1543e−9	1.6168e−9	4.9041e−10	5.0846e−10	2.3251e−10	4.1832e−11
200 − 250	8.8477e−10	1.2235e−9	2.0133e−9	1.5300e−9	6.6946e−10	3.8026e−10	4.9041e−10	4.8554e−10	2.4047e−10	1.0435e−10	2.8220e−11
250 − 300	7.3004e−10	9.6024e−10	1.7999e−9	1.1484e−9	5.3890e−10	3.7673e−10	5.0846e−10	2.4047e−10	2.1469e−10	8.9899e−11	1.9150e−11
300 − 400	3.1467e−10	4.5037e−10	7.8251e−10	5.1780e−10	2.5366e−10	1.6332e−10	2.3251e−10	1.0435e−10	8.9899e−11	4.5537e−11	9.2193e−12
400 − 600	4.8048e−11	1.0029e−10	1.2640e−10	1.0954e−10	6.0876e−11	1.9470e−11	4.1832e−11	2.8220e−11	1.9150e−11	9.2193e−12	2.7264e−12

Table 22: Covariance matrix for $p_{\mathrm{T}}(\ell)$. Each entry in the covariance matrix has units $[1/\mathrm{GeV}^2]$.

$p_{\mathrm{T}}(\ell)$ bins [GeV]	25–30	30–40	40–50	50–60	60–75	75–100	100–140	140–180	180–250	250–350
25 − 30	1.1120e−7	3.1874e−8	1.7242e−8	5.8726e−9	7.2506e−9	6.1402e−9	1.0085e−8	4.0825e−9	1.7578e−9	4.0521e−10
30 − 40	3.1874e−8	1.7064e−8	7.6325e−9	3.0760e−9	3.4538e−9	2.3930e−9	3.7825e−9	1.8002e−9	8.2362e−10	2.7820e−10
40 − 50	1.7242e−8	7.6325e−9	8.3975e−9	2.7487e−9	2.3492e−9	1.6691e−9	2.1651e−9	1.1753e−9	4.7966e−10	1.7717e−10
50 − 60	5.8726e−9	3.0760e−9	2.7487e−9	3.3667e−9	1.1614e−9	6.2974e−10	8.9330e−10	5.4839e−10	2.3695e−10	1.0128e−10
60 − 75	7.2506e−9	3.4538e−9	2.3492e−9	1.1614e−9	2.0848e−9	6.4453e−10	9.3724e−10	5.0765e−10	2.1750e−10	7.6699e−11
75 − 100	6.1402e−9	2.3930e−9	1.6691e−9	6.2974e−10	6.4453e−10	7.8938e−10	6.7594e−10	3.0866e−10	1.2551e−10	3.8967e−11
100 − 140	1.0085e−8	3.7825e−9	2.1651e−9	8.9330e−10	9.3724e−10	6.7594e−10	1.2253e−9	5.2837e−10	2.3816e−10	6.9736e−11
140 − 180	4.0825e−9	1.8002e−9	1.1753e−9	5.4839e−10	5.0765e−10	3.0866e−10	5.2837e−10	2.9122e−10	1.2121e−10	4.2181e−11
180 − 250	1.7578e−9	8.2362e−10	4.7966e−10	2.3695e−10	2.1750e−10	1.2551e−10	2.3816e−10	1.2121e−10	6.3116e−11	2.2309e−11
250 − 350	4.0521e−10	2.7820e−10	1.7717e−10	1.0128e−10	7.6699e−11	3.8967e−11	6.9736e−11	4.2181e−11	2.2309e−11	1.0485e−11

Table 23: Covariance matrix for $E(\ell^{+}) + E(\ell^{-})$. Each entry in the covariance matrix has units $[1/\mathrm{GeV}^2]$.

$E(\ell^{+}) + E(\ell^{-})$ bins [GeV]	50−60	60−70	70−80	80−90	90−110	110−125	125−160	160−200	200−250	250−300	300−370	370−450	450−550	550−700	700−900
50 − 60	1.4291e−10	1.6301e−10	2.4748e−10	1.9119e−10	1.5103e−10	1.3057e−10	1.3669e−10	8.0466e−11	7.0787e−11	7.6004e−11	6.4589e−11	3.2449e−11	1.2443e−11	1.1958e−11	7.0769e−12
60 − 70	1.6301e−10	1.3016e−9	8.8208e−10	8.3089e−10	8.1346e−10	5.0046e−10	9.5668e−10	3.5228e−10	5.5247e−10	4.2038e−10	3.9055e−10	1.1073e−10	4.7637e−11	6.8627e−11	4.4037e−11
70 − 80	2.4748e−10	8.8208e−10	1.7086e−9	1.0855e−9	1.0819e−9	8.8132e−10	9.9827e−10	4.3247e−10	4.5058e−10	4.6663e−10	4.5372e−10	1.8900e−10	8.9336e−11	8.8608e−11	5.6752e−11
80 − 90	1.9119e−10	8.3089e−10	1.0855e−9	2.3373e−9	1.2921e−9	1.0942e−9	1.2191e−9	4.5737e−10	4.2216e−10	5.0599e−10	5.4841e−10	2.6706e−10	1.2911e−10	1.0931e−10	7.2740e−11
90 − 110	1.5103e−10	8.1346e−10	1.0819e−9	1.2921e−9	1.9365e−9	1.1470e−9	1.1900e−9	4.8730e−10	4.0859e−10	5.0145e−10	5.1202e−10	2.6097e−10	1.5619e−10	1.2134e−10	8.0360e−11
110 − 125	1.3057e−10	5.0046e−10	8.8132e−10	1.0942e−9	1.1470e−9	1.9871e−9	9.2042e−10	3.9610e−10	2.4115e−10	3.5889e−10	3.8026e−10	2.5278e−10	1.5347e−10	1.0323e−10	6.9991e−11
125 − 160	1.3669e−10	9.5668e−10	9.9827e−10	1.2191e−9	1.1900e−9	9.2042e−10	1.6542e−9	4.8830e−10	5.5187e−10	5.1278e−10	5.4112e−10	2.1138e−10	1.1418e−10	1.0857e−10	7.5480e−11
160 − 200	8.0466e−11	3.5228e−10	4.3247e−10	4.5737e−10	4.8730e−10	3.9610e−10	4.8830e−10	4.9218e−10	1.6903e−10	1.9480e−10	2.0390e−10	1.0437e−10	5.8375e−11	4.8180e−11	3.5285e−11
200 − 250	7.0787e−11	5.5247e−10	4.5058e−10	4.2216e−10	4.0859e−10	2.4115e−10	5.5187e−10	1.6903e−10	4.9007e−10	2.2934e−10	2.2156e−10	4.8549e−11	2.3220e−11	3.7972e−11	2.6160e−11
250 − 300	7.6004e−11	4.2038e−10	4.6663e−10	5.0599e−10	5.0145e−10	3.5889e−10	5.1278e−10	1.9480e−10	2.2934e−10	3.1485e−10	2.2476e−10	8.2847e−11	4.1380e−11	4.3001e−11	2.8501e−11
300 − 370	6.4589e−11	3.9055e−10	4.5372e−10	5.4841e−10	5.1202e−10	3.8026e−10	5.4112e−10	2.0390e−10	2.2156e−10	2.2476e−10	2.9581e−10	9.6286e−11	4.7416e−11	4.3071e−11	2.9990e−11
370 − 450	3.2449e−11	1.1073e−10	1.8900e−10	2.6706e−10	2.6097e−10	2.5278e−10	2.1138e−10	1.0437e−10	4.8549e−11	8.2847e−11	9.6286e−11	8.4468e−11	3.5140e−11	2.3002e−11	1.6221e−11
450 − 550	1.2443e−11	4.7637e−11	8.9336e−11	1.2911e−10	1.5619e−10	1.5347e−10	1.1418e−10	5.8375e−11	2.3220e−11	4.1380e−11	4.7416e−11	3.5140e−11	3.4774e−11	1.4626e−11	1.0657e−11
550 − 700	1.1958e−11	6.8627e−11	8.8608e−11	1.0931e−10	1.2134e−10	1.0323e−10	1.0857e−10	4.8180e−11	3.7972e−11	4.3001e−11	4.3071e−11	2.3002e−11	1.4626e−11	1.4428e−11	7.7705e−12
700 − 900	7.0769e−12	4.4037e−11	5.6752e−11	7.2740e−11	8.0360e−11	6.9991e−11	7.5480e−11	3.5285e−11	2.6160e−11	2.8501e−11	2.9990e−11	1.6221e−11	1.0657e−11	7.7705e−12	6.5977e−12

Table 24: Covariance matrix for $m(\ell^+\ell^-)$. Each entry in the covariance matrix has units $[1/\mathrm{GeV}^2]$.

$m(\ell^+\ell^-)$ bins [GeV]	0−15	15−20	20−25	25−30	30−35	35−40	40−50	50−60	60−70	70−85	85−100	100−120	120−150	150−175	175−200	200−250	250−300	300−400	400−500	500−650	650−800
0 − 15	7.9502e−10	6.5653e−10	5.5825e−10	3.1830e−10	8.6543e−10	2.4320e−10	1.5184e−9	9.4416e−10	9.6070e−10	3.0767e−10	1.0955e−9	3.3796e−10	1.2219e−10	1.8815e−10	4.4784e−10	1.8161e−10	3.2640e−10	8.5908e−11	3.2423e−11	2.0973e−11	3.7796e−12
15 − 20	6.5653e−10	2.0999e−9	6.9272e−10	4.1393e−10	1.1509e−9	4.4040e−10	2.1095e−9	1.4655e−9	1.4062e−9	5.4487e−10	1.4861e−9	4.7587e−10	2.2731e−10	2.4464e−10	6.5835e−10	2.7137e−10	4.4252e−10	1.3230e−10	4.7342e−11	2.7406e−11	6.1440e−12
20 − 25	5.5825e−10	6.9272e−10	2.0561e−9	4.5217e−10	1.1830e−9	4.7005e−10	1.7407e−9	1.6983e−9	1.6187e−9	6.2838e−10	1.3712e−9	4.2764e−10	2.4598e−10	2.6605e−10	6.4791e−10	3.2003e−10	4.1198e−10	1.4742e−10	4.8201e−11	2.6669e−11	7.7094e−12
25 − 30	3.1830e−10	4.1393e−10	4.5217e−10	2.4931e−9	6.8631e−10	7.0427e−10	1.0482e−9	1.1579e−9	9.6763e−10	8.3494e−10	8.9032e−10	3.5859e−10	1.0692e−10	2.3527e−10	4.0324e−10	3.7703e−10	2.8853e−10	1.7579e−10	7.4517e−11	1.6291e−11	1.5812e−11
30 − 35	8.6543e−10	1.1509e−9	1.1830e−9	6.8631e−10	3.6859e−9	9.4804e−10	2.7793e−9	2.8209e−9	2.9633e−9	1.0500e−9	1.9875e−9	7.1766e−10	4.3554e−10	4.2729e−10	1.1451e−9	5.4261e−10	6.2936e−10	2.2318e−10	6.8116e−11	4.3573e−11	9.5304e−12
35 − 40	2.4320e−10	4.4040e−10	4.7005e−10	7.0427e−10	9.4804e−10	2.8560e−9	7.8171e−10	1.6901e−9	1.8412e−9	1.1027e−9	5.8212e−10	1.9012e−10	2.7951e−10	2.9059e−10	5.3993e−10	4.0308e−10	2.4277e−10	1.5658e−10	4.7378e−11	1.9246e−11	1.1326e−11
40 − 50	1.5184e−9	2.1095e−9	1.7407e−9	1.0482e−9	2.7793e−9	7.8171e−10	6.1231e−9	3.3905e−9	3.2040e−9	1.0581e−9	3.4138e−9	1.1048e−9	4.0716e−10	6.5559e−10	1.5264e−9	6.5248e−10	1.0310e−9	2.9392e−10	1.0994e−10	6.4312e−11	1.3070e−11
50 − 60	9.4416e−10	1.4655e−9	1.6983e−9	1.1579e−9	2.8209e−9	1.6901e−9	3.3905e−9	6.9852e−9	5.5906e−9	1.9442e−9	2.4893e−9	8.5700e−10	9.2117e−10	6.2834e−10	1.8641e−9	1.0337e−9	8.4960e−10	4.0658e−10	1.0602e−10	6.3801e−11	1.9312e−11
60 − 70	9.6070e−10	1.4062e−9	1.6187e−9	9.6763e−10	2.9633e−9	1.8412e−9	3.2040e−9	5.5906e−9	7.8418e−9	2.1107e−9	2.3699e−9	7.1164e−10	9.6650e−10	6.6889e−10	1.9349e−9	1.0623e−9	8.1039e−10	3.8632e−10	8.8042e−11	6.9025e−11	1.6498e−11
70 − 85	3.0767e−10	5.4487e−10	6.2838e−10	8.3494e−10	1.0500e−9	1.1027e−9	1.0581e−9	1.9442e−9	2.1107e−9	2.8128e−9	7.9785e−10	3.4623e−10	2.8332e−10	3.0940e−10	6.8894e−10	5.5761e−10	3.4418e−10	2.2201e−10	6.9899e−11	2.6447e−11	1.6058e−11
85 − 100	1.0955e−9	1.4861e−9	1.3712e−9	8.9032e−10	1.9875e−9	5.8212e−10	3.4138e−9	2.4893e−9	2.3699e−9	7.9785e−10	3.7761e−9	8.2427e−10	2.6563e−10	4.1410e−10	1.1329e−9	5.0848e−10	7.7277e−10	2.4067e−10	9.3039e−11	4.9003e−11	1.2582e−11
100 − 120	3.3796e−10	4.7587e−10	4.2764e−10	3.5859e−10	7.1766e−10	1.9012e−10	1.1048e−9	8.5700e−10	7.1164e−10	3.4623e−10	8.2427e−10	1.1018e−9	7.6623e−11	1.5108e−10	3.7604e−10	1.8844e−10	2.5765e−10	9.4197e−11	3.8301e−11	1.7945e−11	5.7135e−12
120 − 150	1.2219e−10	2.2731e−10	2.4598e−10	1.0692e−10	4.3554e−10	2.7951e−10	4.0716e−10	9.2117e−10	9.6650e−10	2.8332e−10	2.6563e−10	7.6623e−11	5.5341e−10	9.3424e−11	3.1517e−10	1.7736e−10	1.1749e−10	6.0273e−11	1.1880e−11	1.1094e−11	2.8043e−12
150 − 175	1.8815e−10	2.4464e−10	2.6605e−10	2.3527e−10	4.2729e−10	2.9059e−10	6.5559e−10	6.2834e−10	6.6889e−10	3.0940e−10	4.1410e−10	1.5108e−10	9.3424e−11	4.1777e−10	2.5997e−10	1.6655e−10	1.4318e−10	6.1489e−11	2.2821e−11	1.1125e−11	3.7994e−12
175 − 200	4.4784e−10	6.5835e−10	6.4791e−10	4.0324e−10	1.1451e−9	5.3993e−10	1.5264e−9	1.8641e−9	1.9349e−9	6.8894e−10	1.1329e−9	3.7604e−10	3.1517e−10	2.5997e−10	9.3096e−10	3.7678e−10	3.7018e−10	1.5044e−10	4.3292e−11	2.6631e−11	6.9168e−12
200 − 250	1.8161e−10	2.7137e−10	3.2003e−10	3.7703e−10	5.4261e−10	4.0308e−10	6.5248e−10	1.0337e−9	1.0623e−9	5.5761e−10	5.0848e−10	1.8844e−10	1.7736e−10	1.6655e−10	3.7678e−10	3.2241e−10	1.7219e−10	9.5751e−11	3.1158e−11	1.4242e−11	6.3014e−12
250 − 300	3.2640e−10	4.4252e−10	4.1198e−10	2.8853e−10	6.2936e−10	2.4277e−10	1.0310e−9	8.4960e−10	8.1039e−10	3.4418e−10	7.7277e−10	2.5765e−10	1.1749e−10	1.4318e−10	3.7018e−10	1.7219e−10	2.7312e−10	8.1576e−11	2.8477e−11	1.5045e−11	4.1851e−12
300 − 400	8.5908e−11	1.3230e−10	1.4742e−10	1.7579e−10	2.2318e−10	1.5658e−10	2.9392e−10	4.0658e−10	3.8632e−10	2.2201e−10	2.4067e−10	9.4197e−11	6.0273e−11	6.1489e−11	1.5044e−10	9.5751e−11	8.1576e−11	4.8470e−11	1.4636e−11	5.5303e−12	2.8956e−12
400 − 500	3.2423e−11	4.7342e−11	4.8201e−11	7.4517e−11	6.8116e−11	4.7378e−11	1.0994e−10	1.0602e−10	8.8042e−11	6.9899e−11	9.3039e−11	3.8301e−11	1.1880e−11	2.2821e−11	4.3292e−11	3.1158e−11	2.8477e−11	1.4636e−11	7.7843e−12	1.8983e−12	1.1593e−12
500 − 650	2.0973e−11	2.7406e−11	2.6669e−11	1.6291e−11	4.3573e−11	1.9246e−11	6.4312e−11	6.3801e−11	6.9025e−11	2.6447e−11	4.9003e−11	1.7945e−11	1.1094e−11	1.1125e−11	2.6631e−11	1.4242e−11	1.5045e−11	5.5303e−12	1.8983e−12	1.4873e−12	2.9376e−13
650 − 800	3.7796e−12	6.1440e−12	7.7094e−12	1.5812e−11	9.5304e−12	1.1326e−11	1.3070e−11	1.9312e−11	1.6498e−11	1.6058e−11	1.2582e−11	5.7135e−12	2.8043e−12	3.7994e−12	6.9168e−12	6.3014e−12	4.1851e−12	2.8956e−12	1.1593e−12	2.9376e−13	3.5638e−13